Seafloor Deposit Models, Geochemistry, and Petrology of the Mafic-Ultramafic Hosted Big Lake VMS Occurrence, Marathon, Ontario

Marc L. Rinne

A thesis submitted to the Faculty of Graduate Studies in partial fulfillment of the requirements for the degree of Master of Science

Geology Department
Lakehead University
Thunder Bay, Ontario
May 2010

Abstract

The Big Lake volcanogenic massive sulphide (VMS) occurrence, located in the Schreiber-Hemlo belt of the Superior Province, was discovered in March 2006 near Marathon, Ontario. It is hosted in a mafic-ultramafic metavolcanic sequence lacking felsic volcanic or volcaniclastic rock, and consists of a thin, locally anastomosing sheet of veined pyrrhotite, chalcopyrite, and sphalerite (± galena, cobaltite) currently defined over a plan area of approximately 0.5x0.5 km, along the base of a series of peridotite and pyroxenite cumulates termed the Big Lake Ultramafic Complex (BLUC). Hydrothermal alteration at Big Lake is restricted to within a few metres above visible sulphide mineralisation. The geometry of the occurrence may be in part a function of limited permeability in a flow-dominated setting.

Several lines of evidence were used to conclude that the host lithostratigraphy to the Big Lake VMS occurrence is overturned. Moving down hole and up stratigraphy, the sequence consists of cumulate peridotite and pyroxenite, adjacent flows, VMS-hydrothermal alteration and sulphides, siltstone, and flows with interbedded, locally pelitic siltstones and iron formation. The ultramafic cumulates and adjacent underlying volcanic rock are likely a series of ponded ultramafic flows.

The metavolcanic rocks that host the occurrence are basalts to komatiitic basalts, with ~10% of samples having >18 wt. % MgO. Those stratigraphically below the VMS mineralisation are transitional to alkaline basalts, with convex-upward LREE and fractionated HREE. Their NEB-like characteristics can be explained by mixing of depleted and enriched (OIB-like) mantle plume melt components. Basalts stratigraphically overlying the VMS mineralisation have the flat REE patterns (La/Yb_{cn}=1-2) typical of Wawa tholeiitic plateau basalts. As a whole, the lithostratigraphic assemblage at Big Lake is consistent with an oceanic plateau setting, as in the mafic category of VMS deposits, and likely formed by eruption of variably enriched plateau basalts and thick ultramafic flows from a heterogeneous mantle plume.

Depending on the exact roles or effects of shear deformation, different possibilities for heat sources, and other aspects that could not be clearly resolved in this study, four models were developed to describe the genesis of the Big Lake VMS occurrence. The favoured model involves a genetic relationship between the ultramafic cumulates and the stratigraphically overlying VMS occurrence, whereby cooling of the BLUC flow(s) drove the hydrothermal circulation responsible for VMS mineralisation near its upper margins. If this model is accurate, the Big Lake VMS occurrence is the first documented example of a VMS system related to ponded ultramafic flows outside of the Abitibi subprovince, and demonstrates that similar styles of shallow intrusion or komatiite flow-driven VMS convection cells may have developed elsewhere in the Superior Province or in other Archean cratons.

Acknowledgements

I thank the Ontario Centres of Excellence and MetalCORP Ltd. for making this study possible. This research was also supported by a Society of Economic Geologists student research grant and an NSERC PGS-M scholarship.

MetalCORP staff are thanked for providing a great work environment. Lakehead faculty and staff members, too many to list, are appreciated for their help in various aspects of this work, along with Andy Abraham. I have also had the opportunity to work with several mentors in the field or by correspondence, including Charlie Blackburn and Jim Franklin, whose training and advice have already proven to be useful (not to mention a very helpful thesis review by Jim Franklin). I of course thank Pete Hollings, my thesis advisor, for his many hours spent revising drafts and discussing ideas.

Finally, I am grateful to friends, family, and Angela, for their continued support.

Table of Contents

List of Figures

List of Tables

Chapter 1
Introduction

1.1 Location and Background

The Big Lake Cu-Zn-Ag-Au volcanogenic massive sulphide (VMS) occurrence is hosted in mafic-ultramafic strata of the Schreiber-Hemlo greenstone belt near Marathon, Ontario (Fig. 1.1), and is one of few known VMS occurrences in sequences lacking felsic volcanic or volcaniclastic rock. Owing to its recent discovery in March 2006, there are many aspects of the occurrence that have yet to be defined in detail, including age, relationships with overlying ultramafic cumulates, mafic-ultramafic host strata, way-up, and proximity to vent site(s). The academic and potential economic significance of the occurrence has led to a joint research project between MetalCORP Ltd., Lakehead University, and the Ontario Centres of Excellence, of which this thesis forms one part. This project is also funded by NSERC and the Society of Economic Geologists.

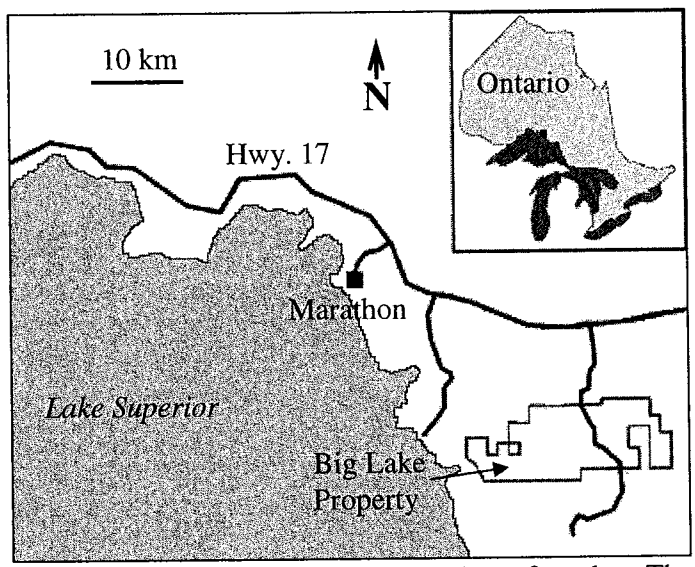

Figure 1.1 - Map showing the location of study. The Big Lake property is about 25 km southeast of Marathon, Ontario.

1.2 Objectives

The key aims of this study were to investigate the nature and origins of the Big Lake VMS occurrence, primarily through detailed studies of its geochemistry in three

dimensions. Modeling and interpretation of whole-rock geochemical data were used to describe the setting and genesis of the occurrence, with the aim of clarifying how and in what conditions significant VMS mineralisation can occur in settings lacking felsic volcanic rocks. Related aims were to classify the occurrence according to host rock lithology and tectonic setting, as in the five-fold classification of Franklin et al. (2005) modified after Barrie and Hannington (1999).

Leapfrog geological modeling software was used to identify and display hydrothermal alteration zones within the occurrence and, where possible, to define its anatomy in terms of stratigraphic hangingwall and footwall, locations of upflow zones or structures, and locations of sulphide precipitation below and above seafloor (e.g., stringer, lens, and/or exhalite sulphides). Observations were ultimately compiled to produce genetic models for the occurrence.

1.3 Review of VMS Systems

Volcanogenic massive sulphide deposits supply approximately 13% of the world's total base metal resource, including 22% of Zn resources, and are also a significant source of gold, silver, and other metals (Singer, 1995). Of the ca. 800 known deposits and documented occurrences with over 200,000 tonnes of geological reserves, over 350 are located in Canada (Galley et al., 2007).

The genesis of volcanogenic massive sulphide deposits is well-understood, based primarily on a number of studies of well-preserved deposits, and also as a result of the discovery of active hydrothermal vents of the East Pacific Rise in 1977 (Gibson et al., 1999) and studies of more than 100 modern analogues discovered since then (Herzig and Hannington, 1999). VMS deposits are hosted within submarine mafic to felsic volcanic and/or volcaniclastic rocks with variable sediment input, in water depths ranging from a few metres to greater than three kilometres (MacGeehan, 1978).

The anatomy of VMS deposits is related to their genesis. The cores of footwall alteration pipes with hydrothermal alteration assemblages and stockwork ore veining are, in brief, formed by wallrock reaction with ascending hydrothermal fluids (Fig. 1.2). Zones of semi-conformable footwall alteration which can extend tens of kilometres along strike (MacGeehan, 1978) imply a regional-scale convection of hydrothermal fluids in

some deposits. Overlying ore lenses feature massive to weakly bedded ore textures mostly conformable with the host volcanic sequence, consistent with a genesis by precipitation from metal-laden hydrothermal fluids (Gibson et al., 1999).

Alteration pipes or stringer zones may not resemble a vertical pipe as shown in Figure 1.2, as their geometry is dictated by footwall permeability (not exclusively fault-related) and later deformation. Also, precipitation of sulphides need not necessarily occur as shown in an open water column, but can also take place just below surface through permeable ocean floor and/or by inflating the base of an already deposited sulphide lens or crust (Galley et al., 2007).

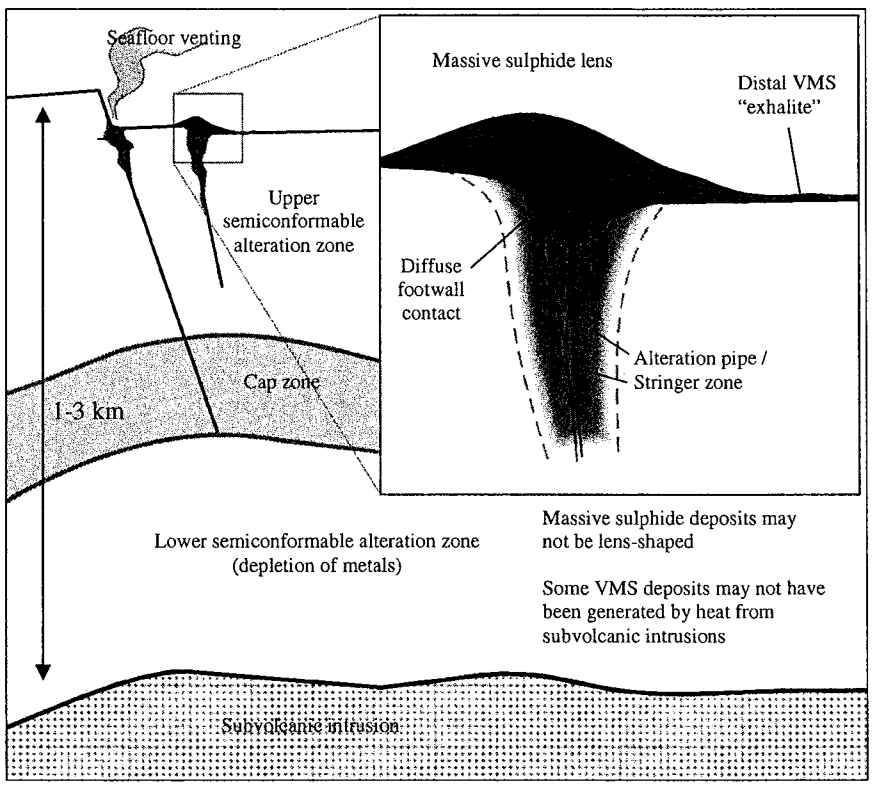

Figure 1.2 - Generalised cross section of a typical VMS-hydrothermal system and associated features discussed in text. Simplified from Franklin et al. (2005) and Lydon (1984).

VMS-hydrothermal systems can subject a large volume of subseafloor rock to high-temperature water-rock reactions, producing semiconformable zones of alteration up to tens of kilometres along strike and three kilometres below paleoseafloor (Galley et al.,

2007; Fig. 1.2). These zones may seal themselves at depth by continued precipitation of smectite-zeolite-carbonate and silica to form an aquaclude or cap zone, which may increase the duration or intensity of metal leaching from rocks in the semiconformable alteration zone below this cap (Franklin et al., 2005; Fig. 1.2). At the seafloor, the formation of a massive sulphide body probably requires some means of capping the diffuse escape of metal-laden fluids into the ocean water column. Sulphide crusts and chimneys, chimney collapse breccias, rhyolite domes, or sedimentary rocks can play this role, and may also protect sulphides from oxidation in modern settings.

Figure 1.2 shows a discrete heat source to drive circulation of seawater. This is usually assumed to be a magma body at least 0.5 km below seafloor (Franklin et al., 2005), but not all VMS deposit areas contain clear examples of such subvolcanic intrusions (Galley, 2002).

1.4 Structure of Thesis

Previous work and mineral exploration on the Big Lake property, sampling methods used, and methods and theory in generating and modeling geochemical data and indices are reviewed in the following chapter. Chapter Three is a summary of the regional geology, and Chapter Four is a discussion of the host lithostratigraphy to the Big Lake VMS occurrence. Chapter Five is a review of whole-rock geochemical data at Big Lake, with emphasis on immobile elements. Analyses of samples collected by the author are used to discuss rock type classifications and tectonic setting of the mafic-ultramafic metavolcanic rocks of the Big Lake VMS host sequence.

Chapter Six combines information from isotope, major, and trace element geochemistry, including assay data not collected by the author, in order to define the shape and extent of hydrothermal alteration related to sulphide mineralisation over a plan scale of approximately 0.5 x 0.5 km. Chapter Seven is a review of the sulphide assemblages and distributions at Big Lake, with discussion of the temperature-pressure conditions of sulphide formation. All information discussed in previous chapters is incorporated into four seafloor deposit models for the occurrence in Chapter Eight. Conclusions and implications are discussed in Chapter Nine.

Chapter 2

Methods

2.1 Property and Access

The MetalCORP Ltd. Big Lake exploration property is located approximately 30 km southeast of Marathon, Ontario, with access from Umbata Falls Rd. south of the Trans Canada Highway 17 (Fig. 2.1). Areas east of Umbata Falls Rd., including the study area, are mostly swamp-covered.

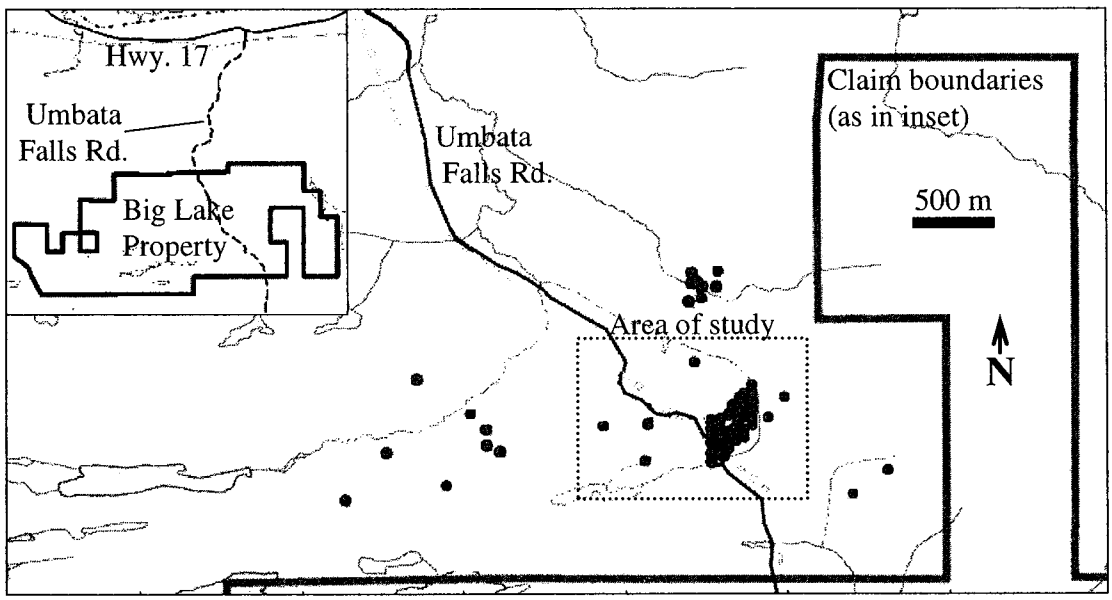

Figure 2.1 - Map of the eastern part of the Big Lake property. Inset at top left shows property boundaries current to 2009 as in Figure 1.1. Grey circles are drill collars, most of which are located within the study area (outlined).

2.2 Previous Work and Mineral Exploration

Geological mapping and sampling of the Schreiber-Hemlo greenstone belt east of the Coldwell Complex was carried out in 1977-78 by T. Muir of the Ontario Geological Survey, with results published by Muir (1982). Prior to 2004, mineral exploration near the Big Lake property had been sporadic and, given the proximity to the Hemlo gold mines, mostly focused on Archean lode gold deposits.

The Big Lake property was staked by MetalCORP in 2003-2004 (additional claims were added in June 2006), with the first phase of drilling targeting airborne EM

conductors. In addition to the VMS occurrence, areas of economic interest identified on the property include a large Mo-Re-bearing quartz vein traced over ~800 m on the far western part of the property that was initially explored by Citadel Mines and Galex Mines from 1968-71 and possibly identified by prospecting in the 1930s. At least two PGE reefs have also been identified within a large layered ultramafic complex spanning most of the property.

The Big Lake VMS occurrence was discovered in March 2006, the first hole intersecting 4.0 m at 7.5 % Cu, 2.2 % Zn, 138.0 gpt Ag, and 9.2 gpt Au. To date, VMS mineralisation has been intersected at depths of approximately 30 to 400 m over an area approximately 500 x 500 m. Due to a lack of outcrop, most geochemical modeling of the Big Lake VMS occurrence was restricted to 53 diamond drill holes in the study area labelled in Figure 2.1. However, property-scale mapping and core and surface sampling are considered for determination of background or least-altered chemistry of the Pulpwood-Playter Harbours sequence, and for general discussion of its structure and tectonic setting.

2.3 Analytical Methods

2.3.1 Petrographic Analysis

Representative core and surface samples were prepared at Lakehead University for petrographic analysis in transmitted and reflected light. The IUGS classification of igneous rocks was used where possible, with names intended to describe protolith compositions. Where not specified, crystal size classifications used were: fine-grained <1 mm, medium-grained 1-3 mm, and coarse-grained 3-10 mm. Petrographic descriptions, as well as core logs and whole-rock geochemical data, are provided in the appendices.

2.3.2 Whole-Rock Geochemical Analysis

Geochemical data used in this study are compiled from many workers, and all data used are whole-rock. Geochemical analyses were mostly performed using X-Ray Fluorescence (XRF), inductively coupled plasma – atomic emission spectrometry (ICP-

AES), and inductively coupled plasma – mass spectrometry (ICP-MS) methods from two laboratories, as follows.

2.3.2.1 OGS Analytical Methods

Drill core samples collected by the author were crushed and pulverised in an agate mill at Lakehead University, with working surfaces cleaned with acetone between samples. Powders were sent to the Ontario Geoscience Laboratories in Sudbury, Ontario, for analysis of major elements by XRF and trace elements (including the REE and HFSE) by ICP–MS. Analyses were performed using a Perkin-Elmer Elan 9000 mass spectrometer, including a two-stage acid digestion of powders in a mixture of HF-HCl-$HClO_4$ followed by a mixture of dilute HCl-$HClO_4$.

2.3.2.2 ALS Chemex Analytical Methods

The majority of core samples used in this study were collected by MetalCORP staff. Standard sampling procedure was applied, with efforts made to avoid sampling across lithological contacts. Split core samples are mostly 0.3-1.1 m long. Chemex analytical procedure codes (e.g., *ME-MS61*) are given for each method described.

Samples were crushed in Thunder Bay and pulverised in a low chrome steel mill. Most core samples were analysed by a standard 47 element assay package (*ME-MS61*) at ALS Chemex. Following four acid (HF, $HN0_3$, $HCL0_4$, HCl) digestion, samples were analysed by ICP-MS for Ag, Al, As, Ba, Be, Bi, Ca, Cd, Ce, Co, Cr, Cs, Cu, Fe, Ga, Ge, Hf, In, K, La, Li, Mg, Mn, Mo, Na, Nb, Ni, P, Pb, Rb, Re, S, Sb, Se, Sn, Sr, Ta, Te, Th, Ti, Tl, U, V, W, Y, Zn, and Zr, as well as for Au, Pt, and Pd. Cu and Zn contents greater than 1 wt. % were analysed by atomic absorption spectra (*AA62*). About one third of the assay samples were instead processed by a 27 element assay package (*ME-ICP61*), by ICP-AES for Ag, Al, As, Ba, Be, Bi, Ca, Cd, Co, Cr, Cu, Fe, K, Mg, Mn, Mo, Na, Ni, P, Pb, S, Sb, Sr, Ti, V, W, and Zn following four-acid digestion. Assay data are not used for rock type classification or discrimination of tectonic setting, but are used in modeling broad-scale distributions of metal ratios (e.g., Cu/Zn) or Mg.

Whole-rock analyses for major element oxides and a larger suite of trace elements were also performed by ALS Chemex labs on representative core samples collected by

MetalCORP staff, which vary in length from 0.1-5 m. As well as the 47 element assay package (*ME-MS61*) described above, major element oxides and LOI were analysed by XRF (*ME-XRF06*) and trace elements (Ce, Dy, Er, Eu, Gd, Ho, La, Lu, Nd, Pr, Sm, Tb, Th, Tm, U, Y, Yb) by ICP-MS (*ME-MS82*) following lithium borate fusion and four acid (HF, $HN0_3$, $HCL0_4$, HCl) digestion.

A limited comparison of major and trace element results obtained by these methods and by those of the Ontario Geoscience Laboratories is presented in Table. 2.1, from overlapping sample intervals. In general, results from OGS and ALS Chemex methods are similar, with the highest differences noted in the REE and Ti, where OGS results are 10-15% lower than ALS Chemex results.

Table 2.1 – Comparison of results from ALS Chemex and OGS lab analyses. Samples with ID in number-letter format were analysed by OGS methods, those with six digit sample ID by ALS Chemex methods. Data are in ppm unless otherwise specified.

					XRF		ICP-MS								
Sample ID	Hole ID	From (m)	To (m)	Rock Type	SiO_2 (wt.%)	MgO (wt.%)	Eu	Hf	La	Lu	Nb	Th	Ti (wt. %)	Yb	Zr
29-M	29	255.1	255.6	Siltstone	69.69	0.52	0.7	3.2	14	0.1	3.3	1.8	0.2	0.3	130
626314	29	255.2	255.4	Siltstone	65.96	1.15	0.6	--	17	0.1	3	2	0.4	0.4	121
71-L	71	222.2	222.8	~Basalt	44.11	16.28	1.1	1.8	7	0.2	4.6	0.4	0.7	1.4	67
645665	71	222.7	229.9	~Basalt	43.00	15.85	1.3	1.9	6.1	0.2	5.2	0.4	0.7	1.3	59
24-M	24	139.4	139.6	Siltstone	67.87	0.83	0.5	2.8	6.4	0	3.3	1.4	0.2	0.3	119
626175	24	140.3	150.6	Siltstone	66.77	0.92	0.6	--	14	0.1	3	2	0.2	0.4	127
7-K	7	170.6	171.1	~Basalt	39.89	9.00	1.5	2.3	7.4	0.2	6	0.6	0.8	1.6	84
626184	7	170.8	170.9	~Basalt	44.16	12.58	1.6	--	9.2	0.3	6	1	1.1	1.9	105
52-K	52	32.8	33.3	~Basalt	46.80	13.55	1	1.6	4.2	0.2	4.8	0.4	0.6	1.2	60
546740	52	32.4	36.4	~Basalt	43.77	14.92	0.7	1.8	5.7	0.1	4.6	0.5	0.7	1.2	51
Mean % difference*					1	-13	1	-5	-13	-10	1	-12	-15	-6	1

Mean % difference is the mean of the five differences in each pair of corresponding OGS and Chemex results (e.g., for SiO_2 in Hole 29 this is calculated as 100(69.69–65.96)/(69.69+65.96)). Negative differences indicate OGS analyses lower than Chemex.

This is not a statistically significant basis for comparison, given the small number of analyses compared, and the fact that samples only partially overlap (samples in Hole 24 do not overlap), which could be responsible for nearly all variation in results. Because OGS and Chemex methods were not proven to produce identical results, attempts were made to note which analyses are used wherever geochemical results are presented, such as in trace element profiles of individual samples.

2.3.2.3 $\delta^{18}O$ Analysis

Several samples were collected from drill core through the study area for analysis of oxygen isotope compositions. Samples were 9-50 cm long, with attention paid to avoid veining and other evidence of alteration, though all contained at least five percent diffuse calcite. For siltstone samples, an attempt was made to sample intervals of identical composition, including overall colour and width of laminae, and to sample intervals of equal proximity to upper contacts with adjacent volcanic rocks.

Samples were crushed and pulverised in an agate ring mill at Lakehead University, with working surfaces cleaned with acetone between samples, and sent to the Queen's University Facility for Isotope Research for determination of whole-rock oxygen isotope compositions. All powders were treated for carbonate by dissolution in 20% HCl, and isotope contents were measured using a Finnigan MAT 252 mass spectrometer, following the method described by Clayton and Mayeda (1963). $\delta^{18}O$ values were calculated by the equation:

$$\delta^{18}O = ([^{18}O / {}^{16}O]_{sample} / [^{18}O / {}^{16}O]_{V\text{-}SMOW} - 1) \times 1000‰$$

where V-SMOW is Vienna Standard Mean Ocean Water.

2.4 Geochemical Modeling

Many aspects of this study required a more accurate and more easily accessible description of the spatial distributions of lithology and geochemistry than was available prior to this study. Leapfrog geological modeling software was used to display raw geochemical and lithological data, the most useful functions including filtering of assay and whole-rock geochemical data (i.e., removing background Zn values), rotation of field of view parallel to strike of relevant surfaces (as in lithological sections displayed in Chapter Four), and display of sections with non-vertical orientations and varying widths. Necessary data included assay results, sampling intervals, drill core logs including lithology and structural measurements, drill hole orientation data (depth, azimuth, and dip at 30 m intervals in each hole), and drill collar locations (easting, northing, and elevation).

Any geochemical or lithological model, hand-drafted or software-generated, is subject to some degree of interpretation or assumption by the author. An attempt was

therefore made to display only raw data (e.g., assay distributions without shell models) wherever practical. However, interpolation or modeling of raw data was necessary in order to reveal and display lithological and geochemical continuities or ratio distributions that were not evident when viewing raw data.

Contours describing the distribution of continuous numerical data, such as assay values or hydrothermal alteration indices, as well as discrete data, such as lithological units, are interpolated in Leapfrog using radial basis functions (Cowan et al., 2004). The recent developments in the practical (reasonably fast) use of radial basis functions to describe point data are reviewed by Beatson et al. (1999) and Carr et al. (2001).

An important constraint defined for Leapfrog modeling of grade or ratio shells in this study is that grade contours follow a general strain ellipsoid, which is somewhat subjectively assumed to have a 4:4:1 ratio, with a strike/dip of 067/55° N. This orientation is based on average schistosity of primary features such as pillows and cumulus crystals, observed at surface and in drill core.

2.5 Qualitative Assessment of Hydrothermal Alteration

In addition to relogging key drill core intervals, drill core was revisited to assess hydrothermal alteration in metavolcanic intervals with corresponding whole-rock data. This was partly in order to better define the relationship between visible hydrothermal alteration and geochemical results. The extent of hydrothermal alteration was graded in drill core using the following scale:

weak = <10% visible hydrothermal minerals by volume, generally diffuse or in sparse veins

moderate = 10-30% by volume, sufficient to change overall colour of rock, either diffuse or in veins

strong = >30% by volume, in dense net-textured veins, in places obscuring primary textures

Chapter 3
Regional Geology

3.1 Superior Province

The Archean craton of the Superior Province consists of nearly two million square kilometres of geologically distinct east-west trending belts ca. 100 km wide, some spanning ~1500 km in length (Fig. 3.1). In general, these belts or subprovinces may be subdivided into four assemblage types: volcano-plutonic subprovinces of metavolcanic and minor metasedimentary rocks metamorphosed to greenschist to amphibolite facies, later intruded by granitoid plutons; metasedimentary subprovinces of mostly turbiditic sandstones and derived migmatites, intruded by felsic plutons; gneissic subprovinces metamorphosed to granulite facies, mostly interpreted as the exposed cores of other belt types; and felsic plutonic subprovinces of mostly mantle-derived granitoid batholiths (Thurston, 1991). In addition to subprovince boundaries, parts of the Superior Province have been divided according to age domains inferred by zircon crystallization ages or isotopic inheritance (Stott et al., 2007) or, based on structural or tectonic relationships, into terranes or composite superterranes (Fig. 3.1).

The ages of rocks forming the Superior Province vary from ca. 3.7 to 2.65 Ga (Skulski et al., 2000; Polat and Kerrich, 1999). Belts forming the southern part of the Superior Province (Wabigoon and Wawa-Abitibi) are volcano-plutonic assemblages of 2.77-2.71 Ga (Stott, 1997). They were accreted northward against a proto-continental margin during the Late Archean in a series of orogenies between 2.72-2.68 Ga, a period collectively named the Kenoran Orogeny (Percival, 2002). These orogenies were estimated by Percival (2002) to be comparable in scale to the Phanerozoic Alpine orogenies, in tectonic settings similar to the modern southwest Pacific Ocean. Though subduction appears to have been an important process at that time (e.g., Calvert et al., 1995), some workers question whether this process was a dominant tectonic process. Concensus, however, is that crustal thickening and magmatism of the Superior Province is mostly attributed to orogeny by subduction-accretion, with later Proterozoic influence from plume magmatism and rifting.

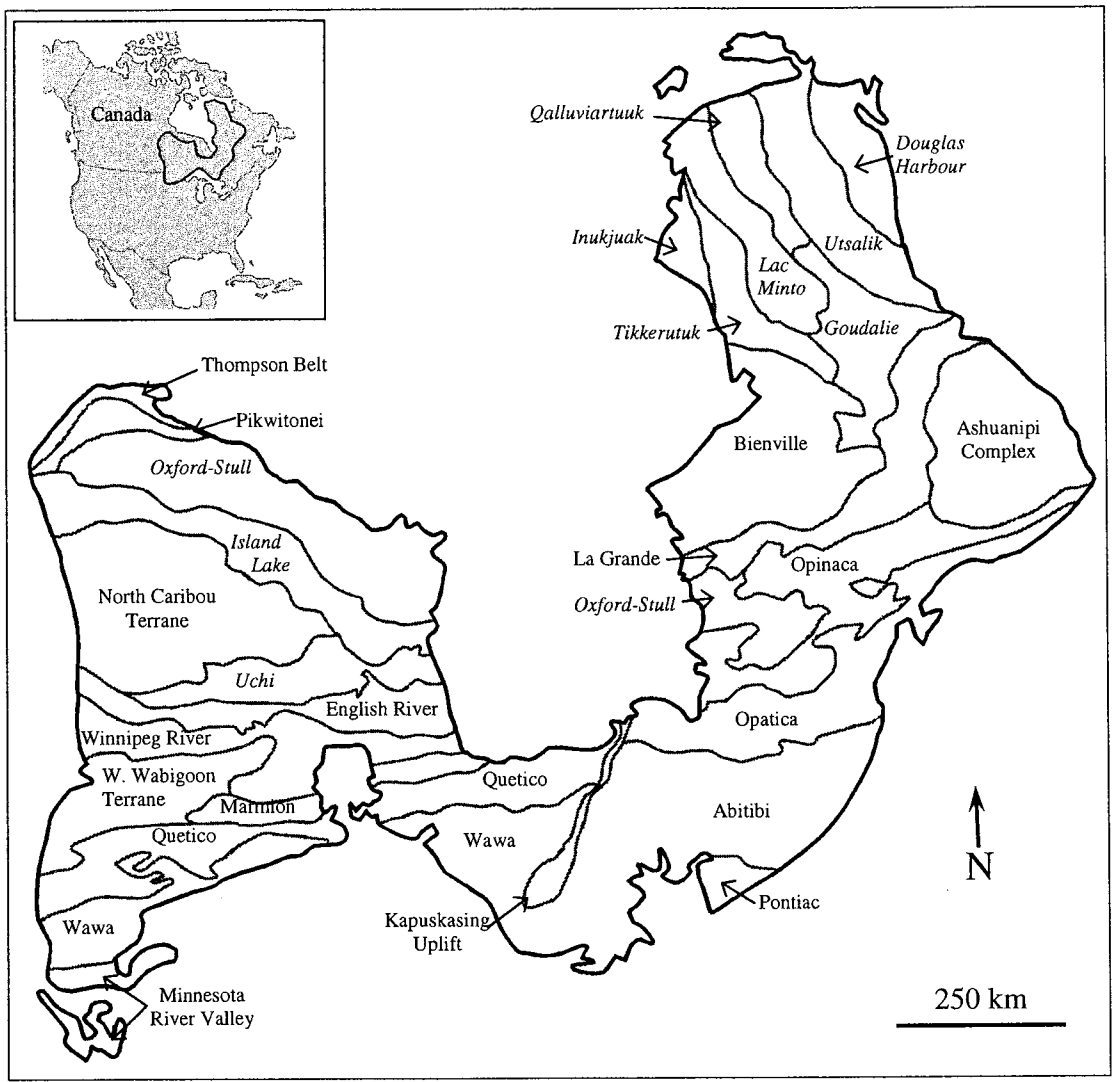

Figure 3.1 – Map of the Superior Province, divided into subprovinces, domains, and terranes. Inset map at top left shows the location of the Superior Province within Canada. Unless indicated as terranes, labels are subprovince names, and domain names are in italics. The Trans-Hudson Orogen and Grenville Province bound the northwest and southeast of the Superior Province, respectively. Compiled from Card and Ciesielski (1986), Stott et al. (2007), and Stevenson et al. (2006).

The tectonic evolution of the Superior Province provides both cause and constraint in the distribution and types of mineral deposits observed throughout the region. Fyon et al. (1992) described the tectonic history of the Superior Province of Ontario in six stages: (1) formation of greenstone belt assemblages; (2) accretion of greenstone assemblages with syn-tectonic calc-alkalic magmatism; (3) erosion of primarily volcanic rocks and filling of sedimentary basins; (4) north-south tectonic

shortening and thickening of crust; (5) local melting of thickened crust; and (6) continued shortening with subprovince-parallel strike-slip faulting. The first stage listed included several mineralising events, as many mineral deposits of the Superior Province are co-genetic with the greenstone belt assemblages, including volcanic massive sulphide, komatiite-hosted Ni-Cu-PGE, iron formation, and orthomagmatic Cu-Ni-PGE in mafic and ultramafic intrusions (Fyon et al., 1992). Most VMS production in the Superior Province appears to have occurred between 2735 and 2698 Ma (Schandl and Gorton, 2002).

3.2 Wawa Subprovince

The Wawa subprovince is a volcano-plutonic belt of 2.88-2.72 Ga rocks (Percival, 2006) accreted to the southern part of the Superior Province during the ca. 2.69 Ga Shebandowanian Orogeny (Fig. 3.1; Kerrich et al., 1999). Extending approximately 1000 km from NE Minnesota to just south of James Bay, it is bounded to the north by the metasedimentary Quetico subprovince and to the southeast by the Kapuskasing Uplift (a.k.a. the Kapuskasing Structural Zone, a gneissic subprovince that accommodated mostly dextral strike-slip shearing; Fig. 3.1). A genetic and temporal relationship between the Wawa and Abitibi subprovinces is generally acknowledged (Williams et al., 1991).

The Wawa subprovince comprises several greenstone belts (Fig. 3.2). These greenstone belts and adjacent siliciclastic metasediments (metawackes and slates) are generally separated by thrust and strike-slip faults (Polat and Kerrich, 2000), and are in turn intruded by syn- to post-kinematic tonalite-trondhjemite-granodiorite (TTG) plutons (Williams et al., 1991; Polat, 1996), as is observed in other volcano-plutonic subprovinces. An important observation at the belt scale is that the TTG plutonism may be derived from dehydration melting of subducting lithosphere, consistent with a genesis by subduction-accretion of island arc complexes (Polat, 1996). Regional metamorphism of the Wawa subprovince ranges from lower greenschist to amphibolite facies, with the latter more common adjacent to batholiths (Polat and Kerrich, 2000).

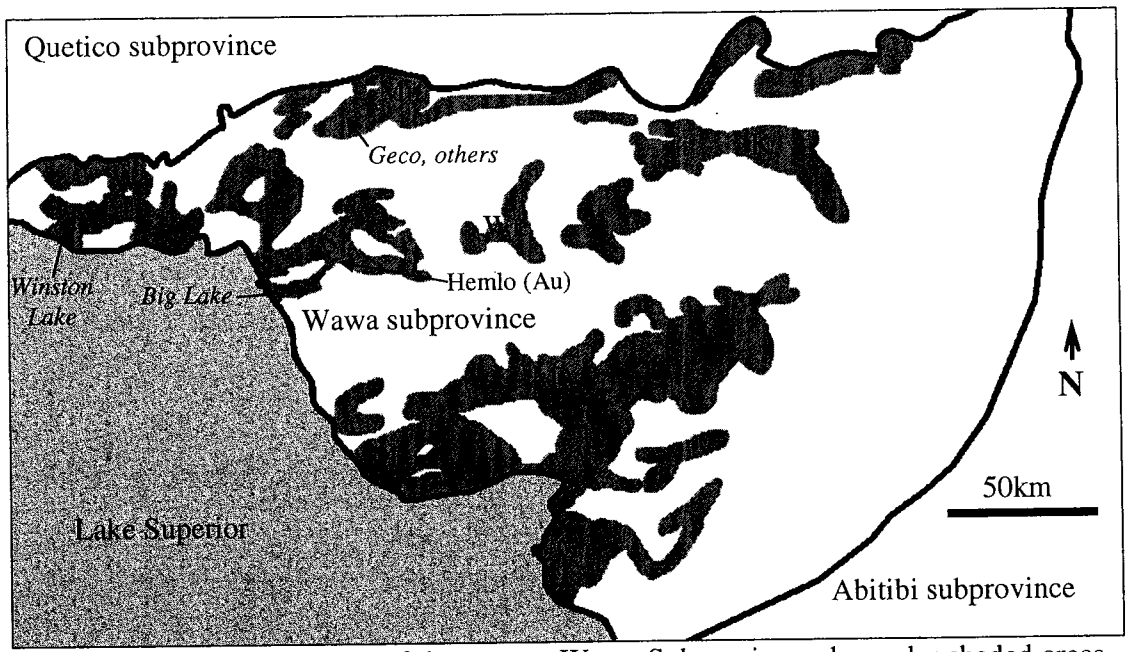

Figure 3.2 - Greenstone belts of the eastern Wawa Subprovince, shown by shaded areas. W-Winston Lake, S-Schreiber-Hemlo, Mn-Manitouwadge, Wr-White River-Dayohessarah, K-Kabinakagami, Mc-Michipicoten, Ms-Mishibishu, G-Gamitagama. VMS occurrences are labeled in italics. Modified after Polat and Kerrich (1999).

Ore deposits of the Wawa subprovince include the Hemlo lode gold and Winston Lake VMS deposits of the Schreiber-Hemlo greenstone belt, and the Geco-Willroy VMS deposits of the Manitouwadge greenstone belt (Fig. 3.2). The Winston Lake VMS deposit contained 4.2 million tonnes of ore at 16.8% Zn, 1% Cu, and 37 g/t Ag (Ministry of Northern Development and Mines, 2006), and is hosted in highly evolved felsic volcanic (± volcaniclastic) rocks and mafic flows. The Manitouwadge deposits (Geco, Willroy, and Big Nama Creek) contained 64 million tonnes of ore grading 2% Cu, 4% Zn, 50 g/t Ag, and 0.3% Pb (Ministry of Northern Development and Mines, 2006). They are hosted in amphibolite-grade felsic metavolcanic rock, near the Quetico subprovince boundary, in an assemblage that Williams et al. (1991) has suggested to be a fore-arc accretionary prism. An igneous crystallization age of 2720 Ma of the Geco host rocks closely matches an age of 2723 Ma for the Winston Lake deposit (Schandl et al., 1991), perhaps implying a shared origin for the two deposits. Both the Winston Lake and Geco deposits are thought to have formed in a back arc rift environment (Eriksson et al., 1994; Polat, 2008). The Big Lake VMS occurrence is located south of these deposits, in the southeast part of the Schreiber-Hemlo greenstone belt (Fig. 3.2).

3.3 Schreiber-Hemlo Greenstone Belt

Williams et al. (1991) divides the Schreiber-Hemlo greenstone belt into three assemblages: the Schreiber assemblage, west of the Coldwell complex; the Hemlo assemblage, north of the Hemlo Fault Zone (a.k.a., the Superior-Hemlo fault zone); and the Heron Bay assemblage, south of the Hemlo Fault Zone (Fig. 3.3). The belt is described by Polat et al. (1998) and Polat and Kerrich (1999) as a subduction-accretion assemblage of oceanic plateau ultramafic to tholeiitic metabasalts, tholeiitic to calc-alkaline arc metabasalts to metadacites, and turbiditic metasandstones interpreted as trench deposits (Polat and Kerrich, 1999).

Unlike comparable Phanerozoic accretionary complexes which consist mostly of island arc-derived siliclastic sediments and volcanic rocks (Shervais, 2006), the Schreiber-Hemlo belt is dominantly made up of plume-derived oceanic plateau volcanic rocks (60-80% by volume; Polat, 2008). The belt was proposed by Polat (2008) to have formed by the start of subduction along an oceanic plateau margin around 2725 Ma. Slab rollback in the resulting oceanic arc environment led to the opening of a back arc rift basin (Polat, 2008). Dextral transpression during subduction-accretion involved orogen-parallel strike-slip faulting, and these faults served as conduits for the upwelling arc-derived tonalite-trondhjemite-granodiorite plutons (Kerrich et al., 1999).

Polat et al. (1998) described three major deformation events in the Schreiber-Hemlo greenstone belt: first, a NNW-SSE compression during subduction-accretion, and accompanying intrusion of subducting slab-derived sills and dykes; second, a NNW-SSE dextral transpression with strike-slip faulting and isoclinal folding at regional scale; and finally, a NW-SE dextral transpression from collision of the Wawa and Quetico subprovinces, with strike-slip faulting and shearing, including the Hemlo Fault Zone. Regional metamorphism is mostly of lower greenschist to lower amphibolite facies (Pan and Fleet, 1993).

Polat and Kerrich (1999) interpret the White River belt (Fig. 3.2) to be part of the same Archean subduction-accretion complex as the Schreiber-Hemlo belt. Alternatively, Reimold and Gibson (2006) suggested that because many komatiites can be interpreted as primitive arc-related as opposed to plume-related volcanic rocks, the Schreiber-Hemlo belt may represent a single arc terrane, rather than an accretionary complex. However, an

accretionary complex including arc- and plume-derived rocks is most widely accepted for the Schreiber-Hemlo belt. The Big Lake VMS occurrence is hosted in metavolcanic rocks of the Heron Bay assemblage, which forms the southeast part of the Schreiber-Hemlo greenstone belt.

3.4 Heron Bay Assemblage

The Heron Bay assemblage of the Schreiber-Hemlo greenstone belt is located south of the Hemlo Fault Zone and east of the Coldwell alkalic complex (Fig. 3.3). Consisting of Archean metasedimentary rocks, ultramafic-mafic (komatiitic basalt) to intermediate metavolcanic rocks, and granitoid plutons, the Heron Bay assemblage includes the Pukaskwa Batholith (ca. 2719 Ma; Muir, 2003) and the Heron Bay Pluton (ca. 2686 Ma; Muir, 2003) to the south and north of the study area, respectively (Fig. 3.3). In general, lithologies of the Heron Bay area are representative of the Schreiber-Hemlo greenstone belt, comprising mostly tholeiitic metabasalts, smaller volumes of metasedimentary rock, and plutons with variable chemistries, except for a) a greater percentage of metasedimentary rock in the far eastern parts of the belt, and b) higher grades of metamorphism and structural complexity observed to the north and northeast of the Heron Bay area (Muir, 2003).

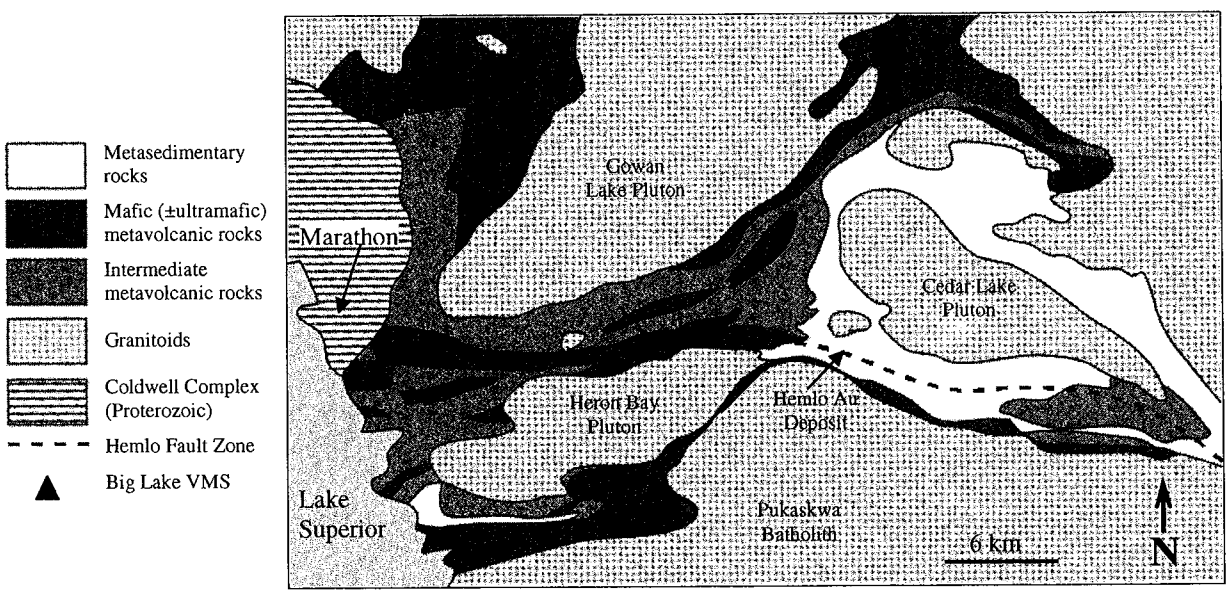

Figure 3.3 - Map showing the Heron Bay assemblage, including the location of the study area. The Heron Bay assemblage is south of the Hemlo Fault Zone in the Schreiber-Hemlo greenstone belt. Modified after Polat et al. (1998).

The mafic to ultramafic metavolcanic rocks located between the Pukaskwa and Heron Bay plutons, the southern part of the Heron Bay area, are part of the tholeiitic Pulpwood-Playter Harbours sequence which hosts the Big Lake VMS occurrence (Fig. 3.3).

3.5 Pulpwood-Playter Harbours Sequence

Named because of extensive outcrops in the Pulpwood and Playter Harbours of Lake Superior, this sequence has an apparent north-south thickness of approximately five km (Muir, 1982). The rocks are massive to pillowed flows and associated subvolcanic gabbros/coarser flow centres, with tholeiitic major element chemistry (Table 3.1). They are regionally metamorphosed to greenschist to lower amphibolite facies, in places featuring randomly oriented amphibole needles <15 mm long (Muir, 1982). According to surface mapping by Muir (1982) and more recently by consulting geologist C. Blackburn (2005-2007) and by the author (2006-2008), top direction is ambiguous in the pillowed flows, ranging from north to south.

Table 3.1 – Major element oxide data (in wt. %) of mafic metavolcanic rocks of the Pulpwood-Playter Harbours Sequence, from Muir (1982).

Sample ID	M36-78	M41-78	M48-78	M112-78	M140A-78	L51-78
SiO_2	53.9	50.0	50.2	49.5	52.9	49.1
TiO_2	1.82	1.61	0.98	1.67	1.29	1.12
Al_2O_3	14.4	14.0	14.4	13.0	14.3	15.2
Fe_2O_3	14.2	16.1	12.5	17.9	15.0	14.4
MnO	0.28	0.31	0.24	0.25	0.27	0.25
MgO	3.80	4.57	5.75	4.67	3.90	6.49
CaO	7.61	9.31	11.20	8.97	8.18	9.02
Na_2O	2.86	2.39	2.71	2.01	3.06	2.67
K_2O	0.18	0.45	0.49	0.19	0.53	0.78
P_2O_5	0.12	0.09	0.09	0.12	0.08	0.09
LOI	0.40	0.80	1.20	1.10	0.50	1.00
Total	99.60	99.80	99.60	99.30	99.80	99.40

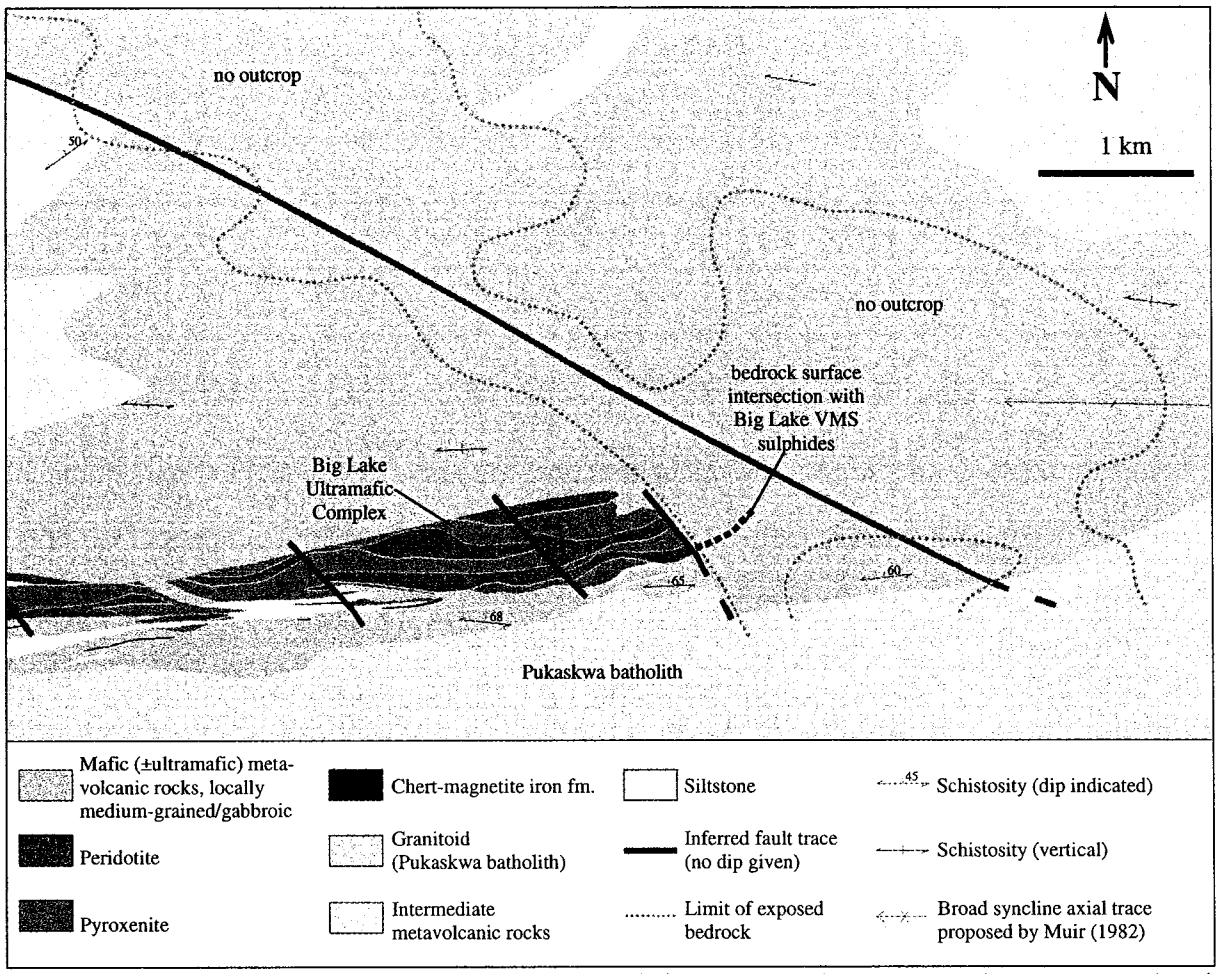

Figure 3.4 - Geological map of the eastern part of the Pulpwood-Playter Harbours metavolcanic sequence, including location of the Big Lake VMS occurrence. Compiled from Blackburn (2008) and Muir (1982).

Small volumes of metasiltstone, metawacke, graphitic metapelite, mafic metasedimentary rock (likely derived from adjacent flows), and a very small volume of oxide-facies iron formation containing chert, magnetite, and amphiboles are generally interbedded with the Pulpwood-Playter Harbours metavolcanic rocks (Fig. 3.4). Small and sparse outcrops of these metasedimentary rocks have made it difficult to map them as continuous stratigraphic units through the Pulpwood-Playter Harbours sequence (Blackburn and MacTavish, 2005). Discordant lensoid ultramafic intrusive bodies were also mapped by Muir (1982) throughout the Pulpwood-Playter Harbours sequence, including parts of what have now been identified as a continuous east-striking series of sill-like bodies named the Big Lake Ultramafic Complex (Fig. 3.4).

A felsic lapilli tuff has been logged in one drill hole approximately 4.5 km northwest of the Big Lake VMS occurrence, in contact with ultramafic intrusive rock. Aside from feldspar porphyry dykes and surrounding batholiths, felsic units have not been observed at surface or in core within approximately four kilometres of the VMS occurrence. However, Blackburn and MacTavish (2005) have suggested that the siltstones may have been derived from felsic volcanic rocks.

3.6 Big Lake Ultramafic Complex

The Big Lake Ultramafic Complex (BLUC) is a prominent, roughly 30 km long east striking sill-like body comprising laterally continuous sequences of cumulate peridotite, pyroxenite, and minor gabbro. Approximately 300 m thick, it is bounded by metavolcanic rocks of the Pulpwood-Playter Harbours sequence, with contacts dipping 5-55° to the north in the area of study. Despite the extent of drill and map exposure it is unclear whether the BLUC is a discrete intrusion, with igneous contacts both north and south of the complex, or the cumulate base and centre to a series of thick mafic-ultramafic flows. These questions will be addressed in later chapters.

Geochronological studies have not been performed on the Big Lake Ultramafic Complex. It is one of three large mafic-ultramafic bodies identified on the Big Lake property (Fig. 3.4), of which the Gus Creek intrusion has been dated to 2669.3 ± 1.8 Ma (Scoates, pers. comm., 2005). A lack of understanding of the relationship between the Gus Creek intrusion and Big Lake cumulates precludes applying the same age to the BLUC.

The Big Lake VMS occurrence immediately underlies (i.e., forms the structural footwall to) the eastern margin of the BLUC. Relationships between the complex and the VMS mineralisation, including possible issues of assimilation, displacement, and contact metamorphism, are addressed in later chapters. No outcrops of the VMS mineralisation have been found, but its location below overburden is noted in Figure 3.4.

3.7 Midcontinent Rift System

The Mesoproterozoic Midcontinent Rift System consists largely of plateau basalts with a thickness of up to 30 km beneath Lake Superior (Cannon et al., 1989), with

associated clastic sediments, in the Lake Superior region. Proterozoic units near the Big Lake property that are associated with the Midcontinent Rift include the Coldwell Alkalic Complex to the northwest, as well as a small number of diabase dykes, most less than a few metres wide, throughout the Pulpwood-Playter Harbours sequence at Big Lake. These dykes are easily identified because they cross-cut all rocks at Big Lake, and are effectively unmetamorphosed and massive, with a sub-ophitic texture defined by plagioclase and intersertal pyroxene. A few Proterozoic lamprophyre dykes, some containing ultramafic xenoliths and garnet phenocrysts, are also seen in the area of study.

3.8 Structure

Property-scale structures identified by air photo interpretation, surface mapping, airborne geophysical surveys, and the correlation of one felsic-fragmental mafic volcanic unit (Muir, 1982) include: a large synform opening westward with a near-vertical east-west striking axial plane (the study area is located on the southern limb of this possible fold; Fig. 3.4); and a northwest trending fault system (Fig. 3.4), with the fault traces largely inferred by aeromagnetic anomalies and offset of map units. Six fault gouge intervals 0.3-1.0 m wide were intersected in core through the study area, and many pre-existing faults may have been intruded by diabase dykes.

Schistosity is strongly developed in most of the metavolcanic and metasedimentary rocks of the Big Lake property, but poorly developed in the centre of the Big Lake Ultramafic Complex. In the area of study, the planar fabric strikes approximately east with a steep northward dip (ca. 65° at surface), shallowing to some extent with depth and to the north. At the property scale, this variable schistosity defines a series of east trending shear structures that can also be inferred by the topography, consisting of a series of steep-sided swamp-filled lineaments (Blackburn and MacTavish, 2005). Two such shear structures may define the northern and southern contacts of the BLUC in Figure 3.4, the southern shear structure also partly running through the zone of Big Lake VMS mineralisation. The shear zones are approximately 5-20 m wide, with gradational contacts. Mylonitic fabric has been documented in a few intervals of siltstone units within the lower shear zone (Appendix B). These shear structures may have several implications that are discussed where relevant.

Chapter 4

Petrography and Lithostratigraphy

4.1 Introduction

This chapter is a review of the host lithostratigraphy to the Big Lake VMS occurrence, with some discussion of structure and classification. Further classification of rock types and tectonic setting is accomplished using geochemical data in Chapter Five. Core logs and petrographic descriptions are referred to throughout the chapter, and are provided in the Appendices.

VMS host sequences include rock formed before and immediately after VMS sulphides, usually within less than 2 m.y. (Franklin et al., 2005). Though all VMS deposits are formed in submarine volcanic settings, there is no general stratigraphic sequence to represent all VMS host sequences, as even the dominant lithology, either volcanic flow, sedimentary, or volcaniclastic rock, varies between deposits. To this end, Franklin et al. (2005) developed a five-fold classification scheme for VMS deposits based on host lithostratigraphy and tectonic setting. Table 4.1 summarises these five lithotectonic types, and serves to illustrate the variety of stratigraphic assemblages or settings known to host VMS deposits.

Table 4.1 - Lithotectonic classification of VMS deposits (summarised from Franklin et al., 2005).

Type	Summary of typical host lithology and *tectonic setting*
Bimodal-mafic	Mostly pillowed to massive basalt flows, <25% felsic volcanic/volcaniclastic rocks, may include terrigenous clastic sediments. *Oceanic arc rift (rifted arcs above ocean-ocean subduction zones).*
Mafic	Mostly pillowed to massive basalt flows, mafic dykes, minor felsic flows, domes, or intrusions, may include ultramafic flows or intrusions, and pelitic sediments. *Ophiolite assemblages (~obducted oceanic arc, oceanic back arc, or ocean island seamounts).*
Pelitic-mafic	Mostly basalt and pelitic sediments (~equal amounts), <25% mafic sills, felsic volcanic rocks absent or <5%, may include siltstone, and mafic-ultramafic flows or sills. *Oceanic back arc rifts, mid-ocean ridges w/ sediment input, or transform basins.*
Bimodal-felsic	~30-70% felsic volcanic rocks, ~20-50% basalt or basaltic andesite, and ~10% terrigenous clastic sediments, may include subaerial components. *Continent margin arcs and back arcs (back arc rifts above ocean-continent subduction zones), or continent rifts.*
Siliciclastic	Mostly clastic sediments, ~20% felsic volcanic/volcaniclastic and intrusive rocks, hangingwall may include ~10% mafic volcanic rocks and chemical sediments. *Continental back arc rifts (back arc rifts above ocean-continent subduction zones).*

4.2 Lithostratigraphy

As described in Chapter Three, lithologies hosting the Big Lake VMS occurrence are broadly divided into ultramafic cumulates, mafic-ultramafic metavolcanic rocks, and metasedimentary rocks. VMS mineralisation occurs as a mostly conformable, in places anastomosing, sheet nearly parallel to and 5-50 m below the base of the cumulate Big Lake Ultramafic Complex (BLUC), with a northward dip of about 60° near surface, shallowing northward to approximately horizontal (Fig. 4.1). This synformal surface of mineralisation generally coincides with the transition from BLUC cumulates (peridotite and pyroxenite) and strongly foliated metavolcanic rocks to an underlying sequence of metavolcanic rocks and interflow metawacke and metasiltstone.

The lithostratigraphy shown in Figure 4.1 differs from previous interpretations by MetalCORP workers in that the clastic metasedimentary rocks below the VMS mineralisation occur in at least two packages not previously recognised, spaced at ~60 m intervals, that are broadly parallel to peridotite-pyroxenite contacts. These bedding packages, along with individual bedding planes, BLUC contacts, and PGE reefs, probably define the paleohorizontal. From the few drill core intervals interpreted to be unintruded/unfaulted flow sequences (e.g., hole 92, interval 333.3-340.2 m in Appendix A), individual flows outside of the BLUC are at least a few metres in thickness after tectonic shortening. These metavolcanic rocks are divided in Figure 4.1 according to stratigraphic relationship to VMS mineralisation: Group I above, and Group II below VMS mineralisation (Groups I and II are labeled with bracketed numerals in the legend of Fig 4.1). Though they are indistinguishable in terms of mineralogy and texture, key differences in chemistry and suggested relationships to the BLUC cumulates will be described in Chapter Five.

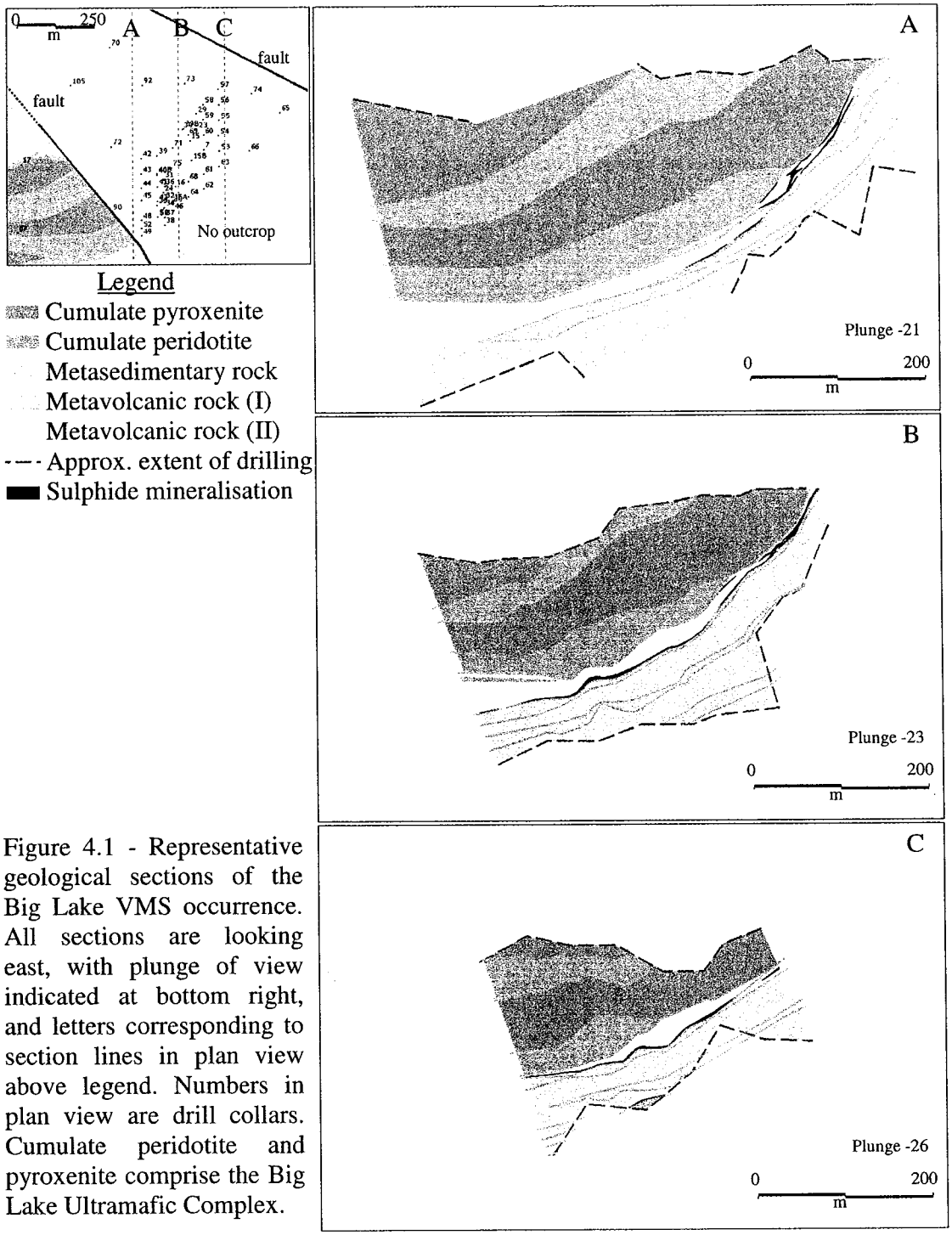

Figure 4.1 - Representative geological sections of the Big Lake VMS occurrence. All sections are looking east, with plunge of view indicated at bottom right, and letters corresponding to section lines in plan view above legend. Numbers in plan view are drill collars. Cumulate peridotite and pyroxenite comprise the Big Lake Ultramafic Complex.

4.3 Petrography

Textural and mineral characteristics of the lithologies presented in Figure 4.1 are summarised in the following sections, and detailed petrographic descriptions are provided in Appendix B. The IUGS classification of igneous rocks is used for the ultramafic cumulates, with names intended to describe protolith compositions. Where omitted, the prefix "meta" can be assumed for all rocks discussed. Crystal size classifications used are: fine-grained <1 mm, medium-grained 1-3 mm, and coarse-grained 3-10 mm.

4.3.1 Ultramafic Cumulates

These rocks comprise the Big Lake Ultramafic Complex, as defined in Chapter Three, forming laterally continuous east-striking layers approximately 20-120 m thick. All samples display at least a weak planar fabric, most commonly from the orientation of metamorphic tremolite-actinolite.

4.3.1.1 Pyroxenite to Feldspathic Pyroxenite

In most pyroxenites sampled, secondary minerals make up at least 75% of the rock; they comprise dark green hornblende or actinolite amphibolites after medium-grained pyroxenite cumulates (Fig. 4.2a,b), with other secondary minerals including magnetite and serpentine. A relict cumulate texture is preserved by amphibole rhombs and needles 0.1-1 mm long in anhedral subequant hexagonal or, in places, rectangular aggregates 1-5mm long that are nearly optically continuous or display wavy extinction where laths are bent, some containing original pyroxene as anhedral fragmented relict cores <0.4 mm across (Fig. 4.2b).

In approximately 95% of pyroxenites, anhedral, subequant plagioclase crystals <0.05 mm long are present at less than 10 modal percent, all in the interstices. Five percent of the BLUC pyroxenites can be described as feldspathic pyroxenites or melagabbros, with 10-30% plagioclase, in places forming diffuse white patches or glomerocrysts several centimetres long. Less than 10% of pyroxenites are magnetic, some with visible magnetite porphyroblasts <1 mm across.

Towards the centre of the BLUC, some pyroxenites contain less than 20% secondary minerals, allowing for more detailed identification of the protolith. Here,

clino- and orthopyroxenes can be distinguished (e.g., Fig. 4.2c), and the samples are medium-grained cumulate-textured websterites, with approximately 3:1 clino- to orthopyroxenes. Pyroxenes are closely packed subhedral to euhedral squares or octagons 0.3-3 mm across, or, in some samples, rectangular laths <4 mm long. Due to anomalously low birefringence (1st order grey to yellow), most clinopyroxenes are distinguished solely by extinction angle, mostly 10-28°.

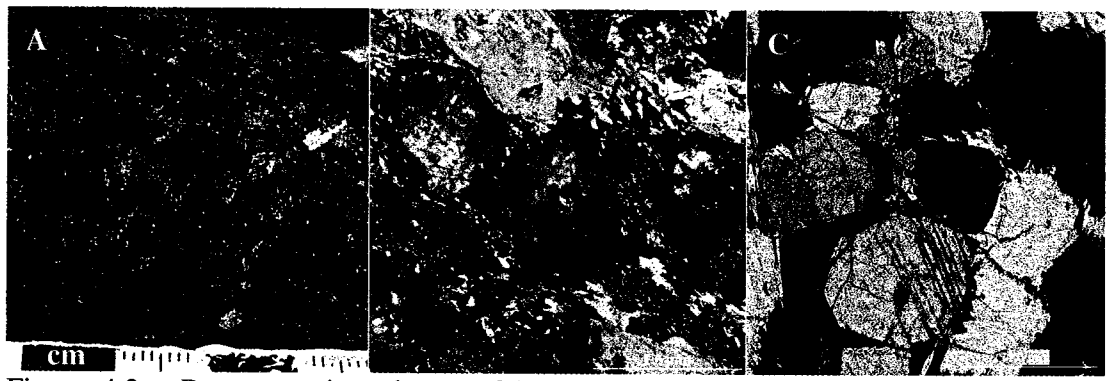

Figure 4.2 - Representative photos of BLUC pyroxenites. A) Core photo showing medium-grained cumulate texture (Hole 17). B) Amphibolite after pyroxenite (sample M-10), preserving relict cumulate texture (PPL). C) Websterite (M-B), with low-birefringence clinopyroxenes (XPL).

4.3.1.2 Peridotite

In hand sample, BLUC peridotites are strongly magnetic and blue-tinged (Fig. 4.3a). All peridotites sampled and logged contain at least 75% serpentine and talc, mostly diffuse and in places as sub-millimetre wide veinlets. The samples consist of densely-packed relict cumulus olivine crystals 0.2-3 mm across, most <1.5 mm across, with cumulate textures preserved by magnetite along rounded crystal boundaries and fractures (Figs. 4.3b,c). Rounded magnetite inclusions <0.5 mm in diameter are observed in most relict olivine grains. In about 10% of drill core, olivine cumulate crystals are either absent or too small to identify in hand sample, and the rock is effectively a serpentinite with a presumed peridotite protolith. Pyroxene is exclusively interstitial to olivine (olivine orthocumulate) and completely encloses only the smallest olivines. Approximately 30% of the interstitial pyroxene is serpentinised, and about half of the remainder retains mid-2nd order birefringence.

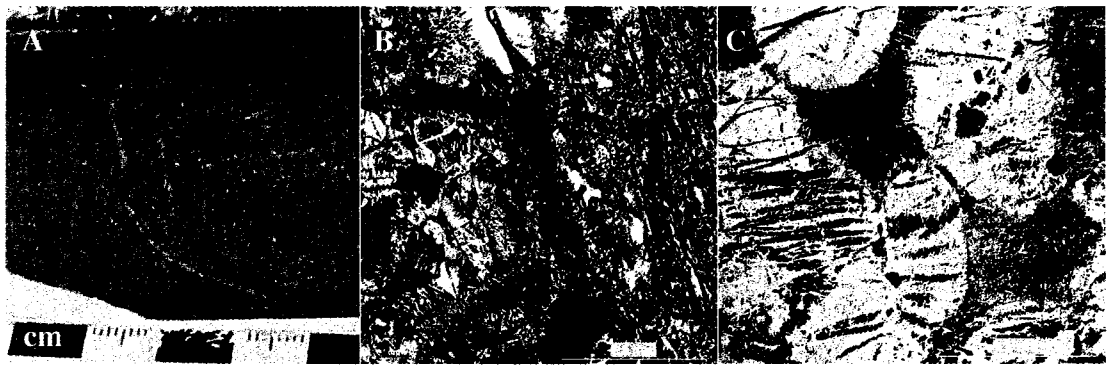

Figure 4.3 - Representative photos of BLUC peridotites. A) Core photo showing blue-grey colour. This sample has a fine-grained cumulate texture, not visible in the photo (Hole 17). B) Serpentinised peridotite (sample M-87) with magnetite-dusted interstitial pyroxene and a few relict cores of olivine (XPL). C) Serpentinised peridotite (M-87), with magnetite preserving relict cumulate olivine texture (PPL).

4.3.2 Mafic-Ultramafic Metavolcanic Rocks

Least-altered samples of metavolcanic rocks at Big Lake are chlorite-actinolite ± serpentine schists (Fig. 4.4d) with up to 15% biotite. Ignoring variable amounts of hydrothermal vein alteration and/or quartz-calcite veining, mineralogy varies little between samples. Most of these rocks lack preserved primary texture, but where observed these textures include cumulus pyroxene crystals 0.5-2 mm across (replaced by actinolite or chlorite; Fig. 4.4c), sparsely distributed plagioclase phenocrysts in a few massive flows, and possible pillow selvages marked either by calcite or darker green chlorite (Fig. 4.4a,b). Outcrops of amygdaloidal basalt have been identified a few kilometres west of the study area, but these features were not observed in core. Neither spinifex nor pepperite textures have been documented in any of these rocks.

These rocks contain a strong planar fabric defined mostly by the orientation of micas and actinolite. Schistosity is most pronounced along the southern contact with the Big Lake Ultramafic Complex, defining a shear zone with gradational contacts over tens of metres.

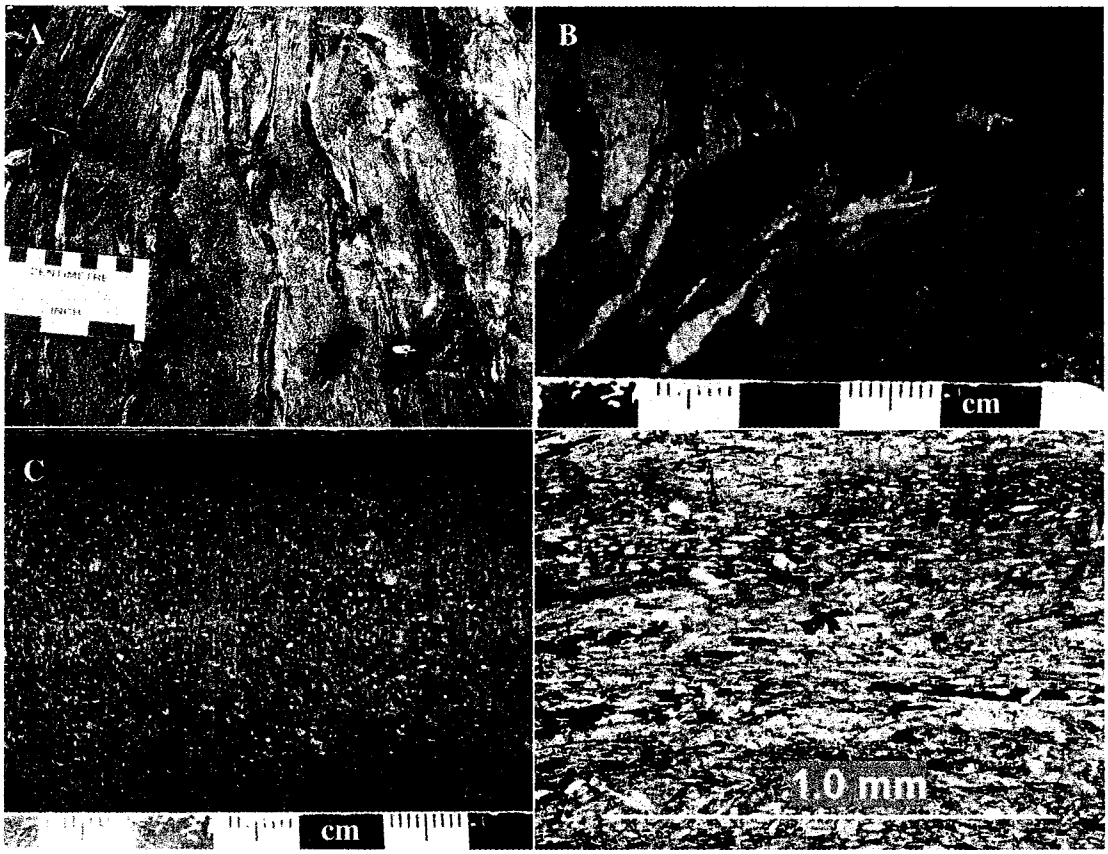

Figure 4.4 - Representative photos of mafic-ultramafic metavolcanic rocks of the Big Lake VMS host sequence. A) Outcrop of deformed pillows with dark green selvages, about 600 m west of the study area (photo by C. Blackburn). B) Possible pillow selvages in drill core (Hole 73; 238-282 m). C) Fine-grained cumulate centre of a metavolcanic flow (Hole 105; 487-493 m). D) Strongly foliated chlorite-actinolite ± biotite schist (M-N) similar to rock in photo B (XPL).

4.3.3 Metasedimentary Rocks

4.3.3.1 Clastic Metasedimentary Rocks

Most of the metasedimentary rocks at Big Lake are light grey, recrystallised metasiltstones (Fig. 4.5a) to darker grey-brown metawackes, mostly consisting of mm-scale laminae, defined by variable mica contents, with no clear indication of graded bedding. Up to 10% rounded white plagioclase clasts 1-4 mm across are distributed along some bedding planes. Less than 10% thin garnetiferous metapelite beds and laminae have also been noted within the siltstone-wacke units.

A few dark green, clearly bedded and fine-grained rocks of mafic composition have been encountered in drill core, some interbedded with metasiltstones and metapelites. These are interpreted to be reworked volcanic material, possibly derived from nearby mafic-ultramafic flows.

4.3.3.2 Chemical Metasedimentary Rocks

In drill core, four intervals less than a metre thick of banded chert-magnetite iron formation have been noted (Fig. 4.5b), but cannot be reliably traced over more than a few tens of metres in drill section. Despite their scarcity, resistance to erosion has resulted in a number of outcrops of this unit being mapped (Fig. 4.5c).

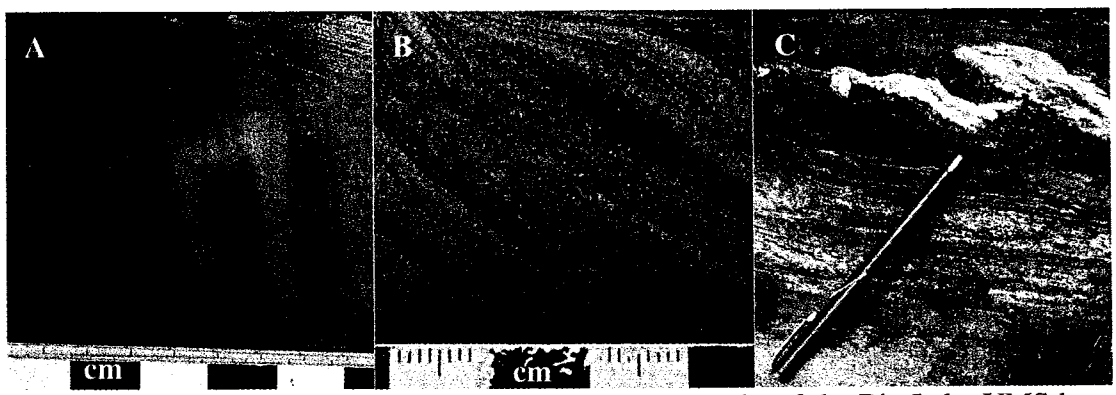

Figure 4.5 - Representative photos of metasedimentary rocks of the Big Lake VMS host sequence. A) Finely laminated non-magnetic siltstone (wetted core) typical of siltstone seen in core (Hole 23). B) Strongly magnetic iron formation with ~20% magnetite laminae (Hole 74; 239.8-240.1 m). C) Outcrop of chert-magnetite iron formation ~1.2 km west of the study area (Photo by C. Blackburn).

4.4 Discussion

Apart from the VMS-related mineral assemblages at Big Lake, the petrographic characteristics of the ultramafic cumulates, mafic-ultramafic metavolcanic rocks, and metasedimentary rocks of the Big Lake VMS occurrence are similar to other parts of the Pulpwood-Playter Harbours sequence, as described by Muir (1982) and reviewed in Chapter Three. The garnet-biotite assemblage in thin metapelite units at Big Lake indicates a minimum metamorphic facies of upper greenschist (garnet zone), consistent with regional upper greenschist-lower amphibolite metamorphic facies estimated by other workers through the Playter Harbours sequence (Polat et al., 1998). Furthermore, there is

no appreciable change in metamorphic grade with distance from the southern BLUC contact.

The petrographic characteristics of hydrothermal alteration and VMS sulphides at Big Lake are reviewed in Chapters Six and Seven, respectively. The remainder of this discussion focuses on the host lithostratigraphy to the Big Lake VMS occurrence, and is divided into sections on younging direction, VMS host sequence classifications, and the relationships between BLUC and adjacent metavolcanic rocks.

4.4.1 Arguments for an Overturned Sequence

It was noted in Chapter Three that younging direction in the Pulpwood-Playter Harbours sequence is ambiguous. While a full review of regional structure through the Pulpwood-Playter Harbours sequence is not possible here, local younging direction can be established in the several hundred metres of VMS host rock intersected by drill core. Because younging direction is relevant to aspects of the lithostratigraphy and structure discussed later, these arguments are presented first.

4.4.1.1 Way-up Indicators in Peridotites

Strictly speaking, whether or not to include the cumulates of the Big Lake Ultramafic Complex as part of the Big Lake VMS lithostratigraphic assemblage depends on whether they were formed prior to VMS formation, and/or whether they share a genetic relationship with the volcanic rocks hosting the VMS occurrence. However, even assuming that the BLUC significantly post-dates VMS mineralisation, the concordant or near-concordant contacts with surrounding rock, an originally horizontal emplacement of the BLUC, and an inferred age of at least 2.68 Ga (Rinne, 2006) make it very unlikely that way up in the BLUC is opposite that in the immediately underlying VMS-mineralised volcanosedimentary sequence. There is no field evidence for isoclinal folding in the area of study.

There are several lines of evidence to support an argument that the BLUC is overturned, with younging downward and to the south:

(a) PGE reef-style mineralisation at tops of peridotites

The term "reef-style" is justified as it describes stratiform and laterally continuous concentrations of PGE in mafic-ultramafic bodies, whether intrusive or flow-hosted (e.g., komatiite-hosted reef-style PGE; Fiorentini et al., 2006). At least two such reefs have been identified in the BLUC, each approximately 1.5-2.0 m thick with 0.8-2.0 ppm combined Pt+Pd, and always in peridotites within a few metres of their upper contacts with pyroxenite (Fig. 4.6b; Rinne, 2006).

A comprehensive review of PGE mineralising processes in layered intrusions is beyond the scope of this study, but some points are relevant to the argument for an overturned sequence. In general, a significant concentration of PGE in igneous systems requires sulphide segregation from a primitive/PGE-rich, initially sulphide-undersaturated magma. Sulphide saturation may be reached (1) by continued crystallization of a magma, (2) by assimilation of country rock to increase silica content, decrease temperature, or provide external sulphur (Mungall and Naldrett, 2008), or (3) by an increase in magma pressure (Cawthorn, 2005). The first sulphide droplets to segregate and settle will contain the highest concentrations of PGE, and in less turbulent systems should be expected to settle to the bottom of the PGE source magma chamber to form a laterally extensive layer (Mungall and Naldrett, 2008). The observation that PGE generally concentrate (if at all) in the lower portions of source magmas holds true in layered intrusions such as the Stillwater and Bushveld (Macdonald, 1987) just as it does in more turbulent systems such as komatiitic flows (e.g., Lesher et al., 1984).

Though PGE reefs do not always coincide with the lower contacts of rock units in layered intrusions, Rinne (2006) noted that regardless of the mechanism(s) responsible for sulphide saturation, the highest accumulation of PGE should not occur along the top of cumulate source chambers. The Pt+Pd (ppm) distributions through BLUC peridotites, shown in Figure 4.6b with highest grades near the upper peridotite contacts, are therefore best explained by an overturned system.

(b) Pyroxenite xenoliths at top of peridotite

At Big Lake, fine-grained pyroxenites hosted within peridotite of a PGE reef outcrop were interpreted by Rinne (2006) to be rip-up xenoliths analogous to those in the Eagle intrusions in Michigan (Rossell and Coombes, 2005). Their location within 30 m of an upper peridotite contact into overlying pyroxenite, and not elsewhere, is consistent with an energetic pulse of hotter, dominantly olivine-crystallising magma along the top of an older pyroxene-cumulate layer, supporting the argument that the sequence has been overturned.

(c) Compatible element contents of peridotites

Fractionation during settling of an olivine-cumulate magma is expected to cause a decrease in olivine-compatible elements such as Mg, and increase in Al and SiO_2 (among many other species), towards the top of the chamber or flow. Mg, Ni, Co, and Cr are most compatible in olivine (Foley and Jenner, 2003) and are likely to be most concentrated in the first olivine to crystallise from a magma, while Al, Si, and Ca contents reflect the presence of pyroxene or feldspar, increasing gradually as the trapped liquid fraction is further depleted in olivine-compatible elements. Although the peridotites of the BLUC display little compositional variation in hand sample, assay results reveal fractionation trends that are consistent with a way up direction pointing downward and to the south (Fig. 4.6c-f).

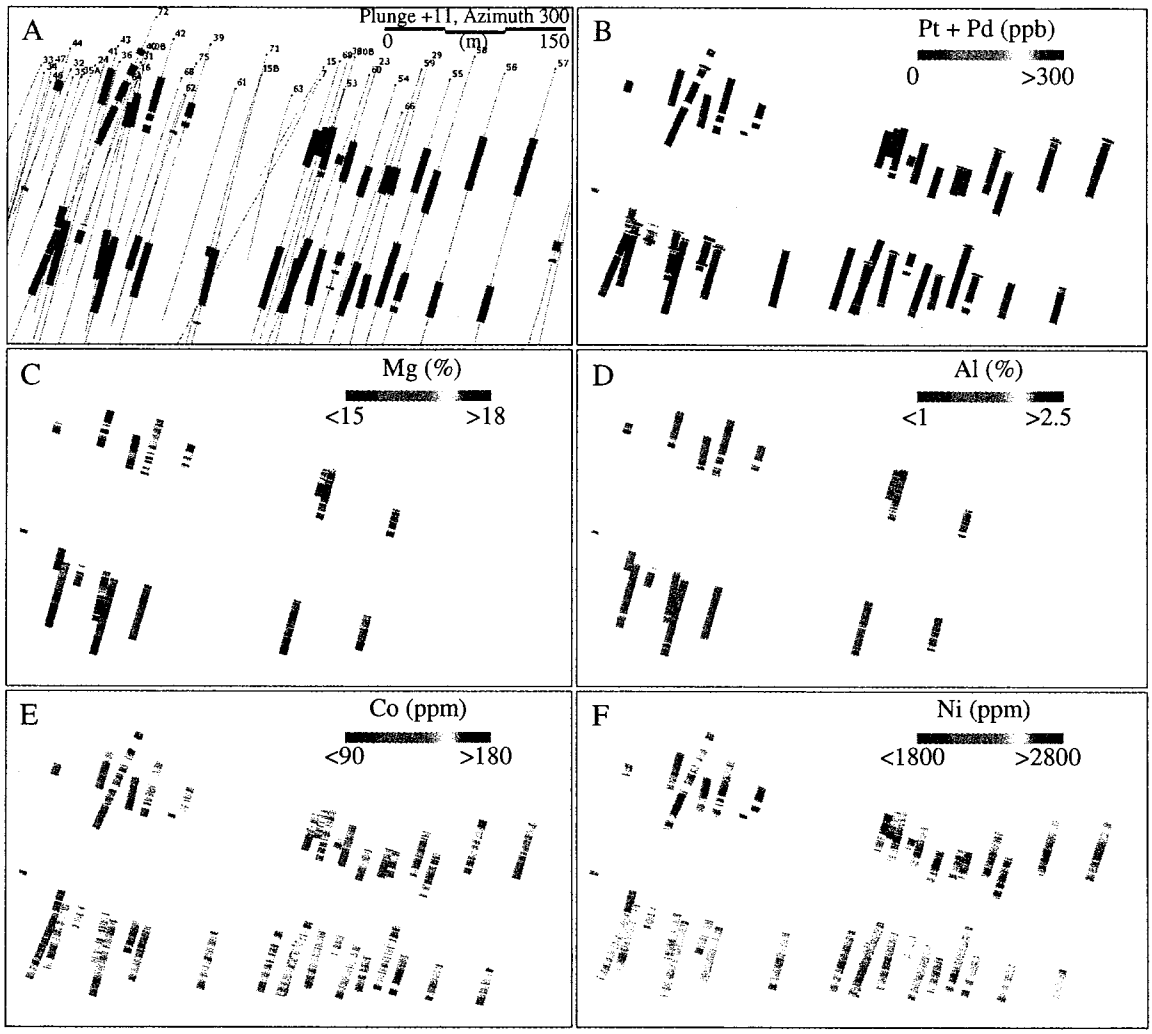

Figure 4.6 - Chemical variations through cumulate peridotites of the Big Lake Ultramafic Complex. A) Spatial distribution of all peridotite intervals in drill core, with scale, drill core traces, and orientation of view (generally NW) indicated. B) Pt+Pd totals, highest totals defining thin reefs near upper contacts with pyroxenite. C) Mg decreases downhole in both peridotite units, and is generally highest in upper unit. D) Al increases downhole, presumably reflecting higher pyroxene or feldspar contents. E) Co decreases downhole in both peridotite units. F) Ni distributions are ambiguous, generally highest at centre of each peridotite unit, and overall contents are higher in the upper peridotite unit.

4.4.1.2 Asymmetry of Hydrothermal Alteration and Mineralisation

Metal and alteration distributions are described in detail in Chapters Six and Seven, but here it is simply noted that in most drill holes the mineralised intervals are adjacent to the uppermost siltstone beds (as in Fig. 4.1), with metal grades decreasing upwards over a few metres into overlying metavolcanic rock. This may imply that,

during VMS activity at Big Lake, most mineralisation and strong hydrothermal alteration occurred immediately adjacent to the structural tops of siltstone layers or beds. If siltstone layers were less permeable to hydrothermal fluids (perhaps as in the case of the impermeable sills of the Rosebery deposits; Large et al., 2001), this may indicate that the sustained hydrothermal fluid flow at Big Lake had a downhole vector component. Since mineralising fluids migrate upwards in a VMS system, this provides some support for an overturned sequence.

4.4.1.3 Downward Fining Flow Sequences

Most of the metavolcanic rock hosting VMS mineralisation at Big Lake is very fine-grained, without obvious primary volcanic features (as described in core logs; Appendix A). However, a few metavolcanic intervals logged in this study represent uninterrupted flows (i.e., without dykes or veining obscuring possible flow contacts). In these flows (Fig. 4.7), relict cumulate pyroxene crystals 0.5-3 mm across are present either at the tops or towards the centres of units, not at the bottoms. These downward fining flows are consistent with an overturned sequence.

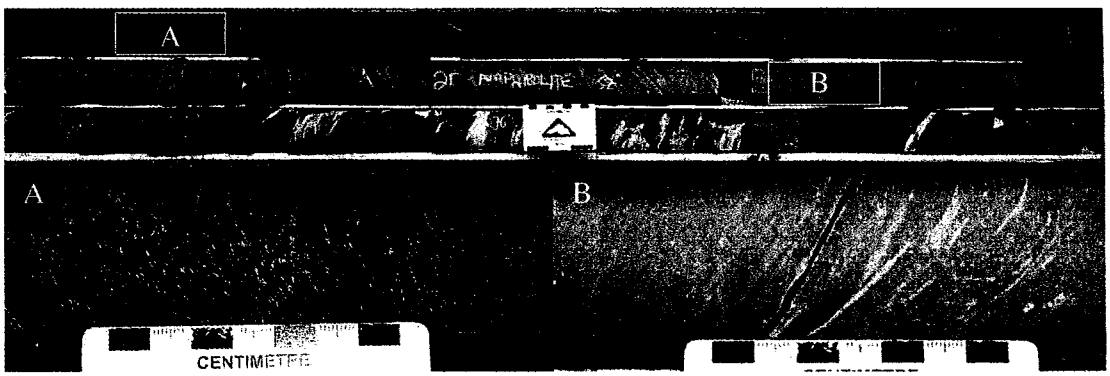

Figure 4.7 - Core photos of an interpreted metavolcanic flow, gradually fining downhole from a uralitised pyroxene-cumulate base (top left, photo A) to an aphanitic flow top (bottom right, represented by photo B). Note inferred down-hole younging direction. Upper and lower contacts of this unit (not shown) are sharp. Log of this interval (hole 92, 333.3-340.2 m) is provided in Appendix A.

Assuming an overturned sequence, metavolcanic rocks of Group II in Figure 4.1 are stratigraphically above VMS mineralisation intersected to date at Big Lake, and are henceforth termed hangingwall metavolcanic rocks.

4.4.2 Origin of BLUC Cumulates

In Chapter Three, it was noted that there is some question concerning whether the BLUC is better described as a thick flow or as a discrete intrusion with upper and lower intrusive contacts. The argument is relevant to the genesis of the Big Lake VMS occurrence: if the former, there are implications for VMS heat source, metal source, and relationships with underlying volcanic rocks; if the latter, assimilation or contact metamorphism of the VMS may have occurred.

The idea that the BLUC might represent one or a series of large near-surface flows was first raised by C. Blackburn (pers. comm., 2008) during his mapping of the Big Lake property. The possible relationship between BLUC cumulates and stratigraphically overlying (structurally underlying) mafic-ultramafic metavolcanic rocks may be analogous to that between basal peridotite/dunite/pyroxenite cumulates and upper portions of thicker ponded ultramafic flows, such as the Empire komatiite flow of the Kidd-Munro assemblage (Barrie et al., 2001). These documented flows have true thicknesses in excess of 300 m (Barrie et al., 2001), comparable to the Big Lake Ultramafic Complex of about 300 m true thickness.

Evidence for a shallow origin for BLUC cumulates includes the small cumulus crystal sizes (relict cumulus pyroxene crystals are mostly <3 mm across in the pyroxenites, and olivine crystals are mostly <1.5 mm across in the peridotites) and generally diffuse lower contacts (stratigraphic tops) into adjacent metavolcanic rock. Upper contacts (stratigraphic bases) of peridotite units of the BLUC are mostly sharp, with up to 30 cm of black biotite alteration extending into overlying rock (e.g., hole 73, 339 m depth; Appendix A). By no means conclusive, the mostly sharp upper contacts (basal contacts in an overturned sequence), mostly gradational lower contacts, and small cumulus crystal sizes suggest the BLUC is more likely one or a series of thick ponded cumulate flows than an intrusion with discrete upper and lower intrusive contacts. This possibility is also explored in a geochemical context in Chapter Five.

4.4.3 VMS Host Sequence Classifications

The lithostratigraphic-tectonic classification of VMS by Franklin et al. (2005) was summarised at the beginning of this chapter to introduce the variety of sequences or

environments known to host VMS (Table 4.1). Metapelites make up less than 5% of the lithostratigraphy shown in Figure 4.1, but the Big Lake VMS occurrence is otherwise consistent with the pelitic-mafic category, given the absence of felsic volcanic/volcaniclastic rocks and the presence of thick ponded ultramafic cumulates, as well as siltstones. As summarised in Table 4.1, this assemblage of rocks may be found in oceanic back arc rifts or ocean ridges with sediment input, the latter more likely to contain shallow ultramafic intrusions or flows like those of the BLUC, as is observed in modern ocean rift settings (Fouquet et al., 2005). The mafic category, associated with ophiolite or ophiolite-like settings, also closely describes the Big Lake occurrence despite its lack of felsic rock. Possible tectonic settings of this class of VMS include those of the pelitic-mafic category (oceanic back arc rifts and ocean ridges), but may also include ocean island seamounts. These possibilities are better explored with respect to tectonic setting in Chapter Five, and the reader is also cautioned that these classifications are best applied to entire volcano-sedimentary assemblages of VMS districts (i.e., typically a larger volume of rock than that mapped and drilled at the Big Lake property).

More relevant to the discussion of Big Lake lithostratigraphy and petrography at this point is lithofacies association, which is, judging from rock available for study, flow-dominated, consisting of flows mostly five to tens of metres thick, and no greater than 60 m thick given the distribution of interflow sedimentary rock as shown in Figure 4.1. Examples of VMS deposits with flow-dominated footwall sequences include the Kidd, Matagami, and Noranda deposits. In these and other settings, workers have been able to identify vent proximal environments according to changes in the distribution of volcanic facies (e.g., lateral change from massive to pillowed facies, distal autobreccia and hyaloclastite facies; Moneckel et al., 2006). While some volcanic features (pillows, amygdules) have been identified in parts of the Big Lake VMS host sequence, mapping its volcanic facies architecture would require a much larger scale of study.

4.4.4 Role of Sedimentation in Preservation of VMS

In a study of Archean through currently active VMS settings, Petersen et al. (2004) discussed the role of sedimentation in producing economic concentrations of VMS precipitate. In settings lacking significant pelagic or turbiditic sedimentation,

notably most mid-ocean ridges, 97% of metals ejected from plumes is lost, or spread over very large areas (Converse et al., 1984). Because ocean ridge volcanism represents the majority of mafic-only seafloor volcanism, this is a likely reason that most mafic-only sequences, such as at Big Lake, are not common hosts to preserved VMS ore. The lithostratigraphy hosting the Big Lake VMS occurrence points to a mafic-only seafloor setting, but sediment input (or, perhaps, the development of a sulphide mound) was apparently sufficient to prevent the total loss of metals to the water column.

4.4.5 Absence of Felsic Volcanism

According to Hart et al. (2004), "all VMS deposits in the Superior province, including Kidd Creek and the deposits in the Noranda and Sturgeon Lake camps, are associated with geochemically distinctive rhyodacites, rhyolites, and high silica rhyolites." The lithostratigraphy of the Big Lake VMS occurrence is therefore unusual in terms of the absence of felsic volcanic or volcaniclastic rock, at least within several kilometres of the mapped and drilled extent of the occurrence.

The association of VMS deposits with camp-scale distributions of felsic volcanic or related volcaniclastic rocks has long been recognised; among the world's ~850 documented deposits and large occurrences, all but the Outukumpu deposit of Finland, the Potter and Potter-Doal deposits, and a few small occurrences above ponded komatiites of the Kidd-Munro assemblage have some documented VMS-proximal synvolcanic felsic rock (J. Franklin, pers. comm., 2007; Barrie et al., 2001). Sampling and geochemical analysis of these rhyolites remains one of the best studied and most popular means of targeting VMS-prospective sites (e.g., Lesher et al., 1986).

Given the strong association between VMS ore and synvolcanic rhyolites, it is perhaps unlikely for VMS-mineralising fluids to be generated or transported, or for sulphides to be deposited or preserved, in suites that are entirely mafic-ultramafic, as at Big Lake. The first and perhaps most likely reason for the global rhyolite-VMS association is that bimodal volcanism typifies an extensional tectonic regime, which is considered productive for VMS systems. A consequence of lithospheric extension/thinning is increased heat flow, sufficient to drive the partial melting of continental crust to produce rhyolites intercalated with mafic flood volcanism.

Extensional arc settings in particular should preserve the transition from a bimodal package of primitive arc basalts and rhyolites to back arc MORB, reflecting a progressively decreasing role of slab dehydration melting, and an increasing upper mantle signature (Franklin et al., 2005). In such environments the combination of extensive normal faulting and intrusion of heat sources probably occurs during this transition from late arc to oceanic rift, and it may be for this reason that VMS deposits are often found at or near the top of a bimodal package (Franklin et al., 2005).

Secondly, despite generally lower metal compatibilities in felsic rocks, degassing of footwall or vent-proximal rhyolites can provide both metals and their complexing agents (e.g., Cl) necessary to the formation of VMS ore. The loss of volatiles, specifically Cl in the absence of water and CO_2, increases in more evolved magmas: "Chloride solubility in basalt melt is an order of magnitude greater than that in silicic melts, so the role of Cl^- in driving the exsolution of vapor and/or liquid from magma will increase dramatically as mafic, H_2O- and CO_2- undersaturated magmas fractionate and evolve to more silicic compositions" (Webster et al., 1999).

Thirdly, the distribution of rhyolites relates to the structural controls on sites of hydrothermal discharge. The higher viscosity of rhyolites leads to their tendency to dome over discharge sites, and rhyolites are therefore local indicators of structural corridors for both volcanism and hydrothermal discharge. By this reasoning, VMS lenses should be more likely to occur in close proximity to rhyolites, regardless of their role in mineralisation processes or products.

Though none of the above indicates that VMS systems cannot develop in settings lacking felsic rocks, the relationships of rhyolites with extensional tectonic settings and structural corridors, and possible role of rhyolites as a source of metals and complexing agents in VMS deposits account in part for the rarity of VMS in mafic-only settings. Unusual circumstances are perhaps required in order for VMS systems to develop in mafic-only settings like Big Lake, such as, for instance, prolonged convection above thick komatiite flows (Barrie et al., 2001) in the absence of subvolcanic intrusions.

4.5 Conclusions

Lithologies of the Big Lake VMS occurrence are broadly divided into ultramafic cumulates (peridotites and pyroxenites), mafic-ultramafic metavolcanic rocks, and sedimentary rocks. Several arguments have been presented to conclude that the host lithostratigraphy to the Big Lake VMS occurrence is overturned. Moving down hole / up stratigraphy, the sequence consists of Big Lake Ultramafic Complex cumulates, adjacent flows, VMS-hydrothermal alteration and sulphides, siltstone, and flows with interbedded, locally pelitic siltstones and iron formation. The ultramafic cumulates and adjacent underlying volcanic rock are likely a series of ponded ultramafic flows.

As a whole, the lithostratigraphic assemblage at Big Lake is consistent with either oceanic arc or sedimented ocean ridge settings (as in the pelitic-mafic category of Franklin et al., 2005) or OIB settings (as in the mafic category). As a VMS host, it is very unusual in its lack of felsic volcanic or volcaniclastic rock.

Chapter 5
Whole-Rock Geochemistry

5.1 Introduction

In this chapter, the genesis, classification, and tectonic environment of the mafic-ultramafic metavolcanic rocks hosting the Big Lake VMS occurrence are examined through whole-rock geochemistry. The origins and possible relationships to VMS mineralisation of the Big Lake Ultramafic Complex cumulates and the metasedimentary rocks are also explored.

5.2 Treatment of Data

A total of 212 samples were used in this section. The majority were collected and described by MetalCORP staff and analysed by ALS Chemex (see Chapter Two). Of the metavolcanic and metasedimentary rock samples, 49 were collected, described, and pulverised by the author and analysed by the Ontario Geoscience Laboratories (Chapter Two). Metavolcanic rock was sampled across a range of degrees of hydrothermal alteration. Assay data are not presented here, but are used in the following chapters. All data shown in this chapter are given in Appendix C. Analyses lower than detection limit were ignored. Where REE totals were used, samples with one or more REE analysis less than detection limit were ignored.

It was shown in Chapter Four that metavolcanic rocks structurally below VMS mineralisation ("Group II" in Fig. 4.1) were stratigraphically above VMS mineralisation, so are here termed hangingwall metavolcanic rocks. They are petrographically indistinguishable from the Group I rocks that are henceforth termed footwall metavolcanic rocks. Apart from the use of the terms stratigraphic footwall and hangingwall, samples considered in this chapter are grouped according to the lithostratigraphic units presented in Figure 4.1, for a total of 63 footwall metavolcanic rocks, 36 hangingwall metavolcanic rocks, three metavolcanic rocks of unknown relation to VMS stratigraphy (from drill core without VMS mineralisation or alteration), 53 cumulate pyroxenites to feldspathic pyroxenites, seven cumulate peridotites, and 48 metasiltstones.

5.3 Results

Table 5.1 - Representative major and trace element data for rocks of the Big Lake VMS host sequence. Samples with six digit ID were analysed by ALS Chemex, and those with ID in number-letter format were analysed by the OGS labs.

	Footwall metavolcanic rocks		Hangingwall metavolcanic rocks		BLUC peridotites		BLUC pyroxenites		Metasiltstones	
Sample ID	73-K	7-K	39-L	546749	626113	546712	626101	626114	73-M	546750
SiO_2	46.35	39.89	48.16	47.44	39.59	39.71	42.73	48.11	69.62	70.13
TiO_2	0.99	1.52	0.75	0.82	0.75	1.39	2.75	0.86	0.30	0.31
Al_2O_3	5.62	7.78	12.64	14.93	2.41	7.32	5.54	13.91	14.40	14.24
Fe_2O_3	14.46	13.42	14.68	11.92	18.79	16.89	21.37	14.83	3.68	2.43
MnO	0.27	0.33	0.22	0.23	0.25	0.24	0.23	0.21	0.04	0.06
MgO	19.61	9.00	9.22	6.58	26.37	20.35	9.14	7.26	1.24	0.84
CaO	9.25	18.78	11.60	13.81	2.80	7.13	15.73	9.88	2.54	2.89
Na_2O	0.32	1.53	2.38	1.78	0.04	0.12	1.05	3.02	4.00	6.75
K_2O	0.05	0.61	0.28	0.42	0.13	0.03	0.36	0.48	3.05	0.08
P_2O_5	0.03	0.12	0.07	0.05	0.05	0.09	0.06	0.07	0.08	0.07
LOI	3.23	7.80	0.75	1.73	7.26	5.19	0.06	0.63	2.13	1.19
Total	100.19	100.78	100.72	99.75	98.84	98.78	98.92	99.31	101.07	99.02
Ti	5390	7665	4039	11920	18790	16890	21370	14830	1490	2430
P				210	220	410	280	280		320
Cr	3706	756	1069	75	2070	1340	18	83	57	27
Co	77.0	53.6	67.1	47.0	161.0	103.0	88.4	60.3	9.1	8.0
Ni	438	261	246	81.5	2220	870	368	118	23	24.4
Rb	1	22	5	10	1	1	2	3	44	1
Sr	79	636	195	190	29	63	103	160	198	209
Cs	0.05	1.33	0.10	0.26	0.18	0.12		0.20	0.99	0.09
Ba	3	132	42	100		10	40	80	685	50
Sc	65.0	34.1	40.8						4.5	
V	248	375	256	258	126	250	799	268	42	41
Ta	0.2	0.4		0.2	0.4	0.5	0.4	0.2	0.3	0.3
Nb	3.2	6.0	2.2	2.2	5.9	7.5	5.9	2.1	3.3	3.6
Zr	43	84	52	17	15	44	3	17	123	77
Hf	1.3	2.3	1.5	0.8	0.4	1.3	1.4	0.6	3.1	2.5
Th	0.3	0.6	0.3	0.3	0.5	0.5	0.9	0.2	2.0	2.2
U	0.1	0.2	0.2	0.1	0.1	0.1	0.2	0.1	0.7	0.4
Y	13.5	19.5	20.0	18.5	5.7	13.5	13.2	15.4	4.4	4.5
La	3.7	7.4	3.7	3.5	6.4	7.5	7.5	3.5	13.0	7.1
Ce	10.9	20.3	10.9	9.2	14.0	19.2	18.0	8.3	25.4	15.9
Pr	1.5	2.8	1.4	1.3	1.8	2.7	2.6	1.4	2.7	2.0
Nd	7.7	14.0	7.0	6.2	7.6	12.1	12.6	6.6	9.7	7.4
Sm	2.3	3.7	2.1	1.9	1.5	3.0	3.2	1.9	1.7	1.4
Eu	1.5	1.5	0.8	0.7	0.5	0.8	1.1	0.7	0.6	0.7
Gd	2.5	3.8	2.6	2.4	1.6	3.2	3.2	2.3	1.3	1.3
Tb	0.4	0.6	0.5	0.4	0.2	0.5	0.6	0.5	0.2	0.2
Dy	2.4	3.6	3.2	3.0	1.2	2.8	2.8	3.0	0.9	0.9
Ho	0.5	0.7	0.7	0.7	0.2	0.6	0.5	0.6	0.2	0.2
Er	1.3	1.8	2.0	2.0	0.6	1.5	1.4	1.9	0.4	0.5
Tm	0.2	0.3	0.3	0.3	0.1	0.2	0.2	0.3	0.1	0.1
Yb	1.2	1.6	2.0	1.9	0.5	1.3	1.1	1.8	0.4	0.5
Lu	0.2	0.2	0.3	0.3	0.1	0.2	0.2	0.3	0.1	0.1
Cu	37	65	6	77	271	103	1185	291	81	143
Zn	80	78	54	68	120	108	98	83	25	19
Mo	0.09	0.29	0.11	0.41	0.09	0.23	0.23	1.62	1.29	0.86
Pb	0.7	6.8	1.3	6.2	1.1	0.6	1.2	3.1	3.2	2.9
Sn	0.9	1.4	0.9	0.4	0.4	0.7	0.9	0.6	0.7	0.4
Sb	0.04	0.10		0.07	0.18	0.14	0.24	0.05		0.05
$(La/Yb)_{cn}$	2.20	3.26	1.33	1.32	9.18	4.14	4.89	1.39	25.40	10.18
$(La/Sm)_{cn}$	1.05	1.27	1.15	1.19	2.76	1.62	1.51	1.19	4.91	3.28
$(Gd/Yb)_{cn}$	1.70	1.96	1.08	1.04	2.65	2.04	2.41	1.06	2.97	2.15
$(Eu/Eu^*)_{cn}$	1.88	1.18	1.00	1.00	0.98	0.78	1.04	1.02	1.13	1.56
Al_2O_3/TiO_2	5.68	5.12	16.85	18.21	3.21	5.27	2.01	16.17	48.00	45.94
Zr/Hf	33	36	35	21	37	33	25	28	40	30
Zr/Y	3.19	4.31	2.60	0.94	2.60	3.24	2.74	1.09	27.89	17.02
Nb/Nb*	0.95	0.84	0.66	0.61	0.75	0.95	0.70	0.53	0.18	0.42
Notes		~10% calcite			magnetic	magnetic	magnetic			
Hole ID	73	7	39	62	6	56	5	7	73	62

5.3.1 Element Mobility

Most schemes that use geochemical data for classification of igneous rocks or tectonic setting require that certain elements are immobile after formation. The Total Alkalies versus Silica diagram of Le Bas et al. (1986), for instance, assumes an unchanged silica and alkali content, and for this reason is rarely applicable to Precambrian rocks, many of which have had alkali elements added or removed during metamorphism. Depending on proximity to recharge or upflow zones, protolith and fluid compositions, fluid pH, temperature, water-rock ratio, and duration of hydrothermal activity, VMS systems can be subject to extreme depletions or enrichments of major elements including Si, Ca, Na, K, or Mg (Galley et al., 2007). Local hydrothermal alteration at Big Lake, coupled with greenschist facies regional metamorphism, may have resulted in mobility of elements even in least-altered samples.

Standard practice to assess element mobility is to plot a given element against another element known to be least mobile, such as Zr, Nb, or TiO_2 (Jenner, 1996). In general, a linear trend among a suite of co-genetic samples on a variation diagram would suggest that both elements are immobile, with co-variation due to igneous processes during formation or to dilution/concentration by addition/removal of other elements. Variation diagrams for rocks of the Big Lake VMS occurrence are shown in Figures 5.1 and 5.2.

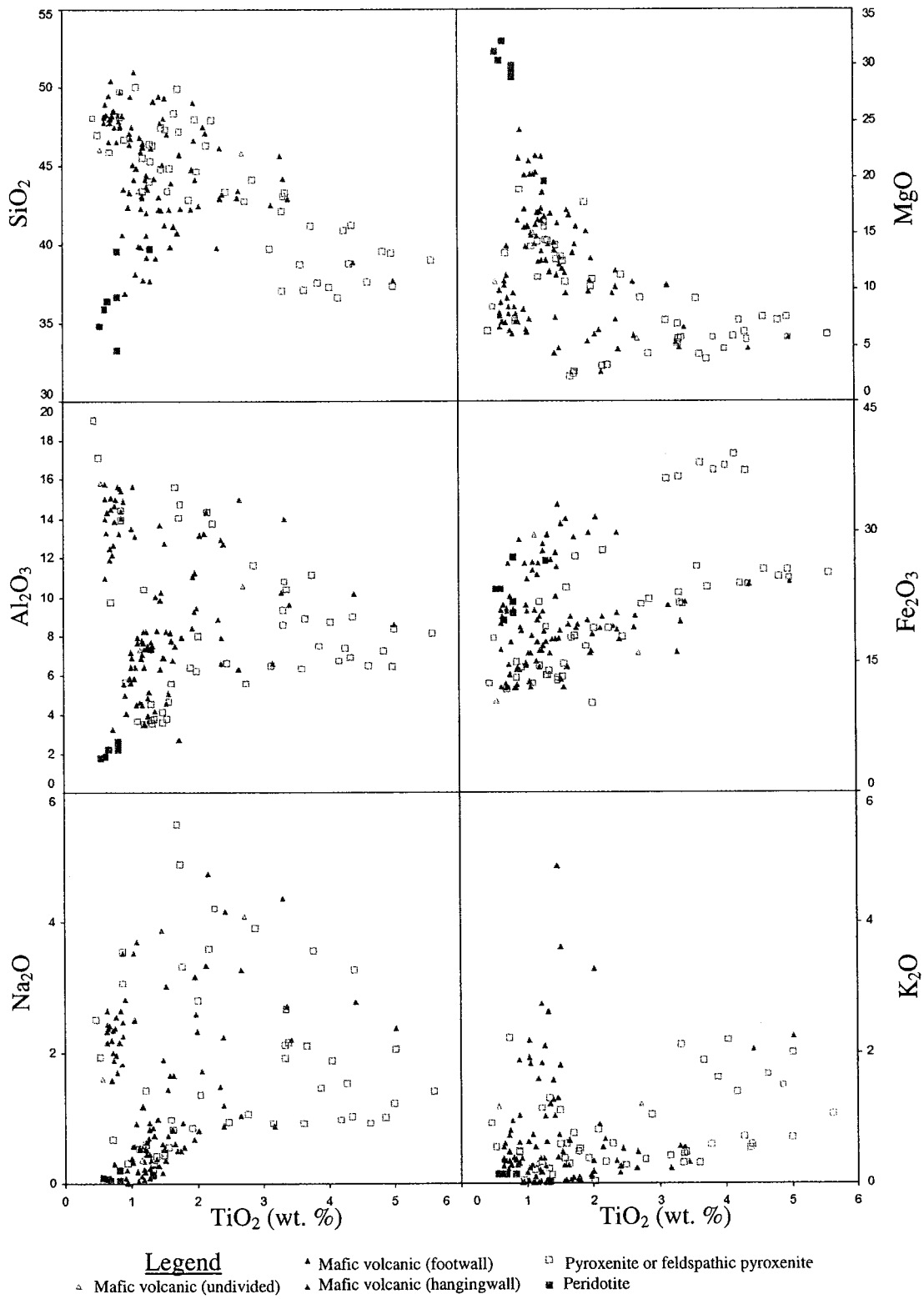

Figure 5.1 - Variation diagrams of major element oxides with TiO_2. All data in wt. %.

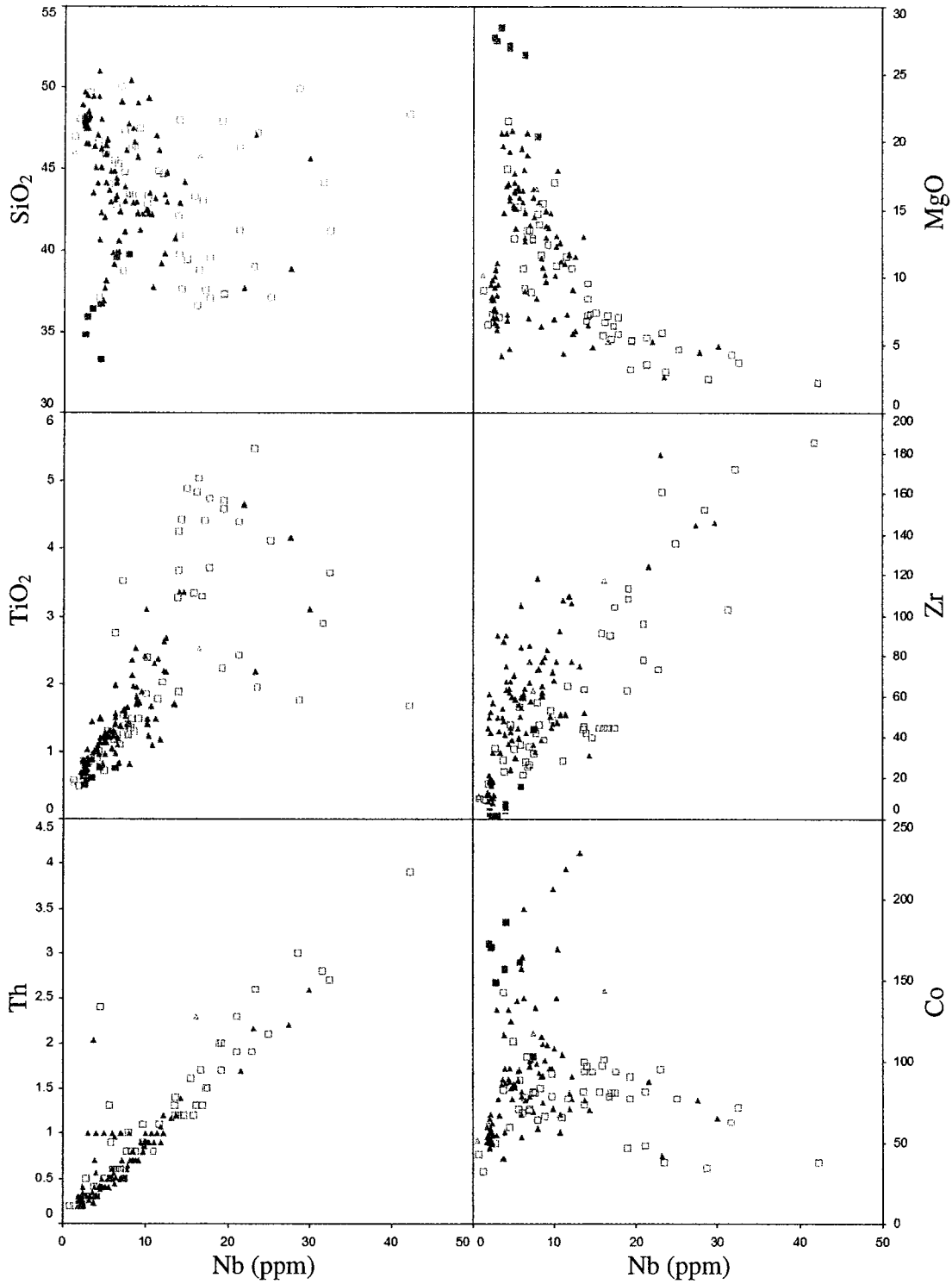

Figure 5.2 - Variation diagrams of major element oxides (in wt. %) and trace elements (in ppm) with Nb. Legend as in Figure 5.1.

Spread of data through all samples suggests that SiO_2, Na_2O, K_2O, and perhaps Co are mobile. Alkali elements, as well as silica depending on P-T conditions, are generally expected to be mobile in VMS-hydrothermal settings (Franklin et al., 2005). Al_2O_3, Zr, and Th are effectively immobile, forming fairly well defined trends in Figures 5.1 and 5.2. In these diagrams, MgO decreases with TiO_2 and Nb, while Zr, Th, and perhaps Co and Al_2O_3 increase with TiO_2 or Nb.

Footwall metavolcanic rocks and the ultramafic cumulates generally define the same trend in the MgO, Fe_2O_3, Al_2O_3, and trace element diagrams. This *may* suggest a common source, with BLUC peridotites perhaps representing the least-evolved members of the suite. This is not unreasonable if the Big Lake Ultramafic Complex represents a series of ponded cumulate flows in sequence with adjacent fine-grained flows, as proposed in Chapter Four. In the MgO and Al_2O_3 diagrams, most hangingwall metavolcanic rocks plot on a trend distinct from the main peridotite-pyroxenite-footwall metavolcanic trend. This may reflect two different volcanic sources.

5.3.2 Geochemical Classifications and Trace Element Geochemistry

In section 5.3.1., SiO_2, Na_2O, and K_2O were shown to be mobile to some degree, so classifications using these elements have limited application to rocks hosting the Big Lake VMS mineralisation. Unlike the alkali and alkaline earth elements, most trace elements—Y and the rare earth elements in particular—are effectively insoluble in aqueous solution (White, 2005) and immobile up to lower amphibolite facies metamorphism (Pearce, 2007). Trace elements as a whole are sensitive to igneous processes not recorded by major element variations, and are thus better suited to igneous rock classifications and tectonic setting indicators.

In the rock type classifications and tectonic discriminant diagrams for igneous rocks presented below, samples are grouped as in previous figures, and BLUC cumulates are included to illustrate their possible relationship to footwall rocks. Though a small part of the following interpretation is based on mobile elements, emphasis is on least-mobile species.

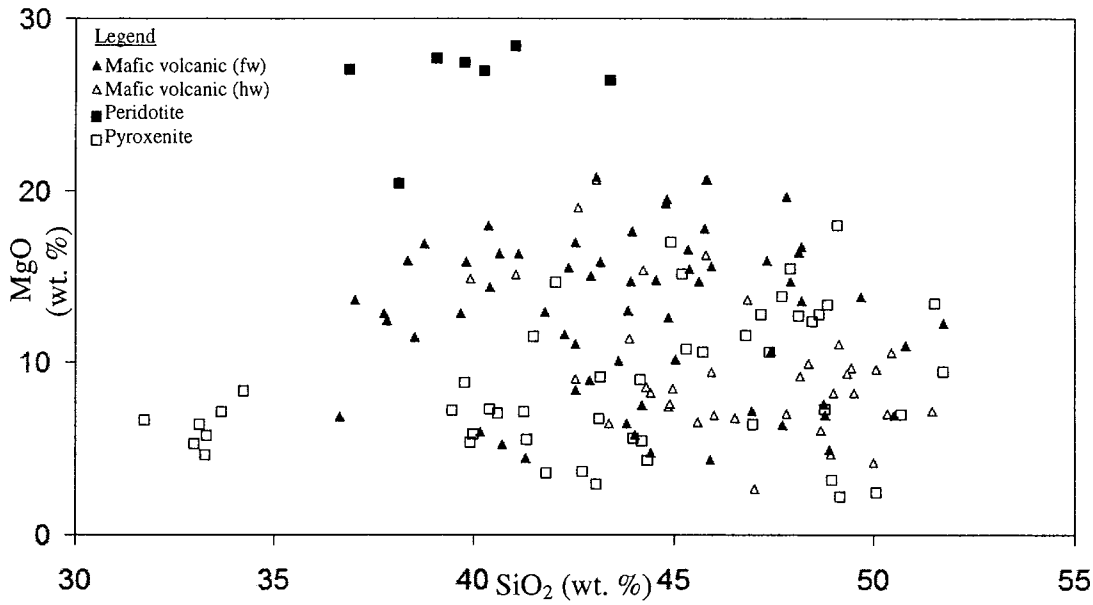

Figure 5.3 - MgO vs. SiO_2 in rocks of the Big Lake VMS host sequence.

In Figure 5.3, only seven of the 99 plotted metavolcanic samples contain >18 wt. % MgO indicative of komatiitic lavas (Arndt and Nesbitt, 1982). Approximately half contain <45% SiO_2 which is typical of ultramafic rocks, and the remainder are mafic. Strictly according to MgO and SiO_2 contents, the metavolcanic rocks can therefore be described as komatiitic basalts. SiO_2 contents of the metavolcanic rocks range from 37-52 wt. % (mean 45 wt. %), compared to peridotites having 37-43 (mean 40) wt. %, and pyroxenites with 32-52 (mean 44) wt. % SiO_2. Hangingwall samples as a whole contain slightly lower MgO and higher SiO_2 than the footwall and BLUC samples.

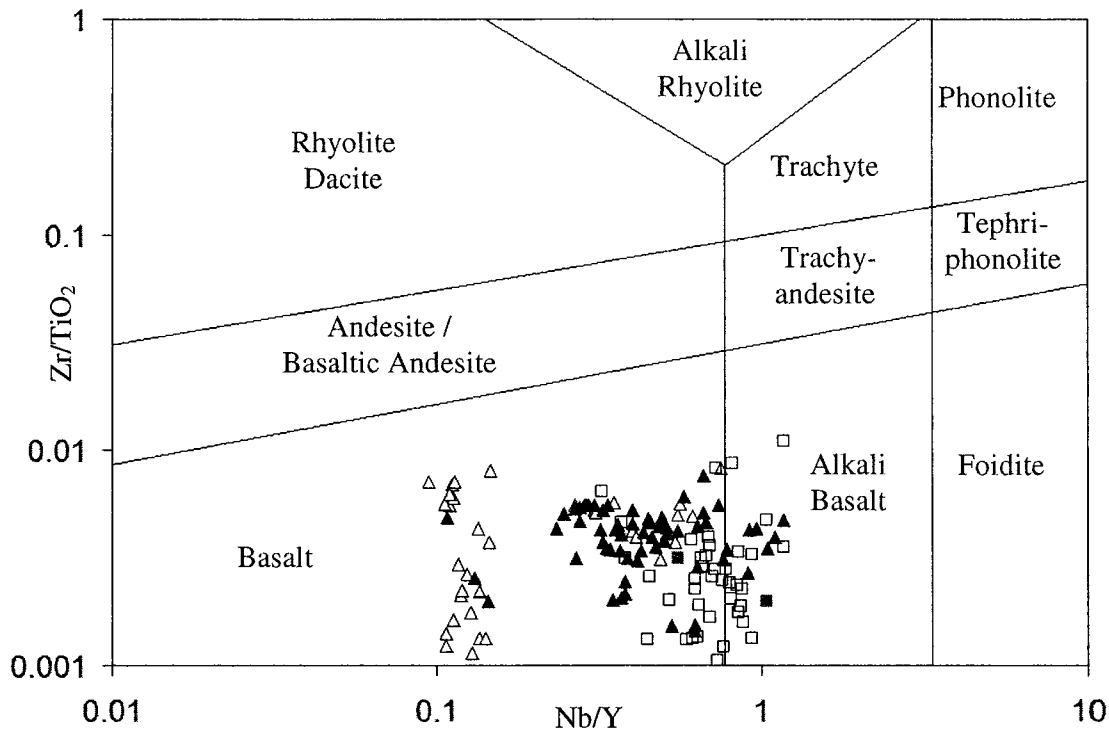

Figure 5.4 - Zr/TiO_2 vs. Nb/Y in rocks of the Big Lake VMS host sequence. Note two distinct sample populations. Fields are from Pearce (1996) after Winchester and Floyd (1977). Legend as in Figure 5.3.

All samples plot in the basalt to alkaline basalt fields of the Zr/TiO_2 vs. Nb/Y diagram of Pearce (1996) after Winchester and Floyd (1977; Fig. 5.4). The consistently low Zr/TiO_2 (<0.01), a least-mobile proxy for silica content, confirms the absence of any possibly misidentified felsic rock in the Big Lake VMS host sequence, since strongly altered rhyolites would still be expected to have Zr/TiO_2 ratios above 0.01. The distribution of Nb/Y ratios is clearly bimodal, defining two groups: sub-alkaline to alkaline footwall metavolcanic rocks and BLUC cumulates; and sub-alkaline hangingwall metavolcanic rocks. The overlap between footwall and hangingwall samples in Figure 5.4 is perhaps better represented by the spatial distribution of Nb/Y of metavolcanic samples above and below 0.2 (Fig. 5.5). Reasons for this overlap are addressed in the discussion.

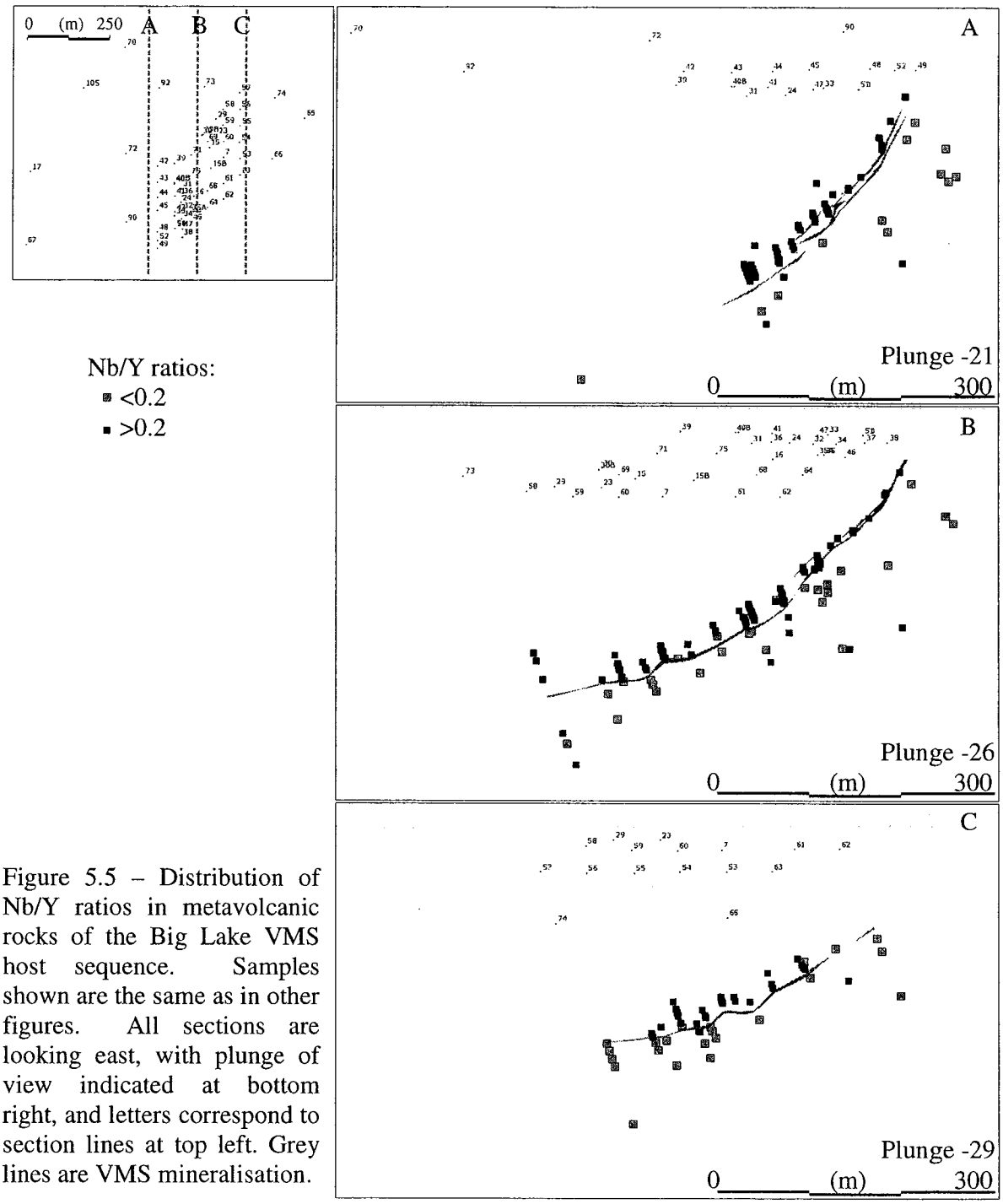

Figure 5.5 – Distribution of Nb/Y ratios in metavolcanic rocks of the Big Lake VMS host sequence. Samples shown are the same as in other figures. All sections are looking east, with plunge of view indicated at bottom right, and letters correspond to section lines at top left. Grey lines are VMS mineralisation.

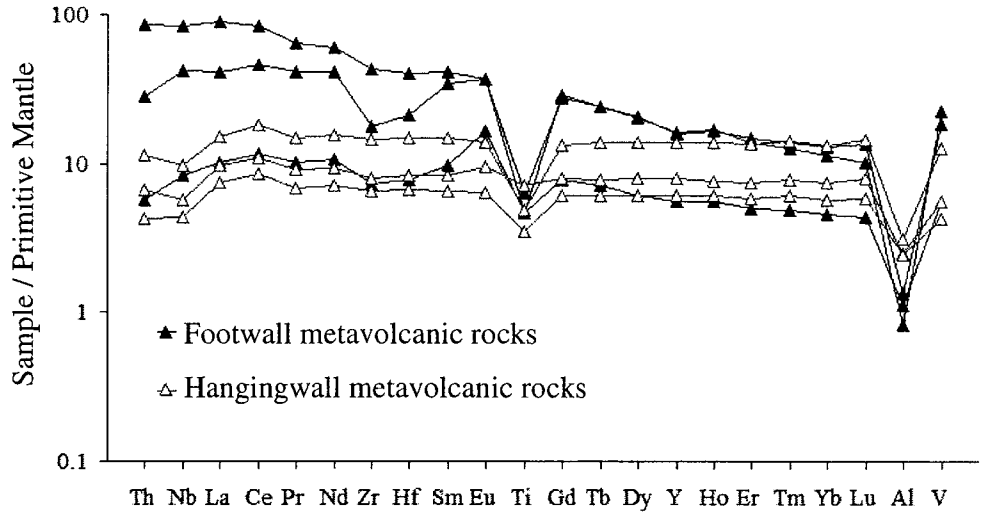

Figure 5.6 - Representative primitive mantle normalised trace element diagrams for metavolcanic rocks stratigraphically below and above VMS mineralisation. All samples shown were analysed by the OGS. Normalising values are from Sun and McDonough (1989).

Figure 5.6 is a comparison of representative trace element profiles of footwall and hangingwall metavolcanic rock normalised to primitive mantle. Footwall samples have weakly fractionated REE (La/Yb_{cn}=2-8) and mostly convex-up LREE patterns, unlike most hangingwall samples with a nearly flat REE profile (La/Yb_{cn}=1-2). Though absolute Nb concentrations are similar in both sample sets (1-38 ppm), most hangingwall samples show weak negative Nb anomalies (Nb/Nb*=0.4-0.9), and generally flat Zr and Hf, whereas footwall samples show generally undepleted Nb (Nb/Nb*=0.6-1.3) and have relative depletions in the other HFSE. Weak positive Eu anomalies are also noted in some of the footwall samples.

Figure 5.7 is a summary of two key differences between hangingwall and footwall groups, where hangingwall samples show negative Nb anomalies (i.e., Nb/Nb* <0.9) and near-flat REE slopes (La/Yb_{cn}=1-2). As was noted in Figure 5.4, there is some overlap between fields: two footwall samples (73-L and 37-L, not shown in Fig. 5.6) have REE profiles resembling hangingwall patterns, and a few hangingwall samples have higher La/Yb as in footwall samples, reasons for which are considered in the discussion.

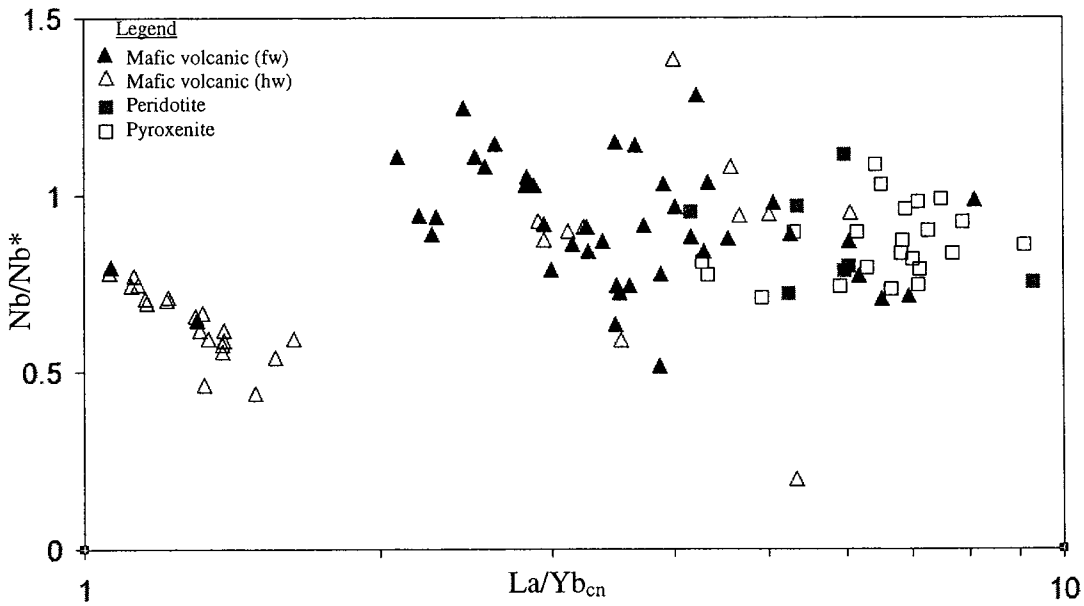

Figure 5.7 - Nb/Nb* vs. La/Yb_{cn} in rocks of the Big Lake VMS host sequence. Note two distinct fields defined by hangingwall samples at left and footwall and cumulate samples at right (overlap is addressed in text).

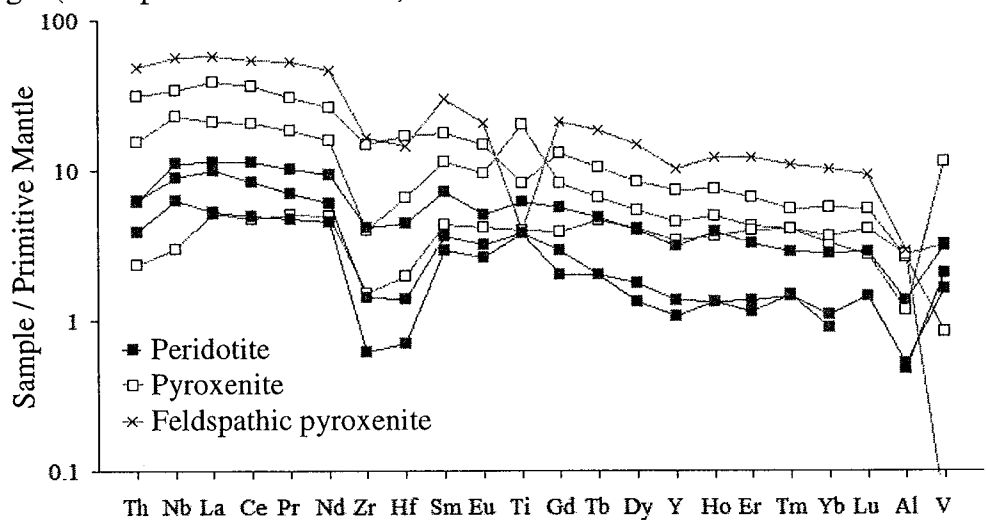

Figure 5.8 - Representative primitive mantle normalised trace element diagrams for ultramafic cumulates of the Big Lake Ultramafic Complex (BLUC). All samples shown were analysed by ALS Chemex methods. Normalising values are from Sun and McDonough (1989).

Trace element patterns of the cumulate peridotites and pyroxenites to feldspathic pyroxenites (Fig. 5.8), stratigraphically below the Big Lake VMS mineralisation, share many similarities with those of footwall metavolcanic rocks in Figure 5.6, including slightly fractionated REE (La/Yb_{cn}= 4-9 in both peridotites and pyroxenites), negative Zr-

Hf anomalies, and generally flat to weak positive Nb anomalies. Unlike the profiles in Figure 5.6, Ti is relatively flat, and in some pyroxenites is enriched reflecting the overall five percent modal abundance of leucoxene/titanite. The uppermost sample of feldspathic pyroxenite contains approximately 30-35% plagioclase, approaching gabbroic composition, with a relative Ti depletion reflecting a lack of visible titanite.

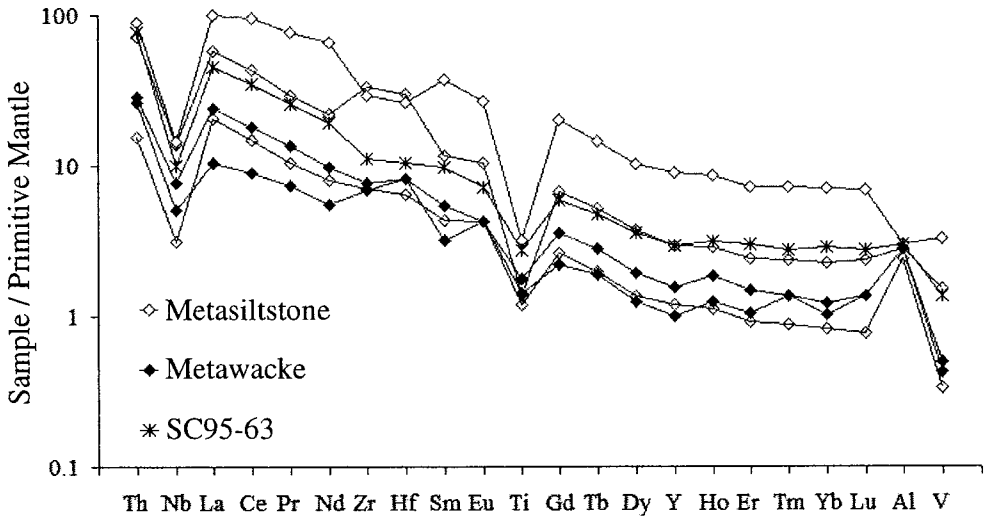

Figure 5.9 - Primitive mantle normalised trace element diagrams for metasedimentary rocks 1-40 m stratigraphically above VMS mineralisation at Big Lake. All siltstone samples shown were analysed by OGS methods, and wacke samples by ALS Chemex methods. Sample SC95-63 is representative Schreiber-Hemlo trench turbidite, from Polat (1998). Normalising values are from Sun and McDonough (1989).

The recrystallised, finely laminated siltstones and wackes are of clear sedimentary origin (bedding planes are clearly visible, and they contain pelitic laminae and beds), but have trace element patterns with evolved arc-like characteristics, including strong negative Nb anomalies (mean Nb/Nb* = 0.2, n = 38) and fractionated REE patterns (mean La/Yb_{cn}= 20, n = 36, two samples omitted due to La or Yb below detection). These resemble other REE-fractionated and HFSE-depleted siliciclastic rocks of the Schreiber-Hemlo greenstone belt interpreted by Polat (1998) and Polat and Kerrich (2001) as trench turbidites (Fig. 5.9). Origin from an intermediate or felsic volcanic arc source is possible, but this does not necessarily imply that the Big Lake VMS occurrence was formed in an arc setting. Regardless, these rocks are interbedded with hangingwall metavolcanic rocks, so they represent a possible component for assimilation by the hangingwall basalts.

5.4 Discussion

5.4.1 Reasons for Overlap in Sample Populations

Some overlap was noted between footwall and hangingwall sample populations on the Nb/Y axis of Figure 5.4, or La/Yb in Figure 5.7. It is important to note that the overlap between some footwall and hangingwall samples has different implications than would samples with composition intermediate between the two sample groups. The bimodal distributions of Nb/Y or La/Yb are contrary to a gradual variation of source chemistry in the volcanic rocks over time or up section (as illustrated in Fig. 5.10b), and instead probably reflect input from two chemically distinct volcanic sources (Figs. 5.10 a,c). It is suggested that the sample overlap in Figures 5.4 or 5.7 is due to the grouping of hangingwall and footwall samples strictly according to their stratigraphic relationship to the VMS mineralisation at Big Lake, since the VMS mineralised surface may not trace the irregular geometry defining the contact(s) between flows derived from two volcanic centres, an idea illustrated in Figure 5.10c.

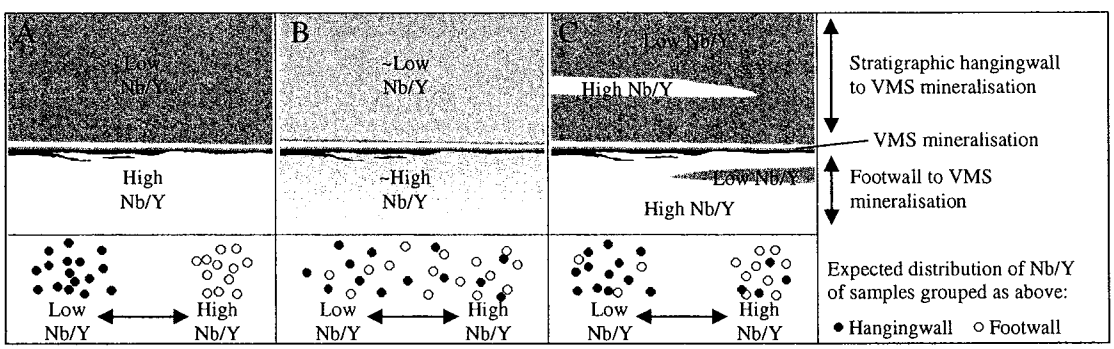

Figure 5.10 - Section sketches comparing three hypothetical scenarios and, in the lower boxes, their expected distributions of Nb/Y values along a horizontal axis. A) In this scenario, the location of VMS mineralisation coincides with a single sharp contact between volcanic flows from two sources, producing a bimodal distribution in Nb/Y with no overlap between hangingwall and footwall samples. This is not observed at Big Lake. B) A gradual decrease in Nb/Y over time or up section produces an even and overlapping distribution in Nb/Y ratios. This is not observed at Big Lake. C) VMS mineralisation does not coincide exactly with the contacts between overlapping flows from two volcanic sources, producing a bimodal distribution in Nb/Y with some overlap between footwall and hangingwall samples. The Nb/Y distribution is similar to that shown in Figure 5.4.

The implication is that the true contact(s) between the footwall and hangingwall flow sequences at Big Lake, evident perhaps in Figure 5.5, would most resemble the sketch in Figure 5.10c, with interfingering/overlapping flows from two chemically and geographically distinct volcanic centres.

5.4.2 Possible Relationships Between BLUC and Metavolcanic Rocks

Covariations in trace and major elements were shown to suggest a trend from BLUC cumulates to the adjacent and stratigraphically overlying footwall metavolcanic rocks. The same was suggested by similar trace element patterns, as summarised in Figure 5.11.

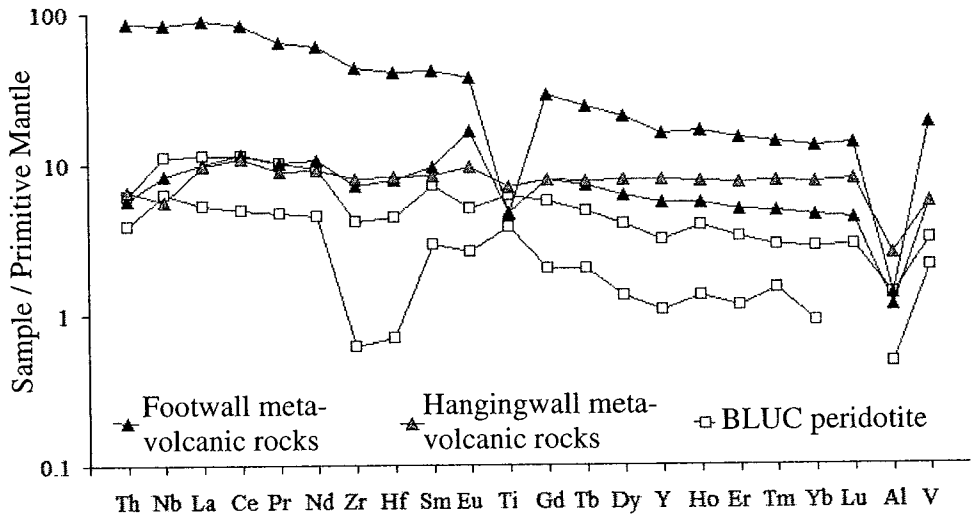

Figure 5.11 - Representative primitive mantle normalised trace element patterns comparing BLUC cumulates and adjacent footwall metavolcanic rocks, which are unlike the hangingwall rocks. Normalising values are from Sun and McDonough (1989).

There is some evidence that footwall metavolcanic rocks are the flow top to the mostly cumulate Big Lake Ultramafic Complex, partly in that profiles in Figure 5.11 may illustrate the fractionation of a weakly LREE-enriched suite from most primitive cumulate peridotite fractionating upward to metavolcanic rock with higher overall trace element abundances and lower relative Ti abundances. In this case, the increasing total REE contents without significant change in LREE/HREE ratio indicates a strong fractional crystallization control, whereas olivine and pyroxene cumulate settling from the BLUC cumulates probably account for the generally decreasing MgO and increasing

Al_2O_3 contents from peridotite to metavolcanic rock. The negative Ti anomalies in the metavolcanic rocks are, in this scenario, possibly conjugate to relative Ti enrichment in the stratigraphically underlying leucoxene-bearing cumulate pyroxenites; that is, they may record crystallization of a Ti-bearing phase, likely titanite/leucoxene in the pyroxenites.

Furthermore, Th-Yb-Nb-Ta characteristics are the same in the BLUC cumulates as in the adjacent footwall basalts or komatiitic basalts (shown later in Fig. 5.12). The possibility that the BLUC is one or a series of large ponded near-surface flows was discussed with respect to contact and field relationships in Chapter Four, and the geochemical evidence presented here provides some support for the idea, implying that some or all of the metavolcanic rocks stratigraphically below the VMS mineralisation are the uppermost preserved part of these thick flows.

5.4.3 Tectonic Setting

Tectonic setting is important to the discussion of the Big Lake VMS occurrence in many respects, with general implications for heat flow, alteration patterns and extents, and potential deposit size. As reviewed in Chapter Four, VMS deposits are known to occur in a range of tectonic settings including oceanic rifts, arcs, and back arcs (Schandl and Gorton, 2002). In collisional settings, they are only known to occur during periods, or in areas, of local extension (Franklin et al., 2005). Rhyolites or equivalent felsic volcanic rocks are well-studied and often useful indicators of tectonic environment in VMS settings (e.g., Schandl and Gorton, 2002), but the absence of rhyolites means that such schemes cannot be applied at Big Lake.

The VMS lithotectonic classification scheme of Franklin et al. (2005) was discussed in Chapter Four with reference to the lithostratigraphy hosting the Big Lake VMS occurrence. Based on the volume of rock available for study, the host lithostratigraphy to the Big Lake VMS occurrence was described as a mafic flow-dominated assemblage with interbedded siltstones and thick ponded ultramafic flows or shallow intrusions, lacking felsic volcanic or volcaniclastic rock. Such an assemblage is most consistent with either the pelitic-mafic category (which may be formed in oceanic

arc settings or sedimented ocean ridges) or the mafic category (which may also include OIB settings).

Both possibilities are in accord with the general observation that late Archean (~2.7 Ga) greenstone belts of the Superior Province are largely made up of two types of volcanic associations: plume-derived oceanic plateau tholeiitic basalts with near-flat REE patterns and associated komatiites; and bimodal (mafic-felsic or mafic-intermediate) tholeiitic to calc-alkaline oceanic arc sequences (Polat and Kerrich, 2001), some containing small volumes of adakite or Nb-enriched basalt (Polat, 2008). This is perhaps not surprising given the low likelihood of preserving other settings (such as MORB) during orogeny by subduction-accretion (Fouquet et al., 2005). The Schreiber-Hemlo greenstone belt in particular contains both types of volcanic associations (Polat and Kerrich, 2001; Polat, 2008).

Pearce (2007) used Th/Yb, Nb/Yb, and TiO_2/Yb ratios to distinguish between MORB, OIB, and volcanic arc settings for basalts (Fig. 5.12). In samples without selective LREE enrichment by arc-related processes, Nb/Yb increases in proportion with Th/Yb, and non-arc basalts should thus plot within the MORB-OIB array of Figure 5.12a (Pearce, 2007). Along this array, the general relationship follows: Increasing Th/Yb *and* Nb/Y = less LREE-depleted / steeper REE pattern = more OIB-like source. This allows for the distinction between N-MORB, E-MORB, and OIB within the array.

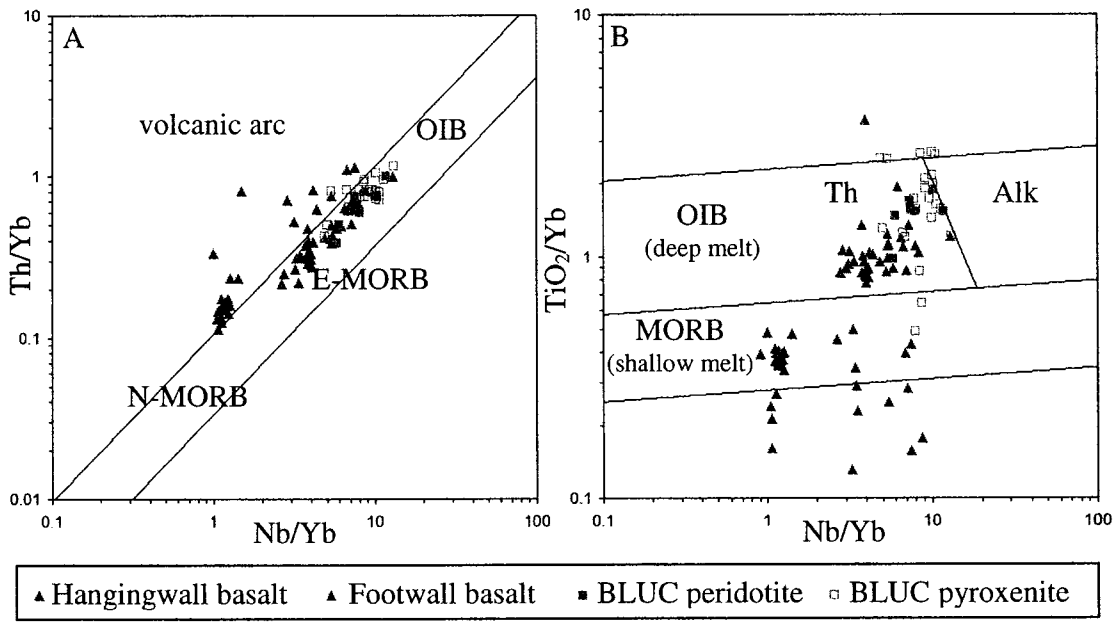

Figure 5.12 - Tectonic discrimination diagrams of Pearce (2007) for basalts. BLUC cumulates are also included to illustrate relationships with Big Lake footwall basalts. A) Th/Yb vs. Nb/Yb in rocks of the Big Lake VMS host sequence. Th/Yb is a proxy for crustal contamination. B) TiO_2/Yb vs. Nb/Yb for rocks that plot within the MORB-OIB array of Figure A. Hangingwall samples may not be of OIB-MORB affinity, but are included for comparison of TiO_2/Yb ratios. TiO_2/Yb is a proxy for depth of melting (see text for discussion).

In samples where selective LREE enrichment has occurred by arc-related processes or crustal contamination, Th/Yb increases independently of Nb/Yb, due to source enrichment of Th by slab-derived fluids or by interaction with contintental crust. Therefore, Th/Yb is a proxy for crustal input in Figure 5.12a, and arc rocks or contaminated rocks will plot along vertical trends above the MORB-OIB array. Means of distinguishing arc rocks from crustally contaminated rocks are discussed later with reference to Figure 5.14.

Footwall basalts and BLUC cumulates plot mostly between E-MORB and OIB in Figure 5.12a, whereas most hangingwall basalts plot above the MORB-OIB array along a near-vertical trend, indicating some crustal input. As noted in previous figures, most hangingwall rocks are also distinctly less alkaline than the footwall rocks and BLUC cumulates in Figure 5.12b.

TiO_2/Yb is a proxy for depth of melting in Figure 5.12b. Ti and Yb have similar partition coefficients in mantle rocks, except that Yb, like other HREE, is more strongly

partitioned into garnet (Pearce, 2007). As a result, partial melting at higher pressures (greater depths) at which garnet is stable will produce magmas with steeper HREE slopes. Higher Ti/Yb in footwall basalts and BLUC cumulates is therefore indicative of deeper melting, and these samples plot mostly in the tholeiitic OIB field (Fig. 5.12b). Whether the BLUC-footwall rocks are plume-derived is questionable (discussed below), but greater HREE fractionation indicates at least that they are unlikely to have formed in a mid-ocean ridge environment (Fig. 5.12b). In contrast, hangingwall samples have lower Ti/Yb as well as lower Gd/Yb (also evident in their generally flat HREE on primitive mantle normalised diagrams) that may indicate shallower depths of melting consistent with either MORB or subducting arc environments. Possible tectonic settings for the BLUC-footwall rocks and hangingwall basalts are examined in detail through the next four sections.

5.4.3.1 Comparison to Wawa Subprovince Basalts

Arc basalts of the Wawa subprovince, such as those north of the Playter Harbours sequence in the western part of the Heron Bay assemblage, have trace element characteristics dissimilar to those of the footwall and hangingwall basalts of the Big Lake VMS occurrence (Figs. 5.13 and 5.16).

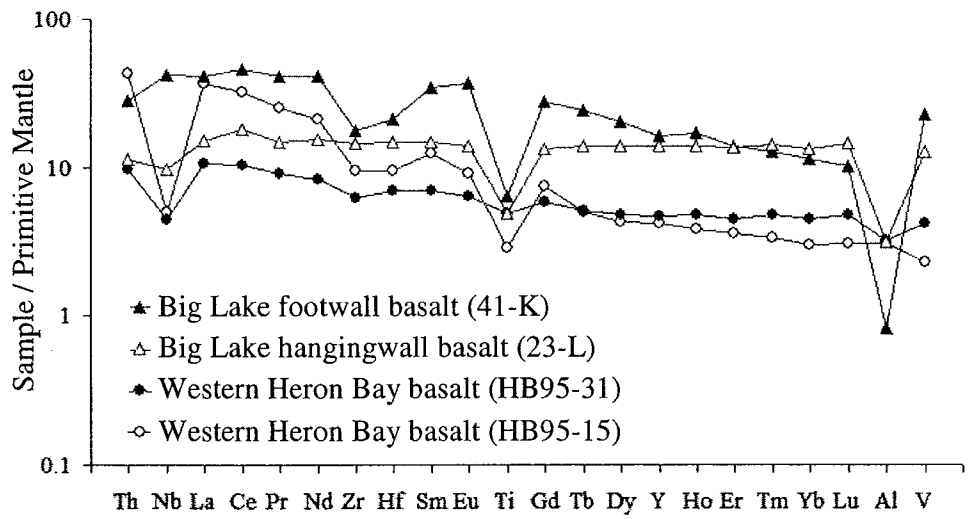

Figure 5.13 - Primitive mantle normalised trace element patterns of representative samples from the Big Lake VMS host sequence compared to Heron Bay data from Polat and Kerrich (2001). Heron Bay samples were taken approximately 15 km west of the Big Lake study area. Normalising values are from Sun and McDonough (1989).

Oceanic plateau basalts of the Wawa subprovince, including those of the tholeiitic Pulpwood-Playter Harbours sequence, are similar to basalts of the Big Lake VMS host sequence, except that Big Lake basalts have larger relative Ti depletions, and some hangingwall basalts have weak relative Nb depletions. In particular, Big Lake footwall basalts have the characteristics of the transitional to alkaline basalts of the Wawa subprovince defined by Polat (2008), including convex-upward LREE and fractionated HREE (Figs. 5.14 and 5.16). Hangingwall basalts have the flat REE patterns typical of tholeiitic plateau basalts that make up most of the Wawa greenstone belts, including the Pulpwood-Playter Harbours sequence of the Heron Bay assemblage (Figs. 5.15 and 5.16).

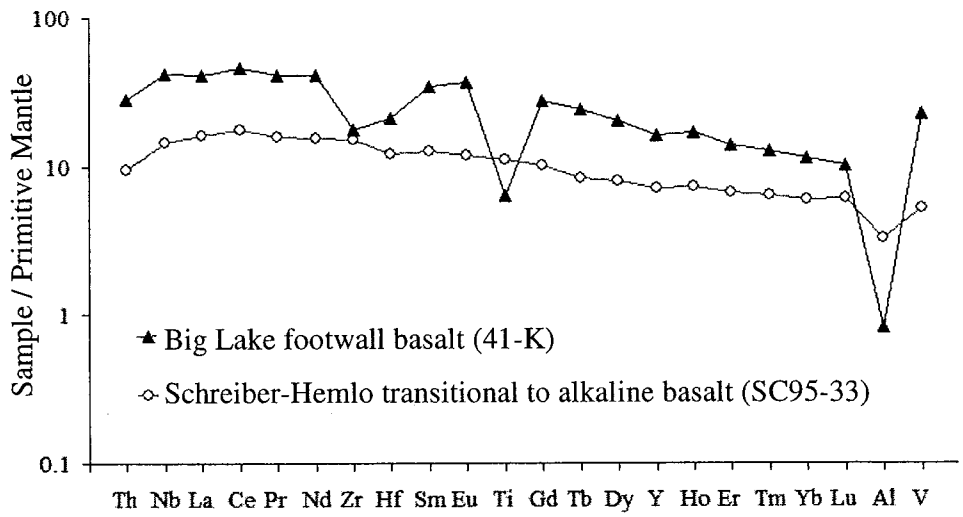

Figure 5.14 - Primitive mantle normalised trace element patterns of a representative Big Lake footwall basalt compared to a representative transitional to alkaline basalt of the Schreiber-Hemlo belt, from Polat (2008). Normalising values are from Sun and McDonough (1989).

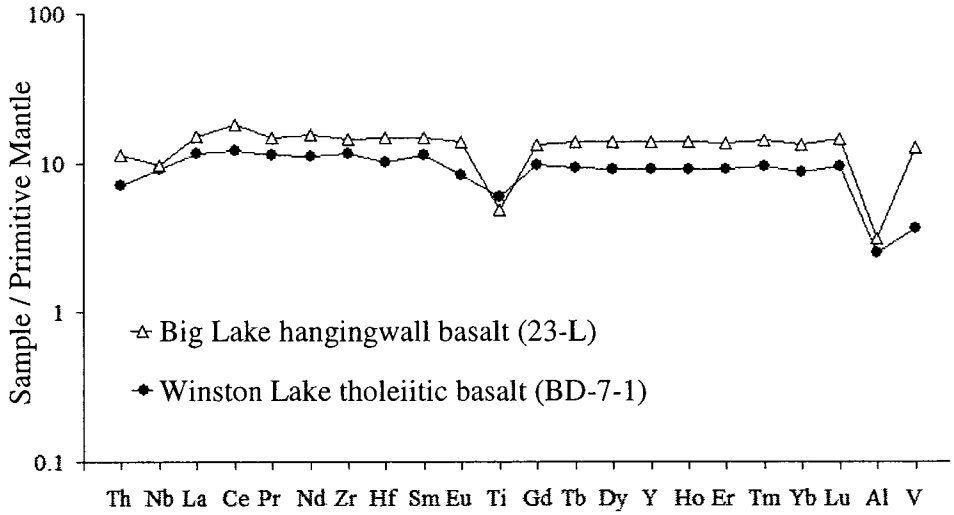

Figure 5.15 - Primitive mantle normalised trace element patterns of a representative Big Lake hangingwall basalt compared to a representative tholeiitic basalt from the Winston (Big Duck) Lake belt, from Polat (2008). Normalising values are from Sun and McDonough (1989).

Polat (2008) adopted a similar tectonic discriminant diagram to that of Pearce (2007) in Figure 5.12, to compare oceanic plateau and arc-associated basalts throughout the Wawa subprovince, including basalts from the Schreiber-Hemlo belt. The Wawa oceanic plateau basalts include both tholeiitic and transitional to alkaline basalts, fields for which are shown in Figure 5.16. The tholeiitic basalts are the most common in the Wawa subprovince and in the Heron Bay area, with near-flat REE patterns (La/Sm_{cn} and Gd/Yb_{cn} <1.15). The transitional to alkaline basalts are less common, and plot between N-MORB and OIB in Figure 5.16. They have fractionated REE (La/Sm_{cn} <1.6 and Gd/Yb_{cn} <3.8) similar to OIB, likely indicating higher depths of partial melting, and some display weak positive Nb anomalies (Polat, 2008). In terms of their Th-Ta-Yb systematics, as well as their trace element patterns shown in Figures 5.14 and 5.15, Big Lake hangingwall basalts are like other oceanic plateau tholeiitic basalts of the Wawa subprovince, and Big Lake footwall basalts are like the transitional to alkaline basalts defined by Polat (2008).

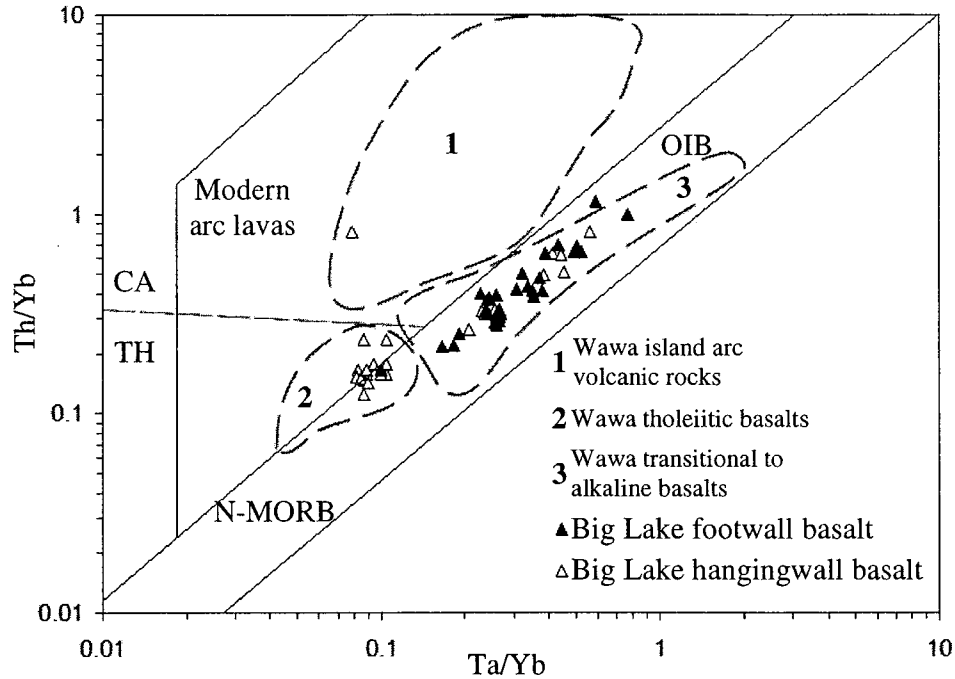

Figure 5.16 - Tectonic discriminant diagram used by Polat (2008) after Pearce (2003), comparing Big Lake basalts to Wawa subprovince data (numbered fields) of Polat (2008).

Polat (2008) noted some difficulty in assessing a plume versus subduction origin for the transitional to alkaline basalts of the Wawa subprovince: they may have been generated by melting of adakite/slab melt-enriched sub-arc mantle (i.e., NEBs), a possibility given the presence of adakites and Mg-andesites in the Schreiber-Hemlo and Manitouwadge belts; or they may have been derived by mixing of enriched/OIB-like and depleted/MORB-like sources, formed respectively by low and high degrees of partial melting at different depths in a mantle plume. Polat (2008) concluded that the latter is most likely, in part because the transitional to alkaline basalts are spatially associated with komatiites/komatiitic basalts and tholeiites, and because some Wawa plume-derived komatiites and komatiitic basalts (not of arc origin) have the same trace element characteristics as the transitional to alkaline basalts. The island arc volcanic rocks of the Schreiber-Hemlo belt are thought to have erupted later, during the start of subduction along the edge of the oceanic plateau (Polat, 2008).

Thus, given the similarities shown in Figures 5.14, 5.15, and 5.16, all of the basalts or basaltic komatiites that host the Big Lake VMS occurrence could be part of the

same oceanic plateau sequence. Apart from weak negative Nb anomalies in some of the hangingwall basalts (discussed below), they are typical of other Wawa plateau basalts. The OIB-like chemistry of the Big Lake footwall basalts could be explained by some degree of mixing with magma from low degrees of partial melting of a mantle plume at garnet-stable depths (as in HIMU OIB), as modeled by Polat (2008) for other transitional to alkaline basalts of the Wawa subprovince.

The mafic-ultramafic geochemistry and relative Zr-Hf depletions of the Big Lake basalts, along with their spatial association with plateau tholeiites of the Pulpwood-Playter Harbours sequence, are supportive of a plume setting. It was also noted in Chapter Four that the occurrence of large shallow ultramafic intrusions or thick flows like the BLUC is consistent with plume-influenced settings, as in the mafic category of the five-fold VMS classification of Franklin et al. (2005). Galley et al. (2007) discussed the evolution of Archean crust as one dominated by mantle plume activity, forming incipient rift basins consisting of basalts and/or komatiites, siliciclastic sediments, iron formation, and mafic-ultramafic sills. Incipient or failed oceanic rift environments are suggested to be productive for VMS (Galley et al., 2007), and it may be that Big Lake formed in such a setting, at least in terms of a plume-derived ultramafic sill or thick flow within mafic-ultramafic volcanic and clastic and chemical sedimentary strata.

5.4.3.2 Arguments for an Arc Setting

Though a plume origin is strongly favoured for the Big Lake komatiitic basalts, a few previously noted features could be consistent with an arc setting. These include the negative Nb anomalies in hangingwall rocks, and the observation that transitional to alkaline basalts have characteristics similar to those of Nb-enriched basalts (NEB) in other parts of the Superior Province.

Relative Nb depletions in hangingwall basalts

Arc basalts can be recognised partly on the basis of negative HFSE anomalies. This is because HFSE (namely Nb, Ti, Zr, and Hf) and HREE are conserved by accessory phases such as rutile and zircon in the subducting slab (Pearce and Peate, 1995), so that the slab-derived fluids that drive the melting of sub-arc mantle wedge are HFSE-

depleted. A higher Th/Yb and Th/Nb ratio (or lower Nb/Nb*) in arc rocks would be present in rocks formed from such fluids as opposed to a more OIB-like source.

The exceptionally high liquidus temperatures of ultramafic lavas increases their likelihood of contamination by assimilation of crust rocks (Naldrett, 1989). The implication at Big Lake is that the hangingwall mafic-ultramafic basalts may have been contaminated specifically by assimilation of the interflow siltstones with strong negative Nb anomalies (Nb/Nb* = 0.1-0.3 in most samples; Fig. 5.9). Assimilation of evolved continental crust can cause an increase in $(La/Sm)_{cn}$ and a decrease in Nb/Nb*, but if siltstone is the contaminant, this is also expected to be accompanied by an increase in SiO_2. The lack of positive correlation between SiO_2 and $(La/Sm)_{cn}$ or SiO_2 and Nb/Nb* (Figs. 5.17 and 5.18) in hangingwall metavolcanic rocks at Big Lake suggests that their weak negative Nb anomalies were not derived from assimilation of crustal material such as the siltstones. Though it has not been shown that assimilation of siltstones has occurred in the hangingwall basalts at Big Lake, their negative Nb anomalies are too small to be conclusive of an arc origin.

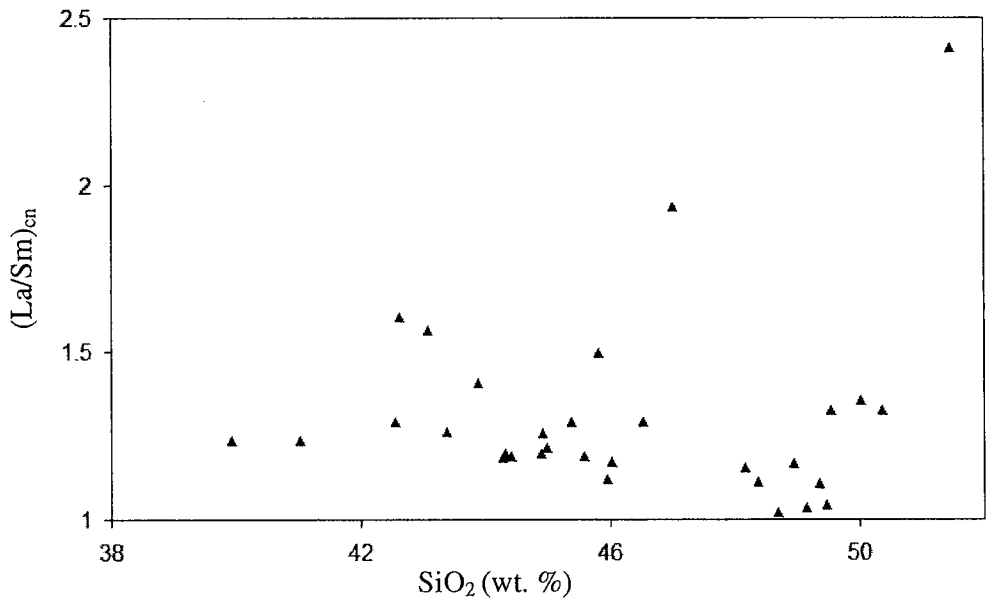

Figure 5.17 - $(La/Sm)_{cn}$ vs. SiO_2 in hangingwall metavolcanic rocks of the Big Lake VMS host sequence.

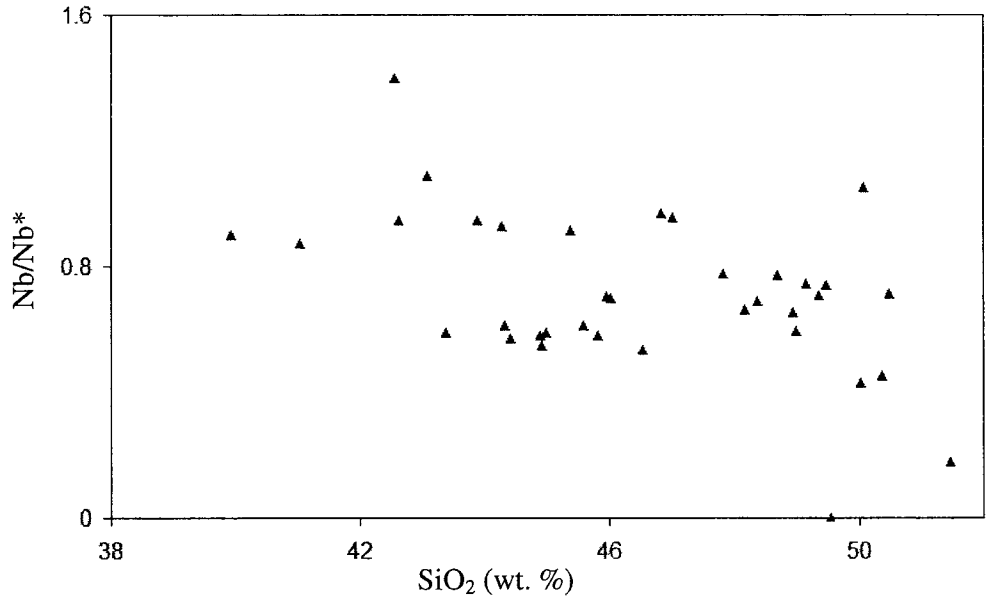

Figure 5.18 - Nb/Nb* vs. SiO_2 in hangingwall metavolcanic rocks of the Big Lake VMS host sequence.

NEB-like chemistry of footwall rocks

Though arc basalts usually display strong negative HFSE anomalies with LREE enrichment, some workers have reported arc-associated basalts with both LREE and HFSE enrichment, showing negative to positive Nb anomalies on trace element patterns with OIB-like characteristics (e.g., Hollings, 2002; Wang et al., 2007). The genesis of these Nb-enriched basalts (NEB) in an arc environment may involve an OIB source component or a component of subduction-modified (adakite/slab-melt enriched) mantle wedge (Wyman et al., 2000). A common association of NEB with adakites implies the latter is a possible scenario in many arc systems, such as in the Wabigoon Subprovince (Wyman et al., 2000). Since adakite-metasomatised mantle should be present in back arc settings, NEB can be indicative of back arc rifts. Owing mostly to high heat flow and/or many subvolcanic intrusions, and the development of synvolcanic faults in an extensional regime, back arc rift settings are cited to be productive environments for VMS (Syme et al., 1996).

Wyman et al. (2000) described Nb-enriched basalts (NEB) in terms of Nb/Th higher than chondrite or mantle-normalised Nb/La (Nb/La_{MN}) between 0.5 and 1.4, and absolute Nb contents greater than 6 ppm. Of the Big Lake samples, 74 of 99 metavolcanic samples yield Nb concentrations greater than 6 ppm (mean 14.8 ppm in the footwall samples and 16.4 ppm in the hangingwall). Using the criteria of Wyman et al. (2000), most footwall samples ($Nb/Nb^* = 0.5\text{-}1.3$ and $Nb/La_{MN} = 0.5\text{-}1.3$) could be considered NEB, with similar trace element patterns to NEB of the Sturgeon Lake belt of the Wabigoon subprovince (Fig. 5.19).

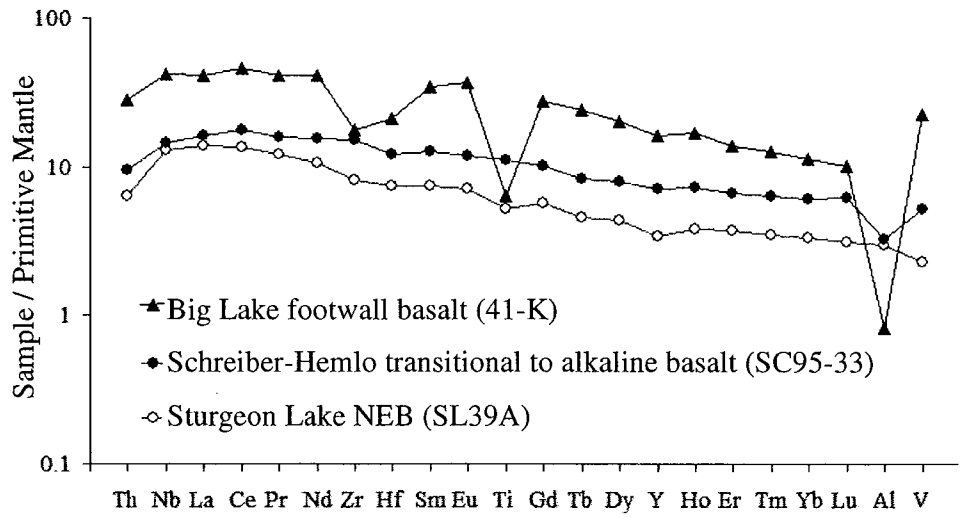

Figure 5.19 - Primitive mantle normalised trace element patterns of a representative Big Lake hangingwall basalt compared to alkaline basalt of the Schreiber-Hemlo belt from Polat (2008), and NEB from the Sturgeon Lake belt from Wyman et al., (2000). Normalising values are from Sun and McDonough (1989).

The Wawa subprovince transitional to alkaline basalts, Big Lake footwall basalts, and Sturgeon Lake NEB share the same OIB-like pattern with REE (particularly HREE) fractionation, convex-upwards LREE, and primitive mantle normalised Nb>Th (Fig. 5.19). If the Big Lake footwall basalts are arc-associated NEB, their association with the unfractionated hangingwall tholeiites could be similar to that proposed by Hollings (2002) between Suite I and III basalts of the Northern Pickle assemblage of the Uchi subprovince. There, NEB-associated tholeiites were proposed to have a back arc as opposed to plume origin, in part due to their association with arc rocks and lack of ultramafic lavas that would be indicative of a plume setting (Hollings, 2002).

However, the rocks of the Pulpwood-Playter Harbours sequence, including those of the study area, are not spatially associated with any adakites, Mg-andesites, or other rocks suggestive of a back arc rift setting. The presence of island arc rocks north of the Playter Harbours sequence were explained by Polat (2008) to be the result of the start of subduction along the edge of the plateau sequence represented by the Playter Harbours sequence. As previously discussed, the NEB-like characteristics of the transitional to alkaline Wawa basalts, including Big Lake footwall basalts, in Figure 5.19 can be explained by mixing of depleted and enriched (OIB-like) mantle plume melt components, shown by Polat (2008) in two-component mixing models. Ultramafic chemistry and relative Zr-Hf depletions in the Big Lake komatiitic basalts are also more consistent with mixing with a deep, low-degree partial melt of a mantle plume.

5.4.4 Summary of Tectonic Setting and Implications for VMS Mineralisation

The footwall and hangingwall basalts at Big Lake are most likely part of the same oceanic plateau sequence, and except for small relative Nb depletions in some hangingwall samples, are typical of other Wawa plateau basalts summarised by Polat (2008). Few non-arc VMS are preserved in the rock record, primarily because of the improbability of preserving mid-ocean ridge settings during subduction-accretion (Galley et al., 2007). Although plume-derived rocks are common in the Archean (e.g., Polat, 2008), plume-influenced oceanic plateau settings are not commonly host to VMS. However, rifting during plume development is thought to be productive for VMS (Franklin et al., 2005). The giant Kidd Creek deposit, for example, may have formed in oceanic lithosphere in which partial melting was induced by a mantle plume (Wyman et al., 1999; Galley et al., 2007).

The distinction between true footwall—essentially all rock extending up to paleoseafloor at the time of VMS mineralisation—and hangingwall of a VMS system is usually an important one, as footwall rocks are often the dominant metal source and may represent source magmas, indicating tectonic setting immediately prior to development of VMS circulation, whereas hangingwall rocks are generally, not always, subject to less hydrothermal alteration and may represent tectonic setting during closure or continued development of a VMS system. In back arc settings, for instance, the onset of rifting can

be recognised by the transition from arc to MORB-like basalts (Franklin et al., 2005), and such transitions are often concurrent with VMS deposits.

VMS mineralisation at Big Lake appears to have occurred during the waning of the transitional to alkaline footwall flows and waxing of the tholeiitic hangingwall flows. While the footwall-hangingwall contact does not likely mark a significant change in tectonic setting (as in an arc to MORB transition, for instance), the apparent timing of VMS mineralisation at Big Lake possibly indicates that the VMS-hydrothermal system formed during cooling of the ponded footwall flows (i.e., the BLUC). It is also possible that venting of VMS-hydrothermal fluids was already occurring, but significant accumulations of sulphides did not occur until the deposition of siltstones in the hangingwall sequence, which may have served to prevent the diffuse escape of hydrothermal fluids by causing them to channel along their base.

5.5 Conclusions

On the basis of a relationship with ultramafic cumulates and a few samples having greater than 18 wt. % MgO, volcanic rocks that host the Big Lake VMS occurrence are basalts or komatiitic basalts. A cumulate centre/base to flow top relationship would account for the chemical similarities and spatial relationship between the BLUC cumulates and footwall basalts. The location of VMS mineralisation at Big Lake is consistent with the idea that the VMS system developed during the cooling of the BLUC-footwall rocks, and/or that VMS-hydrothermal venting was taking place, but sulphides did not accumulate below seafloor until siltstones were deposited in the hangingwall.

In addition to their Ti-Th-Nb-Ta-Yb systematics, previously noted differences in chemistry of the hangingwall basalts compared to footwall-BLUC rocks (including higher silica and lower MgO, Co, Cr, and Ni) support the notion that the BLUC-footwall and hangingwall rocks are derived from two geographically and chemically distinct, but both plume-derived, sources. Both footwall and hangingwall basalts are typical of other Wawa subprovince oceanic plateau basalts summarised by Polat (2008), except for the small negative Nb anomalies in some hangingwall rocks.

As explained in section 5.4.1, the overlap in hangingwall and footwall volcanic rock chemistry (i.e., some transitional to alkaline basalt flows within the tholeiitic hangingwall) is reflective of volcanic input from two separate eruptive centres over a short period of time, rather than a sudden change in chemistry of one centre. If both footwall and hangingwall basalts are plume-derived as suggested here, these local variations lend support to the idea of Polat (2008) of eruption of variably enriched plateau basalts from a heterogeneous mantle plume in Wawa subprovince plateau sequences.

Chapter 6
Mineralisation

6.1 Introduction

The ore mineralogy of most VMS deposits consists of chalcopyrite, pyrrhotite, sphalerite, pyrite, and galena, in no strict order of abundance, with minor phases that may include magnetite, arsenopyrite, bornite, tetrahedrite-tennantite, molybdenite, cobaltite, or stannite, among others (Lydon, 1984). Although a general process of base metal precipitation from upward-convecting fluids is common to all VMS, their variable footwall compositions, temperatures, water depths, degrees of fluid mixing, and a number of other factors produce significant variations in metal contents and ore textures both between and within individual systems (Galley et al., 2007). It follows that specific ore mineral assemblages and distributions can help to constrain conditions of VMS formation, such as temperature, pH, or proximity to seafloor. In this chapter the sulphide assemblages, textures, and metal distributions of the Big Lake VMS occurrence are summarised and later discussed in terms of conditions of its formation.

6.2 Sulphide Textures

The mineralised zone of the Big Lake VMS occurrence consists of veined or wispy to semi-massive pyrrhotite, chalcopyrite, and sphalerite, in decreasing order of abundance, at up to 80% sulphides by volume over a few metres (Fig. 6.1). Other metal-bearing phases include galena (1-2 modal % in samples with ~75% sulphide), cobaltite (2-3 %), pyrite (<1 %), and minerals of the linnaeite-violarite series (<1 %). This assemblage of pyrrhotite-chalcopyrite-sphalerite (±galena, ±cobaltite) is hosted within hydrothermally-altered metavolcanic rock, and with the exception of higher amounts of chalcopyrite towards the southern part of the occurrence, does not differ significantly throughout the occurrence. Sulphide veins are generally parallel to bedding planes if present, mostly against upper contacts of uppermost siltstone units (Fig. 6.1d-f). Sulphide veins are also mostly parallel to each other, and no cross-cutting relationships are evident at any scale. "Chalcopyrite disease," or very small inclusion trains of chalcopyrite in sphalerite, was observed in most sphalerite at Big Lake.

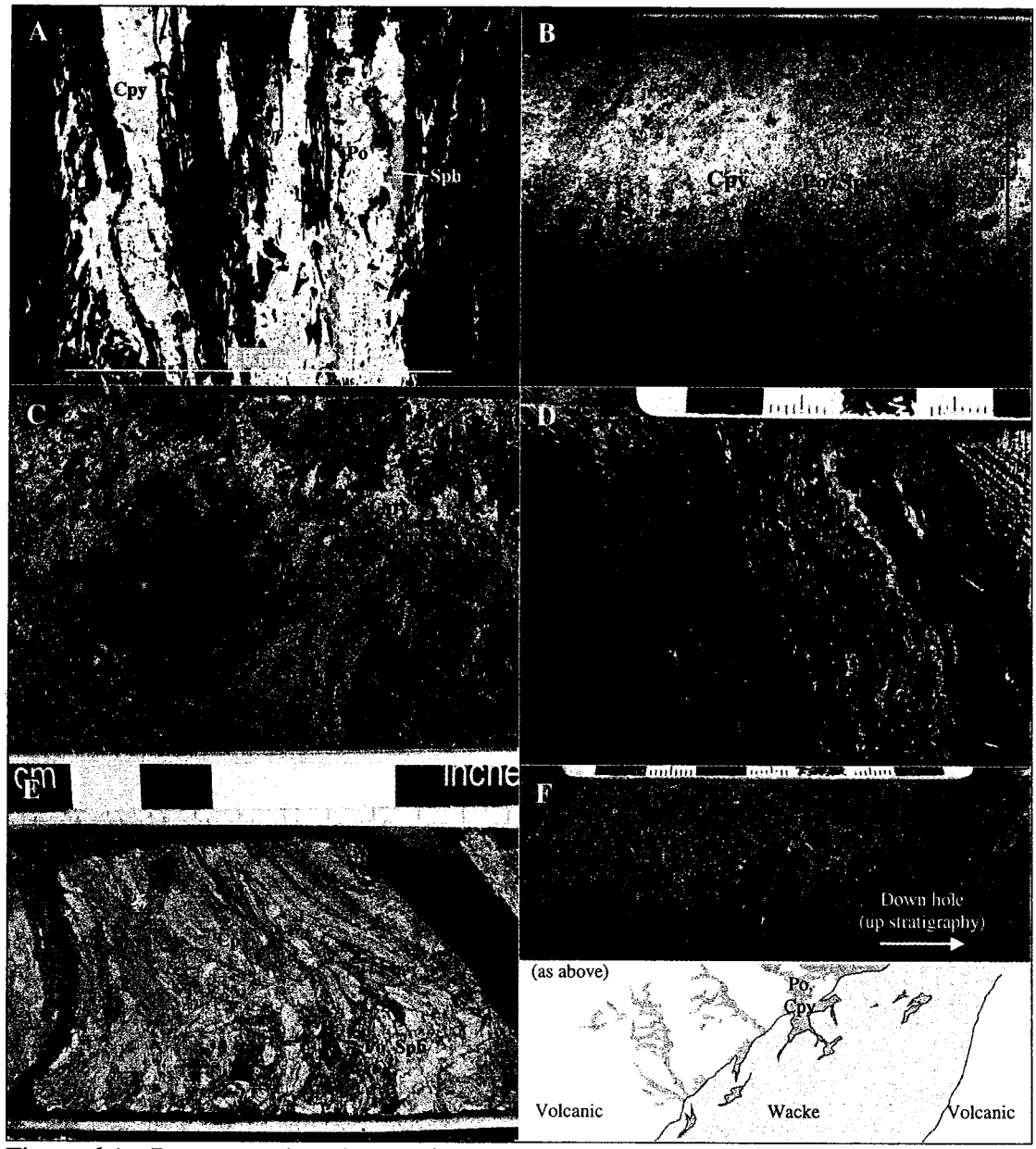

Figure 6.1 - Representative photos of VMS mineralisation at Big Lake. Down hole is to the right in all core photos. A) Typical stringer/vein textures of sulphides hosted in hydrothermally altered metavolcanic rock (sample B682321, reflected light, PPL). B) Best-mineralised intervals have a semi-massive or diffusely banded habit of chalcopyrite and pyrrhotite ± sphalerite. C) Pyrrhotite-chalcopyrite veins surrounding an apparently undeformed siliceous (siltstone?) fragment (Wet core, cut surface). D) Near contacts between metavolcanic and sedimentary units, sulphide veinlets are generally parallel to bedding planes (Wet core, cut surface). E) Some upper contacts (stratigraphic bottoms) of siltstone are marked by brecciated intervals of sulphides surrounding rotated siltstone fragments (Cut surface). F) Sulphide content generally increases against upper contacts (stratigraphic bases) of uppermost siltstone units, at both metre and centimetre scales. Cpy = chalcopyrite, Po = pyrrhotite, Sph = sphalerite.

6.3 Metal Distributions

Best-mineralised drill core intervals of the Big Lake VMS occurrence contain 5.7 % Cu and 1.8 % Zn weighted over 7.0 metres, with significant enrichment in Au, Ag, Pb, and other metals as summarised in Table 6.1. Though 300 ppm Zn is considered typical for VMS stringer zones (compared to ~100 ppm in unmineralised mafic rock; Franklin, 2006), samples with greater than 750 ppm Zn are considered here to define well-mineralised metavolcanic rock of the Big Lake VMS occurrence. Only a limited comparison can be made to metal contents of other VMS deposits/occurrences, in part because the Big Lake occurrence is not a producing mine (average ore grades cannot be calculated).

Table 6.1 - Representative metal contents in well-mineralised Big Lake VMS samples. Analyses are by ALS Chemex. For comparison, "VMS Mean" values are from Franklin et al. (2005), of ore grades from 76 deposits of the mafic category.

Sample ID	B682384	B682387	B683727	B682388	B683696	B684077	VMS Mean
Ag (ppm)	450	181	46.4	50.7	6.06	0.48	10.62
Au (ppb)	8650	2120	274	257	71	4	1400
Bi (ppm)	58.5	39.9	20.7	9.81	2.09	0.49	
Cd (ppm)	192	108.5	51.7	23.2	6.98	1.41	
Co (ppm)	1195	1370	441	240	78.9	72.2	
Cu (ppm)	135000	116500	24200	29200	3200	366	18200
Fe (%)	29.2	26	16.5	12.15	5.59	7.9	
Mn (ppm)	842	1055	1640	2020	875	1410	
Ni (ppm)	646	590	541	309	146.5	349	
Pb (ppm)	3820	2060	1085	529	127.5	21	200
Pd (ppb)	11	37	9	5	2	5	
Pt (ppb)	3.9	3	12	4.5	3.8	5.4	
Zn (ppm)	47500	25800	11300	5120	1520	761	8400

Similarities in behaviour between metals in VMS-mineralised samples (with Zn >750 ppm, n=268) are shown in Table 6.2. The significance of some of these correlations is addressed in the discussion, but in general, higher correlations can be indicative of origin from the same fluid, or a function of similar ion charge or size yielding similar chemical behaviour (e.g., Cd isostructural with Zn in sphalerite). Of particular note in this table are the strong correlations between zinc, cadmium, bismuth, and indium (R^2 = 0.85-0.99), and the correlation between copper and silver (R^2 = 0.91). In these well-mineralised samples, copper and zinc share a weaker correlation (R^2 = 0.63), indicative of variable Cu/Zn ratios that may reflect Cu-Zn zoning discussed later.

Gold does not share a significant correlation with any other metals assayed, but is more strongly correlated with Cu ($R^2 = 0.18$) than with Zn ($R^2 = 0.10$).

Table 6.2 – Squared Pearson correlation coefficients for metals plus As, S, Se, and Te in Big Lake samples with >750 ppm Zn. R^2 values >0.85 are in bold. n=268

	Ag	Au	Cd	Cu	Pb	As	Bi	Co	Fe	In	Ni	Pd	Pt	S	Se	Sn	Te
Ag						0.26	0.69	0.65	0.67	0.78	0.02	0.06	0.02	0.73	0.78	0.66	0.77
Au	0.23					0.00	0.14	0.11	0.09	0.08	0.00	0.01	0.00	0.24	0.14	0.08	0.16
Cd	0.66	0.11				0.27	**0.88**	0.74	0.64	**0.90**	0.03	0.10	0.01	0.66	0.81	0.75	0.64
Cu	**0.91**	0.18	0.66			0.31	0.68	0.67	0.72	0.82	0.02	0.05	0.02	0.70	0.84	0.70	0.73
Pb	0.57	0.11	0.78	0.53		0.20	0.78	0.63	0.53	0.67	0.02	0.13	0.02	0.52	0.64	0.58	0.54
Zn	0.63	0.10	**0.99**	0.63	0.78	0.25	**0.85**	0.71	0.62	**0.87**	0.03	0.10	0.01	0.68	0.77	0.72	0.60

Three-dimensional metal distributions at Big Lake define a surface of mineralisation shallowing with depth and to the north, as shown in plan view and cross sections in Figure 6.2. In general, metal concentrations are highest in the southern part of the mineralised sheet. Cu/Zn ratios are shown in Figure 6.3, and are generally highest where total metal contents are highest.

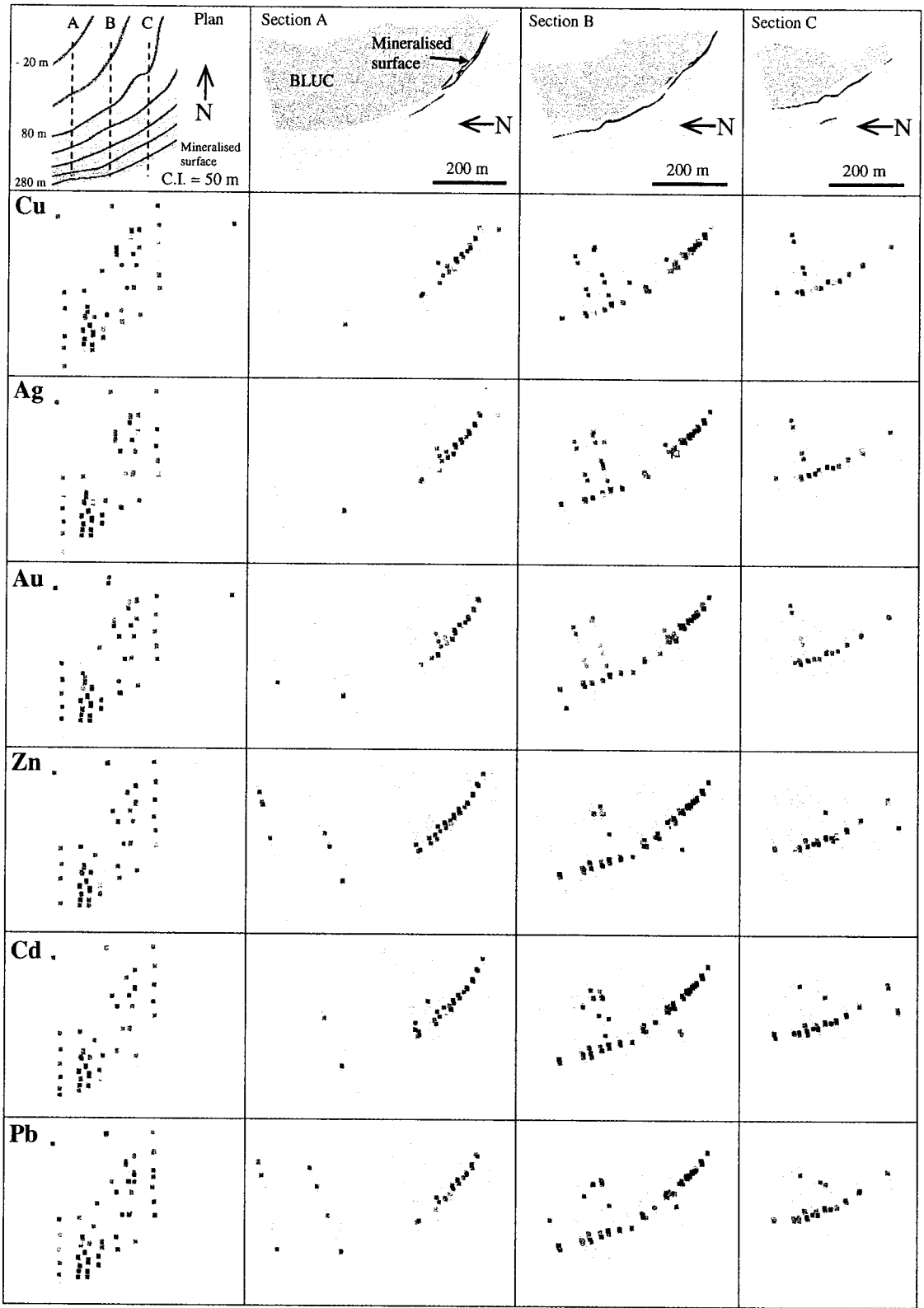

Figure 6.2 - Plan and section views showing metal distributions through the Big Lake VMS occurrence. Blue and grey are low assay values, red are high.

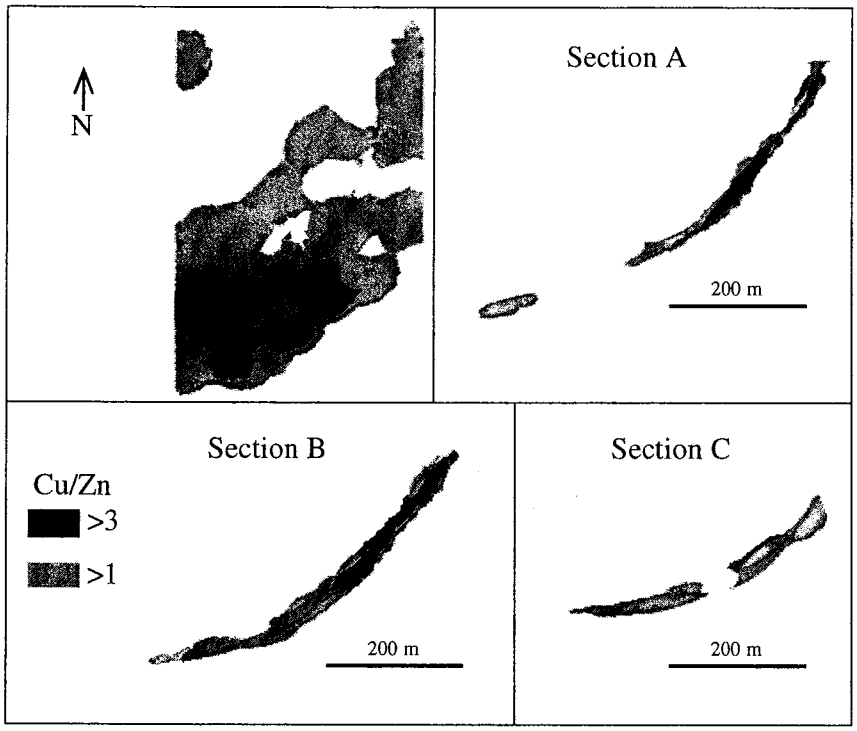

Figure 6.3 - Cu/Zn ratio shells through metavolcanic rock of the Big Lake VMS occurrence. Plan view and sections are the same as in Figure 6.2. Shells were modeled using Leapfrog methods described in Chapter Two.

6.4 Discussion

In general, the sulphide assemblages (pyrrhotite-chalcopyrite-sphalerite ± galena and cobaltite) and metal contents (Table 6.1) of the Big Lake VMS occurrence are consistent with the VMS class of deposits, as summarised by many workers including Franklin et al. (2005) and Galley et al. (2007). In particular, the veined sulphide textures at Big Lake (Fig. 6.1) are consistent with stringer or stockwork zones of VMS deposits. However, given that all mineralisation occurs in rock with a strong planar fabric, these textures may be at least in part a result of post-VMS deformation and/or metamorphism. Regardless, the pyrrhotite-chalcopyrite-sphalerite assemblage, accompanied by hydrothermal alteration minerals and textures, almost certainly originated by VMS-hydrothermal processes.

Due to the absence of cross-cutting relationships, petrographic examination of sulphide assemblages has yielded little information on the paragenetic sequence at Big Lake. However, the general lack of pyrite may be used to infer a replacement of early pyrite-sphalerite assemblages by massive chalcopyrite-pyrrhotite-sphalerite, as would be expected in most VMS deposits (Franklin et al., 2005). This is discussed later in the

context of zone refining at Big Lake. Chalcopyrite disease in sphalerite (Fig. 6.1c) is not necessarily a primary replacement texture in the Big Lake samples, but may instead indicate subsolidus exsolution during crystallisation.

Because an assemblage of pyrrhotite-chalcopyrite-sphalerite (± galena, cobaltite) hosted within hydrothermally-altered metavolcanic rock is typical of VMS mineralisation, the Big Lake occurrence should share some aspects of its genesis with other VMS deposits, where metal distributions have well-reasoned implications for heat flow and proximity to seafloor, among other factors. The processes responsible for VMS metal distributions are reviewed in the next section, and are then discussed as they relate to the Big Lake VMS occurrence.

6.4.1 Review of Metal Zoning Processes

A common characteristic of VMS deposits is a lateral and vertical sulphide zonation of the massive ore lenses, and to a lesser extent in some stringer zones (Lydon, 1988). This was first described by Sangster (1972) as zone-refining, where sphalerite-pyrite ore is replaced by higher-temperature chalcopyrite-pyrrhotite, producing a zonation from base to top, and from the middle to lateral extremities, of chalcopyrite-pyrrhotite-pyrite to sphalerite-pyrite ± galena. Some workers have identified ore replacement textures within ore lenses to support this process (e.g., "preservation of vestiges of massive pyrite and sphalerite within chalcopyrite-pyrrhotite ore" at Kidd Creek; Gibson et al., 2003), but some lenses do not display any systematic zoning, cryptic or otherwise (Solomon et al., 2004).

The zoning of Cu and Zn-Pb in VMS systems is in part a function of differing solubilities of metals at different points throughout a hydrothermal system. The general factors of ion size (larger ions are less mobile) and charge (ions with higher valence are less mobile) apply in hydrothermal systems, along with the more complicated and far more significant factors of solubility in complexes. Many studies have shown that the aqueous solubilities of most base and precious metals are very low as individual dissolved ions, but increase dramatically when in complexes (e.g., Loucks and Mavrogenes, 1999; Berry et al., 2006; Stefansson, 2004). The effectiveness of metal complexing agents is dependent on their concentration, as well as on temperature,

pressure, and other factors including pH and Eh. These agents may include other (non-aqueous) volatile phases such as CO_2, SO_2, HCl, H_2, HF, H_2S (Williams-Jones and Heinrich, 2005), and non-volatile ligands including CH_4, S, H, O, and particularly Cl (Loucks and Mavrogenes, 1999; Franklin et al., 2005).

As bisulphide complexing requires colder and more alkaline conditions than is normal for VMS systems (Ioannou et al., 2007), chloride complexing is the most significant means of transport and deposition of Cu, Zn, and Pb in VMS systems (Figs. 6.4 and 6.5). Cu is transported largely as chloride complexes $[CuCl_2]^-$ and $[CuCl_4]^{2-}$ at temperatures below 500°C (Berry et al., 2006), which form by reaction with free Cl^-:

$$CuCl_2 + 2Cl^- = CuCl_3^- + Cl^- \leftrightarrow CuCl_4^{2-}$$

Zn also occurs primarily as chloride complexes $[ZnCl_3]^-$ and $[ZnCl_4]^{2-}$ in vent fluids (Bourcier and Barnes, 1987) but, as shown in Figure 6.4, behaves differently in pH-T space.

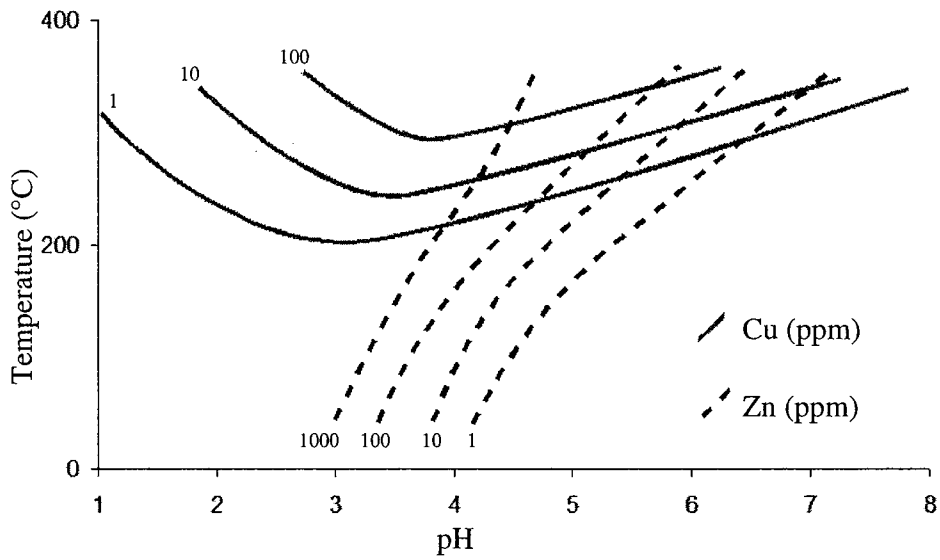

Figure 6.4 - Approximate Cu and Zn solubilities as a function of temperature and pH in a typical VMS fluid with salinity of 1 m NaCl-$CaCl_2$ equivalent. Cu and Zn are in chloride complexes. Pb curves, not shown, are approximately parallel to and 1 pH left of the Zn solubility curves. The dip in solubility of Cu reflects a change in the Cl^-/Cu^{2+} ratio between two Cu chloride complexes. From Franklin et al. (2005).

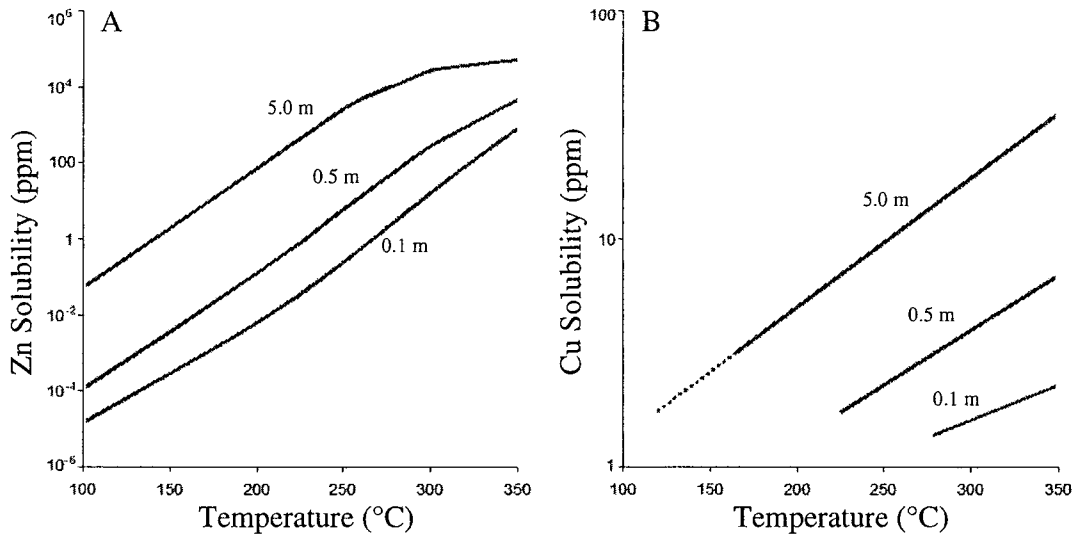

Figure 6.5 - Metal solubilities as chlorides vs. temperature in a pH = 5.0 fluid, numbered lines indicating different salinities (m NaCl-$CaCl_2$ equivalent). A) Zn chloride solubility vs. temperature. B) Cu chloride solubility vs. temperature. From Ioannou et al. (2007).

Key relationships shown in Figures 6.4 and 6.5 are: (1) a lower pH or higher temperature results in higher base metal solubilities; (2) in chloride complexes, Cu solubility is more temperature dependent than Zn (and Pb); (3) higher salinities increase metal chloride solubilities; and (4) Cu is effectively insoluble below 200°C, while Zn and Pb may remain in solution at T < 200°C and low pH. The last point is relevant to sulphide zonation as it describes the tendency for chalcopyrite (+ pyrrhotite) to precipitate in place of sphalerite (+ pyrite ± galena) as temperature increases during development of an ore lens; this is part of the "zone refining process" of Eldridge et al. (1983) discussed earlier. It also accounts for the segregated nature of these ore minerals at the scale of both ore lens and individual sulphide stringers, as shown in Figure 6.1.

6.4.2 Zone Refining at Big Lake

Cu-Zn zonation in VMS stringer zones or pipes, if present, is usually recognised on the order or tens to hundreds of metres (Franklin et al., 2001), and reflects zone refining during increasingly channelled flow of fluids towards the seafloor. At Big Lake, some degree of Cu-Zn zonation at a plan scale of ca. 500 x 500 m reflects an inconsistent degree of chalcopyrite-pyrrhotite deposition at the expense of sphalerite, which could have occurred in any part of a VMS system (Fig. 6.3). If the original geometry of the

occurrence were better preserved, a vertical component of zonation would indicate lens or near-surface mineralisation. However, the original geometry has not been preserved at Big Lake, and no vertical component of Cu-Zn zonation can been observed. Thus, while there is clear evidence for zone refining at Big Lake, consistent with it being a VMS system, the Cu-Zn zoning provides no argument for the depth at which the sulphides were precipitated.

6.4.3 Depth of Sulphide Precipitation

There is some evidence to suggest that the sulphides of the Big Lake occurrence were deposited some distance below the seafloor. A stronger partitioning of Au with Cu than with Zn (Table 6.2) and a lack of Sn-Hg-Bi-Te mineral phases are consistent with a higher-temperature zone of precipitation. A pyrrhotite-dominated sulphide assemblage also indicates a higher temperature of mineralising fluids (>350 °C), which is not typically encountered near the seafloor (Nimis et al., 2006). The lack of pyrite in VMS-mineralised parts of the Big Lake sequence cannot be the result of metamorphic breakdown to pyrrhotite, since some adjacent metasedimentary rocks contain up to 10% pyrite with no indication of pyrrhotite replacement. Veining or diffuse banding textures throughout the Big Lake VMS occurrence are also consistent with sub-seafloor deposition or replacement as opposed to precipitation from an open water column. Finally, a sub-seafloor style of mineralisation may explain, at least in part, the tabular or sheet-like pattern of mineralisation spreading hundreds of metres along a paleohorizontal surface (basal siltstone contacts) in a flow-dominated setting.

However, this stringer zone argument is weakened by poor constraints on the role of deformation on the sulphide distributions, and the possibility of erosion of the VMS prior to its deformation. Upper greenschist facies metamorphism in a shear zone, including possible episodes of hydrothermal metamorphism unrelated to VMS formation, could explain some of the features discussed above, including lower Sn+Hg+Bi+Te contents in the mineralised zone. For instance, these metals may have been remobilised by fluids through a shear structure, rather than by zone refining during the development of a VMS stringer zone. Because the sulphides are hosted in sheared rock immediately adjacent to a siltstone unit, it also is possible that the occurrence instead represents a

strongly deformed and perhaps partially eroded part of a VMS lens, in which sulphides were originally precipitated from an open water column (and stringer textures are secondary). These possibilities are explored in the next two chapters.

6.5 Conclusions

The mineralised zone of the Big Lake VMS occurrence consists of pyrrhotite-chalcopyrite-sphalerite (± galena, cobaltite) associated with hydrothermal veining. This mineral assemblage most likely originated by VMS processes. The sulphides define a thin (< 10 m), locally anastomosing surface against and parallel to the upper contact of the uppermost siltstone unit. Total metal contents and Cu/Zn ratios are highest in the southern part of the mineralised sheet. A sub-seafloor style of mineralisation is proposed based mostly on its sulphide textures, geometry and relationship to siltstone contacts, and pyrrhotite-dominated sulphide assemblage.

Chapter 7

Alteration Patterns and Geochemistry

7.1 Introduction

It was stated in Chapter Five that many geochemical arguments rely on immobile elements. In some contexts, however, recognition of element mobility is useful. It is the relative mass gains and losses of certain elements in VMS-hydrothermal systems that allow these systems to be fingerprinted and recognised at both regional and local scales.

Vent fluids of both modern and preserved VMS occurrences have been loosely constrained to within the conditions listed in Table 7.1. Exceptions to the listed characteristics are that fluids with pH below 2 may be generated by boiling or magmatic input, and fluids with density >1.0 g/cm^3 may occur if the fluid is supercritical or if it has interacted with evaporite (J. Franklin, pers. comm., 2009).

Table 7.1 - General characteristics of seafloor vent fluids

Temperature	150-400 °C (Large, 1992)
pH	2-6 (Embley et al., 2006)
Eh	Reducing
Salinity	6.0-32.4 wt. % NaCl / $CaCl_2$ equivalent (e.g., Ioannou et al., 2007)
Density	Less or greater than seawater, ~1.0 g/cm^3 (Ioannou et al., 2007)
$\delta^{18}O$	-0.5 – 3.5 (Paquette-Mihalasky, 1999)

These vent fluid characteristics are in marked contrast to cold, alkaline, SO_4-rich, metal-poor, and (in modern settings) oxidising ocean water with ~3.2 wt. % Cl salts (Bischoff and Rosenbauer, 1988). The changes to seawater composition during circulation and eventual release at vents can be mostly attributed to footwall interactions, magmatic input, or a combination of the two (Franklin et al., 2005). For instance, hydration reactions at low water-rock ratios increase salinity along with leaching of K^+, $Fe^{2+/3+}$, and other cations in the reaction zone underlying VMS vents (e.g., Ioannou et al., 2007). The presence of native sulfur at some boiling vents is suggestive of these pH-reducing reactions:

$$SO_2 + H_2O \leftrightarrow HSO_3^- + H^+$$

and $$3SO_2 + 2H_2O \leftrightarrow S(s) + 2H_2SO_4$$

The water-rock interactions that produce these changes in water composition are also responsible for changes in seafloor composition. This footwall alteration is an important and recognizable signature of a VMS system, and is known to occur at both circulation-related regional (kilometres) and vent-related local (metres to hundreds of metres) scales.

This chapter is a summary of hydrothermal alteration mineral assemblages and their spatial distributions at Big Lake, defined by chemical alteration indices and by visual estimation in core samples. $\delta^{18}O$ distributions are also discussed in this context, as they are controlled in part by temperatures and water/rock ratios involved in hydrothermal alteration. Most observations are necessarily limited to local (i.e., likely discharge-related) hydrothermal alteration. Comparisons are then made to alteration patterns observed in well documented VMS systems.

7.2 Alteration Mineralogy and Chemistry

In Chapter Four, it was suggested that regional metamorphism at the Big Lake property is of upper greenschist to lower amphibolites facies (based on the garnet-biotite assemblage in metapelite units, and on the actinolite-chlorite assemblage in metavolcanic units), consistent with regional metamorphic grades estimated by other workers through the Playter Harbours sequence (Polat et al., 1998). At Big Lake, regionally metamorphosed *hydrothermal* mineral assemblages, as opposed to regional metamorphic mineral assemblages of least-altered protolith, can be recognised on the basis of their darker colour and textures suggestive of fluid flow (e.g., network veining, Fig.7.1a), as well as visible amounts of veined and diffuse biotite-phlogopite (Fig. 7.1a,c-e) and anthophyllite (Fig. 7.1d). Most hydrothermal alteration at Big Lake also includes diffuse silicification (5-10 % recrystallised quartz by volume; see Appendix B for thin section descriptions) that is not readily apparent in hand sample. Diffuse carbonate alteration (<10 modal % calcite) is present even in least-altered metavolcanic samples at Big Lake, but may be slightly more abundant in strongly altered rocks. Also worth noting at Big Lake is an absence of sericite, or potassic alteration in general, associated with the sulphide mineralisation.

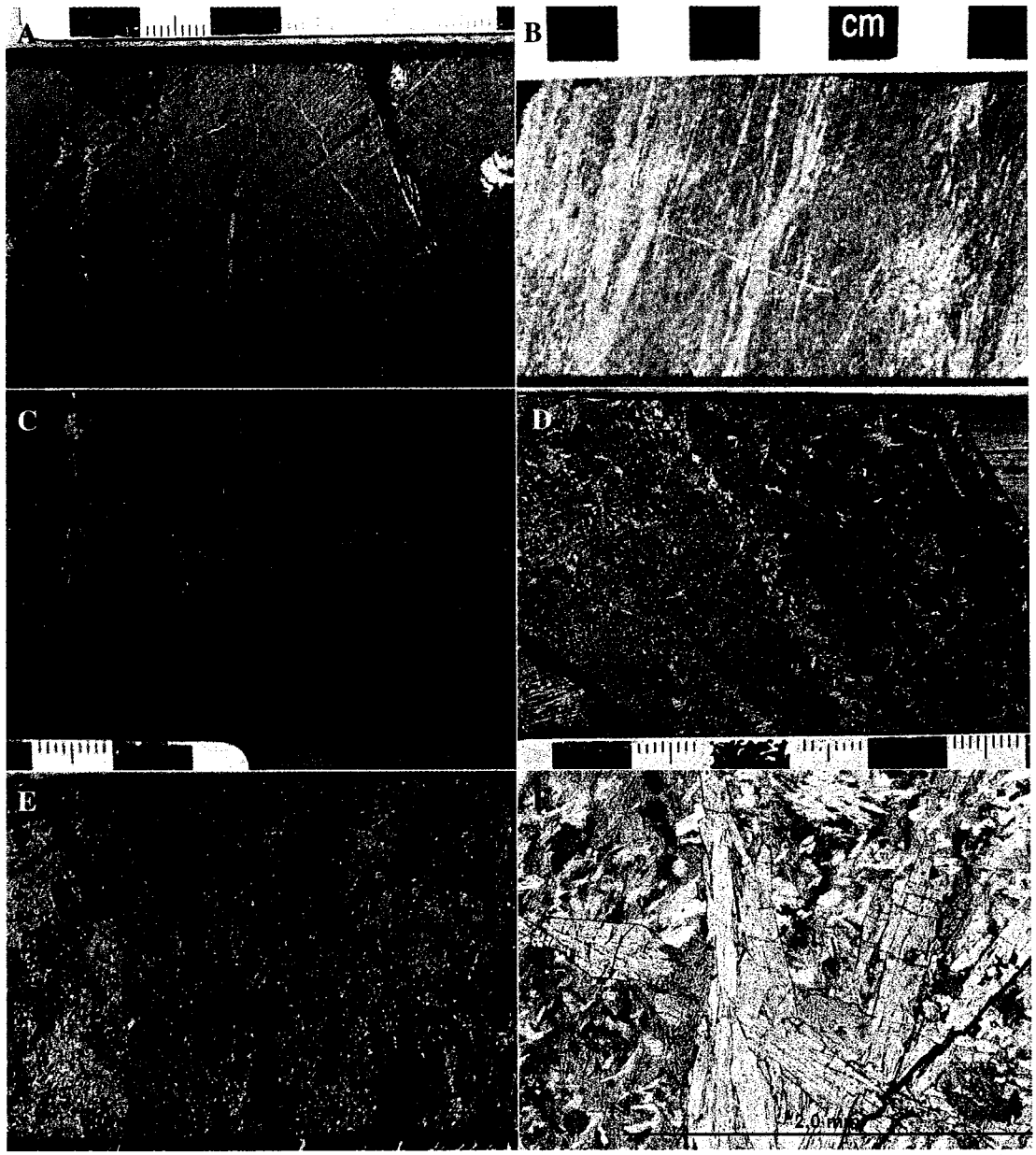

Figure 7.1 - Representative core and thin section photos of hydrothermal alteration associated with VMS sulphides in metavolcanic rocks at Big Lake. A) Hydrothermal alteration is evident in diffuse brown mica (biotite-phlogopite) veins (Cut surface, Hole 32). B) One of few hydrothermally altered intervals in which lighter colour is imparted by ~30% talc (this interval contains very little carbonate). C) Hydrothermal alteration is usually accompanied by darker colour due to increasing biotite content and/or darker chlorite (Hole 73). D) Biotite-chlorite alteration with ~10% anthophyllite visible as lighter radiating fans and veins (Cut surface, Hole 32). E) Sulphides are associated with strongest degrees of hydrothermal alteration (Cut surface, Hole 24). F) Anthophyllite fans in biotite, as in photo D (sample B683718, PPL).

In hydrothermally altered samples associated with VMS mineralisation at Big Lake, there is little distinct variation in relative amounts of chlorite, biotite-phlogopite, anthophyllite, or talc relative to the overall degree or intensity of visible hydrothermal alteration (Table 7.2), as determined in hand sample using the qualitative method described in Chapter Two (Section 2.5). Veined talc, chlorite, anthophyllite, and biotite-phlogopite have been observed across the range of degrees of hydrothermal alteration, but anthophyllite and talc are less commonly seen in weakly altered samples, and anthophyllite is most common in strongly altered samples (Table 7.2). Bias may be significant, as pale green anthophyllite is more easily identified in darker coloured or more strongly altered core samples (e.g., those with higher biotite and darker chlorite contents), though it is generally absent in thin section of least-altered rocks.

Table 7.2 - Sample counts in categories of hydrothermal alteration mineral assemblages and weak, moderate, and strong hydrothermal alteration as defined in Chapter Two

Hydrothermal alteration mineral assemblage	Degree of hydrothermal alteration		
	Weak	Moderate	Strong
Chlorite±biotite-phlogopite only	28	17	3
Chlorite-talc±biotite-phlogopite	9	12	8
Chlorite-biotite-phlogopite-anthophyllite±talc	1	6	7

Least and most altered samples can be distinguished geochemically, as shown in Figure 7.2. Most of the least-altered metavolcanic samples have Na_2O and MgO contents of 1.8-4.1 wt. % and 4.0-18 wt. %, respectively, whereas most of the strongly altered samples (having greater than 30% hydrothermal minerals by volume, in dense net-textured veins, in places obscuring primary textures) contain less than 1.5 wt. % Na_2O and 11-21 wt. % MgO. Other possible means of estimating degrees of hydrothermal alteration, such as the alteration index $(Fe_2O_3(total) + MgO) / (K_2O + Na_2O)$ used by Lentz (1999), or loss on ignition values, are apparently of more limited use in defining intensity of hydrothermal alteration through the Big Lake VMS occurrence, as shown in Figure 7.3.

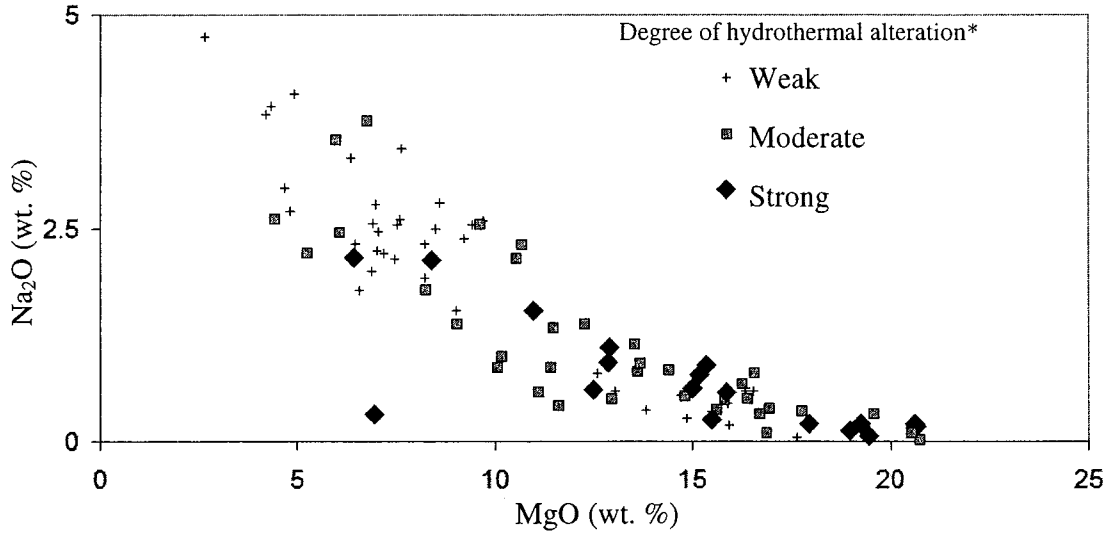

Figure 7.2 - Na_2O vs. MgO in metavolcanic samples of the Big Lake VMS host sequence. *Degrees of hydrothermal alteration were assigned using the method described in Chapter Two.

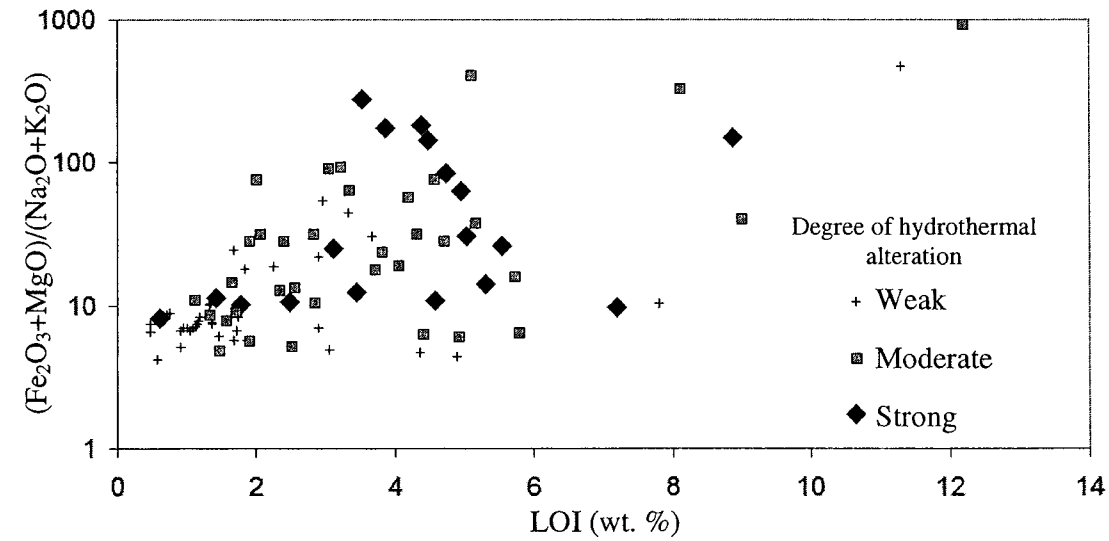

Figure 7.3 - Alteration index used by Lentz (1999) vs. loss on ignition in metavolcanic samples of the Big Lake VMS host sequence.

The alteration box plot of Large et al. (2001) was developed in order to reveal chemical variations related to VMS-hydrothermal alteration, and can be applied to mafic rocks. It is a plot of the Ishikawa (1979) Alteration Index ($100\ [K_2O + MgO] / [K_2O + MgO + Na_2O + CaO]$) in which high numbers are expected to reflect breakdown of feldspars at the expense of sericite and chlorite, against the Chlorite-Carbonate-Pyrite

(CCP) Index *(100 [MgO + FeO] / [MgO + FeO + Na_2O + K_2O]* in which high numbers are expected to reflect increasing chlorite content, as well as possible Mg-Fe-carbonate and pyrite, all of which generally form in alteration pipes below VMS deposits (Large et al., 2001). Big Lake metavolcanic rocks are plotted in the alteration box plot in Figure 7.4. Only 30 analyses included ferrous iron (FeO), required for calculation of the CCP Index, so Figure 7.5 instead includes an index more closely resembling the alteration index used by Lentz (1999): *100 [Fe_2O_3 + MgO] / [Fe_2O_3 + MgO + Na_2O + K_2O].* Numbers generated by this index and the CCP Index are nearly identical at high values (Fig. 7.6), so sample distributions along the y axes of Figures 7.4 and 7.5 are comparable.

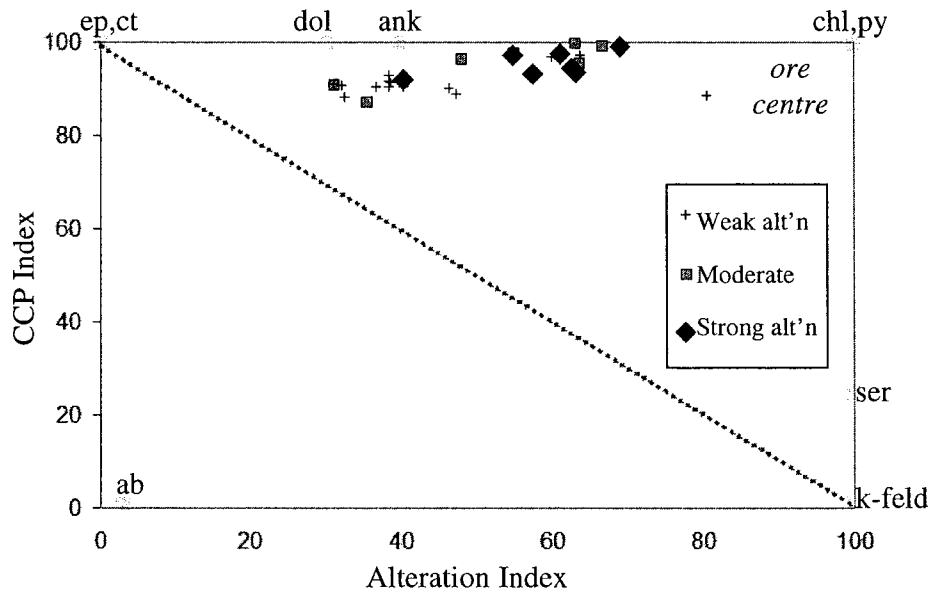

Figure 7.4 - Alteration box plot of Large et al. (2001), with Big Lake metavolcanic samples grouped according to degrees of visible hydrothermal alteration. ep=epidote, ct=calcite, dol=dolomite, ank=ankerite, chl=chlorite, py=pyrite, ser=sericite, k-feld=k-feldspar, ab=albite.

In both figures, Big Lake samples have high CCP indices, due mostly to their ultramafic-mafic character with high Mg and Fe contents and low alkali element contents even in least-altered samples (the CCP index is perhaps best applied to rocks with higher alkali contents). The Big Lake samples occupy a near-horizontal trend towards high CCP and AI that approximates the chlorite-carbonate trend, which is normally traced by samples located immediately below massive sulphide lenses (Large et al., 2001).

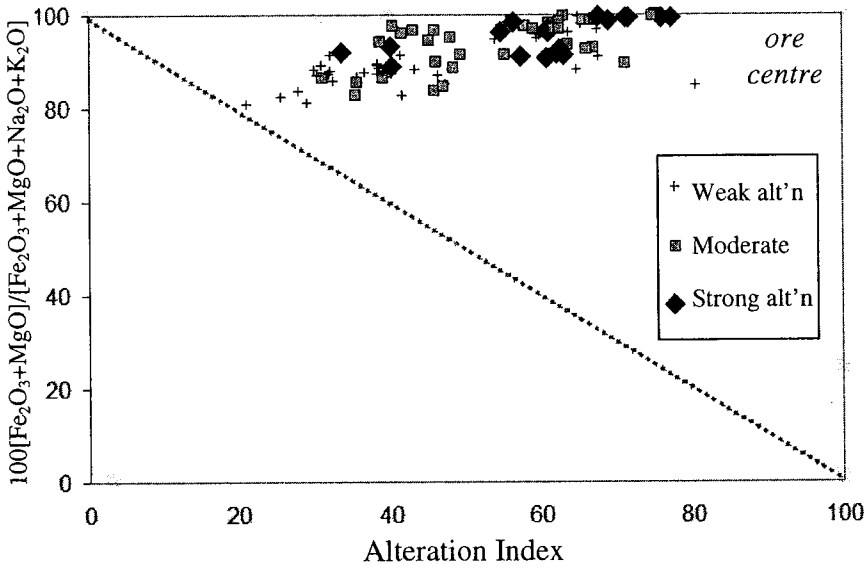

Figure 7.5 - Modified alteration box plot of Large et al. (2001), including Big Lake samples without FeO analyses. Some mineral end members of Figure 7.4 do not include ferric iron, so are not included in this diagram.

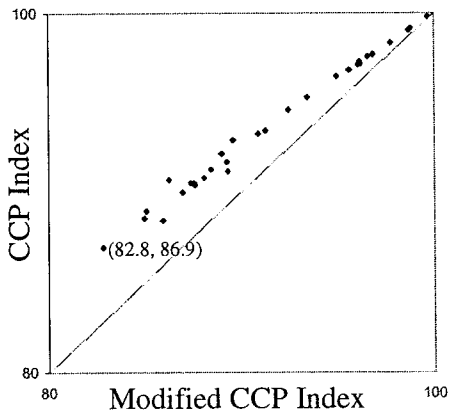

Figure 7.6 - Comparison of sample values calculated from the CCP Index and from the modified CCP Index (*100 [Fe_2O_3 + MgO] / [Fe_2O_3 + MgO + Na_2O + K_2O]*) used in Figure 7.5.

7.3 Alteration Distributions

Hydrothermal alteration of the Big Lake VMS occurrence, recognised either on the basis of darker colour and fluid flow textures or by geochemical indices, is mostly confined to within and up to ten metres above VMS-mineralised rock, as illustrated by Mg assay distributions in Figure 7.7. The hydrothermal alteration also mimics metal distributions in that it is generally most intense immediately above the uppermost siltstone package (Fig. 7.7). The field of view shown in Figure 7.7 is one of very few in

which Mg assays, or any other relevant data, are sufficiently dense to allow for useful observation at metre scales.

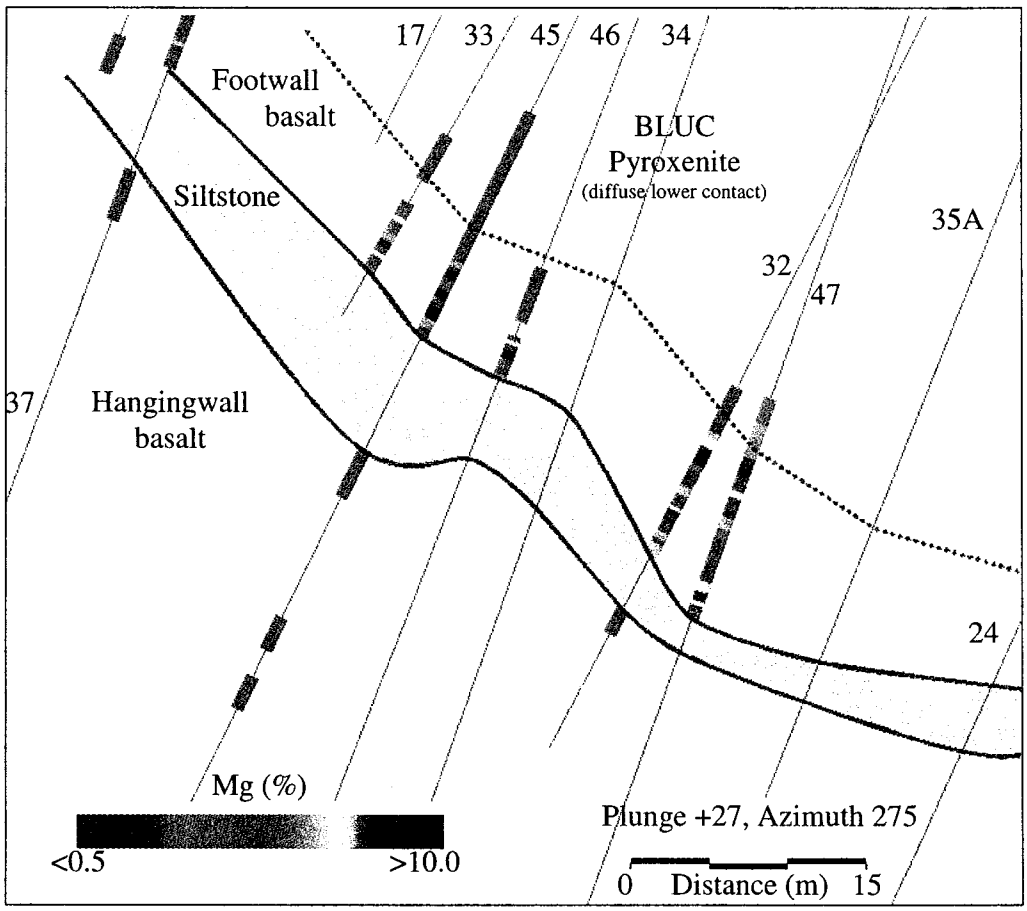

Figure 7.7 - Mg (wt. %) assay values through metavolcanic rocks and cumulates of the Big Lake VMS occurrence. Plunge and azimuth of view (down and to the west) are indicated above scale, and numbers beside drill traces are drill hole numbers. Mg assay data are shown because of their high density of sampling in the metavolcanic rocks, compared to a low density of whole-rock data over the area of study that severely limits the use of alteration indices or ore vectors such as Tl, P_2O_5, Eu, the Alteration Index of Ishikawa (1979), Rb/Sr, or Na_2O/K_2O.

7.4 $\delta^{18}O$ Distributions

7.4.1 Introduction

In hydrothermally altered rocks, $^{18}O/^{16}O$ isotope ratios, which can be expressed by $\delta^{18}O$ as defined in Chapter Two, are a function of water/rock ratio (partly related to permeability), mineralogy or chemistry of the rock, initial isotopic compositions of rock

and hydrothermal fluid, and fluid temperature (Paquette-Mihalasky, 1999). Though it is generally not reasonable to assume constants for all but one of these variables at any scale of study, arguments on general degrees or styles of hydrothermal alteration are possible.

In VMS systems, oxygen isotopic compositions have recently been used to map regional scales of hydrothermal convection (as in semi-conformable zones of silicification), and to map locations of smaller-scale upflow zones (as in alteration pipes; e.g., Roberts et al., 2003, Paquette-Mihalasky, 1999). For this reason, $\delta^{18}O$ distributions at Big Lake complement the existing geochemical data as another possible means of distinction between higher and lower temperature zones of alteration and along-strike vectors towards vent site(s).

7.4.2 Results

Of the 18 drill core samples collected for analysis of oxygen isotopic compositions and calculation of $\delta^{18}O$ values as described in Chapter Two, 11 were siltstone, sampled specifically from the bedding package immediately below VMS mineralisation. Of the lithologies in contact with hydrothermal fluids, the siltstones were assumed to have the least variable range in permeability and water-rock ratio during hydrothermal alteration. In order to provide the most constraints on rock composition and water-rock ratio, intervals of identical colour and width of laminae (1 mm) were sampled, and nine of the siltstone samples were taken from within five metres of their upper contacts with hydrothermally altered metavolcanic rocks (following the observation that hydrothermal alteration was most intense along the stratigraphic bases of the siltstone units; Fig. 7.8a).

The remaining seven $\delta^{18}O$ analyses were chosen from stratigraphic footwall and hangingwall metavolcanic rocks of the study area. They are strongly foliated, making it effectively impossible to estimate their original permeability or water-rock ratios during development of the VMS system at Big Lake. Furthermore, although they are now mineralogically indistinguishable by standard petrographic methods, different chemistries reflecting two distinct sources (Chapter Five) imply that protolith chemistry cannot be assumed to have been the same for both. For this reason, comparisons of $\delta^{18}O$ values

above and below VMS mineralisation may not strictly reflect temperatures or degrees of silicification, and observations are therefore limited to along-strike or plan view, as opposed to down-hole, distributions. Plan distributions of $\delta^{18}O$ values in metavolcanic rocks are shown in Figure 7.8b.

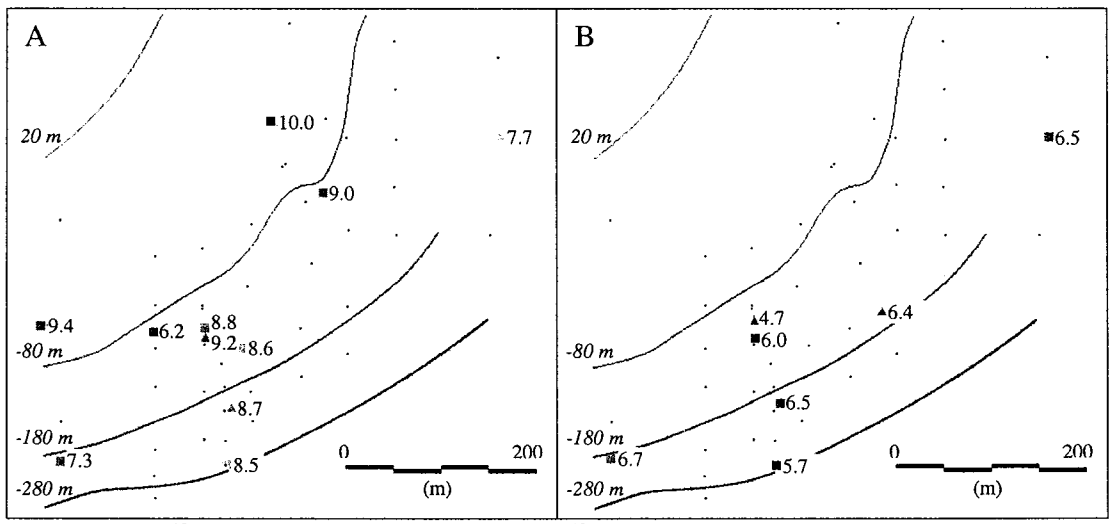

Figure 7.8 - $\delta^{18}O$ distributions in plan view. $\delta^{18}O$ values are indicated beside each sample location. Black dots are drill collar locations as shown in other figures. For spatial reference, black lines are contour intervals through the centre of the VMS mineralised zone. A) $\delta^{18}O$ in siltstones. The two triangles are samples 20 and 28 m below the uppermost siltstone unit, all others are from the uppermost siltstone unit adjacent to VMS mineralisation. B) $\delta^{18}O$ in metavolcanic rocks. The two triangles are from the stratigraphic hangingwall to VMS mineralisation, all other samples are of footwall rock.

$\delta^{18}O$ values in the siltstones vary from 6.2-10.0 (mean = 8.5), and in metavolcanic rocks vary from 4.7-6.7 (Figs. 7.8 and 7.9). $\delta^{18}O$ in Big Lake samples is plotted against major element oxides related to hydrothermal alteration and/or silicification in Figure 7.9. Given significant differences in rock chemistry and permeability between siltstones and volcanic rocks, the only meaningful trends in Figure 7.9 are those within respective lithological groups. $\delta^{18}O$ in the volcanic samples shares no significant correlation with SiO_2, Al_2O_3, CaO, or MgO. In siltstones , $\delta^{18}O$ appears to decrease with Al_2O_3 and MgO (and increases with Na_2O, not shown), the implications of which are noted in the discussion.

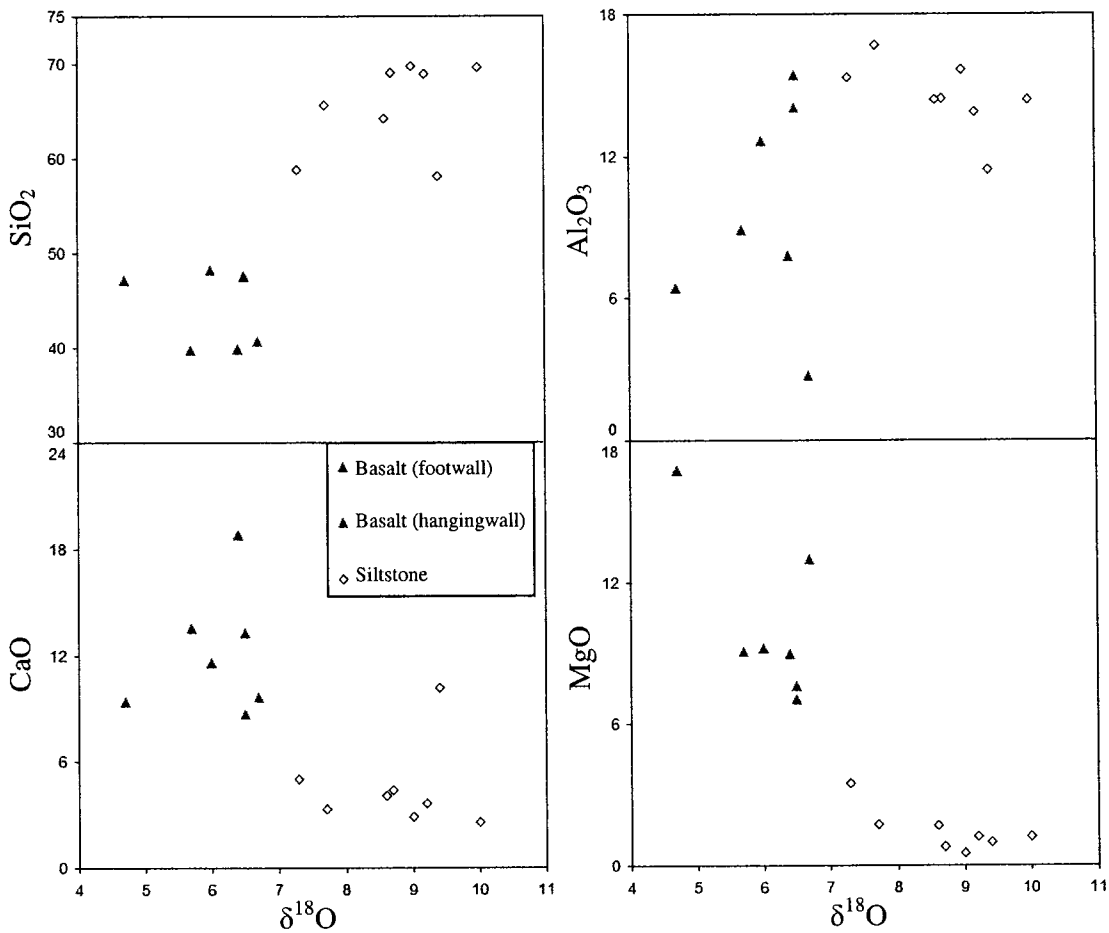

Figure 7.9 - Major element oxide contents versus whole-rock $\delta^{18}O$ values for siltstone and volcanic samples discussed in text. Oxides are in wt. %.

7.5 Discussion

7.5.1 Regional Footwall Alteration

VMS-hydrothermal systems include a large volume of subseafloor rock subject to high-temperature water-rock reaction, producing semiconformable zones of alteration, from top to bottom, of carbonates (carbonatization), albite and chlorite (spilitization), crypto- and microcrystalline quartz (silicification), and epidote with quartz (epidote-quartz alteration), generally increasing in intensity with depth (Franklin et al., 2005). These zones of regional semiconformable alteration, where recognised, can be hundreds of kilometres along strike and up to several kilometres below paleoseafloor. These zones may seal themselves at depth by continued precipitation of smectite-zeolite-carbonate and

silica to form an aquaclude or cap zone (Franklin et al., 2005), which may increase the duration or intensity of metal leaching from rocks in the semiconformable alteration zone below this cap.

Regional increases in silica, Ca, or CO_2 that may help define a zone of regional semiconformable alteration could not recognised at Big Lake given the scale of study, limited by the lack of outcrop and very small volume of volcanic rock intersected in drill core north (down stratigraphy) of the Big Lake Ultramafic Complex. Most observations are instead limited to the confined or vent-related zone of hydrothermal alteration associated with the sulphides of the Big Lake VMS occurrence.

7.5.2 Vent-proximal Footwall Alteration

Along with areas of regional semiconformable footwall alteration, VMS-hydrothermal systems involve smaller zones of alteration immediately below sulphide deposits. These are in many cases described as vertical pipes, cones, or sheets extending up to a kilometre below the seafloor, and are formed by the upward-migrating hydrothermal fluids responsible for VMS mineralisation (Franklin et al., 2005). They normally consist of Fe-chloritised and in some cases silicified cores with chalcopyrite and pyrrhotite, grading to Mg-chloritised and sericitised margins with pyrite and sphalerite (Franklin et al., 2005). Because the geometry of these alteration zones is largely dictated by local permeability (in turn a function of synvolcanic structures and host lithology), shapes and dimensions vary from thin pipes or sheets, to broad, diffuse areas parallel to seafloor (Large et al., 2001). Depending on the duration of venting and timing of overburden emplacement, this alteration may extend into hangingwall rocks.

VMS-hydrothermal alteration at Big Lake, as defined by chemical alteration indices or visual estimation in hand sample, is mostly restricted to within, and a few metres structurally above, visible sulphide mineralisation (Fig. 7.7). This may be a function of limited permeability in a flow-dominated setting, and/or of some degree of tectonic shortening and/or shear deformation, particularly given its location within a shear structure. The increased MgO of altered rocks can be attributed to higher chlorite contents. Lower Na_2O contents probably reflect the breakdown of feldspars or other alkali-bearing phases, as is observed in alteration pipes of all VMS deposits (Large et al.,

2001). However, it is noted that Na_2O of the protolith was likely low, given a mean of 1.6 wt. % Na_2O in the 38 least-altered/"weakly altered" whole-rock metavolcanic samples. This illustrates one of the difficulties in assessing Na depletion in ultramafic rocks that are initially Na-poor. The absence of sericite or other evidence of potassic alteration related to Big Lake VMS mineralisation may be due to this low alkali content and/or a lack of alkali input from felsic rocks in the regional footwall (Lydon, 1989).

The application of $\delta^{18}O$ to map degrees of hydrothermal alteration requires several assumptions. Ferromagnesian minerals such as chlorite contain relatively low $^{18}O/^{16}O$ (compared to quartz or feldspars, for instance), so higher chlorite contents tend to decrease $\delta^{18}O$ values (Faure, 1977). Increasing temperature also tends to decrease $\delta^{18}O$ values of rock during hydrothermal alteration, provided $\delta^{18}O$ of the fluid is less than that of the rock (Faure, 1977), as is almost certainly the case in VMS fluids. In general, assuming a constant fluid (and rock) composition and water/rock ratio, decrease in $\delta^{18}O$ of altered rocks is expected to reflect higher temperature and/or more prolonged hydrothermal alteration (Faure, 1977), which would be expected moving towards the centre of an alteration pipe, for instance. In siltstones sampled, the negative correlation of $\delta^{18}O$ with MgO and Al_2O_3 (not conclusive, given the small number of $\delta^{18}O$ samples) may support this premise, as Al_2O_3 and MgO were shown to increase with apparent intensity or duration of hydrothermal alteration. In terms of proximity to a vent or alteration pipe, however, there is little consistent change of $\delta^{18}O$ in any direction.

The fact that two samples from a siltstone bedding package at least 20 m below the VMS mineralisation produced $\delta^{18}O$ as high as the other samples, which were sampled adjacent to VMS mineralisation, suggests several possibilities, including: (1) oxygen isotope ratios did not survive regional metamorphism, though they are expected to be retained in rocks at up to amphibolite facies metamorphism (Beaty and Taylor, 1982); (2) none of the siltstones sampled were present during VMS-hydrothermal alteration; or most likely (3) the siltstones were effectively impermeable, so water/rock ratios were too low to produce appreciable changes in $\delta^{18}O$ values. Though oxygen isotope compositions still represent a possible means to map small-scale alteration patterns through the Big Lake VMS occurrence, their use is subject to several constraints that are not easily applied at this scale with the number of samples used.

Even given some degree of shear deformation, the geometry of hydrothermal alteration at Big Lake probably had a considerable horizontal dimension, as a thin paleohorizontal sheet immediately below the uppermost thick siltstone unit. Since hydrothermal alteration or mineralisation is generally most intense immediately above the uppermost siltstone package, and again assuming an overturned sequence, it is possible that siltstones acted as local impermeable barriers to fluid ascent, as was suggested for less permeable sills and flows at of the Rosebery deposit (Martin, 2004). Also possible is that the lower surface of alteration and mineralisation defines an erosional unconformity, although minor chalcopyrite-pyrrhotite mineralisation through parts of the uppermost siltstone package makes this a less likely explanation. Regardless, little comment can be made regarding possible locations of major upflow zones or discharge centres; judging only from the alteration, it is not clear from which direction fluid might have originated, other than suggesting the fluid had a likely downhole (up-stratigraphy) vector component.

Mass balance equilibria involved in the formation of VMS ore are not limited to base and alkali earth metals; depletions and enrichments of as little as a few ppm in such elements as Tl, Eu, Mn, Bi, Ba, P, or Se can be used to vector towards seafloor vents, or to define zones of more prolonged or intense hydrothermal alteration (Franklin et al., 2005). The distributions of these elements, along with various element ratios (Rb/Sr, Ba/Sr, S/Na, Mn) and elements normalised to silica, MgO, and total REE contents, were also explored during this study. Though their distributions were examined in detail, their usefulness as ore vectors in this study is severely limited by a lower sampling density (Fig. 7.10) and by a lack of sampling for these elements in drill core or at surface outside of the ~0.5 x 0.5 km study area.

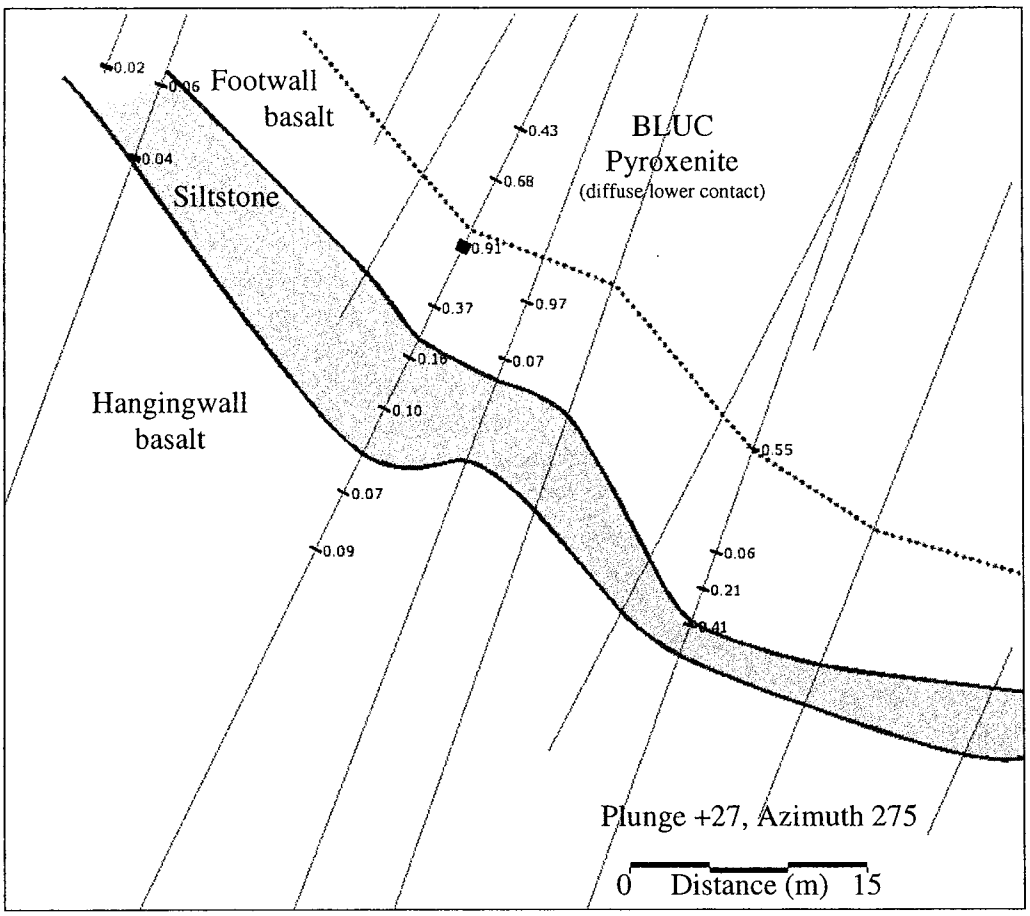

Figure 7.10 - Whole-rock Thallium (ppm) values through part of the Big Lake VMS host sequence, showing a lower sampling density than the assays shown in Figure 7.7. Drill holes and field of view are the same as in Figure 7.7.

7.6 Conclusions

Vent-related (stringer zone) hydrothermal alteration at Big Lake is restricted to within a few metres above visible sulphide mineralisation. This may be in part a function of limited permeability in a flow-dominated setting. The alteration mineral assemblages consist of chlorite, biotite, and anthophyllite, in decreasing order of abundance, and without appreciable zoning or strict relationship to metal contents. The rocks at Big Lake have a high chlorite-carbonate-pyrite (CCP) index, and increasingly altered samples have higher Alteration Indices (AI). In summary, the mineralogy and chemistry of hydrothermal alteration associated with the VMS sulphides at Big Lake is typical of other VMS alteration pipes, including addition of Mg and Na depletion.

Chapter 8
Seafloor Deposit Models

8.1 Introduction

This chapter incorporates information discussed in the previous chapters, with the broad aim of describing the possible formation of the Big Lake VMS occurrence. Based on the evidence presented in the previous chapters, four models are considered, with later discussion of their possible exploration implications.

8.2 Deposit Models

It was previously suggested that regardless of later effects of deformation, the Big Lake occurrence originated by VMS processes, involving seafloor or paleo-seafloor sulphide accumulation in a volcanic setting. Arguments were also made for an overturned host sequence, in which the mineralised sheet was parallel to the paleohorizontal. These assumptions are held for all models considered in this study. However, some aspects of the Big Lake VMS occurrence remain unresolved, most importantly including: the precise roles of shear deformation and general tectonic shortening on its metal and alteration distributions; its timing relationship with the Big Lake Ultramafic Complex; and whether sulphides intersected to date represent a stringer zone or a lens/very near seafloor replacement zone. Exploring these possibilities leads to four general models describing the formation of the Big Lake VMS occurrence, introduced in Table 8.1.

Table 8.1 - Summary of models describing the genesis of the Big Lake VMS occurrence

	Heat Source	Big Lake Ultramafic Complex	Timing of BLUC emplacement	Proximity of sulphides to paleoseafloor	Sulphide remobilisation	Similar examples
Model 1 Stringer zone in situ	No subvolcanic intrusion identified, or footwall mafic-ultramafic package as a whole	Thick ponded cumulate flow or a discrete cumulate intrusion	Before VMS	At least tens of metres below seafloor; occurrence is stringer zone	Although sheared / tectonically shortened, sulphides are effectively in situ.	Kidd Creek (Hannington et al., 1999)
Model 2 Partially remobilised or assimilated by BLUC	None identified, or footwall mafic-ultramafic package as a whole	BLUC is a discrete intrusion, with both upper and lower intrusive contacts	After VMS	Unknown	Sulphides are remobilised by BLUC, may be partially assimilated.	Winston Lake, Flin Flon? (Koo and Mossman, 1975)
Model 3 BLUC-driven convection	Big Lake Ultramafic Complex	BLUC is a thick ponded ultramafic flow	Immediately prior (100s of yrs) to and cooling during VMS formation	Unknown	Sulphides are effectively in situ, though subject to shear deformation.	Terminus VMS occurrence (Barrie et al., 2001)
Model 4 Remobilised through shear zone	None identified, or footwall mafic-ultramafic package as a whole	Not relevant	Not relevant	Unknown	Sulphides derived from nearby VMS, remobilised through shear zone.	Occurrence in Massif Central (Bellot, 2004)

Model 1 - Stringer zone in situ

This model involves the assumption that prior to deformation, the pyrrhotite, chalcopyrite, and sphalerite were precipitated below an already deposited siltstone package, some distance below the seafloor. Metals and alteration minerals therefore comprise a stringer or feeder zone to seafloor vent(s). The presumably less permeable siltstone, possibly coupled with local permeability of the host volcanic rock (e.g., flow tops?), may account for the thin sheet-like geometry of the stringer zone intersected to date, hundreds of metres in lateral extent (Fig. 8.1). A less likely possibility, noted in the previous chapter, is that it was precipitated in situ and partly eroded and overlain by siltstone. The stringer or vein sulphide textures are primary; that is, they are not remobilised sulphides that used to have a bedded or massive habit from precipitation from an open water column.

In this model, the Big Lake Ultramafic Complex represents either a thick ponded cumulate flow or a discrete cumulate intrusion with upper and lower intrusive contacts, and played no active role in the genesis of the VMS system. A potential heat source such as a subvolcanic intrusion was not identified by mapping or drilling at the Big Lake property. However, there are many deposits with no clear heat source (Galley, 2002), and drilling at Big Lake has not targeted any such intrusions. Furthermore, the model does not necessarily require a subvolcanic intrusion, because the entire mafic-ultramafic footwall succession could have generated the heat required to drive convection, as has been proposed for the genesis of the Kidd Creek deposits (Hannington et al., 1999).

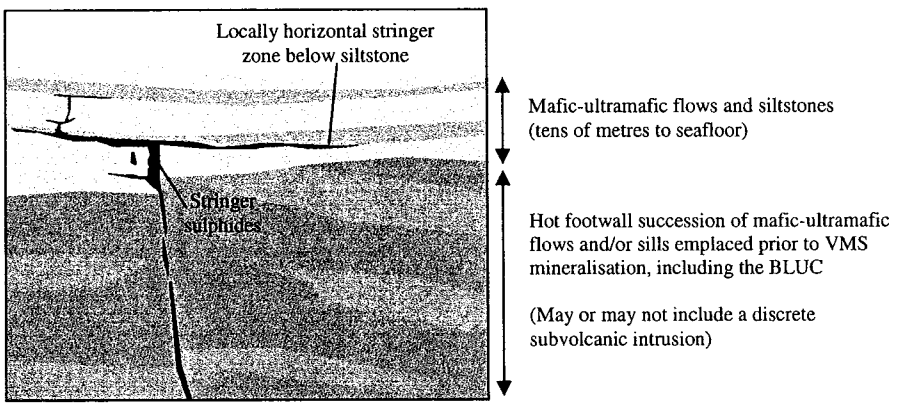

Figure 8.1 - Section diagram illustrating aspects of Model 1, prior to deformation.

Evidence for this model includes all features consistent with a higher-temperature (>350 °C) zone of precipitation, including the vein sulphide textures consistent with sub-seafloor replacement, a stronger partitioning of Au with Cu than with Zn, a lack of Sn-Hg-Bi-Te mineral phases, and a pyrrhotite-dominated sulphide assemblage.

Model 2 - Partially remobilised or assimilated by BLUC

The second model is similar to the first, except that the BLUC is a discrete intrusion that post-dates VMS mineralisation, with both upper and lower intrusive contacts. Proximity to such a large ultramafic intrusion involved contact metamorphism and possible assimilation or displacement of the VMS from or into the edge of the intrusion. In this model, VMS sulphides may not be in situ, and stringer sulphide textures may not be primary; that is, they may have had bedded, massive, or disseminated textures

prior to remobilisation or contact metamorphism. A similar scenario has been proposed for the Winston Lake VMS deposit and Flin Flon deposits, where metal enrichment may have been caused by partial assimilation and contact metamorphism (Koo and Mossman, 1975).

Other than a paleohorizontal sheet-like geometry that is perhaps more consistent with very near-surface sulphide replacement or precipitation at surface than with stringer zone precipitation, there is little evidence to suggest the Big Lake VMS occurrence was remobilised by the BLUC. Earlier evidence of contact metamorphism, such as hornfels texture, would presumably have been overprinted by a planar fabric from regional metamorphism and/or and shearing, and may otherwise be difficult to distinguish from the sulphide-related hydrothermal alteration.

The presence of hydrothermal veining and chalcopyrite-pyrrhotite mineralisation in two intervals within peridotites of the BLUC, and another such occurrence through a BLUC peridotite unit ten kilometres west of the study area, suggests the BLUC was emplaced prior to VMS mineralisation. No evidence of sulphide assimilation was encountered at the margins of the BLUC, again making it unlikely that any VMS mineralised rock was assimilated into the BLUC. Perhaps most importantly, the BLUC has a fine-grained cumulus texture and diffuse lower contacts into adjacent metavolcanic rock, with similar major and trace element characteristics that are distinct from metavolcanic rock structurally underlying the VMS mineralisation. As was argued in Chapter Five, this suggests the BLUC is more likely a thick ponded cumulate flow than an intrusion.

Model 3 - BLUC-driven convection

The most important premise to the third model is that the Big Lake Ultramafic Complex was a shallow heat source directly responsible for VMS mineralisation, as was suggested by Barrie et al. (2001) for the Empire cumulate komatiite flow and Terminus VMS occurrence of the Kidd-Munro assemblage. In this model, the BLUC represents one, or a series of, ponded cumulate mafic-ultramafic flows. Cooling of the BLUC would have driven the hydrothermal system responsible for VMS mineralisation at Big Lake, unlike typical VMS systems that are supposed to have formed by subvolcanic

intrusions at least 0.5 km deep (Franklin et al., 2005). Barrie et al. (2001) proposed that ultramafic magmas can generate significant VMS-hydrothermal circulation due in part to their extremely high liquidus temperatures of approximately 1300-1700 °C. Moreover, because of the insulating effects of serpentinisation, thick komatiite flows could require up to hundreds of years to cool, thus providing a sufficiently prolonged heat source to form VMS deposits as large as those along the Mid-Atlantic Ridge (Barrie et al., 2001). An important aspect of this scenario described by Barrie et al. (2001) is that much of the convective cooling system (the volume of rock through which seawater was drawn during cooling, and in which most metal leaching occurred) lay *below* the ponded flow.

The Empire komatiite flow consists of 70-225 m of medium to fine-grained peridotite-dunite-pyroxenite cumulates, overlain by 0-10 m of flow top breccia (locally absent). These are overlain by thinner basaltic komatiite flows which host the Terminus occurrence, approximately 50-100 m stratigraphically above the Empire flow (Barrie et al., 2001). Although dimensions of the BLUC are larger than those of the Empire flow and may consist of more than one cooling unit or flow, spatial relationships between ultramafic cumulates and VMS sulphides described by Barrie et al. (2001) are almost identical to those observed at Big Lake, as illustrated in Figure 8.2.

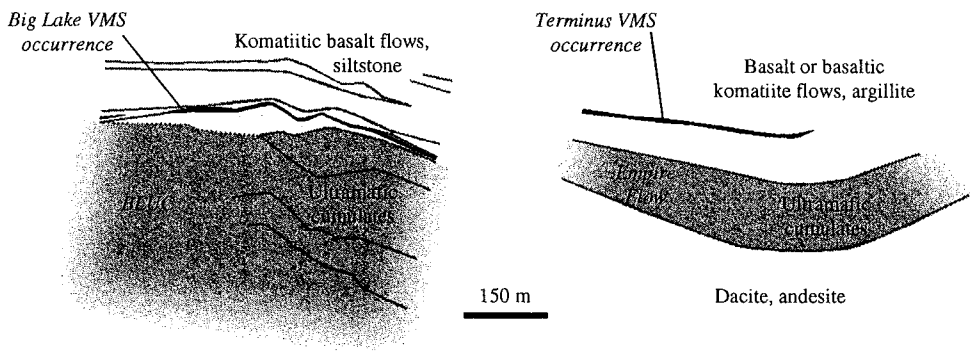

Figure 8.2 - Section diagrams comparing spatial relationships between Empire Flow and BLUC cumulates (dark grey), and their associated VMS mineralisation (black). Both sections are rotated to near horizontal, with no correction for deformation. The Big Lake diagram is from section C of Figure 4.1, and the Empire diagram is modified from Figure 2c of Barrie et al. (2001).

Regardless of whether the model developed by Barrie et al. (2001) accurately describes the circumstances at Big Lake, some genetic relationship between the BLUC

and Big Lake VMS occurrence can be inferred from their general spatial relationship, with VMS mineralisation parallel to and 5-50 m below the base (stratigraphic top) of the BLUC.

If the BLUC was a shallow heat source for VMS-hydrothermal convection, this model requires some mechanism to allow fluids to migrate through the entire stratigraphic thickness of the BLUC. Thermal cracking through a ponded komatiite during cooling is possible (Barrie et al., 2001), and this may explain the few VMS-like intervals cross-cutting BLUC peridotite in drill core (as these intervals may represent thin channels of VMS-hydrothermal fluid that post-date the BLUC). Also possible is that the BLUC was effectively impermeable during convection, in which case upflow zones would be limited to within perhaps ~100s m from the edges of the BLUC. Interestingly, if the currently mapped eastern extent of the BLUC marks its original extent, or if its eastern edge is due to displacement by synvolcanic faulting, then this could account for the location of the Big Lake VMS occurrence around its margin, and for the general lack of VMS sulphides stratigraphically overlying the middle (western) portions of the BLUC.

Apart from the occurrences of the Abitibi subprovince documented by Barrie et al. (2001) and, perhaps, the Big Lake VMS occurrence, there are no preserved examples of VMS occurrences related to shallow ultramafic rocks. In the modern ocean, however, Fouquet et al. (2005) observed that such systems are common. Most are located on slow spreading ridges along rift valley walls and ridge-transform fault intersections. Much like the Big Lake occurrence, most of the mineral deposits are characterised as low pH and high temperature (>350°C) deposits that are enriched in Ni, Co, Cu, Zn, and Au compared to typical basalt-hosted VMS. Fouquet et al. (2005) also noted that these recently formed ultramafic-hosted VMS deposits are more common than in ophiolites, likely because slow-spreading ridges are generally not preserved during orogeny by subduction-accretion. This may explain the rarity of such preserved examples as the Big Lake VMS occurrence, even though the Big Lake occurrence likely formed in an OIB-influenced oceanic plateau setting.

Model 4 - VMS remobilised through a shear zone

The fourth and last model proposed is least similar to the other models in that the spatial relationships between VMS sulphides, the BLUC margin, and metasedimentary rock are secondary. The VMS occurrence is hosted in a structure that happens to follow a metasedimentary unit contact that runs parallel to the base of the BLUC. A similar scenario was documented by Bellot (2004) in the French Massif Central, where chalcopyrite, pyrite, and sphalerite were found to be coeval with deformation in a shear structure adjacent to an undeformed VMS body. Unlike the anhedral sulphides at Big Lake, the remobilised sulphides documented by Bellot (2004) are euhedral, perhaps implying syntectonic emplacement. However, the shear-hosted sulphides at Big Lake may have been both shear-deposited and euhedral prior to further deformation.

While the sulphides of the Big Lake VMS occurrence must have originated by VMS processes, they are hosted mostly within shear structures. It is therefore necessary to consider that, as in the fourth model, they may have been entirely shear-deposited/remobilised. At the same time, it is not difficult to account for shearing through the Big Lake VMS occurrence. In the study area, the planar fabric is generally strongest near both upper and lower contacts of the BLUC, perhaps due in part to mechanical contrasts between the mostly serpentinised ultramafic cumulates and thinner adjacent flows. If VMS sulphides are *in situ*, they are hosted in a shear structure simply because they are located along and may even form a surface of mechanical contrast.

8.3 Discussion

8.3.1 Overview

While a more straightforward approach in this chapter would be to produce one model describing a most likely scenario, too many aspects of the Big Lake VMS occurrence could not be conclusively defined in order to do so. Rather than ignore some of the contradictory aspects (such as whether the BLUC is a discrete intrusion that post-dates, or an intrusion/flow that pre-dates VMS mineralisation), it was decided to separate these into different genetic models. In some cases, it is not unreasonable to consider a combination of models presented, such as that VMS sulphides may have formed by

BLUC-driven convection (model 3), and were later remobilised some distance along a shear zone (model 4).

In some models discussed, the same observations are used to support two or more models. For instance, the spatial relationship of VMS with BLUC contacts is consistent with both a genetic relationship of sulphides with the BLUC (model 3) and with a shear-remobilised occurrence (model 4), given that shear zones also follow the BLUC contacts. Likewise, stringer sulphide textures were said to be consistent with both a VMS stringer zone *in situ* (model 1) or with remobilisation of originally bedded, massive, or veined sulphides through a shear structure (model 4). While efforts were made to keep arguments as concise and simple as possible, it was in some cases unavoidable that the same premise be used in different contexts to support different conclusions.

Of the models presented, the least favoured is model 2, involving VMS remobilisation/displacement or partial displacement at the edges of the BLUC. It requires that the BLUC has two intrusive contacts, which was shown to be less likely in favour of a series of thick cumulate flows.

The model that most likely describes the origin of the Big Lake VMS occurrence is model 3, with BLUC-driven convection causing VMS mineralisation. The documented examples and heat/fluid flow modeling of Barrie et al. (2001) have demonstrated that this scenario is possible, provided that upward-convecting fluids had some means of escaping to seafloor. Barrie et al. (2001) suggested thermal cracking as such a mechanism for the Terminus VMS occurrence, but at Big Lake it was proposed that an impermeable BLUC could explain the occurrence of VMS mineralisation only near the eastern edge of the BLUC. Though mechanical contrasts produced by primary VMS alteration/mineralisation and the BLUC contact could have been responsible for the locations of the shear structures, a qualification added to this preferred model is that it could share some aspects with model 4 (shear-controlled mineralisation).

8.3.2 Exploration Implications

Two of the four models have distinct exploration implications for finding similar occurrences. If model 4 (VMS remobilised though a shear zone) applies at Big Lake, sulphides would still be of VMS origin. Exploration should then involve more detailed

mapping of the shear structure(s) through the Big Lake property, as the original occurrence may lie somewhere along the shear structure(s). If model 3 (BLUC-driven convection) applies, any similar sulphide mineralisation would be expected stratigraphically above the BLUC, perhaps along its margins. Barrie et al. (2001) noted that the Terminus VMS occurrence was thickest stratigraphically above the thickest part of the Empire flow. If the BLUC was permeable to allow upflow through its centre, thicker parts of the BLUC may likewise be prospective for larger accumulations of seafloor sulphide. Finally, as the Big Lake VMS occurrence probably represents a stringer zone, more significant sulphide accumulations such as seafloor lens deposits may be encountered farther up stratigraphy / towards paleoseafloor from the study area.

Of more regional significance is that VMS exploration is typically focused in settings characterised by bimodal volcanism and containing subvolcanic intrusions at least 0.5 km deep, areas deemed favourable for the development of VMS convection cells. Rocks overyling thick ponded ultramafic flows or very shallow (<0.5 km below seafloor) intrusions are not targeted for VMS sulphide accumulations, particularly if they occur in settings lacking bimodal volcanism. If the model (or some variation) of Barrie et al. (2001) is responsible for the Big Lake VMS occurrence, this would be the first documented example preserved outside of the Abitibi subprovince (Barrie et al., 2001), and shows that similar styles of shallow intrusion or komatiite flow-driven VMS convection cells may have developed elsewhere in the Superior Province or other Archean cratons.

Chapter 9
Conclusions

9.1 Introduction

A summary of arguments and observations made in previous chapters is provided here. Conclusions of this study include a brief discussion of its general implications and avenues for future study.

9.2 Summary of Previous Chapters

Lithologies of the Big Lake VMS occurrence are broadly divided into ultramafic cumulates (peridotites and pyroxenites), mafic-ultramafic metavolcanic rocks, and metasedimentary rocks. The host lithostratigraphy to the Big Lake VMS occurrence was shown to be overturned, with a general downhole/up-stratigraphy sequence of Big Lake Ultramafic Complex cumulates, adjacent flows, VMS-hydrothermal alteration and sulphides, siltstone, and flows with interbedded, locally pelitic siltstones and iron formation. The ultramafic cumulates and adjacent underlying volcanic rock are likely a series of ponded ultramafic flows. Their cumulate base-flow top relationship is further supported by their shared chemistry, as footwall metavolcanic rocks and the BLUC cumulates occupy the same fields in most trace and major element variation and tectonic discriminant diagrams.

As a whole, the lithostratigraphic assemblage at Big Lake is consistent with either oceanic arc or sedimented ocean ridge settings (as in the pelitic-mafic category of Franklin et al., 2005) or OIB settings (as in the mafic category). It was shown that the latter is most likely, given that trace element characteristics of the komatiitic basalts at Big Lake are most consistent with a plume origin. Specifically, hangingwall basalts are the same as other tholeiitic plateau basalts of the Wawa subprovince, except that some samples display weak relative Nb depletions. Contamination of tholeiitic plateau basalts by assimilation of trench turbiditic sandstones could explain their weak negative Nb anomalies, though there is limited evidence to support this. Footwall basalts are the same as other transitional to alkaline basalts of the Wawa subprovince. Their NEB-like

characteristics were suggested to be due to mixing with an OIB-like component (a deep, low-degree partial melt of a mantle plume), as modeled by Polat (2008).

The mineralised zone of the Big Lake VMS occurrence consists of pyrrhotite-chalcopyrite-sphalerite (± galena, cobaltite) associated with hydrothermal veining. This mineral assemblage is clear evidence of an origin by VMS processes. The sulphides define a thin (< 10 m), locally anastomosing surface against and parallel to the upper contact of the uppermost siltstone unit. Total metal contents and Cu/Zn ratios are highest in the southern part of the mineralised sheet. A sub-seafloor style of mineralisation is proposed mainly based on its sulphide textures, geometry and relationship to siltstone contacts, and pyrrhotite-dominated sulphide assemblage.

VMS-hydrothermal alteration at Big Lake is marked by visible amounts of veined and diffuse biotite-phlogopite, anthophyllite, veined chlorite, and/or generally darker colour in metavolcanic rocks. Higher degrees of hydrothermal alteration most notably involved increases in MgO and the Alteration Index of Ishikawa (1979), and decreases in Na_2O. Samples plot along the chlorite-carbonate trend of the Large et al. (2001) alteration box plot.

The distribution of hydrothermal alteration closely mimics metal contents (highest degrees of alteration are usually associated with highest metal contents) and is generally restricted to within 10 m above VMS mineralisation. In most holes it is most intense immediately above the uppermost siltstone package, implying that siltstones may have acted as local impermeable barriers to ascent of mineralising fluid. Apart from its unusual (horizontal) geometry, hydrothermal alteration intersected to date at Big Lake is broadly consistent with that in alteration pipes of many VMS deposits, including depletion of Na and addition of Mg and/or hydrothermal chlorite (Galley et al., 2007).

Depending on the roles or effects of shear deformation, different possibilities for heat sources, and other issues that could not be clearly resolved in this study, four models were presented to describe the possible origins of the Big Lake VMS occurrence:

(Model 1) *Stringer zone in situ* – No discrete heat source is implied, and sulphide textures are primary, from higher-temperature precipitation some distance below seafloor.

(Model 2) *Partially remobilised or assimilated by BLUC* – The BLUC is an intrusion with discrete upper and lower contacts, and VMS sulphides were remobilised or partially assimilated at its margins.

(Model 3) *BLUC-driven convection* – The BLUC was a shallow heat source directly responsible for VMS mineralisation, much as in the model of Barrie et al. (2001).

(Model 4) *VMS remobilised through a shear zone* – VMS sulphides were reprecipitated in a shear zone that follows the margin of the BLUC.

A combination of models 3 and 4 was suggested to best describe its origins, whereby cooling of the BLUC flow(s) drove the hydrothermal circulation responsible for VMS mineralisation near its upper margins, with later development of shear zones partly along the surface of VMS mineralisation.

9.3 Study Implications and Future Research

9.3.1 Shallow-Driven Convection in VMS Systems

If a volume of rock and seawater is simply treated as a chemical system, where entropy increases by release of heat and by movement of species down concentration gradients, then VMS processes are much the same as in other deposit types such as SEDEX or even porphyry systems. An implication in this study is to extend this idea further: given that convection of a free or pooled water phase is an efficient means of heat and mass transfer, and given the volume of rock represented by ocean floor settings, it is not unreasonable to suggest that VMS, broadly defined as seafloor accumulations of sulphide by hydrothermal convection, could be more common or present in more varied settings than is currently recognised. These could include areas overlying mafic or ultramafic flows or shallow intrusions in non-bimodal and non-arc settings.

Though the idea introduced by Barrie at al. (2001) of "shallow-driven" convection to form VMS deposits is relatively new in VMS literature, key processes are no different than in better studied VMS occurrences. There are significant exploration implications if the Barrie et al. (2001) model holds true. The Big Lake occurrence would be the first

such documented occurrence outside of the Abitibi Subprovince, and similar undiscovered occurrences may be found in similar settings.

9.3.2 Future Study

Many details regarding the Big Lake VMS occurrence have yet to be resolved. In particular, the possible relationship between BLUC cumulates and adjacent metavolcanic rocks (i.e., the possibility that the BLUC is a series of thick flows), and the possibility that hangingwall basalts are contaminated plume-derived tholeiites can both be explored with a study of their Sm-Nd isotopic compositions. A better understanding of the tectonic setting of the occurrence (both hangingwall and footwall rocks) may be approached at a more regional scale, as the study area does not permit any conclusions to be drawn through the whole of the Pulpwood-Playter Harbours volcanic sequence.

There are several means of testing or mapping hydrothermal alteration at Big Lake that were not undertaken during this study. SEM mineral analyses of Fe-Mg contents are a possible means of distinguishing between regional metamorphic and regionally metamorphosed VMS-hydrothermal micas. This was not deemed practical at the scale of this study, since strong hydrothermal alteration is readily recognised by darker chlorite and higher biotite contents in hand specimen, along with textures suggestive of fluid flow. Nevertheless, a comprehensive study of mica or other mineral compositional variations would be a useful avenue of study to further define alteration patterns and styles of the Big Lake VMS occurrence.

Detailed mapping along the southern BLUC contact and shear structures may help to constrain the role of shear deformation on the shape and location of the VMS occurrence, and may better define the relationship between VMS mineralisation and the BLUC. In order to test the flow-driven convection model developed by Barrie et al. (2001) at Big Lake, their *Akcess.basin* finite element modeling of convection could be used in order to compare modeled and proposed locations of upflow through or around the BLUC, and to highlight other VMS-prospective areas along the length of the BLUC. A more regional examination of regional hydrothermal alteration or other evidence of circulation cells may be applied below the stratigraphic base of the BLUC, which is not extensively drilled.

While many aspects of the Big Lake VMS occurrence have been described with the use of geochemical and lithological modeling in this study, many details have yet to be conclusively defined, including the exact degree of structural control on its morphology, or the shape and permeability controls of its proposed shallow heat source. Future study of such an unusual example of VMS mineralisation should prove useful in expanding understanding of the formation of Archean VMS systems, particularly in non-bimodal or oceanic plateau environments.

References Cited

Allen, R., Weihed, P., and Svesen, S., 1996. *Setting of Zn-Cu-Au-Ag massive sulfide deposits in the evolution and facies architecture of a 1.9 Ga marine volcanic arc, Skellefte district, Sweden.* Economic Geology **91:** 1022-1053.

Alt, J., 1995. *Subseafloor processes in mid-ocean ridge hydrothermal systems.* In: Humphris, S. (Ed.). Seafloor Hydrothermal Systems: Physical, Chemical, Biological, and Geological Interactions. American Geophysical Union Monograph **91:** 85-114.

Araujo, S., Scott, D., and Longstaffe, F., 1996. *Oxygen isotope composition of alteration zones of highly metamorphosed volcanogenic massive sulfide deposits; Geco, Canada, and Palmeiropolis, Brazil.* Economic Geology **91:** 697-712.

Arndt, N., and Nesbitt, E., 1982. In: Arndt, N., and Nisbet, E. (Eds.). *Komatiites*, p. 309-330. Allen & Unwin, London.

Barnes, S., Zientek, M., and Severson, M., 1997. *Ni, Cu, Au, and platinum element contents of sulfides associated with intraplate magmatism: A synthesis.* Canadian Journal of Earth Sciences **34**: 337-351.

Barrie, C., 1999. *Komatiitic flows of the Kidd Creek footwall, Abitibi Subprovince, Canada.* In: Hannington, M., and Barrie, C. (Eds.). The Giant Kidd Creek Volcanogenic Massive Sulfide Deposit, Western Abitibi Subprovince, Canada. Economic Geology Monograph **10:** 143-162.

Barrie, C., and Hannington, M., 1999. *Classification of volcanic-associated massive sulfide deposits based on host-rock composition.* Reviews in Economic Geology **8**: 1-11.

Barrie, C., Erendi, A., and Cathles, L., 2001. *Paleosea-floor volcanic-associated massive sulfide mineralization related to a cooling komatiite flow, Abitibi Subprovince, Canada.* Economic Geology **96:** 1695-1700.

Beatson, R., Cherrie, J., and Mouat, C., 1999. *Fast fitting of radial basis functions: Methods based on preconditioned GMRES iteration.* Advances in Computational Mathematics **11:** 253-270.

Beaty, D., Taylor, H., and Coad, P., 1988. *An oxygen isotope study of the Kidd Creek, Ontario, volcanogenic massive sulfide deposit: Evidence for high heat ^{18}O ore fluid.* Economic Geology **83:** 1-18.

Bellot, J., 2004. *Shear zone-hosted polymetallic sulfides in the South Limousin area, Massif Central, France: remobilized sulfide deposits related to variscan collisional tectonics and amphibolite facies metamorphism.* Economic Geology **99:** 819-827.

Berry, A., Hack, A., Mavrogenes, A., Newville, M., and Sutton, S., 2006. *A XANES study of Cu speciation in high-temperature brines using synthetic fluid inclusions.* American Mineralogist **91**: 1773-1782.

Bischoff, J., and Rosenbauer, R., 1984. *The critical point and two-phase boundary of seawater, 200-500°C.* Earth and Planetary Science Letters **68**: 172-180.

Blackburn, C., and MacTavish, A., 2005. Report on Geological Mapping, Big Lake Property. MetalCORP Ltd. Internal Report, 58 p.

Bleeker, W., 1999. *Structure, stratigraphy, and primary setting of the late Archean Kidd Creek Volcanogenic massive sulfide deposit: A semi-quantitative reconstruction.* In: Hannington, M., and Barrie, C., (Eds.). The Giant Kidd Creek Volcanogenic Massive Sulfide Deposit, Western Abitibi Subprovince, Canada. Economic Geology Monograph **10:** 71-122.

Bloomer, S., Taylor, B., MacLeod, C., Stern, R., Fryer, P., Hawkins J., and Johnson, L., 1995. *Early arc volcanism and the ophiolite problem: A perspective from drilling in the Western Pacific.* Geophysical Monograph **88:** 1-30.

Bourcier, W., and Barnes, H., 1987. *Stabilities of chloride and bisulfide complexes of zinc to 350°C.* Economic Geology **82**: 1839-1863.

Brauhart, C., Huston, D., Groves, D., Mikucki, E., and Gardoll, S., 2001. *Geochemical mass-transfer patterns as indicators of the architecture of a complete volcanic-hosted massive sulfide hydrothermal alteration system, Panorama District, Pilbara, Western Australia.* Economic Geology **96**: 1263-1278.

Calvert, A., Sawyer, E., Davis, W., and Ludden, J., 1995. *Archaean subduction inferred from seismic images of a mantle suture in the Superior Province.* Nature **375:** 670-674.

Calvert, A., and Ludden, J., 1999. *Archean continental assembly in the southeastern Superior Province of Canada.* Tectonics **18**: 412-429.

Campbell, I., and Griffiths, R., 1990. Implications *of mantle plume structures for the evolution of flood basalts.* Earth and Planetary Science Letters **99:** 73-93.

Cannon, W., Green, A., Hutchinson, D., Lee, M., Behrendt, J., Halls, H., Green, J., Dickas, A., Morey, G., Sutcliffe, R., and Spencer, C., 1989. *The North American Midcontinent Rift beneath Lake Superior from GLIMPCE seismic reflection profiling.* Tectonics **8**: 305-332.

Card, K., and Ciesielski, A., 1986. *Subdivisions of the SuperiorProvince of the Canadian Shield.* Geoscience Canada **13**: 5-13.

Carr, J., Beatson, R., Cherrie, J., Mitchell, T., Fright, W., McCallum, B., and Evans, T., 2001. *Reconstruction and representation of 3D objects with radial basis functions.* SIGGRAPH Computer Graphics Proceedings, Annual Conference Series: 67-76.

Cathles, L., 1993. *Oxygen isotope alteration in the Noranda Mining District, Abitibi Greenstone Belt, Quebec.* Economic Geology **88:** 1483-1511.

Cawthorn, R., Barnes, S., Ballhaus, C., and Malitch, K., 2005. *Platinum group element, chromium, and vanadium deposits in mafic and ultramafic rocks.* Economic Geology 100th anniversary volume: 215 -249.

Condie, K., and Kroner, A., 2008. *When did plate tectonics begin? Evidence from the geologic record.* Geological Society of America Special Paper **440:** 281-295.

Converse D., Holland H., and Edmond, J., 1984. *Flow rates in the axial hot springs of the East Pacific Rise (21°N): implications for the heat budget and the formation of massive sulphide deposits.* Earth and Planetary Science Letters **69:** 159-175

Cowan, E., Lane, R., and Ross., H., 2004. *Leapfrog's implicit drawing tool: a new way of drawing geological objects of any shape rapidly in 3D.* In: Berry, M., and Quigley, M. (Eds.). Mining Geology 2004 Workshop, Bulletin **41:** 23-25.

Eldridge, C., Barton, P. Jr., and Ohmoto, H., 1983. *Mineral textures and their bearing on formation of the Kuroko orebodies.* Economic Geology Monograph **5:** 241-281.

Embley, R., Chadwick, W. Jr., Baker, E., Butterfield, D., Resing, J., de Ronde, C., Tunnicliffe, V., Lupton, J., Juniper, S., Rubin, K., Stern, R., Lebon, G., Nakamura, K-I., Merle, S., Hein, J., Wiens, D., and Tamura, Y., 2006. *Long-term eruptive activity at a submarine arc volcano.* Nature **441**: 494-497.

Eriksson, K., Krapez, B., and Fralick, P., 1994. *Sedimentology of greenstone belts: Signature of tectonic evolution.* Earth Science Reviews **37**: 1-88

Faure, G., 1977. *Principles of Isotope Geochemistry.* John Wiley & Sons, New York, 464 p.

Fei, H., and Xiao, R., 2002. *Ore-forming fluid evolution and metallogenetic physical chemistry.* Bulletin of Mineralogy Petrology and Geochemistry **21:** 139-144.

Fiorentini, M., Beresford, S., Grguric, B., Barnes, S., and Stone, W., 2006. *Anomalous reef-type platinum-group element mineralisation in the Wiluna domain, Agnew-Wiluna Greenstone Belt, Western Australia.* Australian Society of Exploration Geophysicists Extended Abstracts, 2006 volume.

Franklin, J., Lydon, J., and Sangster, D., 1981. *Volcanic-associated massive sulfide deposits.* In: Skinner, B. (Ed.). Economic Geology 75th Anniversary Volume: 485-627.

Franklin, J., Gibson, H., Jonasson, I., and Galley, A., 2005. *Volcanogenic massive sulfide deposits.* In: Hedenquist, J., Thompson, J., Goldfarb, R., and Richards, J. (Eds.). Economic Geology 100th Anniversary Volume: 523-560.

Foley, S., and Jenner, G., 2004. *Trace element partitioning in lamproitic magmas—the Gaussberg olivine leucitite.* Lithos **75:** 19-38.

Fouquet, Y., Charlou, J., Barriga, F., and Cherkashov, G., 2005. *Diversity of ultramafic-hosted hydrothermal mineralization along the mid atlantic ridge.* American Geophysical Union, Fall Meeting 2005 abstract.

Fyon, A., Breaks, F., Heather, K., Jackson, S., Muir, T., Stott, G., and Thurston, P., 1992. *Metallogeny of metallic mineral deposits in the Superior Province of Ontario; Geology of Ontario.* Ontario Geological Survey Special Volume **4**: 1091-1176.

Galley, A., 2002. *Composite synvolcanic intrusions associated with Precambrian VMS-related hydrothermal systems.* Mineralium Deposita **38:** 443-473.

Galley, A., and Koski, R., 1999. *Setting and characteristics of ophiolite hosted volcanogenic massive sulfide deposits.* In: Barrie, C., and Hannington, M. (Eds.). Volcanic-Associated Massive Sulfide Deposits: Processes and Examples in Modern and Ancient Settings. Reviews in Economic Geology **8:** 215-236.

Galley, A., Hannington, M., and Jonasson, I., 2007. *Volcanogenic massive sulphide deposits.* In: Goodfellow, W. (Ed.). Mineral Deposits of Canada: A Synthesis of Major Deposit Types, District Metallogeny, the Evolution of Geological Provinces, and Exploration Methods. Geological Association of Canada Special Publication **5:** 141-161.

Gazel, E., Carr, M., Hoernle, K., Feigenson, M., Szymanski, D., Hauff, F., and van den Bogaard, P., 2009. *Galapagos-OIB signature in southern Central America: Mantle refertilization by arc-hot spot interaction.* Geochemistry, Geophysics, Geosystems **10.**

Gemmell, J., and Large, R., 1992. *Stringer system and alteration zones underlying the Hellyer volcanogenic massive sulfide deposit, Tasmania, Australia.* Economic Geology **87:** 620-649.

Gibson, H., and Watkinson, D., 1990. *Volcanogenic massive sulphide deposits of the Noranda cauldron and shield volcano.* Canadian Institute of Mining and Metallurgy Special Volume **43**: 119-132.

Gibson, H., Morton, R., and Hudak, G., 1999. *Submarine volcanic processes, deposits and environments favorable for the location of volcanic associated massive sulfide deposits.* Reviews in Economic Geology **8:** 13-51.

Hannington, M., Barrie, C., and Bleeker, W., 1999. *The giant Kidd Creek volcanogenic massive sulfide deposit, western Abitibi Subprovince, Canada.* In: Hannington, M., and Barrie, C. (Eds.). The Giant Kidd Creek Volcanogenic Massive Sulfide Deposit, Western Abitibi Subprovince, Canada. Economic Geology Monograph **10:** 1-30.

Hart, T., Gibson, H., and Lesher, C., 2004. *Trace element geochemistry and petrogenesis of felsic volcanic rocks associated with volcanogenic Cu-Zn-Pb massive sulfide deposits.* Economic Geology **99:** 1003-1013.

Heaman, L., and Machado, N., 1992. *Timing and origin of midcontinent rift alkaline magmatism, North America: evidence from the Coldwell Complex.* Contributions to Mineralogy and Petrology **110**: 289-303.

Heggie, G., 2005. *Whole rock geochemistry, mineral chemistry, petrology and Pt, Pd mineralization of the Seagull Intrusion, Northwestern Ontario.* Unpublished MSc. Thesis, Lakehead University, Thunder Bay, 364 p.

Hemley, J., Cygan, G., Fein, J., Robinson, G., and D'Angelo, W., 1992. *Hydrothermal ore-forming processes in the light of studies in rock-buffered systems: I. Fe-Cu-Zn-Pb sulphide solubility relations.* Economic Geology **87:** 1-22.

Herzig, P., and Hannington, M., 1995. *Polymetallic massive sulfides at the modern seafloor: A review.* Ore Geology Reviews **10:** 95-115.

Hinchey, J., Hattori, K., and Lavigne, M., 2005. *Geology, petrology, and controls on PGE mineralization of the Southern Roby and Twilight Zones, Lac des Iles Mine, Canada.* Economic Geology **100**: 43-61.

Hollings, P., 2002. *Archean Nb-enriched basalts in the northern Superior Province.* Lithos **64:** 1-14.

Hollings, P., Wyman, D., and Kerrich, R., 1999. *Komatiite-basalt-rhyolite associations in northern Superior Province greenstone belts: significance of plume-arc interaction in the generation of the protocontinental Superior Province.* Lithos **46**: 137-161

Holwell, D., McDonald, I., and Armitage, P., 2006. *Platinum group mineral assemblages in the Platreef at the Sandsloot Mine, northern Bushveld Complex, South Africa.* Mineralogical Magazine **70**: 83-101.

Huston, D. L., Brauhart, C. W., Drieberg, S. L., Davidson, G. J., and Groves, D. I., 2001. *Metal leaching and inorganic sulfate reduction in volcanic-hosted massive sulfide mineral systems: Evidence from the paleo-Archean Panorama district, Western Australia.* Geology **29**: 687-690.

Hutchinson, D., White, R., Cannon, W., and Schulz, K., 1990. *Keweenaw hot spot: geophysical evidence for a 1.1 Ga mantle plume beneath the Midcontinent Rift System.* Journal of Geophysical Research **95**: 10869-10884.

Ioannou, S., and Spooner, E., 2007. *Fluid Temperature and Salinity Characteristics of the Matagami Volcanogenic Massive Sulfide District, Quebec.* Economic Geology **102**: 691-715.

Ishikawa, Y., Sawaguchi, T., Iwaya, S., and Horiuchi, M., 1976. *Delineation of prospecting targets for Kuroko deposits based on modes of volcanism of underlying dacite and alteration halos.* Mining Geology **26:** 105-117 (English abstract only).

Jenner, G., 1996. *Trace element geochemistry of igneous rocks: geochemical nomenclature and analytical geochemistry.* In: Wyman, D. (Ed.). Trace Element Geochemistry of Volcanic Rocks: Applications for Massive Sulphide Exploration. Geological Association of Canada Short Course Notes **12:** 51-77

Koo, J., and Mossman, D., 1975. *Origin and metamorphism of the Flin Flon stratabound Cu-Zn sulfide deposit, Saskatchewan and Manitoba.* Economic Geology **70:** 48-62.

Large, R., 1992. *Australian volcanic-hosted massive sulphide deposits: features, styles and genetic models.* Economic Geology **87:** 471-510.

Large, R., McPhie, J., Gemmell, B., Herrmann, W., and Davidson, G., 2001. *The spectrum of ore deposit types, volcanic environments, alteration halos, and related exploration vectors in submarine volcanic successions: some examples from Australia.* Economic Geology **96:** 913-938.

Large, R., Allen, R., Blake, M., and Herrmann, W., 2001. *Hydrothermal alteration and volatile element halos for the Rosebery K lens volcanic-hosted massive sulfide deposit, western Tasmania.* Economic Geology **96:** 1055-1072.

Lentz, D., 1998. *Petrogenetic evolution of felsic volcanic sequences associated with Phanerozoic volcanic-hosted massive sulfide systems: the role of extensional geodynamics.* Ore Geology Reviews **12:** 289-327.

Lesher, C. M., Goodwin, A. M., Campbell, I. H., and Gorton, M. P., 1986. *Trace-element geochemistry of ore-associated and barren, felsic metavolcanic rocks in the Superior Province, Canada.* Canadian Journal of Earth Sciences **23**: 222-237.

Lesher, C. M., and Campbell, I. H., 1993. *Geochemical and fluid dynamic modeling of compositional variations in Archean komatiite-hosted nickel sulfide ores in Western Australia.* Economic Geology **88**: 804-816.

Li, C., and Ripley, E., 2005. *The roles of fluid in the genesis and modification of reef-type PGE deposits in large layered intrusions.* Geochimica et Cosmochimica Acta **69**.

Loucks, R., and Mavrogenes, J., 1999. *Gold Solubility in Supercritical Hydrothermal Brines Measured in Synthetic Fluid Inclusions.* Science **284**: 2159 - 2163.

Lydon, J., 1984. Ore deposit models: Volcanogenic massive sulfide deposits. Geoscience Canada **11:** 195-202.

Macdonald, A., 1987. *The platinum group element deposits: classification and genesis.* Geoscience Canada **14**: 155-166.

MacGeehan, P., 1978. *The geochemistry of altered volcanic rocks at Matagami, Quebec: A geothermal model for massive sulphide genesis.* Canadian Journal of Earth Sciences **15:** 551-570.

MacLean, W., and Barrett, T., 1993. *Lithogeochemical techniques using immobile elements.* Journal of Geochemical Exploration **48:** 109-133.

McBirney, A., and Noyes, R., 1979. *Crystallization and Layering of the Skaergaard Intrusion.* Journal of Petrology **20**: 487-554.

Monecke1, T.,Gemmell, B., and Herzig, P., 2006. *Geology and volcanic facies architecture of the Lower Ordovician Waterloo massive sufide deposit, Australia.* Economic Geology **101:** 179-197.

Muir, T., 1982. *Geology of the Hemlo area, district of Thunder Bay.* Ontario Geological Survey Report **217**.

Muir, T., 2003. *Structural evolution of the Hemlo greenstone belt in the vicinity of the world-class Hemlo gold deposit.* Canadian Journal of Earth Sciences **40**: 395-430.

Mungall, J., and Naldrett, A., 2008. *Ore Deposits of the Platinum-Group Elements.* Elements **4:** 253-258.

Naldrett, A., 1989. Magmatic Sulphide Deposits. Oxford Monographs on Geology no. 14. Oxford University Press, New York, 186 p.

Naldrett, A., 1999. *World-class Ni-Cu-PGE deposits: key factors in their genesis.* Mineralium Deposita **34**: 227-239.

Nimis, P., Zaykov, V., Omenetto, P., Melekestseva, I., Tesalina, S., and Orgeval, J., 2006. *Peculiarities of some mafic-ultramafic- and ultramafic-hosted massive sulfide deposits from the Main Uralian Fault Zone, southern Urals.* Ore Geology Reviews **33:** 49-69.

Paquette-Mihalasky, F., 1999. *Silicification: oxygen isotope mapping of an Archean geothermal system at Noranda, Quebec.* Unpublished MSc. thesis, Laurentian University, Sudbury.

Pearce, J., 1996. *A user's guide to basalt discrimination diagrams. In: Wyman, D. (Ed.). Trace Element Geochemistry of Volcanic Rocks: Applications for Massive Sulphide Exploration.* Geological Association of Canada Short Course Notes **12:** 79-113.

Pearce, J., 2007. *Geochemical fingerprinting of oceanic basalts with applications to ophiolite classification and the search for Archean oceanic crust.* Lithos **100:** 14-48.

Pearce, J., and Peate, D., 1995. *Tectonic implications of the composition of volcanic arc magmas.* Annual Review of Earth and Planetary Sciences **23:** 251-285.

Percival, J., 2003. *Orogenic framework for the Superior Province: Dissection of the 'Kenoran Orogeny.'* Geological Survey of Canada, Western Superior NATMAP abstracts.

Percival J., 2006. *Geology and metallogeny of the Superior province, Canada.* Geological Survey of Canada: http://gsc.nrcan.gc.ca/mindep/synth_prov/superior/pdf/regional_synthesis.superior.percival.pdf

Percival, J., Sanborn-Barrie, M., Skulski, T., Stott, G., Helmstaedt, H., and White, D., 2006. *Tectonic evolution of the western Superior Province from NATMAP and Lithoprobe studies.* Canadian Journal of Earth Sciences **43**: 1085-1117

Percival, J., Mcnicoll, V., and Bailes, A. 2006. *Strike-slip juxtaposition of ca. 2.72 Ga juvenile arc and >2.98 Ga continent margin sequences and its implications for Archean terrane accretion, western Superior Province, Canada.* Canadian Journal of Earth Sciences **43:** 895-927.

Petersen, S., Schwarz-Schampera, U., Herzig, P., Hannington, M., and Jonasson, I., 2004. *Hydrothermal precipitates associated with bimodal volcanism in the Central Bransfield Strait, Antarctica.* Mineralium Deposita **39:** 358-379.

Polat, A., 1999. *Geochemistry of subduction-related mafic to felsic volcanic rocks of the late Archean Wawa greenstone belts, Superior Province, Canada.* ARI - International Journal for Physical and Engineering Sciences **51**: 277-295.

Polat, A., 2008. *The geochemistry of Neoarchean (ca. 2700 Ma) tholeiitic basalts, transitional to alkaline basalts, and gabbros, Wawa Subprovince, Canada: Implications for petrogenetic and geodynamic processes.* Precambrian Research **168:** 83-105.

Polat, A., Wyman, D., Kerrich, R., and Hollings, P., 1996. *Geochemical characteristics of mafic metavolcanic rocks from the Schreiber-Hemlo greenstone belt, Wawa subprovince: Implications for mantle source and tectonic setting.* Geological Association of Canada-Mineralogical Association of Canada Joint Annual Meeting, Program with Abstracts, 45 p.

Polat, A., Kerrich, R., and Wyman, D., 1998. *The late Archean Schreiber-Hemlo and White River-Dayohessarah greenstone belts, Superior Province: collages of oceanic plateaus, oceanic arcs, and subduction-accretion complexes.* Tectonophysics **289**: 295-326.

Polat, A., and Kerrich, R., 1999. *Formation of an Archean tectonicmelange in the Schreiber-Hemlo greenstone belt, Superior Province, Canada: implications for Archean subduction-accretion processes.* Tectonics **18**: 732-753.

Polat, A. and Kerrich, R., 2001. *Magnesian andesites, Nb-enriched basalts-andesites, and adakites from late Archean 2.7 Ga Wawa greenstone belts, Superior province, Canada: implications for late Archean subduction zone petrogenetic processes.* Contributions to Mineralogy and Petrology **141:** 36-52.

Power, M., Pirrie, D., Jedwab, J., and Stanley, C., 2004. *Platinum-group element mineralization in an As-rich magmatic sulphide system, Talnotry, southwest Scotland.* Mineralogical Magazine **68**: 395-411.

Reimold, W., and Gibson, R., 2006 (Eds.). Processes on the Early Earth. Geological Society of America Special Publication **405**.

Rimstidt, J., and Cole, D., 1983. *The mechanism of formation of the Beowawe, Nevada siliceous sinter deposit.* American Journal of Science **283**: 861-875.

Rinne, M., 2006. *Petrography and genesis of the Big Lake Ultramafic Complex and associated PGE mineralization, Marathon, Ontario.* Unpublished BSc. thesis, Lakehead University, Thunder Bay, 92 p.

Roberts, M., Oliver, N., Fairclough, M., Hölttä, P., and Lahtinen, R., 2003. *Geochemical and oxygen isotope signature of sea-floor alteration associated with a polydeformed and highly metamorphosed massive sulfide deposit, Ruostesuo, Central Finland.* Economic Geology **98**: 535-556.

Rosenberg, N., Spera, F., and Haymon, R., 1993. *The relationship between flow and permeability field in seafloor hydrothermal systems.* Earth and Planetary Science Letters **116**: 135-153.

Rossel, D., and Coombes, S., 2005. *The geology of the Eagle nickle-copper deposit, Michigan, USA.* Geotechnical report, Kennecott Minerals Co., 37 p.

Schandl, E., and Gorton, M., 2002. *Application of high field strength elements to discriminate tectonic settings in VMS environments.* Economic Geology **97:** 629-642.

Schneiders, D., Bickford, M., Cannon, W., Schulz, K., and Hamilton, M., 2002. *Age of volcanic rocks and syndepositional iron formations, Marquette Range Supergroup: implications for the tectonic setting of Paleoproterozoic iron. formations of the Lake Superior region.* Canadian Journal of Earth Sciences **29**: 999-1012.

Shervais, J., 2006. *The significance of subduction-related accretionary complexes in early Earth processes.* In: Reimold, W., and Gibson, R. (Eds.). Processes on the Early Earth. Geological Society of America Special Publication **405:** 173-192.

Sillitoe, R., Hannington, M., and Thompson, J., 1996. *High sulfidation deposits in the volcanogenic massive sulfide environment.* Economic Geology **91:** 204-212.

Singer, D., 1995. *World-class base and precious metal deposits - a quantitative analysis.* Economic Geology **90:** 88-104.

Skulski, T., Corkery, M., Stone, D., Whalen J., and Stern, R., 2000. *Geological and geochronological investigations in the Stull Lake-Edmund Lake greenstone belt and granitoid rocks of the northwestern Superior Province.* Report of Activities, Manitoba Geological Survey (2000): 117-128

Smyk, M., 2005. *Mineral deposits and metallogeny of the Midcontinent Rift in Ontario.* Geological Society of America, Abstracts with Programs 37-74.

Solomon, M., Tornos, F., Large, R., Badham, J., Both, R., and Zaw, K., 2004. *Zn-Pb-Cu volcanic-hosted massive sulphide deposits: criteria for distinguishing brine pool-type from black smoker-type sulphide deposition.* Ore Geology Reviews **25:** 259-283.

Stefansson, A., 2004. *Gold complexing in aqueous sulphide solutions to 500 degrees C at 500 bar.* Geochimica et Cosmochimica Acta **68**: 4121-4143.

Stott, G., 1997. *The Superior Province, Canada.* In: de Wit, M., and Ashwal, L. (Eds.). Greenstone Belts; Oxford Monographs on Geology **35**: 479-505.

Sun, S., and Mcdonough, W., 1989. *Chemical and isotopic systematics of oceanic basalts: implications for mantle composition and processes.* In: Saunders, A., and Norry, M. (Eds.). Magmatism in the Ocean Basins. Geological Society Special Publication: 313-345.

Syme, E., Bailes, A., Stern, R., and Lucas, S., 1996. *Geochemical characteristics of 1.9 Ga tectonostratigraphic assemblages and tectonic setting of massive sulfide deposits in the Paleoproterozoic Flin Flon belt, Canada.* Geological Association of Canada Short Course Notes **12:** 279-327.

Taylor, B., and South, B., 1985. *Regional stable isotope systematics of hydrothermal alteration and massive sulfide deposition in the West Shasta District, California.* Economic Geology **80:** 2149-2163.

Taylor, B., and Martinez, F., 2003. *Back-arc basin basalt systematics.* Earth and Planetary Science Letters **210:** 481-497.

Wang, Y., Qin, K., Tan, Y., and Hou, Z., 2000. *The Derni Cu-Co Massive Sulfide Deposit, Qinghai Province, China: Ultramafic Volcanic-hosted Submarine-exhalative Mineralization.* Exploration and Mining Geology **9:** 253-264.

Webster, J., Kinzler, R., and Mathez, E., 1999. *Chloride and water solubility in basalt and andesite melts and implications for magmatic degassing.* Geochimica et Cosmochimica Acta **63:** 729-738.

White, W., 2005. Geochemistry. (Online textbook: http://www.imwa.info/geochemistry/)

Williams, H., Stott, G., Heather, K., and Muir, T., 1991. In: Thurston, P., Williams, H., Sutcliffe, R., and Stott, G. (Eds.). Geology of Ontario. Ontario Geological Survey Special Volume **4:** 485-593.

Williams-Jones, A., and Heinrich, C., 2005. *Vapor transport of metals and the formation of magmatic-hydrothermal ore deposits.* Economic Geology **100**: 1287-1312.

Wyman, D., 1999. *A 2.7 Ga komatiite, low Ti tholeiite, arc tholeiite transition, and inferred proto-arc geodynamic setting of the Kidd Creek deposit: evidence from precise trace element data.* Economic Geology Monograph **10:** 511-528.

Yang, K., and Scott, S., 2003. *Geochemical relationships of felsic magmas to ore metals in massive sulfide deposits of the Bathurst mining camp, Iberian Pyrite Belt, Hokuroko district and the Abitibi Belt.* In: Goodfellow, W., McCutcheon, S., and Peter, J. (Eds.). Massive Sulfide Deposits of the Bathurst Mining Camp, New Brunswick and Northern Maine. Economic Geology Monograph **11:** 457-478.

Appendix A

Core Log Descriptions

The following logs were completed in July-August 2008 in order to address specific questions regarding the Big Lake VMS occurrence or host lithostratigraphy. For this reason, focus of description varies between hydrothermal alteration, fluid flow directions, and indicators of way-up in cumulate volcanic and sedimentary rocks. Other aims in re-logging key intervals were to define the relationship between cumulate ultramafic rocks and metavolcanic rocks, and to better define lithology within strongly mineralised intervals, which in previous logs are called "mineralized zone" with most emphasis on sulphide mineral assemblages.

Notes on abbreviations used: Where not specified, grain sizes were classified as follows: fgr: <1mm, mgr: 1-3mm, cgr: 3-10mm, vcgr: 10-30mm. CAA (Core Axis Angle) describes the acute angle of planes or linear features from the core axis (0 = parallel to core axis, 90 = perpendicular to core). In lithology names, bracketed modifiers refer to alteration assemblages interpreted to be of hydrothermal origin only, where chl = chlorite (distinguishing between hydrothermal and regional metamorphic chlorite is, in places, not possible in hand specimen), bt = biotite, anth = anthophyllite, tc = talc, K = K-spar or zoisite, and ct = calcite. W, M, and S describe the degree of alteration, generally following the method described in Chapter Two. MZ = mineralised with >10% sulphide content. The prefix "meta" is generally omitted for rocks such as siltstones or peridotites, but should be assumed.

Hole ID	From (m)	To (m)	Lithology	Description
37	72.4	73.4	Thin mafic metavolcanic flows (chl S) and wackes (chl S)	Soft, strongly chlorite-altered grey-green metavolcanic flow or mafic metasedimentary rock. A few sub-intervals <20 cm wide contain rounded white quartz+/-plagioclase grains <1 mm across, weakly distributed along a plane parallel to their contacts with surrounding metavolcanic rock @CAA 85; these may be bedding planes. Consists of >50% chlorite, with <5% calcite as discrete stringers parallel to bedding (most calcite is closely associated with/surrounds chalcopyrite veinlets). Entire unit, including lighter (more qtz-plag fragments) beds, contains 3-5% cpy, 2-3% po, <1% py, and <<1% sphalerite, all as stringers 1-10 mm wide. Sulphides abruptly disappear/trace below 73.4 m.
	73.4	73.9	Interbedded mafic metasedimentary rock and (meta)siltstones	Grey-green mafic metasedimentary rock with brown (brown mica) and white (qtz-rich) laminae parallel to bedding and contacts with adjacent siltstone @CAA 85 (top) to 35 (bottom). Siltstone beds are light grey, with laminae 1-7 mm thick, and < 5% visible brown mica. Towards upper contact with mafic metavolcanic rock, laminae grade to 5-10% brown mica bands.
39	237.0	242.3	Mafic metavolcanic rock (Chl-Bt+/-talc schist)	Grey-green mafic metavolcanic rock, mostly chlorite with <10% biotite and patches of diffuse talc (to judge from bleaching and powdery feel), with many calcite stringers and veinlets up to 5 mm wide, parallel to schistosity @ CAA 68. Below 239.6, uralitised pyroxene phenocrysts are visible, 1 mm across, and there is a segregation of brown mica into bands (bedding? flow banding?).
	242.3	243.3	Mafic metavolcanic rock and siltstone (Mineralised, ChlM, BtM))	As in above, but higher chlorite content and darker brown colour due to brown mica, with approx. 30% siltstone as beds 1-2 cm thick throughout unit. Upper contact is apparently sharp, but core is soft and broken, heavily chloritised. From upper contact with a mafic flow to the next siltstone at 242.7 m, textures are suggestive of fluid flow through the top of the overlying mafic flow? 1-3% cpy, 3-5% po, and <1% sph occur as hair-thin to 1 mm stringers and wisps, immediately adjacent to the top of almost every siltstone bed in this interval. At 243 m, again adjacent to a siltstone bed, a 3 cm band of stringer to semi-massive cpy and po are hosted in a soft and pitted chlorite-biotite vein.
	243.3	247.1	Siltstone	Light grey-green siltstone, with minor interbedded green chloritic mafic metasedimentary rock. Laminae are <1 to 5 mm thick, parallel to sharp upper and lower contacts @ CAA 55 (top) to 70 (bottom).
	247.1	249.0	Mafic metavolcanic rock	As in interval [242.3-243.3], grading to medium-grained leucoxene-bearing pyroxenite to melagabbro with depth.
54	70.9	96.5	Peridotite	Grey-blue talcose and strongly magnetic m-cgr cumulate peridotite, crystals 3-9 mm across. No appreciable fabric.
	96.5	98.3	Mafic dyke	Fine-grained dark green mafic dyke, sharp upper contact with peridotite fragments (rip-up?) obscured by split core, and lower contact with chill parallel to siltstone.
	98.3	98.7	Siltstone	Light grey siltstone with <10% green laminae <1 mm thick (resedimented mafic volcanic material?). Laminae @CAA 25.

54	98.7	107.1	Pyroxenite (possible hornfels and assimilated sedimentary material?)	Grey-green disequilibrium-textured melagabbro to pyroxenite with randomly oriented (only locally, otherwise following planar fabric @CAA 40) amphibole needles 5-15 mm long, in a mottled green to grey groundmass of chl-act-talc-plag. Upper contact is mottled and irregular, with deformed (partially assimilated?) quartz bands diffusing into unit over 5 cm. K-spar (or zoisite?) -epidote+/-pyrite+/-calcite veining <1 cm wide occurs throughout the unit, along with a few sub-intervals containing trace disseminated leucoxene. Lower contact is diffuse into darker green mgr pyroxenite with ~5% disseminated leucoxene.
	107.1	147.0	Pyroxenite	Dark green mgr cumulate pyroxenite, with weak diffuse biotite alteration and <5% calcite veinlets < 2 mm across throughout. Below 113.6 m, rock is moderately to strongly magnetic. Leucoxene content grades from ~10% as aggregates <1 mm across in upper ten metres of unit, to <1% below 125 m. Lower contact is probably diffuse over ~10 cm, but obscured by broken core.
	147.0	156.0	Peridotite	Talcose peridotite with calcite and chl-serp+/-talc veinlets. -156.9-158.2: Increasing biotite content with depth, to 90% biotite and 10% talc/serpentine - may suggest later hydrothermal alteration through the peridotite?
	219.0	225.4	Mafic flow	Thick mafic flow, with px phenocrysts 1mm across with plag visible in groundmass, and in some intervals (<20% total) as phenocrysts <2 mm across. Millimetre-scale calcite-K-spar-epidote veining is common throughout. Fines towards lower contact, to vfgr below 225; suggests top of flow or thick chill margin?
	225.4	233.3	Siltstone	Light grey siltstone, with laminae 1-10 mm thick @ CAA 80, parallel to sharp upper and lower contacts. Upper 90 cm and a few sub-intervals <30 cm wide contain interbedded/laminated mafic beds (reworked mafic volcanic/volcaniclastic material?). Trace cpy and py occur as stringers within the uppermost mafic beds, absent elsewhere. -229.2-232.0: the siltstone contains 1-5% rounded white plagioclase clasts 0.5-2 mm across, and <1% rounded clear quartz clasts <5 mm, with no evident grading in size or abundance.
62	93.0	96.2	Ferropyroxenite (cumulate flow base?)	Dark green strongly magnetic pyroxenite with uralitised pyroxene cumulus crystals <3 mm across along a weak (possibly igneous?) foliation @ CAA 45. Lower contact is obscured by broken core, but is probably sharp or diffuse over only a few cm, marked by strong shearing (previous logs describe a "sheared lower contact @ CAA 58").
	96.2	100.6	Mafic-ultramafic metavolcanic rock (flow or pyroclastic?) (ChlS, BtM, AnthW, TcW)	Grey-green, locally talcose metavolcanic rock (flow, possibly volcaniclastic in some places) with overall trace-1% finely disseminated pyrrhotite and chalcopyrite.
	100.6	103.7	Interbedded mafic-ultramafic metavolcanic rock (flow/resedimented/pyroclastic?) and siltstone	Mostly grey-green chloritic metavolcanic (volcaniclastic?) rock with 10-20% siltstone as beds/laminae 5-20 mm wide. Most siltstone-mafic contacts sharp, but somewhat masked by chl-brown mica+/-anthophyllite alteration and sulphide stringers which tend to occur along these planes @ CAA 69. Hydrothermal alteration assemblages are mostly 40% chlorite, 20-40% brown mica, <5% talc (in diffuse patches), and <1% anthophyllite as radial growths 1 mm across mostly within brown mica bands. Sulphide content is highest within 1 m of lower contact, with 5-8% cpy and <5% po (up to 10% within 10 cm of lower contact) as stringers/veinlets <2 mm wide, and 1% sph within some po veins. Lower contact is diffuse over 5 cm, based on a decrease in overall sulphide content from ~10% to trace, and an appreciable decrease in hydrothermal alteration (lighter colour, lower mica content, lack of diffuse anastomosing veinlets).
	103.7	105.6	Mafic-ultramafic metavolcanic rock and siltstone (unmineralised)	Grey-green metavolcanic rock similar to interval [96.2-100.6], but with a few (overall <5%) siltstone beds/laminae 1-4 mm wide. Also contains radial aggregates of a light green amphibole (anthophyllite?) 3-5 mm across, along a weak planar fabric @ CAA 74. Lower contact is sharp and slightly undulating @ CAA ~70.
	105.6	106.9	Siltstone, locally pelitic	Light grey to light brown-grey finely laminated recrystallised siltstone, ~5% of siltstone laminae having pink garnet porphyroblasts 2-5 mm across. Trace disseminated pyrite and pyrrhotite occur throughout, mostly along bedding planes @ CAA 70-60. Lower contact is sharp and irregular, lined with 2 cm of biotite-calcite veining, @ CAA ~60.
	106.9	113.6	Ferropyroxenite/cumulate flow base	Grey-green, strongly magnetic, locally blue-tinged (olivine-bearing?) pyroxenite with pyroxene cumulus crystals 1-3 mm long. Plagioclase content increases to ~8% below 111 m. Overall <5% calcite (not leucoxene) interstitial to pyroxenes, possibly replacing plagioclase (?), and as hair-thin veinlets. Upper 2.5 m grades from a strong planar fabric @ CAA 55 to a weak planar fabric @ CAA 53. Trace finely disseminated pyrite and pyrrhotite throughout the unit. Lower contact grades over ~20 cm to an aphanitic rock of the same colour.
	113.6	114.9	Mafic-ultramafic metavolcanic rock (flow top?)	Grey-green vfgr metavolcanic rock with 10% calcite (+/- epidote) veins <5 mm wide. Upper 60 cm [illegible] examples of pillows (defined by calcite-replaced selvages?) stretched along a moderate histosity @ CAA 64. Lower contact is sharp @ CAA 58.
	114.9	115.9	Siltstone	Light grey to light brown-grey finely laminated recrystallised siltstone, locally garnetiferous as in interval [105.6-106.9]. Laminae and sharp lower contact both @ CAA 67.

62	115.9	138.3	Feldspathic pyroxenite to gabbro/Plagiophyric mafic metavolcanic flow centre (?) (KW)	Grey-green metavolcanic rock, distinct from other units identified as flow centres in terms of a) slightly lighter colour and plagioclase content ~20-25%, b) smaller pyroxene crystals, most 1 mm across, and c) 2-3% disseminated anhedral white plagioclase (?) phenocrysts (?). 5% calcite-epidote-zoisite+/-K-spar (and a few quartz-epidote veins) 1-30 mm wide, most with diffuse epidote alteration over a few cm into groundmass of surrounding rock.
65	81.6	94.6	Mafic-ultramafic metavolcanic flow	Grey-green, non-magnetic locally blue-tinged metavolcanic rock, grading from a cumulus base with relict cumulate olivine and pyroxene crystals 1-2 mm across (locally <5 mm long dendritic green needles) to a talcose, aphanitic flow with calcite veining (towards flow top?).
	94.6	101.2	Mafic metavolcanic rock (strongly sheared)	Dark grey-green mafic metavolcanic rock, likely a continuation of above interval, but with a strong planar fabric @ CAA 55. ~5% calcite as veining parallel to schistosity, hair-thin to 2 mm wide. Upper and lower contacts are gradational over ~20 cm, based on a change from weak to strong planar fabric.
	101.2	106.6	Pyroxenite/cumulate flow base	Grey-green pyroxenite (or flow base?) with 3-8% leucoxene between pyroxene crystals 1-3 mm across, and a weak planar fabric @ CAA ~45. Grades with depth to non-magnetic metavolcanic rock as in the bottom of interval [81.6-94.6], with one slightly brown-tinged sub-interval 30 cm wide of weak brown mica alteration, and <1% K-spar in hair-thin veinlets. Lower contact is sharp, or diffuse over 1 cm at most, based on increase in magnetism.
	106.6	111.2	Mafic pyroclastic rock(?) (Weakly mineralised)	Grey-green, moderately to strongly magnetic mafic metavolcanic (possibly pyroclastic?) rock with<5% evenly distributed rounded and elongate K-spar grains/lapilli (?) <1 mm long, locally up to 80% in thin beds a few mm wide, @ CAA 68. Rounded pyrite clasts 5 mm long, some enclosing euhedral magnetite crystals <1 mm across, are also disseminated throughout the unit (overall 1%), in a few places scattered along bedding planes. -107.11: Two thin beds/veinlets (?) of cpy parallel to bedding, both <1 mm wide.
	111.2	114.0	Mafic metavolcanic/pyroclastic rock(?) (Weakly mineralised)	As in above interval [106.6-111.2], but only locally pyrite-bearing and magnetic.
	114.0	119.7	Pyroxenite/cumulate flow base	Grey-green pyroxenite (or flow base?), with <5% leucoxene between relict pyroxene crystals 2-3 mm across. Uppermost 3 m contains several cross-cutting light grey lamprophyre dykes. Grades with depth to pyroxene crystals 1-2 mm. Trace disseminated pyrite increases to 2-3% disseminated pyrite within 80 cm of lower contact, as irregular blebs <3 mm across and some along fracture surfaces. Lower contact is sharp and planar @ CAA 79.
	119.7	128.2	Interbanded siltstone and mafic metavolcanic rock	Light grey finely laminated recrystallised siltstone with <20% green chloritic beds with sharp contacts. Trace finely disseminated pyrite occurs along siltstone bedding planes @ CAA 60. Upper 85 cm is strongly magnetic, remainder is non-magnetic, with no visible contact. 126.1-128.2: Two strongly magnetic blue-tinged py-bearing ferropyroxenite dykes (?) with sharp irregular contacts, and surrounded by brown mica-altered metavolcanic rock.
	128.2	152.0	Pyroxenite/cumulate flow base	Locally strongly magnetic grey-green pyroxenite as in interval [114.0-119.7], with pyroxene crystals 1-3 mm across. Trace cpy and 1 % pyrite are finely disseminated through most of the unit, interstitial to pyroxenes or along hair-thin fractures. Lower contact grades over several metres, as pyroxene grain size decreases with depth.
	152.0	157.5	Mafic-ultramafic metavolcanic flow (weakly mineralised)	Fining from upper unit, a grey-green, locally talcose (Ol-rich flow?), strongly magnetic mafic metavolcanic flow. A weak planar fabric is measured @ CAA ~70, along which thin calcite veining occurs. Trace cpy, py, and po are finely disseminated through most of the unit. Lower contact is sharp and irregular. -155.4, 156.9: veinlets <2 mm wide of chalcopyrite, pyrite, and some minor visible magnetite.
	157.5	159.1	Pyroxenite/cumulate flow base	As in interval [128.2-152], fining with depth.
	159.1	175.1	Mafic-ultramafic metavolcanic flow	Continuation of above interval, grey-green moderately magnetic and locally talcose, becoming strongly sheared with depth, with a schistosity, in places crenulated, @ CAA 40-65.
	175.1	181.9	Feldspathic pyroxenite/cumulate flow base	As in interval [128.2-152], but slightly lighter colour from ~15% lighter saussuritised plagioclase in groundmass.
	181.9	188.1	Siltstone/pebbly siltstone	Light grey finely laminated non-magnetic siltstone, with darker laminae 1-2 mm thick containing <25% brown mica and chlorite. A few sub-intervals contain 3-5% rounded white plagioclase +/- quartz (no K-spar) clasts <3 mm long, with no clear fining direction.
	188.1	188.5	Magnetite-bearing siltstone	As in above interval [181.9-188.1] but strongly magnetic due to 5-10% euhedral magnetite crystals <1 mm across along some bedding planes @ CAA 55 (Fe-rich metasedimentary rock? Possible exhalite laminae?). Sharp upper and lower contacts @ CAA 55.

65	188.5	204.5	Pyroxenite to gabbro/cumulate flow base	As in interval [175.1-181.9], dark green pyroxenite at top, but 2 m from upper contact composition is almost gabbroic, with 30-40% pale green saussuritised (and weakly calcite-bleached) plagioclase surrounding uralitised pyroxene cumulus crystals 1-2 mm across. Fines gradually with depth.
	224.0	228.8	Peridotite	Strongly magnetic blue-grey talcose peridotite, many hair-thin serp-talc veinlets throughout. Lower contact is diffuse over 5 cm with little indication of assimilation or cooling.
	228.8	231.3	Mafic-ultramafic metavolcanic rock (Chl S, Tc S, Bt W)	Dark grey-green, non- to moderately magnetic chlorite-talc-brown mica schist with darker green chlorite and dark brown mica in diffuse patches, more common within 1 m of the upper contact with peridotite.
	231.3	232.0	Calcite-ilmenite vein	Patchy calcite-ilmenite vein through metavolcanic unit, consisting of irregular and sometimes radial growths of weakly magnetic euhedral-subhedral ilmenite laths 5-15 mm long within white calcite. Dark green platy mineral (visibly crystalline serpentine?) rims ~1 mm wide are observed at the edges of the vein and at ilmenite-calcite interfaces.
	232.0	232.8	Mafic-ultramafic metavolcanic rock (Chl S, Tc M, Bt W-M)	Similar to 228.8-231.3.
	232.8	237.9	Peridotite	Strongly magnetic and talcose peridotite, diffuse upper and lower contacts are marked in part by darker colour (brown mica) and decreased magnetism over ~ 5cm.
	237.9	281.9	Mafic-ultramafic metavolcanic rock (Chl S, Tc W, Bt W-S)	Grey-green to dark brown-green mafic (to ultramafic, judging from colour and talc alteration) metavolcanic rock, similar to overlying metavolcanic rock. Three diffuse sub-intervals ~0.5-1 m wide are darker due to >60% brown mica, and most of the unit features fluid flow/alteration textures (brown mica net-textured veining) along a moderate schistosity @ CAA 45-70. Two sub-intervals 0.6 and 1 m wide have 20-40% calcite as thick veining (some have suggested these are remnants of stretched pillow selvages).
	281.9	282.7	Mafic-ultramafic metavolcanic rock (?) (Mineralized chl-talc schist)	As in above interval, lighter grey-green with 5-10% po, 3-5% cpy, and 1% sph as stringers 1-7 mm wide. Sphalerite is blackjack variety, apparently associated with pyrrhotite stringers and not with chalcopyrite. Stringer mineralisation decreases abruptly at the lower contact, defined by an irregular siltstone fragment (?) that is partially overprinted by soft chl+/-talc veining. Sulphide stringers adjacent to this contact contain irregular siltstone fragments 3-15 mm across.
73	282.7	285.5	Interbedded mafic metavolcanic rock (resedimented/volcaniclastic?) and siltstone (Mineralised, chlS, tcS)	Mafic metavolcanic (or metasedimentary?) rock interbedded with light grey siltstone beds 5-30 mm wide. Primary bedding textures are partially masked by chloritic stringers and sulphide stringers/veins. ~5-10% total sulphide, higher immediately adjacent to siltstone beds, even very thin beds---this may suggest down-hole direction of mineralising fluid flow.
	285.5	288.9	Pyroxenite/olivine websterite	Grey-green, in places blue-tinged (higher olivine content) pyroxenite with trace disseminated leucoxene. Upper contact is diffuse over 1 m, lighter in colour than surrounding rock with up to 40% talc +/- serpentine, and grades to a medium-grained pyroxenite with pyroxene phenocrysts 1-4 mm across. Lower contact is diffuse over 3 cm, marked by brown mica and disseminated to semi-massive pyrrhotite.
	288.9	301.7	Interbedded mafic flows and wacke (ChlM)	Mostly grey-green mafic metavolcanic rock, with <10% interbedded grey wacke beds 1-15 cm wide consisting of recrystallised quartz and brown mica. Two of these wacke beds contain 5% finely disseminated pyrrhotite along lamination surfaces @ CAA 40. Hair-thin to 6 cm K-spar-calcite-epidote veining increases with depth, and trace pyrite and K-spar occur along fracture surfaces throughout.
	301.7	314.9	Mafic metavolcanic rock	As in above interval, lacking sedimentary rocks, and relict pyroxene phenocrysts (uralitised) grade from <<1 mm to 1 mm across towards the centre of the unit. K-spar-epidote-calcite veining is common, epidote also replacing white plagioclase in diffuse patches. Becomes moderately magnetic within ~3 m of lower contact, and lowermost 5 cm contain <5% visible magnetite porphyroblasts 1 mm across. Lower contact is sharp, parallel to schistosity @ CAA 56.
	314.9	322.9	Siltstone	Light grey recrystallised siltstone (sugary texture on broken surfaces), with laminae/beds <1 to 15 mm wide @ CAA 60. Many laminae contain rounded plagioclase and quartz clasts/pebbles <1 mm across, and two beds 5 cm wide are green due to <50% chlorite (reworked mafic metasedimentary rock?). K-spar-epidote veinlets are common throughout.
	322.9	329.6	Mafic metavolcanic rock	Dark grey-green, non-magnetic mafic metavolcanic rock/flow. Sharp, irregular upper contact cross-cuts siltstone bedding by a few degrees, @ CAA 60. Lower contact is sharp and parallel to adjacent siltstone bedding @ CAA 52.
	329.6	333.4	Siltstone	As in interval [314.9-322.9]
	333.4	339.0	Mafic metavolcanic rock	As in interval [322.9-329.6], with strong biotite alteration within 20 cm of lower contact (contact metamorphosed?).

73	339.0	340.0	Peridotite	Light grey-blue, strongly magnetic and talcose peridotite. 1% finely disseminated cpy and trace py throughout unit.
	127.0	134.5	Peridotite	As in interval [224-228.8], strongly talcose.
	134.5	141.7	Mafic metavolcanic rock (BtS, ChlM, TcM)	Dark grey-green mafic metavolcanic rock(?), locally dark from >60% chlorite and 20% brown mica, often in discrete bands <1 mm wide. Locally weakly magnetic, likely due to trace finely disseminated pyrrhotite. Strong schistosity @ CAA 45. Upper contact with peridotite is diffuse over ~10 cm, lower contact sharp @ CAA 50.
	141.7	144.2	Peridotite	As in interval [127-134.5], slightly more talc alteration and talc-serpentine veining, very soft and friable. Within 20 cm of lower contact, up to 10% brown mica occurs in stringers parallel to schistosity @ CAA 41. Lower contact is sharp @ CAA 52.
	144.2	150.7	Mafic metavolcanic rock (no/little hydrothermal alt'n)	Dark grey-green mafic metavolcanic rock(?) as in interval [134.5-141.7], but overall lighter colour, lower chlorite and brown mica content; only local hydrothermal alteration within upper 40 cm adjacent to peridotite, which grades from black (biotite+chlorite) to dark green (chlorite+biotite) to usual grey-green (chlorite). 5% calcite veining hair-thin to 5 mm wide throughout, mostly parallel to schistosity. Upper 6 cm contains 5% pyrite as irregular blebs 3-7 mm across, as well as 1-2% disseminated to wispy cpy and 1% finely disseminated po. Remainder of unit contains trace finely disseminated pyrite +/- pyrrhotite, usually concentrated along schistosity plane @ CAA 48-40.
	150.7	150.8	Metapelite	Dark green strongly magnetic garnetiferous metapelite. Contains 10% visible magnetite porphyroblasts 1 mm across and 5% red rounded garnet porphyroblasts 3-15 mm across. 5-10% disseminated pyrrhotite and 2-3% finely disseminated pyrite, sometimes in larger aggregates cut by dark green acicular actinolite. Sharp upper and lower contacts @ CAA 38.
	150.8	166.1	Mafic metavolcanic flow	Grey-green non-magnetic mafic metavolcanic rock, possibly a thick flow centre, with uralitised pyroxene cumulus crystals 1-2 mm across in a white plag-calcite-chlorite +/- brown mica groundmass. Grain size does not decrease with depth as is often observed elsewhere. Several sub-intervals ~10 cm wide, generally with diffuse contacts over a few cm, have up to 30% brown mica defining a strong schistosity @ CAA 35. Sharp lower contact @ CAA 35.
74	166.1	175.1	Mafic metavolcanic rock (resedimented / volcaniclastic?)	Grey-green locally moderately magnetic mafic metavolcanic rock with 30% white (plag-rich, quartz unlikely) laminae/beds 1-15 mm wide with sharp contacts. These are interpreted to have a sedimentary rather than a metamorphic origin, in part due to a) sharp, not particularly sheared contact of this unit with overlying unbanded rock, with sharp increase in pyrite, epidote, and magnetism, and b) two sub-intervals within this unit 3 and 21 cm wide of finely laminated metasiltstone with sharp upper and lower contacts. Overall trace finely disseminated po and 2-3% pyrite, finely disseminated and locally as larger elongate blebs <7 mm long. Sharp lower contact @ CAA 39. (Previous logs describe an ultramafic dyke from [168.22-169.47], which is now obscured by broken core).
	175.1	179.0	Siltstone	Light grey recrystallised siltstone with laminae 1-2 mm wide (a few beds <2 cm wide) up to 20% brown mica in some beds. No apparent grading in grain size or composition. Trace disseminated po is observed only at edges of sparse calcite veins. Sharp lower contact @ CAA 45.
	179.0	182.5	Ferropyroxenite (ultramafic-mafic cumulate flow base?)	Dark grey-green mafic-ultramafic metavolcanic rock (likely a cumulate flow centre/base), as in interval [144.2-150.7], but darker with <10% plagioclase, and slightly coarser-grained; uralitised pyroxene phenocrysts and <10% blue-tinged serpentinised olivine phenocrysts are 1-3 mm across. Trace finely disseminated pyrite. Non-magnetic to locally strongly magnetic where up to 25% magnetite crystals <1 mm across are visible, with 1-3% finely disseminated white leucoxene. Moderate schistosity @ CAA 40.
	182.5	183.1	K-spar porphyry dyke	Pink-grey crowded K-spar porphyry dyke, granitic composition with K-spar phenocrysts 1-3 mm across. Upper contact irregular and sharp, lower contact sharp @ CAA 30, both lined with calcite+/-pyrite.
	183.1	210.0	Pyroxenite to mafic metavolcanic flow(s) (?)	Continuation of interval [179-182.5], fines gradually with depth to a non-magnetic slightly lighter-coloured grey-green mafic metavolcanic rock with 10-15% white minerals (likely plagioclase +/- calcite and talc). Strong planar fabric @ CAA 46, very strong from 203-205 m, with 10-40% calcite as stripes 1-7 mm wide @ CAA 48.
	210.0	210.4	Metapelite	Strongly sheared dark green chloritic rock as in adjacent rock, but with ~5% elongate pink garnet porphyroblasts 1-6 mm long, with trace disseminated py along bedding surfaces.
	210.4	227.4	Mafic metavolcanic rock (KW)	Grey-green, locally talc-bleached mafic metavolcanic rock (flows, mafic metasedimentary rock, or pyroclastic rock?), likely a continuation of the base of interval [183.1-210.0]. Diffuse K-spar alteration yields a pinkish colour in a few sub-intervals ~20 cm wide. - 221.20-221.25: strongly magnetic light grey sub-interval with 20% euhedral magnetite crystals <2 mm across, and 3-5% irregular pyrite aggregates.
	227.4	231.6	Mafic metavolcanic flow (ChlS, BtS)	Grey-green moderately magnetic feldspathic pyroxenite, with uralitised pyroxene cumulus crystals 1-3 mm across in a light groundmass of plagioclase (~15% overall), calcite, and minor diffuse K-spar alteration (?) in some sub-intervals. Grades with depth to a non-magnetic fine-grained grey-green metavolcanic flow. Below ~230.6 m, colour is darker due to higher chlorite and brown mica content (~50% chl, 20-30% brown mica, in diffuse bands 5-15 mm wide). Below 231 m, 1% pyrite occurs as rounded subequant crystals up to 6 mm across. Sharp lower contact with siltstone @ CAA 47.

74	231.6	239.8	Siltstone (MZ)	Light grey recrystallised siltstone with laminae/beds 1-45 mm wide. Upper 1.1 m contains <30% brown beds/laminae with <40% brown mica. -234.4-239.6: pebbly siltstone, with 10-20% rounded, equant white feldspar clasts 1-5 mm in diameter, often concentrated along certain bedding surfaces @ CAA 46. Despite an apparently low degree of deformation in this interval there is no appreciable direction of grading in size or concentration of grains. Locally weakly magnetic. -Below 239.6: <5% disseminated euhedral magnetite crystals <1 mm across. Sulphide content is limited to pyrite within the uppermost 60 cm of this unit, as disseminated to semi-massive beds of anhedral crystals/aggregates <1.5 mm across within darker (containing brown mica) beds only. This bedded habit is likely sedimentary, not stringer-textured, as seen elsewhere. Trace pyrrhotite and trace finely disseminated euhedral magnetite are also observed within these pyritiferous beds.
	239.8	240.1	Iron formation (?)	Strongly magnetic siltstone (possibly recrystallised chert-magnetite or silicate facies banded iron formation?) with distinct magnetite laminae <1 mm wide. Bedding contacts are sharp and slightly undulating @ CAA ~48, and unit contacts are sharp based on appearance of pure magnetite laminae, although magnetite is present ~20 cm beyond both contacts into siltstone.
	240.1	241.4	Siltstone, pebbly siltstone	Light grey recrystallised siltstone with 30% darker chloritic bands. 2-3% euhedral magnetite crystals <1 mm across are disseminated through most beds. Previous logs describe up 25% rounded clasts in a few sub-intervals in this unit. Lower contact is probably sharp, but obscured by a single calcite vein 2 cm wide running @ CAA ~80.
	241.4	250.0	Mafic metavolcanic rock (KW)	Grey-green, non-magnetic mafic metavolcanic rock (flow centre?) with cumulus pyroxene crystals <1 mm across. Minor K-spar (or zoisite?) + epidote veining 2-5 mm cross-cuts most of the unit.
	108.2	127.8	Peridotite	Blue-grey strongly magnetic peridotite, with relict serpentinised olivine cumulus crystals 1-3 mm across. Sharp lower contact @ CAA 47.
	127.8	138.6	Mafic metavolcanic flows and minor siltstone (ChlM, BtW)	Grey-green mafic-ultramafic metavolcanic rock, locally moderately magnetic (around po) with <10 % brown mica in diffuse bands several cm wide. Trace finely disseminated pyrite and 1-2% stringer and disseminated pyrrhotite occur throughout the unit, particularly against upper contact of siltstone at [129.72]. Sharp lower contact @ CAA 45. -129.72-129.97: Light grey finely laminated siltstone with sharp contacts and laminae @ CAA 38. -130.88-131.09: Siltstone with trace stringer and disseminated pyrrhotite, sharp contacts and laminae @ CAA 43-45. -131.88-133.28: Green mafic metavolcanic rock (pyroclastic?) with 5% white clasts <2 mm across. -133.85-138.52; Interflow/interbedded siltstone and chloritic metavolcanic/volcaniclastic bands ~1 cm across, with a strong schistosity, generally sharp contacts, and bedding planes @ CAA 48 (at 133.9 m) to 77 (138 m).
	138.6	148.1	Siltstone, pebbly siltstone	Light grey finely laminated recrystallised siltstone, non-magnetic, with <10% green chloritic (volcanic/volcaniclastic?) beds/laminae with trace disseminated pyrite. Laminae @ CAA 60-70. -140.3-141.7: Siltstone with several beds containing rounded K-spar +/- plagioclase clasts 2-4 mm across. Non-magnetic fine grained light grey siltstone. Sulfide mineralisation only in volcanic subunits: finely disseminated pyrite (trace). Sharp lower contact @ CAA 68.
90	148.1	150.3	Ferropyroxenite/cumulate flow base (?)	Grey-green locally magnetic pyroxenite or cumulus flow centre/base, with pyroxene crystals 1-3 mm across. 1-2% finely disseminated pyrite. Lower contact fines downcore over ~1 m, to a fgr metavolcanic rock of the same colour.
	150.3	150.9	Mafic-ultramafic metavolcanic rock (ChlM, BtM)	Grey-green to brown-green metavolcanic rock with 10-20% calcite veining 1-15 mm wide (possible pillows?). Trace, locally 5% disseminated pyrite, and trace finely disseminated and stringer pyrrhotite. Sharp lower contact @ CAA 55.
	150.9	154.6	Pyroxenite-ferropyroxenite/Cumulate flow base	Non- to locally moderately magnetic grey-green pyroxenite to ferropyroxenite, likely a cumulate flow base/centre, grading to a metavolcanic rock with depth. Magnetic only from [151.5-153.0]; i.e., centre of unit. 1-2% finely disseminated pyrite and trace disseminated leucoxene. Lowermost 60 cm fines downward into an aphanitic metavolcanic rock, which then grades into a lighter grey colour with increasing abundance of siltstone laminae (there is likely a sharp volcanic-sedimentary contact, but based on colour, lower contact is diffuse over 10 cm).
	154.6	155.3	Pebbly Siltstone	Light grey non-magnetic recrystallised siltstone with <5% rounded white clasts 2-4 mm across. Sharp lower contact and laminae @ CAA 57.
	155.3	158.6	Pyroxenite-ferropyroxenite/Cumulate flow base	Grey-green pyroxenite-ferropyroxenite, grading to a metavolcanic flow with depth, almost identical to interval [150.9-154.6], including magnetism observed only in the centre of the unit, in interval [156.7-157]. Sharp lower contact @ CAA 41.
	158.6	160.1	Siltstone	Light grey finely laminated siltstone, with increasing brown mica content with depth to 40% below 159.3 m. Weakly magnetic, with trace finely disseminated pyrite. Sharp lower contact @ CAA 64.

	160.1	164.6	Ferropyroxenite/cumulate flow base (?)	Grey-green strongly magnetic ferropyroxenite, with 5-8% subhedral magnetite 1-2 mm across. Trace finely disseminated pyrite and pyrrhotite. Sharp, slightly undulating lower contact @ CAA ~20, lined with 2 mm of calcite.
90	164.6	166.7	Pyroxenite/cumulate flow base (?)	Grey-green non-magnetic pyroxenite, otherwise similar to interval [160.1-164.58]. Lower 50 cm is fgr, with an apparently diffuse lower contact over 5 cm.
	166.7	171.0	Siltstone	Light grey non-magnetic finely laminated and locally calcite-bleached siltstone, with laminae 1-5 mm wide @ CAA 54.
	171.0		End of Hole	
	318.1	327.0	Peridotite	Grey-blue strongly magnetic peridotite, with serpentinised cumulus olivine crystals 1-2 mm across. Strongly talcose and cross-cut by talc+/-serpentine veinlets < 1mm wide. Upper contact sharp @ CAA 38. Lower contact broken, soft, dark (chl, actinolite?), diffuse over 10 cm.
	327.0	333.3	Siltstone	Light grey siltstone, recrystallised, finely laminated. 10% pelitic laminae <2 mm wide. 2-3% pyrrhotite occurs throughout unit as stringers <1 mm wide parallel to bedding planes @ CAA 60, and locally up to 30% within 40 cm of upper contact. Upper 5 m is white, talc-bleached (consider proximity to peridotite).
	333.3	340.2	Mafic metavolcanic flow	Grey-green non-magnetic cumulus flow base (or pyroxenite) with relict pyroxene crystals 1-3 mm across, and 1% finely disseminated leucoxene. Moderate schistosity @ CAA 69. Grades slowly with depth into a moderately schistose vfgr flow with calcite veining 5-20 mm wide. Upper contact sharp @ CAA 66, marked by 1 cm of >50% biotite; lower contact sharp @ CAA 70.
	340.2	343.2	Mafic metavolcanic flow	As in interval [333.3-340.2]; grey-green metavolcanic flow with relict pyroxene crystals <5 mm across in a lighter grey (plag-talc+/-calcite) groundmass with decreasing grain size and increasing calcite veining with depth. Lower contact sharp @ CAA 55.
	343.2	345.4	K-spar porphyry dyke	Pink-grey groundmass-supported porphyry with 15% K-spar phenocrysts < 2-6 mm across in a K-spar-quartz-biotite groundmass. Weak schistosity @ CAA 60, and sharp upper and lower contacts @ CAA 70 and 85 respectively. Contains ~5% dark green chloritic xenoliths (country rock fragments?) <1 cm across.
	345.4	347.1	Mafic metavolcanic flow (BtW)	Grey-green non-magnetic cumulus flow centre, slightly higher brown mica content (~10-20%) than interval [333.3-340.2]. Strong schistosity @ CAA 63. Sharp lower contact @ CAA 50. Locally 10% pyrrhotite occurs as stringers 1-2 mm wide within the lowest 10 cm (adjacent to downhole siltstone).
92	347.1	347.5	Siltstone	Light grey siltstone, as in interval [327-333.3], with 3-5% po and trace cpy in hair-thin stringers parallel to and occasionally cross-cutting bedding planes. Sharp lower contact parallel to siltstone laminae @ CAA 44.
	350	353.5	Peridotite	Grey-blue strongly magnetic talcose peridotite, as in interval [318.1-327], but with smaller cumulus olivine (~1 mm across). Talc veining and strong schistosity @ CAA 60. Lower contact is diffuse over 20 cm (flow centre?).
	353.5	354	Mafic-ultramafic metavolcanic flow (Mineralised, TcM, ChlM, BtM)	Grey-green, slightly blue-tinged metavolcanic rock as in interval [347.5-350], but weakly magnetic and slightly darker colour due to increased chlorite-brown mica alteration (~30% chlorite and 20% brown mica). Lower contact is sharp, defined by top of a siltstone bed, @ CAA 58. Lowermost 6 cm, adjacent to downhole siltstone, is a 6 cm wide band of massive to stringer-textured sulphides, overall 50% po, 30% cpy, and 5% sph, surrounding rounded siltstone fragments <5 mm and dark green chloritic (likely metavolcanic?) fragments <3 mm across.
	354	357.9	Interbanded mafic metavolcanic rock and siltstone (MZ, ChlS, BtM-S)	60% Dark grey-green mafic, locally weakly magnetic metavolcanic (or reworked metasedimentary?) rock, with 40% interbedded/interflow siltstone beds 1-15 cm wide. Contacts between siltstones and mafic rock are sharp and planar, parallel to siltstone laminae, @ CAA 55-70. Overall 3-5% po, 1-2% cpy, and trace sph occur as stringers <3 mm wide or irregular patches <1 cm across, following bedding planes and immediately adjacent to upper contacts of siltstone bands. (3% pyrite has also been reported in previous logs, but was not observed, possibly due to split core.)
	357.9	396	Interbanded mafic metavolcanic rock and siltstone (KW, ChlW-M, BtM)	Similar to interval [354.0-357.9], but with 60% siltstone and 40% mafic metavolcanic/metasedimentary/metavolcaniclastic rock, lower chlorite and brown mica alteration with depth, and the first appearance of K-spar (or zoisite?)-epidote-calcite+/-pyrite veining below 360 m. Some mafic units contain extremely elongate white clasts up to 3 mm along short dimension, along strong schistosity and bedding planes @ CAA 65-- these may also be interpreted as mafic pyroclastic beds?

	441	453.1	Interbedded siltstone and mafic metavolcanic/metasedimentary rock (KM)	Light grey recrystallised siltstone with 10% dark green chloritic beds with bedding surfaces @ CAA 30-55. K-spar-epidote+/-calcite+/-pyrite diffuse alteration and mm-scale veining are common throughout, especially towards lower contact with diabase dyke.
105	477.9	480.1	Mafic metavolcanic flow centre	Grey-green cumulate-textured flow centre/base(?) with uralitised pyroxene crystals <1 mm across in a light green calcite-bleached groundmass. Overall pink and green mottled hues due to diffuse K-spar and epidote alteration. Upper 40 cm (below diabase) contains 20% epidote and 10-20% pyrite as irregular aggregates and subhedral crystals 1-3 mm across.
	480.1	487	Diabase	Dark grey diabase as in [453.1-477.9]. Upper contact sharp @ CAA 85, lower contact sharp and undulose, with weak chill margin, @ CAA ~ 23.
	487	492.8	Mafic metavolcanic flow centre	Grey-green cumulate-textured flow centre (?) as in [477.9-480.1], with slighter larger (<2 mm) cumulus crystals and very little K-spar-epidote alteration, though sparse calcite veinlets <1 mm wide are observed.
	492.8	506	Diabase	Dark grey diabase as in [453.1-477.9]. Upper contact sharp and undulose, running near-parallel to core direction, @ CAA ~5 (contact spans 90 cm of core).

Appendix B

Petrographic Descriptions

B682321: VMS-mineralised mafic-ultramafic metavolcanic rock
(footwall basalt/mineralised zone)

Consisting of:

Biotite	25%
Actinolite	15%
Chlorite	10%
Chalcopyrite	25%
Pyrrhotite	20%
Sphalerite	5%
Galena	<1%
Titanite	<1%
Zircon	<1%

The sample is a strongly mineralised and hydrothermally altered metavolcanic rock, likely from a mafic-ultramafic protolith. Veined sulphides make up about half of the sample, and are associated with biotite and actinolite which define a strong planar fabric.

a. Biotite: As anhedral laths 0.1-1 mm long, in veins or elongate aggregates with a strongly preferred orientation. Some laths display very small pleochroic halos from zircon inclusions (not visible).

b. Actinolite: Weakly pleochroic white-pale green, subhedral-euhedral needles 0.1-1.5 mm long, intergrown with biotite in veins parallel to sulphide veins. Maximum extinction angles are at 5-10° in longitudinal section.

d. Chlorite: Small anhedral, diffuse patches replacing edges of some biotite laths.

e. Chalcopyrite: As mostly sharp-walled veins/veinlets 1-8 mm wide.

f. Pyrrhotite: As veins/ veinlets <5 mm wide, parallel to but distinct from chalcopyrite, and intergrown with sphalerite.

g. Sphalerite: Veinlets or small aggregates <1 mm wide rimming or within pyrrhotite veins. Contains very small inclusion trains of chalcopyrite along cleavage planes.

h. Galena: Very small (0.05 mm across) inclusions within or rimming sphalerite.

i. Titanite: Anhedral aggregates <0.5 mm across sparsely dispersed throughout biotite-actinolite.

j. Zircon: Not visible, evident only from pleochroic halos 0.05 mm across in biotite laths.

B683718: Intensely hydrothermally altered metavolcanic rock
(footwall basalt)

Consisting of:

Biotite	82%
Anthophyllite	10%
Chlorite	5%
Actinolite	2%
Opaque	1%

The sample is from an interval of strongly hydrothermally altered metavolcanic rock adjacent to the VMS mineralised zone. It consists almost entirely of small biotite laths with a weak planar fabric, surrounding radiating fans of acicular anthophyllite that are pale green or white in hand specimen.

a. Biotite: Makes up most of the slide as strongly pleochroic anhedral-subhedral laths 0.05-0.4 mm long, with a weakly preferred orientation. Zircon inclusion halos are visible in many of the biotite laths.

b. Anthophyllite: Subhedral needles or elongate, in places twinned rhombs 1-3 mm long in radiating aggregates up to 5 mm across throughout the slide. Needles are very weakly pleochroic white-pale green, with first-order interference colours and parallel extinction.

c. Chlorite: Barely evident in diffuse, irregular patches a few mm across throughout the biotite.

d. Actinolite (?): Unlike actinolite through most other samples, these occur throughout the slide as subhedral-euhedral, almost equant rhombs or hexagons 0.5-1 mm across. They are cross-cut by the anthophyllite needles.

e. Opaque: Anhedral grains mostly 0.5 mm across, disseminated throughout biotite.

M-N: Mafic-ultramafic metavolcanic rock
(footwall basalt)

Consisting of:

Chlorite	65%
Actinolite	20%
Biotite	5%
Opaque	5%
Calcite	5%
Titanite	<1%

The sample is a strongly foliated chlorite-actinolite schist, with a mafic to ultramafic protolith.

a. Chlorite: Anhedral laths < 0.05-0.5 mm long with a preferred orientation throughout the slide.

b. Actinolite: Anhedral-subhedral needles < 0.1mm-0.5 mm long throughout slide, with white-pale green pleochroism almost identical to that of chlorite.

c. Biotite: As in chlorite, generally replaced by chlorite along edges of laths/plates.

d. Opaque: Anhedral grains 0.05-0.2 mm across, mostly in long aggregates, perhaps veinlets.

e. Calcite: Anhedral crystals <0.5 mm across disseminated throughout the slide, some in veinlets <1 mm wide.

f. Titanite: In dark grey anhedral aggregates ("leucoxene") <0.4 m across, sparsely distributed throughout the sample.

M-1: Mafic-ultramafic metavolcanic rock
(hangingwall basalt)

Consisting of:

Chlorite	55%
Calcite	15%
Actinolite	15%
Opaque	10%
Biotite	5%
Quartz	<1%

The sample is a very fine-grained metavolcanic rock, with a mafic to ultramafic protolith. A moderate planar fabric is defined by the orientation of larger actinolite needles, opaque aggregates, and where visible, chlorite laths. Patches of fine-grained calcite occur in irregular patches or stringers with sharp contacts to fine chloritic rock.

a. Chlorite: Randomly oriented laths <0.05 mm long throughout the slide, and occasionally as disseminated subhedral laths 0.1-0.5 mm long with a weakly preferred orientation. Crystals are moderately pleochroic clear to pale green.

b. Calcite: Anhedral crystals 0.2-0.4mm across, exclusively within irregular centimetre-size patches and stringers with sharp contacts to chloritic rock.

c. Actinolite: Subhedral needles <0.1mm long throughout slide, less commonly as euhedral rhombs to needles 0.3-0.6mm long associated with biotite patches. Larger needles display a strongly preferred orientation.

d. Opaque: Anhedral aggregates and laths (replacing mica or amphibole?) 0.1mm long throughout slide except in calcite, with a preferred orientation parallel to actinolite.

e. Biotite: Disseminated anhedral laths 0.1-0.3mm long, more commonly lining calcite veins/patches, rarely enclosing actinolite inclusions <0.1mm long.

f. Quartz: Anhedral grains <0.05mm across, randomly disseminated throughout slide, except in calcite.

B27417: Finely laminated, locally mylonitic siltstone

Consisting of:

Quartz	50%
Plagioclase	30%
White mica	10%
Orthoclase	7%
Opaque	2%

The sample is a light grey siltstone in which laminae 0.5-1 mm thick are defined by the distribution of white micas. A few rounded clasts of plagioclase <1 mm across are distributed along some bedding planes. A centimetre-wide band through the section diplays a mylonitic fabric, in which feldspar clasts (porphyroclasts) are disaggregated and flattened, with pressure shadows containing slightly larger recrystallised quartz (~0.05 mm across), and in which laminae or mica layers are spaced only 0.1 mm apart. In this mylonitic zone, core-and mantle texture is evident on a quartz porphyroclast 2 mm long.

a. Quartz: Mostly as finely recrystallised crystals or subgrains <0.05 mm across throughout the section, slightly coarser along rims or in pressure shadows of feldspar porphyroclasts.

b. Plagioclase: The majority of pebbles/porphyroclasts <1 mm across are anhedral plagioclase, generally flattened and disaggregated.

d. White mica: Fine laths or aggregates concentrated in very thin, in places wispy layers 0.05 mm wide that define the laminae 0.5-1 mm wide.

e. Orthoclase: As porphyroclasts <1 mm across, and may also be present with finely recrystallised quartz as anhedral crystals <0.05 mm.

f. Opaque: Anhedral crystals or aggregates 0.1-1 mm long distributed along some bedding planes/laminae.

M-87: Serpentinised peridotite cumulate
(Big Lake Ultramafic Complex)

Consisting of:

Serpentine	55%
Opaque (magnetite)	25%
Olivine	7%
Clinopyroxene	13%

The sample is a fine- to medium-grained serpentinised peridotite, with a relict cumulate olivine texture preserved by opaque minerals (mostly magnetite) along rounded grain boundaries and fractures. More than 90% of the olivine has been replaced by snakeskin-textured serpentine. Pyroxene is interstitial to olivines. Many parallel, linear, sharp-walled serpentine veins 1-3mm thick occur at 0.5-2cm intervals throughout the slide, as is also observed in the field. Relict olivine grains within 5mm of all veins have opaque-filled fractures running parallel to the veins; elsewhere, such fracturing is absent. Similarly, primary olivine is observed more frequently with distance from serpentine veins.

a. Serpentine: Fibrous masses replacing olivine and pyroxene grains. Snakeskin textured 100% serpentine veins 1-3mm wide consist of "scales" <0.1mm across with very faint white to pale green pleochroism.

b. Opaque: 99% magnetite, 1% chalcopyrite (in reflected light), as a microcrystalline dusting throughout the slide, and defining relict cumulate olivine texture. Relict olivine grains are anhedral to subhedral, equant, 0.2-2mm in diameter. Chalcopyrite occurs only interstitial to olivines as very fine disseminations <<0.05mm across.

c. Clinopyroxene: Heavily opaque-dusted anhedral crystals <0.3mm across, interstitial to serpentinised olivine grains. Crystals display 2nd order birefringence.

d. Olivine: Anhedral fragments <0.5mm across within some serpentinised grains, heavily fractured. Moderate relief and high birefringence are still observed. A few fractures have a yellow colour in PPL. Olivine becomes less common with proximity to serpentine veins.

M-A: Serpentinised peridotite cumulate
(Big Lake Ultramafic Complex)

Consisting of:

Serpentine	65%
Magnetite	20%
Clinopyroxene	15%

The sample is a medium-grained serpentinised peridotite with a relict cumulate olivine texture preserved by magnetite along rounded grain boundaries and fractures. Linear fractures run parallel to the preferred orientation of slightly elliptical relict olivine; this weak linear fabric is not observed in hand sample. Pyroxene is exclusively interstitial to olivine (i.e., the cumulate is grain-supported) and completely encloses only the smallest olivines. About 30% of the interstitial clinopyroxene is serpentinised, and the remainder retains mid-2nd order birefringence.

a. Serpentine: Fibrous, often radiating masses completely replacing olivine and about 1/3 of pyroxene as fibrous rinds 0.05mm wide along edges of crystal.

b. Magnetite: As a microcrystalline dusting throughout the slide, and distinctly tracing rounded serpentinised olivine grain boundaries and many intergranular sub-linear fractures <0.05mm wide, preserving a relict texture. Relict olivine grains are anhedral, rounded, 0.5-3mm in diameter, often slightly elliptical with a preferred orientation parallel to fracturing.

c. Clinopyroxene: Anhedral crystals interstitial to serpentinised olivine grains. Partly serpentinised at edges, and commonly cross-cut by opaque-filled fractures <0.05mm wide. May have been single crystals, but now occur as optically discontinuous aggregates 0.1-5mm long of individual crystals <0.5mm, sometimes with simple twinning. Crystals display 2nd order birefringence.

B26861: Serpentinised peridotite cumulate
(Big Lake Ultramafic Complex)

Consisting of:

Serpentine	70%
Opaque (magnetite)	20%
Cummingtonite	10%

The sample is a serpentinised fine- to medium-grained cumulate-textured peridotite. Secondary minerals make up most or all of the sample.

a. Serpentine: Irregular aggregates with snakeskin texture, with fibrous scales <0.2mm across, and as randomly oriented fibrous growths. Contact with opaques is always diffuse.

b. Opaque: Cryptocrystalline dusting lining subhedral hexagonal serpentinised olivine grains 0.7-2mm in diameter, preserving relict cumulate texture. Also as subhedral cubic inclusions 0.1-0.5mm across within relict olivine.

c. Cummingtonite: Laths to very fine needles <0.2mm long extending from subhedral opaque inclusions into serpentinised olivine grains. Lower 3rd-order birefringence and amphibole cleavage are observed. These growths lining opaque inclusions are either radial or in parallel aggregates.

B26832: Peridotite cumulate
(Big Lake Ultramafic Complex)

Consisting of:

Olivine	48%
Actinolite	35%
Opaque (magnetite)	8%
Clinopyroxene	6%
Serpentine	4%
Orthopyroxene	2%

The sample is an amphibolitised fine- to medium-grained peridotite, possibly lherzolite, with cumulate olivine crystals <5mm in diameter with interstitial pyroxenes. Serpentinisation is limited in this sample.

a. Olivine: Subhedral pseudohexagonal, heavily fractured crystals 0.5-5mm across. Commonly serpentinised and with occasionally low (1^{st}-order) birefringence. Sub-linear fractures through crystals have a strongly preferred orientation.

b. Actinolite: Subhedral rhombs <0.1mm long, rarely up to 1mm long, in fibrous aggregates replacing olivine and pyroxene from edges and along cleavage planes and fractures.

c. Opaque: Subhedral to euhedral cubic/cuboctahedral crystals 0.2-1mm across in aggregates up to 4mm long. Mostly occurring interstitial to olivine crystals, as aggregates with diffuse edges, intergrown with amphibole.

d. Pyroxenes: Subhedral hexagons and laths 1-7mm long, commonly fractured, some with simple twinning, interstitial to olivine.

e. Serpentine: Fibrous cryptocrystalline masses occurring in fractures of olivine crystals and along edges of olivine and pyroxene crystals.

M-B: Websterite cumulate
(Big Lake Ultramafic Complex)

Consisting of:

Clinopyroxene	50%
Orthopyroxene	20%
Serpentine	10%
Anthophyllite	5%
Magnetite	5%

The sample is a medium-grained magnetite-bearing websterite cumulate with well-preserved primary mineralogy and texture.

a. Clinopyroxene: Cumulate subhedral to euhedral squares or octagons 0.3-2mm across, or rarely as rectangular laths <4mm long. Anomalously low birefringence (1st order grey to yellow) may be due to serpentinisation(?), and maximum extinction angle is 28°.

b. Orthopyroxene: As in clinopyroxene, with parallel extinction.

c. Serpentine: Fibrous masses <0.6mm interstitial to closely packed pyroxene crystals.

d. Anthophyllite: As acicular rims around pyroxene crystals, with needles <0.3mm running parallel to parent pyroxene, with the same 1st order birefringence. Also rarely as fine needles 0.05mm long within serpentine patches.

e. Magnetite: As irregular grains/aggregates <1mm interstitial to pyroxenes.

M-E: Hornblende amphibolite after pyroxenite cumulate
(Big Lake Ultramafic Complex)

Consisting of:

Hornblende	80%
Calcite	10%
Quartz	5%
Leucoxene	3%
Serpentine	2%
Diopside	<1%
Chlorite	<1%

The sample is a uralitised (amphibolitised) medium-grained pyroxenite/websterite cumulate as observed unaltered in slide M-B. Secondary minerals make up >90% of the sample. A relict texture is preserved in most of the slide as subequant rhombs 1.2-2 mm long are completely replaced by nearly optically continuous aggregates of fine-grained sub-parallel amphibole needles fining from edges inward. Some relict grains contain inclusions (original grain?) <0.5mm long of weakly pleochroic anhedral diopside.

a. Hornblende: Strongly pleochroic pale to green-blue subhedral to euhedral needles (>6:1 aspect ratio) 0.05-0.3mm long. Pleochroism is darker than in actinolite-ferroactinolite observed elsewhere. Occurring mostly in rhomb- and occasionally lath-shaped aggregates 0.5-(rarely)5mm long that are nearly optically continuous or have wavy extinction where laths are bent. Also as disaggregated randomly oriented needles 0.2mm long throughout calcite+qtz groundmass.

b. Calcite: Anhedral crystals 0.1-1mm across, clear, usually in aggregates <2mm across interstitial to relict amphibolitised grains 1-2mm long (best observed in hand sample). Strong reaction to 10% HCl in hand sample.

c. Quartz: Anhedral grains <0.1mm with wavy extinction and no sub-grains, randomly intergrown with calcite.

d. Leucoxene: Appearing as dark grey subhedral rhomb-shaped aggregates 0.1-1mm long of individual subhedral diamond-shaped titanite grains <0.05 mm long with very high relief and extreme birefringence, where possible to observe. Dense packing of high-relief titanite crystals seems to impart the overall dark colour to the leucoxene grains.

e. Serpentine: Mostly as "snakeskin textured" fibrous masses of ~equant scales 0.05mm across within veinlets 0.2-1 mm wide.

f. Chlorite: Lining serpentine veinlets, displaying anomalous blue interference colours in XPL.

B26840: Serpentinised websterite cumulate
(Big Lake Ultramafic Complex)

Consisting of:

Clinopyroxene	45%
Orthopyroxene	22%
Serpentine	20%
Opaque	8%
Actinolite	5%

The sample is a fine- to medium-grained serpentinised websterite.

a. Clinopyroxene: Subhedral hexagons or laths 0.5-2mm long, occasionally as fractured anhedral pieces <0.5mm long. Simple twinning is sometimes observed.

b. Orthopyroxene: As in clinopyroxene, most 0.5mm in diameter, having low birefringence and parallel extinction.

c. Serpentine: Interstitial to pyroxenes, surrounding opaques as fibrous to scaly pale green aggregates.

d. Opaque: Subhedral to euhedral rhombs <0.5mm long, in aggregates interstitial to pyroxene grains.

e. Actinolite: Very fine pale green fibers <0.3mm long, or rarely as euhedral laths <0.5mm long, extending from edges of pyroxenes into serpentine interstices.

B26828: Hornblende amphibolite after pyroxenite cumulate
(Big Lake Ultramafic Complex)

Consisting of:

Hornblende	75%
Leucoxene	11%
Epidote	5%
Orthopyroxene	4%
Chlorite	2%
Clinopyroxene	1%
Opaque	1%

The sample is a uralitised medium-grained pyroxenite cumulate, with relict pyroxene crystals <1 cm long, some with original pyroxene cores.

a. Hornblende: Subhedral rhombs to needles <0.2 mm long in aggregates preserving a relict pyroxene-phyric texture; nearly optically continuous aggregates are rhombs and laths 2-9 mm long, fining from edges inward, and containing small pyroxene inclusions.

b. Leucoxene: Dark grey subhedral rhomb-shaped aggregates 0.1-2 mm long of individual subhedral diamond-shaped or hexagonal anisotropic titanite grains <0.05 mm long with very high relief and extreme birefringence. Dense packing of titanite crystals gives overall dark grey isotropic appearance to leucoxene grains in XPL.

c. Epidote: Very fine anhedral disseminations in groundmass, with a pale green-yellow colour in PPL.

d. Pyroxenes: Clear, heavily fractured anhedral inclusions 0.1-1 mm across within amphibolitised grains (relict cores?), sometimes showing simple twinning. A few larger grains have many pyroxene inclusions that are optically continuous, suggesting one original grain. Clinopyroxene is rare, with inclined extinction but low birefringence.

e. Chlorite: Sometimes within pyroxene inclusions, and as rare patches <0.5 mm across in amphiboles, showing anomalous blue interference colours and bird's eye extinction.

f. Opaque: Exclusively as irregular inclusions <0.1 mm across within center of leucoxene grains.

M-11: Websterite cumulate
(Big Lake Ultramafic Complex)

Consisting of:

Clinopyroxene	55%
Orthopyroxene	15%
Calcite	5%
Biotite	3%
Opaque	3%
Chlorite	2%
Zircon	<<1%

The sample is a medium-grained websterite cumulate featuring calcite veining 2 cm wide, diffuse into pyroxenite by replacing pyroxenes along cleavages.

a. Clinopyroxene: Cumulate subhedral to euhedral hexagons 0.5-3mm across, or rectangular grains <4mm long. Up to 2nd order birefringence, though some have 1st order, with extinction at 20-46°. Grains have a dusty appearance.

b. Orthopyroxene: As in clinopyroxene, with parallel extinction.

c. Calcite: In thick veins 2cm wide of anhedral crystals <2mm across, replacing pyroxenes along cleavages.

d. Biotite: Subhedral laths <0.5mm long, interstitial to pyroxenes, often containing zircon inclusions <<0.05mm in diameter with pleochroic haloes.

e. Opaque: As irregular grains <1mm across, interstitial to pyroxenes.

f. Chlorite: Replacing biotite grains along cleavage.

g. Zircon: As inclusions <<0.05mm in diameter within biotite, with pleochroic haloes.

B26802: Feldspathic pyroxenite
(Big Lake Ultramafic Complex)

Consisting of:

Actinolite	85%
Plagioclase	9%
Opaque	5%
Apatite	1%
Calcite	<1%

The sample is a medium- to coarse-grained melagabbro with randomly oriented, in places diablastic patches of actinolite laths <1 cm long in a feldspathic groundmass. Unlike most BLUC cumulates, no primary igneous features are preserved in this sample.

a. Actinolite: Anhedral laths 1-7mm long in diablastic patches with ragged edges, and as subhedral needles 0.05-1mm long through the quartz-rich groundmass. Laths are often bent.

b. Plagioclase: Anhedral, equigranular, rounded grains <0.1mm in diameter (a few 0.5mm across) surrounding amphiboles.

c. Opaque: Anhedral aggregates 0.1-10mm long, interstitial to amphiboles and as smaller inclusions within amphibole crystals.

d. Apatite: Subhedral grains <0.2mm in diameter, in groundmass, a few as anhedral inclusions in amphiboles.

e. Calcite: Disseminated anhedral crystals <0.3mm across throughout groundmass.

M-C: Feldspathic pyroxenite
(Big Lake Ultramafic Complex)

Consisting of:

Hornblende	65%
Plagioclase	30%
Leucoxene	2%
Serpentine	2%
Chlorite	1%
Opaque	<1%

The sample is a melagabbro without planar or linear fabric.

a. Hornblende: Anhedral ragged crystals 0.1-8mm long, and as very fine acicular radial aggregates of needles 0.05-0.2mm long extending into plagioclase. Pale to dark green-blue pleochroism. Containing many rounded high-relief epidote inclusions <0.05mm as well as anhedral leucoxene grains <2mm long.

b. Plagioclase: Anhedral crystals 0.05-1mm long, intergrown with amphibole. Maximum extinction angle of 30° = 55% An content (labradorite). Possibly forming smaller sub-grains; dislocation creep in plagioclase = T>500°C?

c. Leucoxene: Anhedral to subhedral rhombic fractured, disaggregated grains 0.05-2mm long, often containing irregular opaques. Occurring mostly within larger amphibole crystals.

d. Serpentine: Patches of very fine fibrous masses, usually associated with chlorite.

e. Chlorite: In pleochroic green radial aggregates associated with serpentine, with anomalous blue birefringence.

f. Opaque: Exclusively within leucoxene grains as irregular grains 0.05mm across.

M-4: Lamprophyre and cumulate-textured pyroxenite
(within Big Lake Ultramafic Complex)

The sample features a sharp contact between a fine-grained white lamprophyre dyke that has intruded a medium-grained dark green uralitised pyroxenite cumulate. The lamprophyre features a strong planar fabric from the orientation of hornblende phenocrysts and fine needles within a plagioclase-rich groundmass. The contact features no chill margin or rip-ups to either side, and is lined with plagioclase and less abundant quartz crystals <0.6 mm across.

Lamprophyre consisting of:

Plagioclase	60%
Hornblende	15%
Quartz	14%
K-feldspar	10%
Calcite	1%
Opaque	<1%

a. Hornblende: Zoned anhedral to subhedral rhombic phenocrysts 0.1-1 mm long, with darker opaque-dusted centres and clear rims. Also occurring as extremely fine (<<0.05 mm long) groundmass needles (actinolite?). Phenocrysts and groundmass needles share a strongly preferred orientation.

b. Plagioclase: Equigranular, subequant groundmass grains <0.05mm across, and rarely as elongate anhedral microphenocrysts <0.5 mm across. Also lining the amphibolite contact as anhedral crystals <0.2 mm across.

c. Quartz: Size and habit as in plagioclase, often with wavy extinction.

d. K-feldspar: Size and habit as in plagioclase.

e. Calcite: In random anhedral patches <0.3 mm across within groundmass.

f. Opaque: Subhedral to euhedral cubic crystals 0.05-0.2 mm across within groundmass.

Uralitised pyroxenite consisting of:

Hornblende	80%
Leucoxene	10%
Plagioclase	8%
Quartz	2%
Zircon	<1%
Epidote	<1%

a. Hornblende: Strongly pleochroic pale to green-blue subhedral to euhedral rhombs and needles 0.1-1mm long in rhomb- and hexagon-shaped aggregates 1-5mm long that are

nearly optically continuous or have wavy extinction where laths are bent. Also as randomly oriented needles 0.2 mm long throughout plagioclase and quartz groundmass.

b. Leucoxene: Anhedral fragments 0.2-2 mm long, only as inclusions within amphibolitised grains.

c. Plagioclase: Anhedral, subequant crystals <0.05 mm across, rarely up to 0.1 mm across, interstitial to amphibolitised/uralitised grains. Twinning and faint sericite dusting distinguish it from quartz.

d. Quartz: As in plagioclase.

e. Zircon: Crystals << 0.05 mm in diameter, as inclusions identified by pleochroic haloes in amphiboles.

f. Epidote: Lining larger amphibolitised/uralitised grains as anhedral crystals <0.05 mm in diameter.

Appendix C

Whole-Rock Geochemical Data

The following data are from core samples collected by MetalCORP staff and by the author. Samples with six digit ID were analysed at ALS Chemex labs, and those in number-letter format were analysed by OGS labs (see Chapter Two). Numbers of elements analysed, reported decimal places, and detection limits vary depending on the lab.

	Peridotite (BLUC)							Pyroxenite (BLUC)		
Sample ID	546712	626103	626104	626105	626110	626111	626113	546652	546653	546654
SiO_2	39.71	34.76	36.36	36.70	33.29	35.89	39.59	45.85	49.97	46.28
TiO_2	1.39	0.50	0.61	0.76	0.74	0.58	0.75	0.71	1.09	1.34
Al_2O_3	7.32	1.76	2.23	2.59	2.18	1.83	2.41	9.72	3.68	3.78
Fe_2O_3	16.89	20.73	17.54	19.99	24.32	21.04	18.79	11.58	12.18	13.56
MnO	0.24	0.28	0.24	0.26	0.27	0.30	0.25	0.19	0.17	0.20
MgO	20.35	27.65	28.39	26.91	27.03	27.40	26.37	12.79	13.42	13.85
CaO	7.13	3.01	2.97	3.73	2.06	2.94	2.80	13.27	15.71	17.39
Na_2O	0.12	0.08	0.04	0.05	0.19	0.07	0.04	0.66	0.51	0.40
K_2O	0.03	0.12	0.12	0.13	0.13	0.12	0.13	2.16	0.20	0.12
P_2O_5	0.09	0.02	0.03	0.05	0.03	0.03	0.05	0.18	0.05	0.05
LOI	5.19	9.66	9.79	8.21	8.59	8.22	7.26	1.31	0.97	1.43
Total	98.78	98.92	98.86	99.87	99.00	98.83	98.84	98.75	98.17	98.63
P	410	120	170	210	160	130	220	960	220	240
Cr	1340	1840	2680	2680	954	2220	2070	670	906	930
Co	103	173	149	157	186	170	161	60	77	80
Ni	870	1845	2230	2140	1705	1680	2220	219	574	483
Rb	0.6	0.2	0.1	0.2	0.2	<0.1	0.2	89.9	2.9	0.9
Sr	63.1	107.5	43.2	57.3	48.2	16.2	29.4	1325	155	116
Cs	0.12	0.14	0.12	0.11	0.12	0.09	0.18	4.15	0.16	0.08
Ba	10	<10	<10	<10	<10	<10	<10	740	30	10
Sc										
V	250	127	127	162	157	123	126	216	227	279
Ta	0.45	0.17	0.21	0.29	0.31	0.18	0.4	0.27	0.38	0.48
Nb	7.5	2.2	3	4	4.1	2.4	5.9	4.6	6.5	7.8
Zr	43.7	2.7	1.8	4.3	6.3	2	14.8	45.6	27.4	42
Hf	1.3	0.1	0.1	0.2	0.2	0.1	0.4	1.4	1.1	1.4
Th	0.5	0.2	0.3	0.3	0.3	0.2	0.5	2.4	0.6	0.8
U	0.1	0.1	0.1	0.1	0.1	<0.1	0.1	0.3	0.2	0.2
Y	13.5	4	4.4	5.4	4.4	4.1	5.7	14.2	10.4	11.9
La	7.5	2.5	3.3	3.7	3.3	2.9	6.4	19.6	7.4	8.7
Ce	19.2	6.1	7.6	8.9	8.0	6.7	14.0	39.7	17.8	20.2
Pr	2.7	1.0	1.2	1.3	1.2	1.0	1.8			
Nd	12.1	4.4	5.4	6.2	5.6	4.7	7.6			
Sm	3.0	1.0	1.3	1.5	1.2	1.2	1.5			
Eu	0.8	0.4	0.4	0.5	0.4	0.4	0.5			
Gd	3.2	1.0	1.2	1.4	1.1	1.0	1.6			
Tb	0.5	0.2	0.2	0.2	0.2	0.2	0.2			
Dy	2.8	0.9	1.1	1.2	0.9	0.9	1.2			
Ho	0.6	0.2	0.2	0.2	0.2	0.2	0.2			
Er	1.5	0.4	0.5	0.6	0.5	0.5	0.6			
Tm	0.2	<0.1	0.1	0.1	0.1	<0.1	0.1			
Yb	1.3	0.3	0.4	0.5	0.4	0.4	0.5			
Lu	0.2	<0.1	0.1	<0.1	<0.1	<0.1	0.1			
Cu	103	234	182	365	433	124.5	271	42.1	859	823
Zn	108	102	104	108	114	99	120	121	75	74
Mo	0.23	0.19	0.13	0.19	0.13	0.14	0.09	0.26	0.37	0.54
Tl	<0.02	<0.02	<0.02	<0.02	<0.02	<0.02	0.05	0.64	0.02	<0.02
Pb	0.6	0.6	0.6	0.8	1.1	<0.5	1.1	12.3	2.5	1.5
Sn	0.7	0.4	0.4	0.5	0.5	0.3	0.4	0.9	0.6	0.7
Sb	0.14	0.49	0.67	0.2	0.27	0.11	0.18	0.17	0.16	0.12
$(La/Yb)_{cn}$	4.14	5.98	5.92	5.31	5.92	5.20	9.18			
$(La/Sm)_{cn}$	1.62	1.62	1.64	1.59	1.78	1.56	2.76			
$(Gd/Yb)_{cn}$	2.04	2.76	2.48	2.32	2.27	2.07	2.65			
$(Eu/Eu^*)_{cn}$	0.78	1.21	0.96	1.04	1.05	1.09	0.98			
Al_2O_3/TiO_2	5.27	3.52	3.66	3.41	2.95	3.16	3.21	13.69	3.38	2.82
Zr/Hf	33.62	27.00	18.00	21.50	31.50	20.00	37.00	32.57	24.91	30.00
Zr/Y	3.24	0.68	0.41	0.80	1.43	0.49	2.60	3.21	2.63	3.53
Nb/Nb*	0.95	0.79	0.78	0.97	1.12	0.72	0.75	0.18	0.79	0.78
Notes										

	Pyroxenite (BLUC)									
Sample ID	546655	546656	546657	546664	546666	546667	546678	546685	546686	546689
SiO_2	45.32	45.52	44.77	43.36	39.53	37.60	36.57	37.54	37.02	38.79
TiO_2	1.25	1.17	1.38	2.38	4.73	4.42	4.82	4.40	3.71	5.02
Al_2O_3	3.56	10.39	3.57	6.62	7.23	6.47	6.75	7.45	8.58	6.92
Fe_2O_3	12.43	14.02	11.93	17.15	24.14	24.36	23.31	22.13	21.08	24.24
MnO	0.16	0.21	0.18	0.22	0.27	0.26	0.27	0.26	0.23	0.27
MgO	13.36	10.59	12.75	10.74	7.00	7.18	6.63	6.39	5.74	7.15
CaO	15.15	11.54	16.39	13.91	11.89	12.39	12.56	11.73	11.02	12.62
Na_2O	0.25	1.37	0.44	0.90	0.98	0.87	1.12	1.65	2.12	1.18
K_2O	1.21	1.10	0.55	0.27	1.46	1.59	1.60	1.83	2.35	0.63
P_2O_5	0.05	0.13	0.05	0.10	0.11	0.10	0.10	0.11	0.13	0.09
LOI	5.54	2.60	6.01	3.65	1.30	3.77	5.69	5.72	6.81	1.38
Total	98.54	98.81	98.28	99.39	98.69	99.06	99.52	99.31	98.95	98.34
P	230	620	210	500	510	440	430	480	590	420
Cr	852	95	872	305	5	7	<1	<1	<1	2
Co	68	70	70	78	94	96	97	81	81	101
Ni	564	73	383	229	98	135	86	93	79	105
Rb	52	31.5	29.1	4.4	54.2	63	63.5	76.4	92.9	22.4
Sr	395	695	352	122.5	147.5	122	443	392	569	235
Cs	2.87	1.07	1.45	0.17	4.31	5.27	6.07	6.51	10.3	1.44
Ba	390	780	260	40	230	200	430	500	860	160
Sc										
V	257	250	288	480	782	1015	789	751	808	940
Ta	0.37	0.28	0.42	0.69	1.17	0.91	0.99	1.11	1.19	1.02
Nb	6.2	5.8	7	9.8	17.6	14	15.9	17	17.5	16.2
Zr	21	54.3	26.2	48	43.9	41.7	91.3	89.9	104	43.8
Hf	0.7	1.9	1	1.7	1.8	1.5	3	3.1	3.5	2
Th	0.6	1.3	0.6	1.1	1.5	1.2	1.2	1.3	1.5	1.3
U	0.1	0.3	0.1	0.2	0.3	0.3	0.3	0.3	0.3	0.3
Y	8.9	15.6	10.9	18.8	20.8	17.5	18.5	21.1	22.6	20.2
La	6.2	14.4	7.8	11.8	15.7	13.4	14.7	16.2	19.1	14.2
Ce	16.0	34.2	18.9	28.0	37.7	31.6	35.9	39.8	46.6	36.4
Pr							4.5	5.3	6.2	5.0
Nd							19.2	22.8	26.1	21.2
Sm							4.6	5.5	5.9	5.0
Eu							1.5	1.7	1.9	1.6
Gd							4.6	5.3	5.6	4.8
Tb							0.7	0.8	0.8	0.7
Dy							3.8	4.3	4.5	3.9
Ho							0.7	0.8	0.9	0.8
Er							1.9	2.1	2.3	2.0
Tm							0.3	0.3	0.3	0.3
Yb							1.5	1.7	1.8	1.6
Lu							0.2	0.3	0.3	0.2
Cu	1045	235	859	829	713	852	679	311	660	741
Zn	69	113	77	101	146	131	236	128	105	148
Mo	0.14	3.26	0.22	0.28	0.48	0.26	0.6	0.46	0.86	1
Tl	0.75	0.37	0.48	0.02	0.43	0.68	0.97	0.79	1.27	0.11
Pb	3.7	5.5	3.4	2.4	1.9	2.2	10.9	5.3	12.5	2.5
Sn	0.5	1.3	0.8	1.1	1.4	1	1.3	1.2	1	1.3
Sb	0.12	0.15	0.09	0.06	0.28	0.15	0.08	0.08	0.06	0.34
$(La/Yb)_{cn}$							7.03	6.83	7.61	6.36
$(La/Sm)_{cn}$							2.06	1.90	2.09	1.83
$(Gd/Yb)_{cn}$							2.54	2.58	2.57	2.48
$(Eu/Eu^*)_{cn}$							0.99	0.95	1.00	0.98
Al_2O_3/TiO_2	2.85	8.88	2.59	2.78	1.53	1.46	1.40	1.69	2.31	1.38
Zr/Hf	30.00	28.58	26.20	28.24	24.39	27.80	30.43	29.00	29.71	21.90
Zr/Y	2.36	3.48	2.40	2.55	2.11	2.38	4.94	4.26	4.60	2.17
Nb/Nb*	0.96	0.36	0.81	0.73	1.00	0.92	0.99	0.96	0.83	1.09
Notes										

	Pyroxenite (BLUC)									
Sample ID	546690	546694	546695	546701	546725	546726	546739	546745	546746	626101
SiO_2	37.13	39.72	44.85	43.42	48.01	46.97	37.27	47.20	46.33	42.73
TiO_2	4.10	3.67	1.77	1.26	0.48	0.57	4.57	1.95	2.42	2.75
Al_2O_3	8.87	6.50	5.58	3.46	19.03	17.13	8.68	14.72	14.32	5.54
Fe_2O_3	22.03	24.72	13.51	12.74	8.23	10.74	21.93	16.90	19.08	21.37
MnO	0.27	0.25	0.20	0.19	0.13	0.16	0.28	0.28	0.26	0.23
MgO	4.63	8.36	11.48	14.63	6.42	8.99	5.26	2.94	3.52	9.14
CaO	9.81	14.09	17.51	16.67	11.78	10.93	9.75	8.30	8.61	15.73
Na_2O	2.35	1.07	0.89	0.61	2.55	2.06	2.12	3.64	3.96	1.05
K_2O	2.09	0.49	0.31	0.35	0.94	0.60	2.47	0.58	0.37	0.36
P_2O_5	0.16	0.09	0.08	0.05	0.04	0.05	0.11	0.26	0.23	0.06
LOI	6.58	0.71	3.50	6.24	2.06	1.57	6.50	2.87	0.56	-0.06
Total	98.12	99.72	99.78	99.85	99.77	99.83	99.05	99.71	99.74	98.92
P	740	390	350	210	160	200	480	1170	1060	280
Cr	<1	12	207	770	229	175	7	11	7	18
Co	77	99	66	81	32	43	77	37	48	88
Ni	23	333	280	580	101	191	36	9	10	368
Rb	77.8	3.3	3.2	14.8	15.4	12.6	102.5	17.8	3.4	1.8
Sr	346	227	287	110.5	284	169.5	360	452	454	102.5
Cs	8.17	0.24	0.09	0.9	0.58	0.87	11.7	1.48	0.44	<0.05
Ba	610	70	90	10	170	20	670	160	140	40
Sc										
V	290	857	326	252	184	193	420	69	169	799
Ta	1.62	0.88	0.65	0.46	0.15	0.13	1.2	1.38	1.26	0.41
Nb	25.1	13.8	11.1	7.5	1.4	0.9	19.3	23.5	21.2	5.9
Zr	135	44.9	27.9	31.4	8.6	9.3	108	160.5	95.9	36.2
Hf	4.4	2	1.2	1.1	0.4	0.5	3.9	5.1	2.8	1.4
Th	2.1	1.2	0.8	0.5	0.2	0.2	2	2.6	2.3	0.9
U	0.5	0.3	0.2	0.1	0.1	<0.1	0.5	0.6	0.6	0.2
Y	27	18	12.7	9.9	10.1	11.9	22.9	32.3	30.9	13.2
La	22.8	14.2	9.9	7.6	1.6	2.4	19.1	26.1	24.6	7.5
Ce	55.0	34.1	24.5	19.1	4.3	6.5	45.6	63.5	60.2	18.0
Pr	7.0	4.7	3.5	2.2	0.7	0.9	6.4	8.2	8.1	2.6
Nd	28.7	20.0	15.0	9.8	3.5	4.6	27.2	34.5	34.0	12.6
Sm	6.7	4.7	3.6	2.4	1.1	1.3	5.9	7.6	7.6	3.2
Eu	2.2	1.5	1.2	0.7	0.5	0.5	1.8	2.4	2.5	1.1
Gd	6.5	4.6	3.6	2.3	1.4	1.7	5.9	7.5	7.5	3.2
Tb	0.9	0.7	0.5	0.3	0.2	0.3	0.9	1.1	1.1	0.6
Dy	5.1	3.7	2.8	1.9	1.8	2.1	4.8	6.0	6.0	2.8
Ho	1.0	0.7	0.5	0.4	0.4	0.5	0.9	1.2	1.2	0.5
Er	2.6	1.9	1.4	0.9	1.2	1.3	2.4	3.1	3.1	1.4
Tm	0.4	0.2	0.2	0.1	0.1	0.2	0.3	0.4	0.4	0.2
Yb	2.2	1.5	1.1	0.7	1.1	1.3	1.9	2.7	2.5	1.1
Lu	0.3	0.2	0.2	0.1	0.1	0.2	0.2	0.4	0.3	0.2
Cu	367	971	345	778	93.9	40.4	413	44.9	43	1185
Zn	166	147	100	74	60	70	116	158	113	98
Mo	0.85	0.62	0.52	0.25	3.17	0.27	0.7	3.4	0.97	0.23
Tl	1.13	0.02	<0.02	0.09	0.16	0.09	1.28	0.15	<0.02	0.02
Pb	10	5.2	5.7	2.8	4	2.7	9.4	8.7	2.8	1.2
Sn	1.6	1.2	1	0.4	0.4	0.6	1.3	2.6	1.3	0.9
Sb	0.09	0.17	0.13	0.07	0.07	<0.05	0.05	0.06	0.08	0.24
$(La/Yb)_{cn}$	7.43	6.79	6.45	7.78	1.04	1.32	7.21	6.93	7.06	4.89
$(La/Sm)_{cn}$	2.20	1.95	1.78	2.05	0.94	1.19	2.09	2.22	2.09	1.51
$(Gd/Yb)_{cn}$	2.44	2.54	2.71	2.72	1.05	1.08	2.57	2.30	2.48	2.41
$(Eu/Eu^*)_{cn}$	1.01	0.97	1.01	0.90	1.23	1.03	0.92	0.96	1.00	1.04
Al_2O_3/TiO_2	2.16	1.77	3.15	2.75	39.65	30.05	1.90	7.55	5.92	2.01
Zr/Hf	30.68	22.45	23.25	28.55	21.50	18.60	27.69	31.47	34.25	25.86
Zr/Y	5.00	2.49	2.20	3.17	0.85	0.78	4.72	4.97	3.10	2.74
Nb/Nb*	0.99	0.87	1.03	0.92	0.88	0.38	0.90	0.82	0.79	0.70
Notes										

	Pyroxenite (BLUC)									
Sample ID	626102	626106	626107	626108	626109	626112	626114	626115	626116	626173
SiO_2	44.01	42.84	44.13	41.22	47.30	40.85	48.11	49.91	54.87	43.44
TiO_2	1.29	1.84	2.88	4.38	1.54	4.24	0.86	1.76	0.86	1.48
Al_2O_3	4.55	6.40	11.58	8.99	3.75	7.36	13.91	14.05	14.85	4.62
Fe_2O_3	18.51	16.02	22.02	23.80	13.10	23.78	14.83	17.98	15.24	13.71
MnO	0.25	0.24	0.31	0.30	0.19	0.27	0.21	0.28	0.27	0.21
MgO	15.13	16.96	4.25	5.47	12.69	7.15	7.26	2.41	1.32	11.57
CaO	13.06	9.79	9.18	11.53	18.73	13.03	9.88	7.47	4.69	16.24
Na_2O	0.22	0.81	3.90	3.26	0.55	1.51	3.02	4.87	6.32	0.90
K_2O	0.22	0.37	1.03	0.59	0.38	0.70	0.48	0.48	0.48	0.56
P_2O_5	0.06	0.03	0.24	0.14	0.05	0.12	0.07	0.43	0.29	0.06
LOI	2.01	3.02	0.33	0.21	0.55	0.38	0.63	0.08	-0.03	5.58
Total	99.33	98.57	99.96	99.91	99.04	99.44	99.31	99.77	99.23	98.43
P	270	200	1030	580	240	530	280	1890	1200	310
Cr	106	1110	40	16	773	25	83	24	10	115
Co	113	92	62	81	69	93	60	34	17	64
Ni	557	1175	92	84	409	194	118	38	15	287
Rb	0.2	4.4	22	5.3	6.2	2.3	3	1.7	2.4	20
Sr	45.1	156	491	287	194	274	160	496	331	243
Cs	0.1	0.31	0.71	0.11	0.33	<0.05	0.2	0.07	0.43	
Ba	<10	50	340	150	50	120	80	200	360	130
Sc										
V	287	293	227	537	293	813	268	26	4	302
Ta	0.37	0.67	2.13	1.53	0.47	0.95	0.16	1.93	2.66	
Nb	5	9.7	31.6	21.2	7	13.8	2.1	28.7	40.5	8
Zr	33.4	52.7	102.5	77.4	35	44.7	16.8	152	184	57
Hf	1.1	1.7	2.8	3	1.2	2	0.6	3.7	4.5	
Th	0.5	0.9	2.8	1.9	0.6	1.2	0.2	3	4.1	1
U	0.1	0.1	0.6	0.4	0.1	0.3	0.1	0.7	1	<0.5
Y	11	14.7	27	25.1	11.2	18.8	15.4	35.3	46.6	13.1
La	6.0	10.2	30.1	21.7	8.3	15.7	3.5	31.3	40.1	9.8
Ce	14.9	25.8	65.9	49.7	19.2	35.6	8.3	72.6	95.5	23.8
Pr	2.3	4.0	9.5	7.3	2.7	5.4	1.4	11.6	14.7	3.3
Nd	10.6	18.0	40.2	31.0	12.8	23.8	6.6	49.6	62.4	15.0
Sm	2.7	4.3	7.9	6.8	3.0	5.6	1.9	10.8	13.3	3.3
Eu	0.8	1.3	2.5	2.1	1.0	1.6	0.7	3.1	3.5	1.1
Gd	2.8	3.9	7.5	6.6	2.9	5.2	2.3	10.0	12.6	3.4
Tb	0.4	0.6	1.1	1.0	0.5	0.8	0.5	1.6	2.0	0.5
Dy	2.3	3.2	6.0	5.4	2.4	4.0	3.0	8.1	11.0	2.8
Ho	0.4	0.6	1.1	1.0	0.4	0.8	0.6	1.6	2.0	0.5
Er	1.2	1.6	3.0	2.7	1.1	2.0	1.9	4.2	5.9	1.3
Tm	0.1	0.2	0.4	0.3	0.1	0.3	0.3	0.5	0.8	0.2
Yb	1.0	1.2	2.4	2.3	0.9	1.6	1.8	3.6	5.0	1.2
Lu	0.1	0.2	0.4	0.3	0.1	0.2	0.3	0.5	0.7	0.2
Cu	751	160	343	491	716	768	291	30.7	38.7	684
Zn	82	158	173	140	66	134	83	126	212	78
Mo	0.17	0.2	1.52	0.22	0.22	0.41	1.62	0.84	1.4	<1
Tl	<0.02	0.03	0.08	0.02	0.02	0.04	<0.02	<0.02	0.03	
Pb	0.5	2.7	3.7	1	0.8	1.7	3.1	1.8	3.6	11
Sn	0.5	2	2	1.6	0.7	1.3	0.6	1.6	4.2	
Sb	0.5	0.12	0.11	0.09	0.12	0.14	0.05	<0.05	<0.05	<5
$(La/Yb)_{cn}$	4.30	6.09	8.99	6.76	6.61	7.04	1.39	6.23	5.75	5.86
$(La/Sm)_{cn}$	1.44	1.53	2.46	2.06	1.79	1.81	1.19	1.87	1.95	1.92
$(Gd/Yb)_{cn}$	2.32	2.69	2.58	2.37	2.66	2.69	1.06	2.30	2.08	2.34
$(Eu/Eu^*)_{cn}$	0.88	0.95	0.98	0.95	1.02	0.89	1.02	0.90	0.81	1.00
Al_2O_3/TiO_2	3.53	3.48	4.02	2.05	2.44	1.74	16.17	7.98	17.27	3.12
Zr/Hf	30.36	31.00	36.61	25.80	29.17	22.35	28.00	41.08	40.89	
Zr/Y	3.04	3.59	3.80	3.08	3.13	2.38	1.09	4.31	3.95	4.35
Nb/Nb*	0.77	0.90	0.86	0.83	0.73	0.74	0.53	0.79	0.90	0.74
Notes										

	Pyroxenite (BLUC)									
Sample ID	626385	626386	626387	626388	626391	626392	626399	626400	626461	626462
SiO_2	46.38	39.40	38.97	37.33	41.13	48.30	43.04	43.26	49.69	47.87
TiO_2	1.28	4.87	5.46	4.69	3.64	1.67	3.28	3.34	0.86	2.23
Al_2O_3	3.69	6.45	8.14	8.37	11.11	15.59	10.78	10.38	14.44	13.73
Fe_2O_3	12.99	24.89	24.54	23.04	22.72	17.36	21.17	21.30	12.89	18.52
MnO	0.21	0.27	0.31	0.30	0.32	0.30	0.28	0.27	0.14	0.30
MgO	15.41	7.29	5.84	5.30	3.62	2.18	5.42	5.61	6.98	3.17
CaO	16.52	12.38	11.66	10.56	9.60	6.36	10.16	11.41	8.98	7.02
Na_2O	0.21	1.19	1.37	1.92	3.44	5.40	2.59	2.12	3.47	4.11
K_2O	0.02	0.67	1.04	1.87	0.57	0.76	0.44	0.47	0.46	0.59
P_2O_5	0.06	0.09	0.13	0.15	0.15	0.29	0.15	0.16	0.09	0.21
LOI	1.83	1.05	0.57	4.57	1.96	0.94	0.77	1.06	0.90	0.70
Total	98.88	98.62	98.10	98.20	98.32	99.28	98.13	99.43	98.97	98.52
P	280	450	630	750	730	1370	730	760	360	970
Cr	1145	8	6	<1	5	5	4	<1	73	1
Co	84	94	95	91	72	38	78	81	50	46
Ni	603	131	44	36	7	3	60	59	77	10
Rb	0.3	21.9	35.1	76.1	9.5	18	5.4	5.2	9.3	10.5
Sr	53.3	175.5	161	329	307	609	346	340	261	389
Cs	0.06	1.52	2.4	6.62	0.39	1.44	0.49	0.41	0.27	0.63
Ba	10	220	300	530	310	590	130	150	90	260
Sc										
V	210	1130	446	388	99	7	531	528	229	154
Ta	0.57	1.05	1.61	1.36	2.37	2.82	1.11	1.05	0.19	1.2
Nb	8.3	14.8	23.1	19.3	32.5	42.2	16.7	15.6	2.8	19.1
Zr	45.8	39.6	73.1	113	171.5	185	44.2	44.3	34.4	62.4
Hf	1.6	1.8	2.8	3.7	5.2	4.9	1.7	1.7	1.1	2
Th	0.8	1.2	1.9	1.7	2.7	3.9	1.7	1.6	0.5	2
U	0.2	0.3	0.5	0.4	0.6	0.9	0.4	0.4	0.1	0.5
Y	12	17.8	24.8	24.1	31.5	36	26.2	26.6	19.7	26.6
La	8.7	12.3	19.2	15.6	24.8	35.1	16.4	16.1	4.9	22.7
Ce	20.1	30.3	45.1	38.2	55.8	76.3	38.2	38.1	11.5	54.1
Pr										
Nd										
Sm										
Eu										
Gd										
Tb										
Dy										
Ho										
Er										
Tm										
Yb										
Lu										
Cu	751	746	532	463	77.3	42.6	192.5	244	78.1	55.2
Zn	72	191	210	175	161	210	143	145	56	166
Mo	0.27	0.53	0.59	0.74	0.42	1.41	1.57	3.45	0.37	3.73
Tl	<0.02	0.11	0.27	1.14	0.05	0.14	0.02	0.02	0.06	0.06
Pb	1.2	3.5	4.2	6.8	4.4	6.1	2.4	2.1	4.4	4.7
Sn	0.6	1.3	1.6	1.5	2.1	2.5	1.7	1.6	0.5	2
Sb	0.14	0.24	0.21	0.07	0.08	0.07	0.13	0.09	0.27	0.08
$(La/Yb)_{cn}$										
$(La/Sm)_{cn}$										
$(Gd/Yb)_{cn}$										
$(Eu/Eu^*)_{cn}$										
Al_2O_3/TiO_2	2.88	1.32	1.49	1.78	3.05	9.34	3.29	3.11	16.79	6.16
Zr/Hf	28.63	22.00	26.11	30.54	32.98	37.76	26.00	26.06	31.27	31.20
Zr/Y	3.82	2.22	2.95	4.69	5.44	5.14	1.69	1.67	1.75	2.35
Nb/Nb*	0.82	1.11	1.05	1.13	1.10	0.97	0.88	0.86	0.50	0.75
Notes										

	Pyroxenite (BLUC)								Basalt (footwall)	
Sample ID	626464	626466	626468	626476	626484	626494	626499	626500	546662	546669
SiO_2	37.06	46.64	47.97	72.64	69.68	67.74	42.09	47.50	36.86	38.12
TiO_2	1.00	0.90	1.87	0.33	0.29	0.25	3.27	1.47	0.81	0.95
Al_2O_3	2.99	5.62	6.20	13.23	16.39	14.06	9.35	4.14	4.07	4.53
Fe_2O_3	20.38	13.60	9.52	4.07	2.00	2.39	22.45	12.85	15.93	15.64
MnO	0.22	0.21	0.18	0.04	0.02	0.16	0.26	0.19	0.22	0.22
MgO	21.48	17.92	9.48	1.35	0.79	0.78	6.72	12.38	20.78	17.63
CaO	4.80	9.69	14.79	0.64	0.79	5.32	10.89	17.83	6.83	9.47
Na_2O	0.02	0.30	2.59	6.57	8.78	2.86	2.07	0.43	0.02	0.05
K_2O	<0.01	0.05	0.04	0.29	0.05	2.56	0.31	1.09	0.02	0.02
P_2O_5	0.05	0.05	0.09	0.07	0.08	0.07	0.14	0.08	0.06	0.06
LOI	9.99	3.57	5.71	0.51	0.67	3.32	1.47	0.43	12.20	11.30
Total	98.35	98.91	98.49	99.75	99.55	99.57	99.08	98.59	98.18	98.33
P	180	210	440	340	350	300	620	350	270	260
Cr	1690	1520	207	30	49	52	80	758	1810	1610
Co	142	82	73	9	6	7	82	66	132	125
Ni	1570	914	348	22	21	24	143	357	1500	1340
Rb	0.1	0.7	0.5	9.8	1.8	36.8	3.5	46.1	0.9	1
Sr	104	105.5	197	96.1	114	147.5	322	233	201	114
Cs	0.19	0.24	0.06	1.4	0.17	1.03	0.44	2.27	0.36	0.24
Ba	<10	10	20	90	30	390	80	270	10	10
Sc										
V	220	180	335	29	33	30	605	287	171	197
Ta	0.25	0.23	0.94	0.5	0.31	0.33	0.79	0.51	0.26	0.29
Nb	3.9	3.8	13.8	6.6	3.8	3.7	13.6	8.9	4.4	4.7
Zr	22.6	28.5	63.2	205	75.1	99.1	43.6	38	36.7	42.1
Hf	0.7	0.9	2.3	5.9	2.4	2.6	1.5	1.4	1	1.2
Th	0.4	0.4	1.4	5.4	1.8	1.5	1.3	0.8	0.4	0.4
U	0.1	0.1	0.3	1.1	0.5	0.4	0.3	0.2	0.1	0.1
Y	4.5	10	16.3	12	3.6	3.5	22.1	12.6	8.8	9.7
La	4.9	4.2	13.7	35.6	12.5	7.8	14.1	9.8	4.8	6.2
Ce	11.9	10.9	33.0	73.0	23.2	16.1	35.8	24.3	11.8	14.3
Pr										
Nd										
Sm										
Eu										
Gd										
Tb										
Dy										
Ho										
Er										
Tm										
Yb										
Lu										
Cu	921	333	1080	133.5	23.6	17.6	378	519	87.9	105.5
Zn	113	101	99	78	69	43	125	73	104	107
Mo	0.16	0.91	0.76	1.18	0.64	1.13	0.62	0.42	0.46	0.27
Tl	0.2	0.04	0.02	0.12	<0.02	0.09	0.04	0.29	0.03	0.37
Pb	0.7	1.5	3.6	7.1	4.8	3	1.7	2.9	12	2.7
Sn	0.4	0.4	1.2	0.5	0.5	0.4	1.3	0.7	0.3	<0.2
Sb	0.05	0.15	0.31	<0.05	<0.05	0.07	0.18	0.09	0.29	0.12
$(La/Yb)_{cn}$										
$(La/Sm)_{cn}$										
$(Gd/Yb)_{cn}$										
$(Eu/Eu^*)_{cn}$										
Al_2O_3/TiO_2		6.24	3.32	40.09	56.52	56.24	2.86	2.82	5.02	4.77
Zr/Hf	32.29	31.67	27.48	34.75	31.29	38.12	29.07	27.14	36.70	35.08
Zr/Y	5.02	2.85	3.88	17.08	20.86	28.31	1.97	3.02	4.17	4.34
Nb/Nb*	0.72	0.87	0.90	0.14	0.21	0.37	0.91	0.84	0.84	0.65
Notes										

	Basalt (footwall)									
Sample ID	546682	546683	546691	546702	546703	546705	546713	546714	546728	546729
SiO_2	44.75	41.25	42.14	47.72	43.07	44.89	43.09	46.75	42.45	45.91
TiO_2	2.18	1.72	1.67	1.66	1.64	1.24	1.28	1.13	2.40	1.29
Al_2O_3	11.06	8.24	6.90	10.24	9.83	7.96	7.64	6.87	13.17	7.79
Fe_2O_3	17.23	17.98	19.94	15.58	16.11	15.32	14.78	13.80	19.52	14.12
MnO	0.27	0.26	0.36	0.37	0.20	0.24	0.21	0.21	0.36	0.22
MgO	5.98	13.63	12.49	8.40	15.93	16.34	17.95	15.01	6.88	16.97
CaO	10.07	10.65	8.13	11.57	5.02	9.14	7.96	9.43	10.71	8.18
Na_2O	3.53	0.81	0.60	2.12	0.19	0.62	0.20	0.63	2.00	0.38
K_2O	0.15	0.31	2.02	0.83	5.46	0.62	0.19	2.11	1.04	0.03
P_2O_5	0.15	0.11	0.10	0.10	0.10	0.08	0.08	0.07	0.14	0.08
LOI	4.41	4.71	3.46	0.61	1.86	3.10	4.73	2.49	0.71	4.57
Total	99.86	99.87	98.18	99.65	99.66	99.94	98.47	98.82	99.88	99.90
P	660	450	460	450	440	370	360	290	590	340
Cr	85	704	1550	764	468	1280	1520	1120	918	1570
Co	77	101	139	69	79	89	95	84	95	88
Ni	134	638	1265	276	368	791	899	670	639	956
Rb	4.1	12.2	69.4	9.4	217	22	8.3	86	33.2	0.8
Sr	316	128	110	1440	48.2	59.6	59.6	90.2	1495	60.2
Cs	0.55	1.78	9.93	0.07	15.15	2.24	1.01	8.18	1.26	0.35
Ba	210	80	400	1150	800	80	30	390	1220	10
Sc										
V	362	289	266	316	281	244	239	240	370	237
Ta	0.78	0.6	0.66	0.47	0.46	0.36	0.37	0.32	0.6	0.29
Nb	12.2	8.9	10.3	7.4	7	5.6	5.8	4.8	9.5	4.6
Zr	106	79.5	77	35.8	66.9	39.2	50.1	38.4	49.6	44.5
Hf	3	2.3	2.4	1.4	2	1.3	1.6	1.3	2.2	1.6
Th	1	0.7	0.9	0.5	0.5	0.4	0.5	0.4	0.9	0.4
U	0.2	0.2	0.2	0.1	0.1	0.1	0.1	0.1	0.2	0.1
Y	24.6	19.4	15.2	19.4	13.7	14.5	12.6	13	25.5	13.4
La	13.2	10.1	7.6	7.1	6.3	5.6	6.2	4.4	10.4	6.0
Ce	33.6	25.9	19.5	19.3	17.6	15.5	16.3	12.5	27.8	15.6
Pr	4.4	3.5	2.7	2.9	2.6	2.2	2.3	1.7	4.0	2.2
Nd	19.9	15.6	11.7	13.6	12.0	10.3	10.5	8.3	18.9	11.0
Sm	5.2	4.1	3.2	3.9	3.4	2.8	2.6	2.4	4.9	3.1
Eu	2.0	1.3	1.0	1.3	0.8	1.6	0.6	0.9	2.0	1.1
Gd	5.3	4.2	3.3	4.1	3.6	3.1	2.8	2.6	5.2	3.2
Tb	0.8	0.7	0.5	0.7	0.6	0.5	0.4	0.4	0.8	0.5
Dy	4.7	3.8	3.0	3.9	3.2	2.9	2.6	2.6	5.0	2.7
Ho	1.0	0.8	0.6	0.8	0.6	0.6	0.6	0.5	1.0	0.6
Er	2.5	2.0	1.5	2.1	1.6	1.6	1.4	1.4	2.6	1.4
Tm	0.3	0.3	0.2	0.3	0.2	0.2	0.1	0.2	0.3	0.2
Yb	2.1	1.7	1.3	1.8	1.3	1.4	1.2	1.2	2.3	1.2
Lu	0.3	0.2	0.2	0.3	0.2	0.2	0.1	0.1	0.3	0.1
Cu	531	218	786	14.9	7.4	84.5	187	87.8	15.6	163.5
Zn	139	122	363	109	107	107	90	87	177	142
Mo	1.06	0.51	0.84	0.85	0.12	0.45	0.4	0.36	1.24	0.36
Tl	0.06	0.21	1.62	0.02	1.63	0.23	0.09	0.95	0.43	0.06
Pb	9.2	8.1	31.6	4.1	0.5	5	3.6	2.3	5.9	1.8
Sn	1.3	1.2	1.9	1.1	0.4	1.7	0.5	0.9	1.3	0.6
Sb	0.18	0.19	0.1	0.05	<0.05	0.05	0.27	0.08	0.13	0.07
$(La/Yb)_{cn}$	4.51	4.26	4.19	2.83	3.47	2.87	3.70	2.63	3.24	3.59
$(La/Sm)_{cn}$	1.64	1.59	1.53	1.18	1.20	1.29	1.54	1.18	1.37	1.25
$(Gd/Yb)_{cn}$	2.09	2.04	2.10	1.88	2.29	1.83	1.93	1.79	1.87	2.21
$(Eu/Eu^*)_{cn}$	1.15	0.95	0.93	0.99	0.69	1.65	0.68	1.10	1.20	1.06
Al_2O_3/TiO_2	5.07	4.79	4.13	6.17	5.99	6.42	5.97	6.08	5.49	6.04
Zr/Hf	35.33	34.57	32.08	25.57	33.45	30.15	31.31	29.54	22.55	27.81
Zr/Y	4.31	4.10	5.07	1.85	4.88	2.70	3.98	2.95	1.95	3.32
Nb/Nb*	0.88	0.84	1.30	1.06	1.16	1.03	0.92	1.16	0.91	0.74
Notes										

	Basalt (footwall)									
Sample ID	546730	546735	546743	626166	626167	626168	626169	626174	626183	626184
SiO_2	42.24	46.19	40.64	42.35	43.58	43.57	41.19	46.22	45.04	44.16
TiO_2	1.81	1.53	0.96	1.13	0.88	1.23	1.61	1.20	1.48	1.98
Al_2O_3	8.19	7.53	5.57	7.10	5.01	5.18	7.45	6.44	6.88	9.46
Fe_2O_3	18.40	17.67	15.53	16.44	18.10	17.67	19.33	15.92	17.37	17.96
MnO	0.26	0.27	0.20	0.26	0.26	0.26	0.24	0.23	0.23	0.27
MgO	12.85	14.40	16.90	19.26	20.63	17.79	15.83	15.89	15.61	12.58
CaO	10.02	8.20	9.81	7.61	6.38	8.99	9.06	8.51	7.42	7.83
Na_2O	0.93	0.83	0.09	0.21	0.20	0.35	0.48	0.45	0.36	0.80
K_2O	0.31	1.40	0.01	0.04	0.02	0.04	0.08	2.69	3.55	3.23
P_2O_5	0.11	0.08	0.06	0.09	0.07	0.08	0.10	0.10	0.07	0.12
LOI	3.12	1.66	8.12	4.47	3.86	3.06	3.36	1.33	1.35	1.36
Total	98.43	99.99	98.23	99.32	99.38	98.51	98.92	99.27	99.58	100.10
P	480	390	280	340	300	420	460	380	400	520
Cr	687	844	1430	1520	2060	1450	870	1305	904	1265
Co	91	102	117	96	132	108	100	87	87	78
Ni	634	784	1235	1010	1385	1215	808	823	731	589
Rb	11.6	53.9	0.9	3	2	2	3	87	123	116
Sr	106	49.4	107.5	108	69	91	93	46	65	134
Cs	1.07	8.73	0.31							
Ba	70	230	10	10	<10	10	10	370	310	840
Sc										
V	302	281	194	251	188	209	292	234	271	355
Ta	0.52	0.43	0.23							
Nb	8.6	7.1	3.9	4	3	10	7	4	4	6
Zr	61.8	57.6	41	63	49	68	85	67	75	105
Hf	2.2	2.1	1.5							
Th	0.8	0.7	0.4	<1	<1	1	1	<1	1	1
U	0.2	0.2	0.1	<0.5	<0.5	<0.5	<0.5	<0.5	<0.5	<0.5
Y	20.1	14.1	12.2	13.8	10.2	13.6	17.4	14	16.2	22.4
La	8.9	8.0	4.1	5.0	3.2	10.0	8.6	3.8	7.5	9.2
Ce	24.0	21.6	10.7	13.2	8.6	23.4	22.0	10.8	19.1	23.8
Pr	3.3	2.9	1.6	2.0	1.3	3.1	3.1	1.7	2.8	3.6
Nd	15.6	13.2	7.5	9.7	6.6	13.4	14.9	8.2	13.0	17.2
Sm	4.0	3.3	2.1	2.7	1.8	3.1	3.7	2.6	3.3	4.5
Eu	1.3	0.7	0.7	0.6	0.3	0.4	1.0	0.8	1.1	1.6
Gd	4.2	3.3	2.2	2.8	2.0	3.2	3.8	2.8	3.4	4.8
Tb	0.6	0.5	0.3	0.5	0.3	0.5	0.6	0.5	0.6	0.8
Dy	3.7	2.7	2.1	2.7	1.9	2.8	3.6	2.8	3.1	4.4
Ho	0.8	0.6	0.5	0.5	0.4	0.5	0.7	0.5	0.6	0.9
Er	2.0	1.4	1.1	1.4	1.2	1.5	1.9	1.5	1.7	2.3
Tm	0.2	0.1	0.1	0.2	0.1	0.2	0.2	0.2	0.2	0.3
Yb	1.6	1.1	1.0	1.2	1.0	1.2	1.6	1.3	1.4	1.9
Lu	0.2	0.1	0.1	0.2	0.2	0.2	0.2	0.2	0.2	0.3
Cu	233	100	48.2	71	215	454	212	106	192	1
Zn	120	171	99	112	149	143	116	100	110	123
Mo	0.53	0.31	0.32	<1	<1	<1	<1	<1	<1	1
Tl	0.16	1.08	0.02							
Pb	2.2	5.2	1.2	4	11	2	6	8	5	4
Sn	1	0.9	0.3							
Sb	0.12	0.19	0.52	<5	<5	<5	5	<5	<5	<5
$(La/Yb)_{cn}$	3.99	5.21	2.94	2.99	2.29	5.98	3.85	2.10	3.84	3.47
$(La/Sm)_{cn}$	1.44	1.57	1.26	1.20	1.15	2.08	1.50	0.94	1.47	1.32
$(Gd/Yb)_{cn}$	2.17	2.48	1.82	1.93	1.65	2.21	1.96	1.78	2.01	2.09
$(Eu/Eu^*)_{cn}$	0.96	0.64	0.99	0.66	0.48	0.38	0.81	0.90	1.00	1.05
Al_2O_3/TiO_2	4.52	4.92	5.80	6.28	5.69	4.21	4.63	5.37	4.65	4.78
Zr/Hf	28.09	27.43	27.33							
Zr/Y	3.07	4.09	3.36	4.57	4.80	5.00	4.89	4.79	4.63	4.69
Nb/Nb*	0.97	0.89	0.92	0.79	0.94	0.87	0.78	1.12	0.51	0.63
Notes										

	Basalt (footwall)									
Sample ID	626185	626186	626187	626389	626396	626451	626452	626453	626454	626455
SiO_2	47.43	43.93	43.34	37.69	38.87	43.16	45.65	37.74	47.06	46.19
TiO_2	2.12	1.60	0.97	4.64	4.15	2.29	3.09	1.09	1.47	2.36
Al_2O_3	13.23	6.78	7.21	8.56	10.15	12.67	10.27	3.54	5.09	12.93
Fe_2O_3	18.74	18.73	20.38	22.45	22.61	16.59	15.12	17.93	11.26	18.44
MnO	0.22	0.25	0.24	0.28	0.31	0.23	0.32	0.44	0.21	0.31
MgO	6.37	16.55	14.71	5.25	4.45	4.35	4.91	11.11	10.96	7.20
CaO	7.31	8.27	6.87	9.27	8.85	10.11	9.23	16.05	14.92	8.31
Na_2O	3.32	0.59	0.54	2.21	2.61	3.93	4.08	0.57	1.53	2.21
K_2O	0.55	0.06	0.61	2.09	1.93	0.50	0.53	0.16	0.05	0.25
P_2O_5	0.13	0.10	0.06	0.13	0.16	0.16	0.18	0.07	0.07	0.14
LOI	0.48	2.96	3.66	5.80	4.93	4.36	4.89	9.02	5.30	1.34
Total	99.93	100.00	98.83	98.48	99.15	98.42	98.37	98.31	98.16	99.89
P	620	430	260	630	710	790	890	320	350	710
Cr	31	891	1265	<1	19	48	18	2880	1020	887
Co	59	97	157	88	76	57	66	170	68	105
Ni	75	787	315	36	14	75	70	1510	338	584
Rb	15	3	24	76.3	65.9	13.4	18.4	6	0.5	6.3
Sr	252	39	48	374	327	432	347	452	239	391
Cs				8.49	7.98	1.8	2.27	0.78	0.09	0.67
Ba	170	10	80	590	680	260	560	50	20	200
Sc										
V	370	298	174	389	158	368	357	171	279	418
Ta				1.5	1.96	0.66	1.89	0.63	0.69	0.67
Nb	8	7	6	21.7	27.5	10.7	29.9	10.5	10.8	11.1
Zr	118	77	59	124	144.5	92.1	145.5	47.1	51	107.5
Hf				4	4.5	2.4	3.9	1.3	1.7	3
Th	1	1	1	1.7	2.2	1	2.6	0.9	1	0.9
U	<0.5	<0.5	<0.5	0.4	0.5	0.2	0.6	0.2	0.2	0.2
Y	23.8	15.6	10.4	23.8	26.3	28.7	25.5	10.9	13.8	27.7
La	10.2	7.5	5.4	18.7	21.3	10.9	26.3	10.7	11.4	11.2
Ce	25.8	19.0	13.6	43.9	48.0	27.9	60.2	23.8	26.4	29.1
Pr	3.8	2.8	1.9							
Nd	18.0	12.9	9.0							
Sm	4.6	3.2	2.2							
Eu	1.3	0.8	0.8							
Gd	5.0	3.5	2.4							
Tb	0.8	0.6	0.4							
Dy	4.5	3.1	2.0							
Ho	0.9	0.6	0.4							
Er	2.5	1.7	1.1							
Tm	0.4	0.2	0.2							
Yb	2.1	1.3	0.9							
Lu	0.3	0.2	0.1							
Cu	207	208	7830	305	99.4	11.3	227	325	578	329
Zn	137	132	2000	213	176	106	184	134	87	167
Mo	<1	<1	2	1.08	0.91	0.6	1.02	0.6	0.44	0.67
Tl				1.18	1.02	0.14	0.2	0.09	<0.02	0.09
Pb	8	8	119	13.5	21.5	3.7	4	3.1	2	2.3
Sn				1.7	1.6	0.8	2.8	0.7	0.9	1.4
Sb	<5	<5	<5	0.06	0.08	0.05	1.17	0.18	0.23	0.16
$(La/Yb)_{cn}$	3.48	4.14	4.30							
$(La/Sm)_{cn}$	1.43	1.51	1.59							
$(Gd/Yb)_{cn}$	1.97	2.23	2.21							
$(Eu/Eu^*)_{cn}$	0.82	0.73	1.06							
Al_2O_3/TiO_2	6.24	4.24	7.43	1.84	2.45	5.53	3.32	3.25	3.46	5.48
Zr/Hf				31.00	32.11	38.38	37.31	36.23	30.00	35.83
Zr/Y	4.96	4.94	5.67	5.21	5.49	3.21	5.71	4.32	3.70	3.88
Nb/Nb*	0.74	0.88	1.04	1.02	1.09	0.94	0.97	0.81	0.82	0.96
Notes										

	Basalt (footwall)									
Sample ID	626456	626457	626458	626459	626473	626474	626475	626480	626485	626486
SiO_2	42.35	39.84	69.01	42.97	44.17	48.22	39.16	68.36	39.21	49.32
TiO_2	1.70	1.05	0.28	2.53	3.35	0.90	1.31	0.32	1.19	1.48
Al_2O_3	7.97	4.53	15.81	6.30	13.95	14.87	8.27	14.39	3.95	4.57
Fe_2O_3	18.28	17.65	3.55	18.19	19.63	13.92	16.27	2.78	26.46	12.37
MnO	0.24	0.20	0.08	0.23	0.25	0.20	0.34	0.04	0.71	0.22
MgO	14.83	19.48	1.41	10.19	4.80	6.98	15.49	1.82	11.64	12.27
CaO	8.96	5.76	3.74	13.66	9.85	10.45	10.29	5.17	8.48	13.60
Na_2O	0.53	0.06	3.18	0.99	2.70	2.78	0.26	3.79	0.42	1.37
K_2O	0.05	0.19	1.53	0.23	0.55	0.38	0.96	1.18	0.60	0.04
P_2O_5	0.10	0.07	0.08	0.07	0.14	0.10	0.08	0.09	0.09	0.07
LOI	4.20	8.87	0.92	3.83	0.47	1.04	5.55	1.48	5.17	3.73
Total	99.46	98.09	99.66	99.23	99.96	99.88	98.28	99.51	98.57	99.30
P	510	340	390	330	670	450	370	450	400	320
Cr	1130	1840	47	107	16	83	1150	33	3200	1020
Co	115	138	10	91	71	55	94	10	219	71
Ni	966	1460	25	259	33	80	746	19	1890	383
Rb	0.8	7.9	37.4	2.8	23.3	6.9	28.2	21.9	21.2	0.4
Sr	68.7	187	357	182.5	586	209	185.5	383	338	121
Cs	0.26	1.75	1.08	0.32	1.47	0.39	3.41	0.69	3.42	0.07
Ba	10	30	340	20	380	50	40	460	260	10
Sc										
V	308	203	34	551	391	269	267	45	196	271
Ta	0.52	0.33	0.36	0.52	0.95	0.15	0.34	0.3	0.73	0.65
Nb	8.5	5.5	4.3	8.4	14.3	2.5	5.6	3.4	11.4	9.9
Zr	60.2	44.3	95.3	38.4	31	17.8	55.7	61.4	50.8	46.2
Hf	1.8	1.3	2.6	1.3	1.3	0.7	1.9	1.9	1.6	1.8
Th	0.8	0.5	2.4	0.7	1.4	0.3	0.5	1.8	1	0.9
U	0.2	0.1	0.6	0.2	0.3	0.1	0.1	0.5	0.2	0.2
Y	17.9	9.9	4.7	15.8	20.5	17.3	15.7	4.7	12.4	13
La	9.1	4.7	14.3	8.8	14.6	3.9	5.6	11.9	11.5	10.1
Ce	22.7	12.3	27.0	21.4	35.5	9.7	14.8	24.0	25.6	25.1
Pr										
Nd										
Sm										
Eu										
Gd										
Tb										
Dy										
Ho										
Er										
Tm										
Yb										
Lu										
Cu	268	129	18.3	575	71.8	200	104	14.6	250	621
Zn	127	126	27	107	147	99	202	32	182	98
Mo	0.47	0.22	0.97	0.13	0.63	9.74	0.57	0.69	0.87	0.42
Tl	<0.02	0.16	0.13	<0.02	0.07	0.05	0.35	0.09	0.26	<0.02
Pb	1	18.3	3.3	1.3	2.2	3.9	6.3	7	4.2	2.3
Sn	0.8	0.4	1.1	0.9	1.3	0.5	2	1.1	0.6	0.8
Sb	0.22	0.28	<0.05	0.09	0.11	0.08	<0.05	<0.05	0.06	<0.05
$(La/Yb)_{cn}$										
$(La/Sm)_{cn}$										
$(Gd/Yb)_{cn}$										
$(Eu/Eu^*)_{cn}$										
Al_2O_3/TiO_2	4.69	4.31	56.46	2.49	4.16	16.52	6.31	44.97	3.32	3.09
Zr/Hf	33.44	34.08	36.65	29.54	23.85	25.43	29.32	32.32	31.75	25.67
Zr/Y	3.36	4.47	20.28	2.43	1.51	1.03	3.55	13.06	4.10	3.55
Nb/Nb*	0.87	1.14	0.21	0.87	0.89	0.60	0.98	0.21	0.82	0.91
Notes			silicified					silicified		

	Basalt (footwall)									
Sample ID	626487	626489	626490	626491	626495	645653	645654	645658	645659	645662
SiO_2	46.68	63.47	42.55	46.47	42.90	44.21	42.98	50.46	44.86	47.77
TiO_2	1.97	0.40	3.09	1.18	3.36	1.56	2.67	0.82	1.22	0.78
Al_2O_3	11.23	13.85	6.63	7.38	9.61	10.03	7.96	3.22	7.65	15.07
Fe_2O_3	16.09	3.88	20.98	14.03	21.51	16.02	17.41	15.74	14.71	13.05
MnO	0.23	0.19	0.26	0.23	0.26	0.22	0.27	0.29	0.30	0.23
MgO	10.70	1.62	10.07	16.39	6.43	12.89	11.47	15.48	16.35	7.53
CaO	8.88	6.71	12.76	8.47	11.18	9.78	11.32	10.34	9.95	11.13
Na_2O	2.30	2.01	0.87	0.50	2.16	1.10	1.33	0.35	0.59	2.54
K_2O	0.18	2.86	0.24	1.78	0.32	1.77	0.20	0.91	0.11	0.38
P_2O_5	0.13	0.08	0.07	0.08	0.14	0.09	0.11	0.05	0.08	0.06
LOI	1.13	4.64	2.41	2.56	1.42	1.77	4.06	1.68	3.33	1.09
Total	99.73	99.80	99.95	99.43	99.34	99.70	99.96	99.72	99.52	99.67
P	600	350	300	360	640	400	530	200	310	250
Cr	782	51	49	1240	14	558	530	1640	1400	98
Co	93	11	96	83	76	68	91	133	85	56
Ni	589	33	256	752	106	299	589	1220	793	104
Rb	2.9	61.7	2.5	75.2	3.6	66	6.6	49.7	1.6	7.7
Sr	218	263	99.3	118	341	99.6	193	56.8	157.5	122.5
Cs	0.17	1.28	0.36	4.87	0.45	4.5	0.76	3.11	0.29	0.34
Ba	80	480	20	530	80	910	240	190	10	60
Sc										
V	331	57	579	231	620	290	469	116	216	218
Ta	0.52	0.36	0.6	0.33	0.88	0.39	0.74	0.46	0.34	0.18
Nb	8.1	4.2	9.7	4.7	13.8	6	12.2	7.7	5.2	2.2
Zr	73.4	81.4	44.9	23.6	51.7	54.5	77	32.4	29.8	19.8
Hf	2.6	2.6	1.7	1	1.5	2.1	2.7	1	1.1	0.7
Th	0.7	2	0.8	0.5	1.2	0.6	1.2	0.6	0.4	0.3
U	0.2	0.4	0.2	0.1	0.3	0.1	0.3	0.1	0.1	0.1
Y	24.9	5.6	15.5	13.4	22.1	17.9	19.2	7	13.7	16.8
La	8.7	13.3	8.7	4.4	13.9	7.0	11.9	6.7	5.1	3.3
Ce	23.5	26.2	21.4	12.6	34.2	18.9	30.6	15.5	13.9	8.5
Pr						2.8	4.2	1.9	2.2	1.2
Nd						13.2	18.4	7.9	10.2	5.8
Sm						3.7	4.6	1.8	2.9	1.8
Eu						1.0	1.5	0.4	0.9	0.7
Gd						3.8	4.5	1.7	2.9	2.3
Tb						0.6	0.7	0.2	0.5	0.4
Dy						3.6	3.9	1.4	2.8	2.9
Ho						0.7	0.8	0.3	0.5	0.6
Er						1.9	2.0	0.7	1.5	1.8
Tm						0.3	0.3	0.1	0.2	0.3
Yb						1.6	1.7	0.6	1.3	1.8
Lu						0.3	0.2	0.1	0.2	0.3
Cu	228	19.8	534	204	387	9.9	393	286	141	78.8
Zn	114	23	112	88	130	107	131	119	130	78
Mo	0.68	0.49	0.27	1.05	0.62	0.24	0.68	0.35	0.44	1.31
Tl	0.04	0.13	0.03	0.68	0.04	0.47	0.13	0.54	0.02	0.03
Pb	10.8	2.4	1.2	3.1	1.4	3.4	4.2	1.9	8.8	1.5
Sn	1.1	0.7	1.1	0.7	1.3	1	1	0.4	0.7	0.6
Sb	0.14	<0.05	0.33	0.15	0.21	0.09	0.23	0.11	0.06	0.05
$(La/Yb)_{cn}$						3.14	5.02	8.01	2.81	1.31
$(La/Sm)_{cn}$						1.22	1.67	2.40	1.14	1.18
$(Gd/Yb)_{cn}$						1.96	2.19	2.34	1.84	1.06
$(Eu/Eu^*)_{cn}$						0.81	1.00	0.69	0.94	1.05
Al_2O_3/TiO_2	5.70	34.63	2.15	6.25	2.86	6.43	2.98	3.93	6.27	19.32
Zr/Hf	28.23	31.31	26.41	23.60	34.47	25.95	28.52	32.40	27.09	28.29
Zr/Y	2.95	14.54	2.90	1.76	2.34	3.04	4.01	4.63	2.18	1.18
Nb/Nb*	0.94	0.23	1.02	1.14	0.91	0.86	0.98	0.99	1.03	0.64
Notes		silicified								

					Basalt (footwall)					
Sample ID	645665	24-B	36-K	39-K	41-K	52-K	73-1	73-K	7-K	90-1
SiO_2	43.00	42.39	47.47	47.10	49.11	46.80	44.16	46.35	39.89	42.27
TiO_2	1.30	0.84	0.86	1.00	1.37	1.14	1.05	0.99	1.52	1.41
Al_2O_3	8.21	5.85	14.04	6.45	4.17	6.83	6.45	5.62	7.78	6.29
Fe_2O_3	15.00	22.08	13.91	14.23	15.91	14.68	15.51	14.46	13.42	21.77
MnO	0.20	0.13	0.21	0.27	0.22	0.24	0.26	0.27	0.33	0.56
MgO	15.85	6.93	7.62	16.72	13.81	13.55	20.65	19.61	9.00	13.02
CaO	9.89	5.17	8.73	9.42	12.52	11.10	8.01	9.25	18.78	9.13
Na_2O	0.58	0.32	3.43	0.32	0.37	1.14	0.18	0.32	1.53	0.59
K_2O	0.42	0.14	1.01	2.15	1.27	1.56	0.02	0.05	0.61	1.25
P_2O_5	0.08	0.07	0.06	0.07	0.05	0.04	0.05	0.03	0.12	0.09
LOI	5.02	4.94	3.05	2.34	1.84	2.85	4.38	3.23	7.80	2.25
Total	99.89	88.87	100.38	100.07	100.63	99.93	100.71	100.19	100.78	98.62
P	340									
Cr	1290	733	164	2207	414	1656	3057	3706	756	3588
Co	84	194	53	85	76	77	89	77	54	206
Ni	727	75	94	715	423	661	495	438	261	1813
Rb	10	7	31	104	46	44	1	1	22	43
Sr	118.5	48	442	133	133	277	85	79	636	147
Cs	0.91	1.789	0.767	5.317	3.817	7.22	0.053	0.05	1.332	5.203
Ba	70	35.4	394	622.7	247.9	377.8	1.1	2.7	131.6	1043.1
Sc		16.2	41.3	28.9	95.1	27.7	60	65	34.1	29.9
V	232	207	319	238	409	226	229	248	375	254
Ta	0.35	0.5	<0.2	0.3	0.4	0.3	0.2	0.2	0.4	0.7
Nb	5.2	6.34	2.24	3.63	6.45	4.83	3.68	3.17	6	9.92
Zr	58.7	64	42	54	42	60	49	43	84	72
Hf	1.9	1.65	1.13	1.44	1.38	1.59	1.37	1.28	2.31	1.89
Th	0.4	0.97	0.28	0.35	0.51	0.4	0.24	0.26	0.61	0.86
U	0.1	0.27	0.13	0.1	0.14	0.11	0.07	0.07	0.16	0.23
Y	14.4	9.54	20.77	13.12	15.57	14.84	13.34	13.47	19.5	14.9
La	6.1	8.1	3.2	3.9	6.0	4.2	5.3	3.7	7.4	11.3
Ce	16.7	19.7	9.8	12.5	17.3	12.4	14.9	10.9	20.3	26.8
Pr	2.4	2.4	1.2	1.7	2.4	1.8	2.0	1.5	2.8	3.5
Nd	11.3	10.8	5.8	8.4	12.0	9.2	9.6	7.7	14.0	15.4
Sm	3.0	2.4	1.8	2.4	3.3	2.8	2.6	2.3	3.7	3.4
Eu	1.3	0.8	0.7	0.8	1.3	1.0	0.8	1.5	1.5	1.0
Gd	3.2	2.3	2.4	2.7	3.5	2.9	2.6	2.5	3.8	3.1
Tb	0.5	0.3	0.4	0.4	0.6	0.5	0.4	0.4	0.6	0.5
Dy	2.9	2.0	3.0	2.5	3.2	2.8	2.6	2.4	3.6	2.8
Ho	0.6	0.4	0.7	0.5	0.6	0.5	0.5	0.5	0.7	0.5
Er	1.6	0.9	2.0	1.3	1.4	1.4	1.2	1.3	1.8	1.4
Tm	0.2	0.1	0.3	0.2	0.2	0.2	0.2	0.2	0.3	0.2
Yb	1.3	0.8	2.1	1.1	1.2	1.2	1.1	1.2	1.6	1.3
Lu	0.2	0.1	0.3	0.2	0.2	0.2	0.2	0.2	0.2	0.2
Cu	157	>800	27	62	16	35	4	37	65	277
Zn	74	>2400	75	91	81	126	83	80	78	234
Mo	0.44	4.93	0.13	0.34	0.12	0.26	0.08	0.09	0.29	1.01
Tl	0.1	0.983	0.176	1.271	0.792	0.624	<0.005	<0.005	0.31	0.636
Pb	1.1	>400	5.4	5.5	6.1	17.3	0.6	0.7	6.8	6.5
Sn	1	5.2	0.34	0.37	1.11	1.11	0.58	0.93	1.43	0.87
Sb	0.05	0.49	0.04	0.06	0.08	0.04	<0.04	0.04	0.1	0.04
$(La/Yb)_{cn}$	3.36	6.86	1.08	2.51	3.64	2.44	3.51	2.20	3.26	6.12
$(La/Sm)_{cn}$	1.31	2.16	1.13	1.06	1.19	0.98	1.31	1.05	1.27	2.14
$(Gd/Yb)_{cn}$	2.04	2.23	0.94	1.98	2.44	1.93	2.00	1.70	1.96	1.95
$(Eu/Eu^*)_{cn}$	1.27	1.05	1.03	0.96	1.19	1.03	0.88	1.88	1.18	0.88
Al_2O_3/TiO_2	6.32	6.96	16.33	6.45	3.04	5.99	6.14	5.68	5.12	4.46
Zr/Hf	30.89	38.79	37.17	37.50	30.43	37.74	35.77	33.59	36.36	38.10
Zr/Y	4.08	6.71	2.02	4.12	2.70	4.04	3.67	3.19	4.31	4.83
Nb/Nb*	0.87	0.71	0.79	1.12	1.15	1.26	0.72	0.95	0.84	0.77
Notes		high sulphide content							~10% calcite	

	Basalt (fw)	Basalt (hangingwall)								
Sample ID	90-K	546675	546676	546677	546732	546733	546736	546738	546748	546749
SiO_2	40.69	49.46	47.92	45.69	48.26	48.92	46.51	48.19	47.74	47.44
TiO_2	1.70	0.70	0.85	1.73	0.72	0.69	0.88	0.68	0.69	0.82
Al_2O_3	2.74	12.49	15.53	7.97	14.32	13.28	15.66	15.04	13.99	14.93
Fe_2O_3	28.56	11.80	11.83	18.40	13.05	11.98	13.61	12.10	13.42	11.92
MnO	0.42	0.17	0.19	0.27	0.18	0.22	0.29	0.18	0.20	0.23
MgO	12.97	10.56	8.24	13.70	7.60	9.43	6.45	8.48	8.22	6.58
CaO	9.65	9.89	9.58	8.67	10.21	9.13	12.23	10.73	11.37	13.81
Na_2O	0.49	2.14	1.78	0.91	2.60	2.54	2.31	2.49	2.31	1.78
K_2O	0.06	0.72	1.84	0.11	0.37	0.65	0.39	0.41	0.28	0.42
P_2O_5	0.13	0.06	0.06	0.10	0.06	0.05	0.06	0.06	0.07	0.05
LOI	2.01	1.57	1.92	2.08	1.00	1.72	1.36	1.13	1.19	1.73
Total	99.41	99.69	99.87	99.89	98.42	98.69	99.81	99.54	99.54	99.75
P		320	300	450	300	210	280	260	290	210
Cr	5440	412	242	1080	99	103	86	133	114	75
Co	229	59	51	111	51	54	62	50	55	47
Ni	1585	194	142	879	104	119	112	118	114	82
Rb	1	20	77.2	3.9	8.6	19.8	10.9	11.9	2.5	10.2
Sr	55	143	163.5	74.3	143	158	201	157.5	104.5	189.5
Cs	0.134	0.41	1.41	0.45	0.23	0.86	0.28	0.3	0.14	0.26
Ba	14.7	260	520	60	90	330	90	80	60	100
Sc	37.6									
V	439	230	253	293	236	232	279	227	223	258
Ta	0.9	0.15	0.13	0.52	0.16	0.14	0.18	0.16	0.15	0.16
Nb	13.2	2.3	1.9	8.6	2.1	1.8	2.4	1.9	2.1	2.2
Zr	75	15.7	11.9	65	21.1	11.3	10	8.4	18.2	17.3
Hf	2.04	0.6	0.5	2	0.9	0.5	0.6	0.4	0.8	0.8
Th	1.17	0.3	0.3	0.7	0.3	0.2	0.4	0.3	0.3	0.3
U	0.29	0.1	0.1	0.2	0.1	0.1	0.1	0.1	0.1	0.1
Y	20.71	19.2	17.8	15.8	17.9	16	18.7	17.7	16.9	18.5
La	16.3	3.2	3.1	8.5	3.5	2.6	3.9	3.2	3.5	3.5
Ce	38.1	8.5	8.1	21.8	8.6	7.1	10.0	8.5	8.9	9.2
Pr	5.1				1.2	1.0	1.4	1.2	1.3	1.3
Nd	22.3				5.7	4.9	6.6	5.7	6.2	6.2
Sm	4.7				1.8	1.5	2.0	1.7	1.9	1.9
Eu	1.5				0.7	0.5	0.8	0.6	0.7	0.7
Gd	4.2				2.3	2.0	2.6	2.3	2.3	2.4
Tb	0.6				0.4	0.3	0.4	0.4	0.4	0.4
Dy	3.6				2.8	2.6	3.0	2.8	2.9	3.0
Ho	0.7				0.7	0.6	0.7	0.7	0.7	0.7
Er	1.9				1.9	1.7	1.9	1.8	1.9	2.0
Tm	0.3				0.2	0.2	0.2	0.2	0.3	0.3
Yb	1.8				1.8	1.6	1.7	1.7	1.8	1.9
Lu	0.3				0.2	0.2	0.2	0.2	0.3	0.3
Cu	>800	259	131	228	87.3	116	166.5	87.8	193.5	77.1
Zn	507	64	101	126	78	78	113	81	102	68
Mo	1	0.55	2.15	0.44	0.33	0.38	2.84	0.96	4.93	0.41
Tl	0.204	0.08	0.43	0.07	0.04	0.1	0.05	0.05	<0.02	0.04
Pb	6.9	2.6	1.7	4.5	1.6	2.5	3.4	2	3.4	6.2
Sn	1.46	0.6	0.6	1	0.5	0.2	0.6	0.4	0.5	0.4
Sb	0.14	<0.05	<0.05	0.17	0.05	<0.05	0.07	<0.05	0.08	0.07
$(La/Yb)_{cn}$	6.46				1.39	1.17	1.64	1.35	1.39	1.32
$(La/Sm)_{cn}$	2.26				1.26	1.12	1.26	1.22	1.19	1.19
$(Gd/Yb)_{cn}$	1.91				1.06	1.03	1.26	1.12	1.06	1.04
$(Eu/Eu^*)_{cn}$	1.00				1.05	0.88	1.07	0.93	1.02	1.00
Al_2O_3/TiO_2	1.61	17.84	18.27	4.61	19.89	19.25	17.80	22.12	20.28	18.21
Zr/Hf	36.76	26.17	23.80	32.50	23.44	22.60	16.67	21.00	22.75	21.63
Zr/Y	3.62	0.82	0.67	4.11	1.18	0.71	0.53	0.47	1.08	0.94
Nb/Nb*	0.71	0.71	0.60	0.97	0.55	0.71	0.59	0.59	0.57	0.61

Notes

	Basalt (hangingwall)									
Sample ID	626188	626189	626192	626193	626477	645651	645656	645660	645663	645666
SiO_2	49.43	49.74	48.47	43.66	49.03	49.45	48.10	47.95	44.41	48.53
TiO_2	1.44	0.86	0.76	1.23	1.95	1.10	0.67	0.77	1.41	0.85
Al_2O_3	13.71	14.37	13.88	7.53	9.30	13.51	15.78	14.47	7.48	14.69
Fe_2O_3	17.40	13.96	13.27	16.19	15.72	12.58	11.08	13.08	16.07	13.40
MnO	0.24	0.24	0.22	0.23	0.25	0.18	0.22	0.20	0.22	0.20
MgO	4.20	7.03	8.23	16.59	9.62	6.77	6.92	7.47	14.84	8.60
CaO	8.07	9.63	10.11	9.67	9.08	8.98	12.64	10.61	10.48	7.96
Na_2O	3.84	2.23	1.92	0.80	2.54	3.76	2.55	2.14	0.27	2.79
K_2O	0.39	0.61	0.94	0.25	0.34	0.25	0.39	0.52	1.15	1.05
P_2O_5	0.11	0.08	0.05	0.08	0.11	0.11	0.05	0.07	0.09	0.07
LOI	0.91	0.61	1.14	2.83	1.72	1.47	1.46	1.16	2.90	1.67
Total	99.78	99.42	99.05	99.33	99.88	98.21	99.91	98.49	99.57	99.94
P	510	340	290	350	530	480	220	290	330	290
Cr	51	66	86	1125	850	139	49	112	907	72
Co	54	50	50	86	74	40	46	56	81	50
Ni	53	74	92	779	250	76	80	107	641	86
Rb	7	15	29	8	12.8	3.2	10.9	19.3	37.3	23.6
Sr	277	145	264	81	143	174.5	202	132	51.4	357
Cs					1.81	0.18	0.25	0.29	3.5	0.85
Ba	100	90	120	40	230	50	110	100	180	460
Sc										
V	409	266	244	266	396	264	217	223	234	237
Ta					0.57	0.26	0.18	0.2	0.39	0.19
Nb	3	2	<2	5	8.6	3.8	2.1	2.3	6	2.4
Zr	90	61	52	70	76.9	47.6	11.8	17	59.7	31.9
Hf					2.8	1.7	0.5	0.7	1.9	1.1
Th	1	<1	<1	1	0.8	0.7	0.3	0.3	0.5	0.3
U	<0.5	<0.5	<0.5	<0.5	0.2	0.1	0.1	0.1	0.1	0.1
Y	27.2	21.1	20	14.2	20.8	28.4	16.5	16.9	14.9	16.5
La	6.3	4.1	4.1	5.4	8.3	6.6	2.9	3.7	6.5	3.7
Ce	15.2	10.2	9.7	14.3	22.6	16.4	7.5	9.3	17.0	9.4
Pr	2.2	1.5	1.4	2.1		2.3	1.1	1.4	2.6	1.4
Nd	10.4	7.1	6.6	10.2		10.8	5.2	6.6	12.3	6.7
Sm	3.0	2.0	2.0	2.7		3.3	1.6	2.0	3.4	2.0
Eu	1.0	0.8	0.8	0.9		1.2	0.7	0.7	0.8	0.8
Gd	3.9	2.7	2.6	3.0		3.9	2.1	2.5	3.5	2.5
Tb	0.7	0.5	0.5	0.5		0.7	0.4	0.5	0.6	0.5
Dy	4.6	3.5	3.3	2.7		4.9	2.7	3.0	3.2	3.0
Ho	1.1	0.8	0.8	0.5		1.1	0.6	0.7	0.6	0.7
Er	3.1	2.4	2.2	1.5		3.2	1.8	2.0	1.7	2.0
Tm	0.5	0.4	0.3	0.2		0.5	0.3	0.3	0.2	0.3
Yb	3.0	2.2	2.1	1.2		3.0	1.7	1.9	1.5	1.9
Lu	0.5	0.4	0.3	0.2		0.5	0.3	0.3	0.2	0.3
Cu	337	133	121	254	262	100.5	40	139	161.5	77.3
Zn	125	102	93	101	114	80	56	73	91	66
Mo	<1	<1	<1	<1	0.58	5.56	1.4	2.1	0.25	0.32
Tl					0.19	0.02	0.04	0.07	0.35	0.14
Pb	17	4	12	13	2.6	42.7	5.7	1.1	8.9	6.9
Sn					1.3	0.6	0.3	0.7	0.8	0.5
Sb	<5	<5	<5	<5	0.1	0.17	0.07	0.05	0.25	0.19
$(La/Yb)_{cn}$	1.51	1.34	1.40	3.23		1.58	1.22	1.40	3.11	1.40
$(La/Sm)_{cn}$	1.36	1.32	1.32	1.29		1.29	1.17	1.20	1.24	1.20
$(Gd/Yb)_{cn}$	1.08	1.01	1.02	2.07		1.08	1.02	1.09	1.93	1.09
$(Eu/Eu^*)_{cn}$	0.89	1.05	1.07	0.96		1.02	1.17	0.96	0.70	1.09
Al_2O_3/TiO_2	9.52	16.71	18.26	6.12	4.77	12.28	23.55	18.79	5.30	17.28
Zr/Hf					27.46	28.00	23.60	24.29	31.42	29.00
Zr/Y	3.31	2.89	2.60	4.93	3.70	1.68	0.72	1.01	4.01	1.93
Nb/Nb*	0.43	0.45		0.91	1.05	0.53	0.70	0.58	0.90	0.61
Notes										

	Basalt (hangingwall)									
Sample ID	23-L	30-L	37-L	39-L	46-L	50-L	71-L	72-2	72-L	73-3
SiO_2	47.46	48.06	39.80	48.16	48.17	47.08	44.11	42.03	37.70	39.93
TiO_2	1.03	1.50	2.19	0.75	0.62	2.17	1.21	1.21	1.22	1.09
Al_2O_3	15.65	12.75	8.87	12.64	10.95	14.33	8.21	7.39	7.72	4.61
Fe_2O_3	15.68	18.33	17.92	14.68	11.87	20.27	15.68	16.08	15.92	19.65
MnO	0.48	0.47	0.32	0.22	0.23	0.32	0.21	0.27	0.27	0.25
MgO	6.07	4.69	9.06	9.22	9.71	2.64	16.28	15.33	15.16	18.97
CaO	6.82	8.83	13.52	11.60	12.65	7.70	9.33	9.68	10.57	8.99
Na_2O	2.44	2.97	1.38	2.38	2.58	4.75	0.67	0.89	0.79	0.12
K_2O	1.78	0.47	0.32	0.28	0.54	0.68	0.36	1.99	2.42	0.02
P_2O_5	0.08	0.13	0.15	0.07	0.06	0.19	0.20	0.08	0.08	0.07
LOI	2.53	0.91	5.74	0.75	2.90	0.57	4.31	4.58	7.19	3.53
Total	100.02	99.11	99.24	100.72	100.28	100.70	100.57	99.52	99.05	97.25
P										
Cr	73	68	744	1069	916	17	2561	2375	2560	2104
Co	50	56	81	67	59	42	96	89	89	165
Ni	46	32	256	246	245	6	814	776	767	2612
Rb	57	12	6	5	15	16	8	61	74	1
Sr	120	128	153	195	215	485	64	212	313	43
Cs	0.822	0.256	0.286	0.096	1.795	0.347	0.517	11.68	13.601	0.076
Ba	615.7	235.8	34.8	41.7	130.2	298	46.3	425.9	535.2	2
Sc	43.8	43.9	63.5	40.8	31.6	9.5	34.7	30.5	32	28.1
V	373	467	499	256	242	49	287	264	278	186
Ta	0.2	0.3	0.7	<0.2	<0.2	1.5	0.3	0.3	0.3	0.4
Nb	2.44	4.05	11.94	2.24	1.92	23.24	4.63	4.46	4.46	6.19
Zr	57	90	109	52	44	179	67	62	64	61
Hf	1.61	2.55	3.01	1.47	1.23	4.6	1.79	1.71	1.75	1.59
Th	0.34	0.56	1.07	0.26	0.25	2.16	0.38	0.4	0.42	0.56
U	0.1	0.15	0.28	0.18	0.08	0.54	0.14	0.11	0.12	0.16
Y	22.19	35.92	21.5	19.99	16.86	31.09	17.36	14.4	14.59	10.96
La	3.7	6.7	9.4	3.7	2.8	22.3	7.0	5.1	5.3	6.2
Ce	11.3	19.4	27.7	10.9	8.0	54.7	16.7	14.6	14.8	16.0
Pr	1.4	2.5	3.8	1.4	1.1	7.2	2.3	2.1	2.1	2.2
Nd	7.4	12.5	17.9	7.0	5.6	33.2	11.1	10.5	10.3	10.2
Sm	2.3	3.7	4.7	2.1	1.7	7.4	3.0	2.8	2.8	2.5
Eu	0.8	1.6	1.4	0.8	0.6	2.5	1.1	1.0	0.9	0.8
Gd	2.8	4.7	4.7	2.6	2.1	7.2	3.3	2.9	2.9	2.5
Tb	0.5	0.8	0.7	0.5	0.4	1.1	0.5	0.5	0.4	0.4
Dy	3.6	5.8	4.1	3.2	2.8	6.0	3.0	2.6	2.6	2.1
Ho	0.8	1.3	0.8	0.7	0.6	1.1	0.6	0.5	0.5	0.4
Er	2.3	3.6	2.0	2.0	1.7	3.0	1.6	1.4	1.3	1.0
Tm	0.4	0.6	0.3	0.3	0.3	0.4	0.2	0.2	0.2	0.2
Yb	2.3	3.7	1.7	2.0	1.8	2.7	1.4	1.3	1.3	0.9
Lu	0.4	0.6	0.2	0.3	0.3	0.4	0.2	0.2	0.2	0.1
Cu	104	220	418	6	30	39	19	44	51	>800
Zn	1280	1799	95	54	76	150	91	114	112	127
Mo	0.21	0.52	1.21	0.11	0.11	1.98	0.44	0.42	0.39	0.11
Tl	0.287	0.084	0.042	0.019	0.083	0.076	0.114	0.664	0.779	0.051
Pb	38.8	14.8	1.7	1.3	4	5.6	0.7	3.3	4.3	1.6
Sn	0.48	2.07	0.84	0.9	0.51	2.09	0.81	0.56	0.45	0.87
Sb	0.06	0.11	0.07	<0.04	<0.04	0.06	0.07	<0.04	<0.04	0.05
$(La/Yb)_{cn}$	1.14	1.31	3.97	1.33	1.13	6.01	3.52	2.90	2.94	4.96
$(La/Sm)_{cn}$	1.02	1.17	1.29	1.15	1.04	1.93	1.50	1.18	1.23	1.61
$(Gd/Yb)_{cn}$	0.99	1.06	2.30	1.08	0.99	2.23	1.88	1.90	1.83	2.27
$(Eu/Eu^*)_{cn}$	0.98	1.18	0.92	1.00	0.89	1.03	1.08	1.02	0.96	0.93
Al_2O_3/TiO_2	15.19	8.50	4.05	16.85	17.66	6.60	6.79	6.11	6.33	4.23
Zr/Hf	35.40	35.29	36.21	35.37	35.77	38.91	37.43	36.26	36.57	38.36
Zr/Y	2.57	2.51	5.07	2.60	2.61	5.76	3.86	4.31	4.39	5.57
Nb/Nb*	0.77	0.65	1.40	0.66	0.74	0.96	0.58	0.93	0.87	0.95
Notes										

	Basalt (hangingwall)			Basalt (unkown relationship to VMS stratigraphy)			Siltstone			
Sample ID	73-L	74-L	90-2	546699	626467	105-1	546663	546670	546672	546680
SiO_2	40.60	47.60	42.93	43.38	45.80	45.99	70.91	66.12	43.53	70.46
TiO_2	1.20	0.87	2.34	1.27	2.53	0.54	0.27	0.32	3.31	0.28
Al_2O_3	4.87	15.41	6.63	7.33	10.57	15.82	13.81	17.04	10.26	15.33
Fe_2O_3	19.70	12.32	20.16	16.70	14.91	10.15	1.91	2.99	22.31	1.57
MnO	0.26	0.19	0.26	0.25	0.28	0.16	0.04	0.04	0.24	0.02
MgO	20.58	7.05	11.42	16.50	5.18	10.21	1.43	1.46	6.10	1.02
CaO	6.83	13.27	12.87	7.69	8.72	10.23	4.42	3.49	10.39	3.67
Na_2O	0.09	2.46	0.87	0.40	3.81	1.54	4.09	5.15	2.25	4.58
K_2O	0.01	0.31	0.25	0.35	1.14	1.13	0.87	1.29	0.42	0.90
P_2O_5	0.09	0.07	0.08	0.08	0.16	0.04	0.07	0.08	0.15	0.08
LOI	5.11	0.95	1.92	4.09	4.99	2.57	1.89	1.07	0.72	1.72
Total	99.33	100.50	99.74	98.32	98.49	98.53	99.78	99.17	99.72	99.70
P				390	780	130	330	390	750	340
Cr	2127	374	553	1310	1770	459	36	53	19	18
Co	139	52	99	118	144	51	7	11	89	6
Ni	1433	153	409	761	1300	178	26	30	149	17
Rb	1	5	3	12.3	51.6	37.3	22.6	33.4	4.9	19.3
Sr	30	158	53	43.1	371	147	280	493	351	255
Cs	0.071	0.24	0.14	2.59	3.85	1.11	1.38	1.33	0.18	0.72
Ba	1.2	28.7	17.1	50	630	80	330	310	100	390
Sc	27.3	38.9	49.8							
V	202	263	533	258	400	179	30	40	704	30
Ta	0.4	<0.2	0.5	0.48	1.1	0.07	0.23	0.37	1.05	0.21
Nb	6.29	2.05	7.94	7.4	16.2	0.7	2.4	4.2	16.3	2.1
Zr	59	49	73	62.6	117	10.2	88.9	108	49.7	94.9
Hf	1.6	1.35	2.15	1.9	3.9	0.4	2.3	2.7	1.6	2.7
Th	0.45	0.22	0.64	0.6	2.3	<0.2	2	2.2	1.7	1.8
U	0.14	0.07	0.14	0.1	0.6	<0.1	0.5	0.7	0.4	0.4
Y	10.26	19.21	16.18	14.5	25.7	10.1	4.3	4.4	25.2	3.7
La	5.6	2.9	8.3	5.5	17.0	1.5	12.6	13.2	17.4	10.9
Ce	14.4	8.5	22.2	14.9	41.4	3.9	24.5	25.8	41.5	21.3
Pr	1.9	1.2	3.1	2.2		0.7				2.5
Nd	8.9	6.3	15.1	10.1		3.4				8.6
Sm	2.3	2.0	3.8	3.1		1.1				1.5
Eu	0.6	0.7	1.0	1.0		0.5				0.5
Gd	2.3	2.6	3.7	3.1		1.4				1.3
Tb	0.4	0.5	0.6	0.5		0.3				0.2
Dy	2.0	3.2	3.2	2.9		1.8				0.8
Ho	0.4	0.7	0.6	0.6		0.4				0.1
Er	1.0	1.9	1.5	1.6		1.2				0.4
Tm	0.1	0.3	0.2	0.2		0.2				<0.1
Yb	0.9	1.9	1.3	1.3		1.2				0.3
Lu	0.1	0.3	0.2	0.2		0.2				<0.1
Cu	>800	103	448	651	766	37.7	16.9	18.8	562	9.1
Zn	125	83	99	2620	632	93	16	44	131	20
Mo	0.19	3.04	0.39	1.2	3.3	0.16	1.78	1.79	2.32	0.53
Tl	0.025	0.035	0.019	0.22	0.85	0.26	0.07	0.16	0.03	0.07
Pb	0.8	2.8	3.5	30.4	13.2	1	4.8	6.5	3.6	4.6
Sn	0.58	0.57	1	3.1	3.5	0.5	0.6	0.7	1.7	0.4
Sb	<0.04	0.05	<0.04	<0.05	0.45	0.05	0.06	0.06	0.08	0.06
$(La/Yb)_{cn}$	4.54	1.07	4.63	3.03		0.90				26.05
$(La/Sm)_{cn}$	1.56	0.94	1.41	1.15		0.88				4.69
$(Gd/Yb)_{cn}$	2.17	1.09	2.40	1.97		0.96				3.58
$(Eu/Eu^*)_{cn}$	0.75	0.99	0.80	0.98		1.23				1.07
Al_2O_3/TiO_2	4.06	17.71	2.83	5.77	4.18	29.30	51.15	53.25	3.10	54.75
Zr/Hf	36.88	36.30	33.95	32.95	30.00	25.50	38.65	40.00	31.06	35.15
Zr/Y	5.75	2.55	4.51	4.32	4.55	1.01	20.67	24.55	1.97	25.65
Nb/Nb*	1.09	0.78	0.95	1.36	0.87	0.46	0.14	0.23	0.83	0.14
Notes									~10-50% chloritic laminae	

	Siltstone									
Sample ID	546684	546688	546692	546710	546718	546722	546724	546727	546734	546737
SiO_2	65.07	67.20	66.07	70.38	67.52	69.00	62.06	60.92	69.06	68.26
TiO_2	0.29	0.32	0.41	0.31	0.32	0.24	0.44	0.42	0.28	0.27
Al_2O_3	17.17	15.47	15.22	15.59	15.61	15.27	16.70	16.86	15.51	15.87
Fe_2O_3	3.86	3.30	3.28	2.45	3.24	3.38	7.69	8.40	3.14	2.86
MnO	0.05	0.08	0.06	0.01	0.03	0.04	0.15	0.15	0.03	0.02
MgO	2.55	1.67	1.67	0.95	1.58	0.97	2.79	2.64	1.27	1.04
CaO	3.14	4.36	3.26	3.01	2.76	2.75	1.95	2.11	1.88	2.75
Na_2O	4.56	3.79	3.94	4.71	4.25	4.32	4.30	5.67	4.72	3.98
K_2O	1.82	1.49	2.71	0.90	1.42	1.64	1.44	0.35	1.77	2.80
P_2O_5	0.08	0.07	0.11	0.08	0.08	0.07	0.16	0.15	0.08	0.08
LOI	1.15	2.03	3.06	1.06	1.16	2.24	2.12	1.82	1.94	1.69
Total	99.85	99.87	99.95	99.52	98.06	100.00	99.92	99.55	99.77	99.72
P	350	290	540	350	350	290	750	690	330	360
Cr	16	13	53	19	17	21	17	19	16	17
Co	23	7	10	11	6	8	12	42	6	7
Ni	69	11	44	14	10	15	19	57	12	13
Rb	49.2	32.4	85.3	17.3	25.3	36.7	28.4	9.2	39.2	41.7
Sr	199	354	328	291	397	233	416	329	230	242
Cs	2.97	1.5	1.4	0.26	1.11	0.7	1.03	1.16	0.72	0.77
Ba	720	480	1040	270	440	420	660	110	630	570
Sc										
V	37	37	44	33	31	34	75	71	33	34
Ta	0.4	0.37	0.37	0.39	0.38	0.32	0.25	0.26	0.31	0.33
Nb	3.7	3.6	4.1	4.2	3.8	3.3	3.7	4	3.5	3.6
Zr	93.5	79.5	100.5	100.5	105.5	67.3	58.5	66.4	90.3	88
Hf	2.9	2.4	3	2.9	3.1	2.2	2.1	2.3	3.1	3.1
Th	1.7	1.5	1.8	2.1	2	1.9	3.1	3	2.2	2.1
U	0.4	0.3	0.4	0.5	0.5	0.5	1.4	0.9	0.5	0.5
Y	4.5	4.1	5.9	4.4	4.4	4.5	10.7	10.8	4.5	4.4
La	10.5	10.3	13.9	13.2	11.9	11.5	26.8	9.8	13.2	12.4
Ce	21.6	22.2	29.5	26.2	24.5	22.6	57.7	22.0	26.0	25.4
Pr	2.6	2.8	4.1	3.1	2.8	2.6	7.0	2.9	2.9	3.0
Nd	9.3	9.7	14.3	10.4	9.8	9.2	25.9	12.3	10.1	10.3
Sm	1.7	1.7	2.6	1.9	1.7	1.6	4.3	2.7	1.7	1.7
Eu	0.6	0.6	0.7	0.5	0.4	0.5	1.4	0.6	0.5	0.5
Gd	1.5	1.5	2.3	1.7	1.5	1.5	3.5	2.6	1.6	1.6
Tb	0.2	0.2	0.3	0.2	0.1	0.1	0.4	0.4	0.2	0.2
Dy	0.9	0.9	1.3	1.0	0.8	0.9	1.9	2.1	0.9	0.9
Ho	0.2	0.2	0.2	0.2	0.2	0.2	0.4	0.5	0.2	0.2
Er	0.5	0.4	0.6	0.5	0.4	0.4	1.0	1.1	0.4	0.4
Tm	0.1	<0.1	0.1	0.1	<0.1	<0.1	0.1	0.1	<0.1	<0.1
Yb	0.4	0.4	0.5	0.4	0.4	0.4	0.9	0.8	0.3	0.3
Lu	0.1	<0.1	0.1	0.1	<0.1	<0.1	0.1	0.1	<0.1	<0.1
Cu	7.7	10.3	35.7	3.7	3.8	15.4	347	344	38.2	4.1
Zn	34	17	55	12	14	39	83	631	12	14
Mo	1.84	0.87	3.56	1.07	0.77	0.68	4.85	0.83	0.58	0.43
Tl	0.41	0.14	0.49	0.04	0.07	0.12	0.12	0.04	0.14	0.11
Pb	6.7	3.9	49.3	4	2.8	4.8	5.2	8.8	1.7	3.2
Sn	0.4	0.5	0.6	0.5	0.3	0.6	1.7	1.3	0.5	0.4
Sb	0.08	0.06	0.08	<0.05	<0.05	0.06	<0.05	<0.05	<0.05	<0.05
$(La/Yb)_{cn}$	18.82	18.46	19.93	23.66	21.33	20.61	21.35	8.78	31.55	29.64
$(La/Sm)_{cn}$	3.99	3.91	3.45	4.49	4.52	4.64	4.03	2.34	5.02	4.71
$(Gd/Yb)_{cn}$	3.10	3.10	3.80	3.51	3.10	3.10	3.22	2.69	4.41	4.41
$(Eu/Eu^*)_{cn}$	1.12	1.12	0.86	0.83	0.75	0.97	1.07	0.68	0.91	0.91
Al_2O_3/TiO_2	59.21	48.34	37.12	50.29	48.78	63.63	37.95	40.14	55.39	58.78
Zr/Hf	32.24	33.13	33.50	34.66	34.03	30.59	27.86	28.87	29.13	28.39
Zr/Y	20.78	19.39	17.03	22.84	23.98	14.96	5.47	6.15	20.07	20.00
Nb/Nb*	0.27	0.28	0.23	0.24	0.25	0.21	0.11	0.34	0.19	0.22
Notes										

	Siltstone									
Sample ID	546741	546747	546750	626175	626190	626195	626390	626397	626398	626460
SiO_2	67.71	68.19	70.13	66.77	69.62	69.37	72.48	55.92	69.54	42.13
TiO_2	0.39	0.27	0.31	0.40	0.30	0.32	0.37	0.45	0.30	3.60
Al_2O_3	15.03	15.38	14.24	15.36	14.04	14.69	15.12	21.92	15.74	10.58
Fe_2O_3	2.99	4.94	2.43	3.32	3.16	3.05	1.51	3.74	2.47	21.97
MnO	0.03	0.04	0.06	0.16	0.03	0.11	0.02	0.03	0.06	0.27
MgO	1.67	1.46	0.84	0.92	2.49	1.48	0.72	2.68	0.73	5.76
CaO	3.50	2.31	2.89	4.73	1.63	3.26	3.12	3.63	3.97	10.58
Na_2O	4.25	1.68	6.75	2.97	7.74	2.70	4.78	5.82	3.47	2.01
K_2O	1.76	3.19	0.08	2.77	0.23	2.81	0.77	2.79	1.64	0.41
P_2O_5	0.11	0.07	0.07	0.09	0.06	0.07	0.09	0.11	0.07	0.16
LOI	1.39	1.86	1.19	1.43	0.45	1.26	1.00	1.62	1.12	2.09
Total	98.96	99.45	99.02	98.99	99.81	99.25	100.05	98.85	99.23	99.61
P	560	320	320	380	270	360	430	500	350	700
Cr	31	15	27	25	67	34	15	20	11	10
Co	9	6	8	9	13	8	4	21	7	78
Ni	24	12	24	14	35	13	8	77	11	63
Rb	42.6	60.2	0.9	56	7	72	19.2	67.1	29.4	6.5
Sr	459	167.5	209	163	399	238	268	282	339	308
Cs	1.97	2.34	0.09				0.87	3.81	1.28	0.7
Ba	690	330	50	510	40	720	280	860	600	150
Sc										
V	50	32	41	41	35	34	30	45	31	552
Ta	0.3	0.29	0.33				0.27	0.41	0.37	0.98
Nb	3.6	3.2	3.6	3	5	3	2.7	4.3	3.9	15.2
Zr	97	47.7	76.6	127	95	123	103	130.5	90.1	57.5
Hf	3.3	1.6	2.5				3.1	3.7	2.5	1.8
Th	2.2	1.9	2.2	2	3	2	2.4	3	2	1.5
U	0.5	0.4	0.4	0.5	0.9	0.6	0.6	0.9	0.5	0.4
Y	6.5	4.1	4.5	5.1	6.9	5.5	4.5	6.2	4.1	23.7
La	14.8	12.2	7.1	14.0	11.4	15.8	11.7	13.5	9.9	16.1
Ce	32.3	23.3	15.9	25.7	24.1	28.4	22.8	29.0	20.4	39.4
Pr	4.3	2.4	2.0	2.7	2.8	3.0				
Nd	15.8	8.2	7.4	10.2	10.4	10.6				
Sm	2.7	1.4	1.4	1.7	1.9	1.8				
Eu	0.7	0.5	0.7	0.6	0.4	0.7				
Gd	2.3	1.3	1.3	1.6	1.8	1.8				
Tb	0.2	0.1	0.2	0.2	0.2	0.2				
Dy	1.3	0.7	0.9	0.9	1.2	1.0				
Ho	0.3	0.2	0.2	0.1	0.2	0.2				
Er	0.7	0.3	0.5	0.5	0.6	0.5				
Tm	<0.1	<0.1	0.1	<0.1	0.1	0.1				
Yb	0.5	0.3	0.5	0.4	0.6	0.4				
Lu	<0.1	<0.1	0.1	0.1	0.1	0.1				
Cu	11.4	20.5	143	19	125	14	11.6	14.7	11.2	288
Zn	33	45	19	23	39	31	12	25	21	138
Mo	1.41	0.67	0.86	<1	23	<1	1.91	3.99	2.8	0.91
Tl	0.21	0.14	<0.02				0.06	0.52	0.1	0.03
Pb	5.3	2.3	2.9	7	18	6	6.1	9.3	3.5	2.2
Sn	0.5	0.5	0.4				0.5	0.6	0.5	1.5
Sb	0.09	<0.05	0.05	<5	<5	<5	0.06	<0.05	<0.05	0.09
$(La/Yb)_{cn}$	21.22	29.16	10.18	25.10	13.62	28.32				
$(La/Sm)_{cn}$	3.54	5.63	3.28	5.32	3.88	5.67				
$(Gd/Yb)_{cn}$	3.80	3.58	2.15	3.31	2.48	3.72				
$(Eu/Eu^*)_{cn}$	0.84	1.11	1.56	1.09	0.65	1.18				
Al_2O_3/TiO_2	38.54	56.96	45.94	38.40	46.80	45.91	40.86	48.71	52.47	2.94
Zr/Hf	29.39	29.81	30.64				33.23	35.27	36.04	31.94
Zr/Y	14.92	11.63	17.02	24.90	13.77	22.36	22.89	21.05	21.98	2.43
Nb/Nb*	0.20	0.19	0.42	0.15	0.35	0.13	0.17	0.26	0.30	0.86
Notes										~10-50% chloritic laminae

	Siltstone									
Sample ID	626483	626488	626492	626493	626498	645655	645661	645672	24-M	29-M
SiO_2	48.87	71.68	48.60	38.57	66.91	68.20	48.48	67.80	67.87	69.69
TiO_2	0.82	0.35	1.49	1.07	0.25	0.30	0.61	0.39	0.32	0.33
Al_2O_3	4.91	14.28	4.87	6.28	13.74	15.90	11.09	14.39	14.44	15.66
Fe_2O_3	14.93	1.99	11.67	17.88	2.68	2.71	11.64	4.56	1.71	2.00
MnO	0.22	0.04	0.27	0.24	0.15	0.06	0.21	0.05	0.10	0.04
MgO	16.31	1.25	10.97	19.68	0.69	1.55	11.70	1.38	0.83	0.52
CaO	8.71	4.01	14.71	5.04	5.13	3.37	10.56	2.78	4.62	2.86
Na_2O	0.26	3.92	1.75	0.05	2.81	3.16	1.61	4.78	5.03	5.51
K_2O	2.21	0.77	0.04	0.02	2.52	2.54	0.49	0.86	2.33	2.19
P_2O_5	0.06	0.09	0.08	0.08	0.07	0.08	0.06	0.09	0.06	0.09
LOI	2.01	1.49	4.32	9.06	3.28	1.66	1.50	0.93	2.67	1.63
Total	99.73	99.94	98.96	98.33	98.30	99.66	98.11	98.07	99.98	100.51
P	240	400	320	370	320	340	240	420		
Cr	1660	54	770	1590	27	17	573	21	42	41
Co	106	6	85	115	8	6	59	10	7	4
Ni	1050	21	465	1105	24	13	306	15	19	11
Rb	81.9	12.5	1	0.9	48.6	51.9	19.5	22.2	51	32
Sr	56.3	246	161	138.5	158.5	305	113.5	277	198	156
Cs	5.88	0.3	0.13	0.29	1.06	1.15	1.76	1.24	0.76	0.688
Ba	380	350	10	<10	420	680	120	230	446.9	962.5
Sc									4	5.1
V	153	40	265	211	29	36	186	35	43	46
Ta	0.22	0.29	0.73	0.28	0.31	0.31	0.18	0.46	0.3	0.3
Nb	3.3	2.9	11.4	4.4	4	3.5	2.2	5.4	3.29	3.25
Zr	36	92.1	54.2	60.5	99.5	92.1	13	84.4	119	130
Hf	1.2	3.1	1.8	1.5	2.9	3	0.5	2.5	2.84	3.24
Th	0.3	2.1	1	0.4	2.1	2	0.2	2.4	1.36	1.82
U	0.1	0.5	0.2	0.1	0.6	0.4	<0.1	0.6	0.35	0.48
Y	8	4.4	14.7	14.5	4.4	4.2	16.3	7	3.33	4.38
La	4.0	11.8	11.9	4.4	11.9	12.0	2.7	16.4	6.4	14.2
Ce	10.3	23.6	28.0	12.1	22.6	24.6	7.3	31.8	12.4	27.2
Pr						3.0	1.1	3.7	1.2	2.7
Nd						10.6	5.6	13.2	4.7	10.1
Sm						1.8	1.8	2.4	0.9	1.7
Eu						0.6	0.7	0.7	0.5	0.7
Gd						1.6	2.3	2.1	0.8	1.4
Tb						0.2	0.4	0.3	0.1	0.2
Dy						1.0	2.9	1.4	0.5	0.8
Ho						0.2	0.6	0.3	0.1	0.2
Er						0.5	1.9	0.7	0.3	0.4
Tm						0.1	0.3	0.1	0.0	0.1
Yb						0.4	1.8	0.6	0.3	0.3
Lu						<0.1	0.3	0.1	0.0	0.1
Cu	315	10.4	776	146.5	13.7	4.9	1.8	108	391	53
Zn	454	16	90	98	43	14	66	30	76	49
Mo	0.47	1.03	0.49	0.31	1.21	0.43	0.74	0.86	0.17	0.32
Tl	0.91	0.05	0.04	0.05	0.09	0.21	0.07	0.1	0.207	0.122
Pb	4.9	5.1	9.9	4.2	3.2	4	0.7	5.3	14	2.5
Sn	1.2	0.5	0.8	0.3	0.4	0.8	0.5	0.7	0.67	0.41
Sb	<0.05	<0.05	0.13	0.24	0.06	<0.05	0.05	<0.05	<0.04	<0.04
$(La/Yb)_{cn}$						21.51	1.08	19.60	18.32	29.17
$(La/Sm)_{cn}$						4.31	0.97	4.41	4.78	5.30
$(Gd/Yb)_{cn}$						3.31	1.06	2.89	2.76	3.25
$(Eu/Eu^*)_{cn}$						1.06	1.05	0.93	1.79	1.37
Al_2O_3/TiO_2	5.99	40.80	3.27	5.87	54.96	53.00	18.18	36.90	45.13	47.45
Zr/Hf	30.00	29.71	30.11	40.33	34.31	30.70	26.00	33.76	41.90	40.12
Zr/Y	4.50	20.93	3.69	4.17	22.61	21.93	0.80	12.06	35.74	29.68
Nb/Nb*	0.79	0.18	0.84	1.02	0.24	0.22	0.83	0.24	0.37	0.16
Notes	~10-50% chloritic laminae		~10-50% chloritic laminae							

	Siltstone									
Sample ID	29-N	36-M	39-N	41-L	46-M	52-P	72-1	72-M	73-M	74-M
SiO_2	49.13	68.97	68.91	45.82	66.03	72.28	61.31	58.05	69.62	65.62
TiO_2	0.66	0.30	0.35	0.85	0.30	0.25	0.25	0.24	0.30	0.39
Al_2O_3	2.58	14.44	13.88	13.53	14.78	15.07	12.11	11.42	14.40	16.70
Fe_2O_3	15.66	2.14	3.98	13.05	3.70	1.81	2.67	4.08	3.68	3.83
MnO	0.22	0.04	0.08	0.21	0.05	0.02	0.04	0.07	0.04	0.05
MgO	19.43	0.82	1.21	6.38	1.31	1.21	0.64	0.99	1.24	1.73
CaO	10.55	4.38	3.64	9.63	3.88	1.28	8.53	10.13	2.54	3.35
Na_2O	0.15	3.89	4.45	3.96	6.33	5.15	7.40	7.02	4.00	6.68
K_2O	0.02	3.18	1.49	2.11	1.24	2.99	0.16	0.05	3.05	0.80
P_2O_5	0.03	0.07	0.08	0.10	0.07	0.07	0.06	0.06	0.08	0.11
LOI	2.24	2.61	1.72	4.68	1.88	1.00	5.90	6.66	2.13	1.59
Total	100.68	100.83	99.79	100.32	99.57	101.11	99.09	98.77	101.07	100.86
P										
Cr	1642	30	47	133	36	39	32	42	57	74
Co	113	5	8	42	8	5	5	7	9	9
Ni	851	15	18	79	14	11	9	17	23	15
Rb	1	46	33	103	27	39	9	4	44	22
Sr	19	196	217	344	266	152	292	418	198	408
Cs	0.036	0.668	0.861	14.092	2.5	0.447	0.461	0.211	0.985	1.683
Ba	4	523.7	371.8	293.1	196.9	1180.2	141.3	44.1	685.3	223.8
Sc	25.8	3.7	5.8	39	4.4	3.6	2.7	4.2	4.5	5.9
V	156	34	52	313	40	33	34	31	42	57
Ta	0.2	0.3	0.4	0.2	0.3	0.3	0.2	0.2	0.3	0.3
Nb	2.91	3	3.82	2.39	3.27	2.91	2.49	2.46	3.27	4.49
Zr	27	116	116	55	123	112	93	86	123	93
Hf	0.78	3	2.92	1.55	3.07	2.77	2.36	2.17	3.06	2.31
Th	0.75	1.84	2.37	0.37	2.01	1.82	1.65	1.44	2.01	2.78
U	0.55	0.55	0.6	0.09	0.39	0.47	0.48	0.43	0.71	0.81
Y	6.22	3.66	6.05	22.94	4.33	4.03	4.66	5.98	4.41	6.44
La	1.4	11.4	14.9	4.4	9.0	10.7	14.3	15.5	13.0	13.2
Ce	6.1	22.7	29.1	11.9	19.4	21.3	26.1	29.1	25.4	38.5
Pr	0.7	2.2	3.0	1.6	2.2	2.2	2.8	3.2	2.7	5.1
Nd	3.7	7.9	11.0	8.0	8.7	8.6	10.4	11.8	9.7	20.9
Sm	1.3	1.4	1.9	2.3	1.6	1.5	1.8	2.1	1.7	3.3
Eu	0.2	0.5	0.6	0.8	0.5	0.6	0.6	0.8	0.6	1.0
Gd	1.4	1.1	1.6	3.0	1.3	1.2	1.4	1.7	1.3	2.2
Tb	0.2	0.1	0.2	0.5	0.2	0.2	0.2	0.2	0.2	0.3
Dy	1.2	0.7	1.1	3.7	0.8	0.7	0.9	1.1	0.9	1.2
Ho	0.2	0.1	0.2	0.8	0.2	0.1	0.2	0.2	0.2	0.2
Er	0.6	0.3	0.5	2.3	0.4	0.4	0.4	0.5	0.4	0.5
Tm	0.1	0.0	0.1	0.4	0.1	0.1	0.1	0.1	0.1	0.1
Yb	0.5	0.3	0.5	2.3	0.3	0.3	0.3	0.4	0.4	0.5
Lu	0.1	0.0	0.1	0.4	0.1	0.0	0.1	0.1	0.1	0.1
Cu	537	17	27	42	52	7	76	131	81	72
Zn	69	15	42	49	20	24	15	18	25	85
Mo	0.11	0.8	0.57	0.15	0.64	0.44	0.52	0.44	1.29	0.13
Tl	<0.005	0.099	0.161	0.517	0.119	0.135	0.062	0.015	0.167	0.096
Pb	1.7	2.6	5.9	3.8	4.7	3.4	3.1	3.4	3.2	6.5
Sn	0.18	0.25	0.69	0.3	0.15	0.38	0.6	0.33	0.68	2.31
Sb	0.08	<0.04	<0.04	<0.04	<0.04	<0.04	<0.04	<0.04	<0.04	<0.04
$(La/Yb)_{cn}$	1.96	27.45	21.61	1.35	18.55	24.26	30.77	24.76	25.40	18.19
$(La/Sm)_{cn}$	0.68	5.32	5.03	1.24	3.53	4.54	5.23	4.71	4.91	2.57
$(Gd/Yb)_{cn}$	2.34	2.98	2.63	1.05	3.01	3.25	3.41	3.16	2.97	3.51
$(Eu/Eu^*)_{cn}$	0.54	1.19	0.95	0.91	1.12	1.22	1.14	1.22	1.13	1.06
Al_2O_3/TiO_2	3.91	48.13	39.66	15.92	49.27	60.28	48.44	47.58	48.00	42.82
Zr/Hf	34.62	38.67	39.73	35.48	40.07	40.43	39.41	39.63	40.20	40.26
Zr/Y	4.34	31.69	19.17	2.40	28.41	27.79	19.96	14.38	27.89	14.44
Nb/Nb*	3.63	0.20	0.19	0.55	0.30	0.20	0.12	0.11	0.18	0.37
Notes	~10-50% chloritic laminae			~10-50% chloritic laminae						

	Siltstone		
Sample ID	75-M	81-P	90-M
SiO_2	64.18	41.98	58.73
TiO_2	0.30	0.92	0.69
Al_2O_3	14.39	5.74	15.34
Fe_2O_3	4.16	14.85	6.54
MnO	0.10	0.21	0.10
MgO	1.67	20.70	3.50
CaO	4.07	7.53	5.01
Na_2O	5.04	0.13	6.69
K_2O	1.87	0.10	1.79
P_2O_5	0.08	0.06	0.34
LOI	2.74	7.55	1.27
Total	98.59	99.77	100.00
P			
Cr	30	3721	195
Co	5	105	21
Ni	11	1150	71
Rb	46	3	50
Sr	281	93	633
Cs	1.381	1.225	0.897
Ba	655.4	4.9	1305.8
Sc	4.2	22.8	12.3
V	38	224	117
Ta	0.3	0.2	0.3
Nb	3.21	3.48	4.4
Zr	114	47	139
Hf	2.86	1.28	3.49
Th	1.9	0.27	3.26
U	0.56	0.08	0.8
Y	6.27	10.01	17.42
La	14.5	3.2	30.9
Ce	26.5	9.7	72.0
Pr	2.8	1.4	9.0
Nd	10.6	7.3	38.4
Sm	2.1	2.0	7.1
Eu	0.9	0.5	1.9
Gd	1.8	2.2	5.1
Tb	0.2	0.3	0.7
Dy	1.2	1.9	3.2
Ho	0.2	0.4	0.6
Er	0.5	1.0	1.5
Tm	0.1	0.1	0.2
Yb	0.4	0.9	1.5
Lu	0.1	0.1	0.2
Cu	49	127	161
Zn	653	85	59
Mo	0.68	0.08	2.35
Tl	0.246	0.043	0.318
Pb	23.2	1.1	9.7
Sn	1.02	0.49	0.7
Sb	0.1	<0.04	0.06
$(La/Yb)_{cn}$	23.71	2.56	14.84
$(La/Sm)_{cn}$	4.47	1.03	2.81
$(Gd/Yb)_{cn}$	3.30	1.97	2.84
$(Eu/Eu^*)_{cn}$	1.32	0.70	0.94
Al_2O_3/TiO_2	47.97	6.24	22.23
Zr/Hf	39.86	36.72	39.83
Zr/Y	18.18	4.70	7.98
Nb/Nb*	0.15	1.21	0.12
Notes			